AGSO JOURNAL
OF AUSTRALIAN GEOLOGY & GEOPHYSICS

BMR PUBLICATIONS COMPACTUS
(LENDING SECTION)

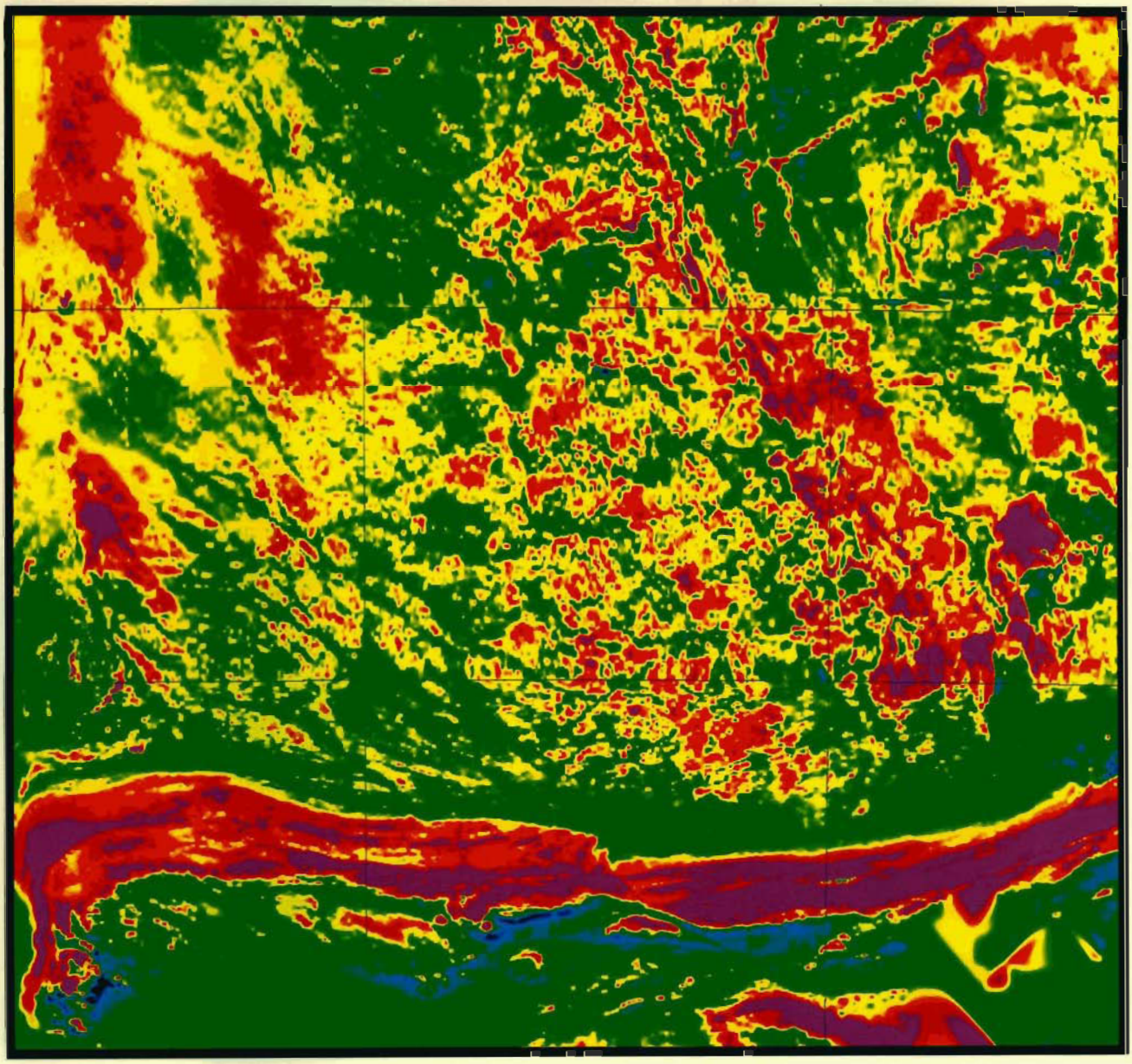

BMR
SSS(94)
AGS. 5
C3

VOLUME 15, NUMBER 3
1994

AUSTRALIAN GEOLOGICAL SURVEY ORGANISATION
LIBRARY
- 7 DEC 1994

AGSO Journal of Australian Geology & Geophysics

Editor: Karl H. Wolf, Corporate Publications, Australian Geological Survey Organisation

Editorial Board

C.E. Barton, Geophysical Observatories & Mapping Division, AGSO

J. Bauld, Environmental Geoscience & Groundwater Division, AGSO

A.R. Chivas, Research School of Earth Sciences, Australian National University

B.J.J. Embleton, CSIRO Office of Space Science and Applications, Australian National University Campus

Shen-Su Sun, Regional Geology & Minerals Division, AGSO

J.M. Kennard, Marine, Petroleum & Sedimentary Resources Division, AGSO

I.H. Lavering, Petroleum Resource Branch, Bureau of Resource Sciences

J.H. Shergold, Marine, Petroleum & Sedimentary Resources Division, AGSO

J.B. Willcox, Marine, Petroleum & Sedimentary Resources Division, AGSO

L.A.I. Wyborn, Regional Geology & Minerals Division, AGSO

Policy

The *AGSO Journal of Australian Geology & Geophysics* is a quarterly journal of geoscientific research results relating to the program and interests of the Australian Geological Survey Organisation (AGSO). It complements other earth science journals by focusing on Australia, and includes papers covering the broader Australasian and SW Pacific region.

The *Journal*'s target audience is the world-wide geoscientific community, catering for the interests of the resource, exploration and environmental industries, as well as those of researchers in universities and State and Federal agencies.

The Editorial Board is responsible for the scientific policies and standards of the *Journal*, which will publish papers on fundamental research, applied research and review topics. Contributions are invited from anyone. Scientific excellence and relevance to the broad aims of AGSO are the main criteria for acceptance of manuscripts for publication. Peer review and editorial and production standards are similar to those of leading international journals.

Guide for contributors

Submission of a paper to the *Journal* implies that the paper is original and unpublished, and is not being considered for publication elsewhere. Papers published in the *AGSO Journal of Australian Geology & Geophysics* become Commonwealth copyright. Authors are responsible for obtaining permission to reproduce any material, especially a figure, that has been published previously.

All submissions will be peer-reviewed. Submissions by AGSO authors will normally be reviewed by non-AGSO referees; those by non-AGSO authors, by at least one AGSO referee.

When your paper has been accepted you will be asked to supply a copy on an IBM-compatible diskette. Do not send this until it is requested.

Submission of manuscripts

- Three copies of the complete manuscript should be sent to the Editor.
- Your manuscript should be double-spaced, with margins of at least 25 mm, on one side only of A4 paper, with all pages numbered. Single-spaced copies are not suitable for refereeing or editing and will not be accepted.
- Use a straightforward print-out in Times or Courier font. Do not use desktop publishing software to prepare your manuscript.
- Photocopies of draft figures are acceptable when the manuscript is first submitted, as long as they are clear enough for the reviewers. Final versions of figures must be supplied when the final version of the manuscript is accepted for publication.
- Photographs should be supplied as glossy prints.

Style

Contributions should be written in English, and spelling should follow the latest edition of *The Macquarie Dictionary*. Refer to a recent issue of the *Journal* for further guidance on general style. But note that a revised style for references is being introduced with these instructions. Heading hierarchy should be indicated in the margin by ringed capital letters; A for main headings, B for second level headings, etc.

Abstract and key words

An abstract is required at the beginning of the manuscript. It should provide an informative summary of the main results and conclusions contained in the manuscript. It should not exceed 300 words. (An abstract is not adequate if it states that certain work was done, but fails to summarise the outcomes.) Up to 10 key words or short phrases should be supplied to assist indexing of your paper.

References

The Journal does not cite 'in prep' references. References 'in press' are acceptable only if the journal and issue can be supplied. References to unpublished data, if necessary, should be quoted as personal communications, giving the affiliation of the person being quoted and the date of communication. References should be cited in the text by author(s) and year in the normal Harvard style. For example: 'Ernest (1976, p. 312) showed that ..' or as described by earlier workers (Zagreb 1931; Ernest 1976; Melway & Murray 1977; Melway et al. 1978). References should be listed at the end of the text, in alphabetical order and in the style shown below. Please note that all journal titles are spelt out in full.

Continued inside back cover

AGSO JOURNAL

OF AUSTRALIAN GEOLOGY & GEOPHYSICS

VOLUME 15, NUMBER 3, 1994

CONTENTS

David W. Durney & Hanan J. Kisch
A field classification and intensity scale for first-generation cleavages 257

T.P. Mernagh & W.K. Witt
Early, methane-rich fluids and their role in Archaean gold mineralisation at the Sand King and Missouri deposits, Eastern Goldfields Province, Western Australia 297

Alan J. Whitaker
Integrated geological and geophysical mapping of southwestern Western Australia 313

Marion O. Michael-Leiba
Fluctuations in seismicity in the Dalton area, NSW, Australia, and their relevance to earthquake forecasting 329

C.D. Ollier & C.F. Pain
Landscape evolution and tectonics in southeastern Australia 335

Ian H. Lavering
Marine benthic communities in the Early Carboniferous of New South Wales (Visean—*Delepinea aspinosa* Zone) 347

V. Palmieri, C.B. Foster & E.V. Bondareva
First record of shared species of Late Permian small foraminiferids in Australia and Russia: time correlations and plate reconstructions 359

Robert S. Nicoll
Seximembrate apparatus structure of the Late Cambrian coniform conodont *Teridontus nakamurai* from the Chatsworth Limestone, Georgina Basin, Queensland 367

I.C. Roach, K.G. McQueen & M.C. Brown
Physical and petrological characteristics of basaltic eruption sites in the Monaro Volcanic Province, southeastern New South Wales, Australia 381

AUSTRALIAN GEOLOGICAL SURVEY ORGANISATION
LIBRARY
- 7 DEC 1994

© Commonwealth of Australia 1994

ISSN 1320–1271

This work is copyright. Apart from any use as permitted under the Copyright Act 1968, no part may be reproduced by any process without written permission from the Manager, Commonwealth Information Services, AGPS. Inquiries should be directed to the Manager, AGPS Press, Australian Government Publishing Service, GPO Box 84, Canberra ACT 2601

Subscriptions to the AGSO Journal are available through the Australian Geological Survey Organisation (GPO Box 378, Canberra ACT 2601; tel. 06 249 9642, fax 06 249 9982).

Other matters concerning the Journal should be sent to the Editor, AGSO Journal

Editor, AGSO Journal: Dr. Karl H. Wolf
Cover design and figures prepared by AGSO Cartographic Services Unit unless otherwise indicated
Prepared for publication by Lin Kay

Printed in Australia by National Capital Printing Fyshwick, A.C.T. 2609

AUSTRALIAN GOVERNMENT PUBLISHING SERVICE CANBERRA 1994

Front-cover illustration: **Total Magnetic Intensity (low blue–high pink) image of the onshore Albany 1:1M sheet. Towards the bottom of the image is an east–west band of red to pink, which corresponds with highly magnetised felsic and mafic granulites of the northern zone of the Albany Province. To the south, in blue to green, are poorly magnetised gneiss and granite of the southern zone. To the north of the Albany Province and corresponding to the area mottled green, yellow and red, is the Archaean Yilgarn Craton. Magnetic anomalies attributed to compositional banding in the craton are largely oriented north-northwest to north. Poorly magnetised lineaments, oriented west-northwest, are particularly evident in the southwest of the craton. The southern margin of the craton has been deformed and demagnetised and is represented in the image by an irregular width zone of green abutting the northern zone of the Albany Province. This deformation was caused by thrusting of the Albany Province during the Mid Proterozoic.**

AGSO Journal of Australian Geology & Geophysics, 15 (3), 257–295 © Commonwealth of Australia 1994

A field classification and intensity scale for first-generation cleavages

David W. Durney[1] & Hanan J. Kisch[2]

The chief morphological characteristics and lithological associations of naturally occurring cleavage fabrics are reviewed with the aim of differentiating qualities that represent fabric type from those that represent fabric intensity, and incidental partings from the cleavage fabric itself. This leads to field-based descriptive classifications for types and intensity of rock cleavage which unify diverse previous observations and allow a more formal approach to the description of cleavage. Particular attention is given to first-generation cleavage and incipient cleavage in clastic rocks of low to very low metamorphic grade, although all cleavage types are considered.

Two main divisions of cleavage type are recognised: (a) *penetrative* and (b) *non-penetrative*, according to the spacing of cleavage domains (where present) with respect to the width of dominant clastic (or detrital) grains. Each division includes three types, each of which is closely related to the lithology and texture of the parent rock (*type 1, clay* and *slaty* penetrative types; *spaced, crenulation* and *scaly* non-penetrative types). Each of the six cleavage types may display one (or less commonly both) of two kinds of intensity modulation at the mesoscale: *shear zones* and *'stripes'*.

Fissility, defined as the small-scale crack-structure which develops along planes of bedding- and cleavage-fabric anisotropy in weathered mudrocks, is proposed as an index property reflecting the relative intensity of cleavage, bedding and intersection fabrics in these lithologies. Fissility-ratios can be quantified in the field by measurements of dimensional ratios of fissility-fragments. The ratios are given named class intervals and are quantitatively discussed with the aid of a logarithmic 3-axis diagram. A reference field-example illustrates a full progression of relative cleavage-fissility intensity from none, through incipient, to strong, in relation to a natural strain gradient. The influences of rock type, initial bedding anisotropy, strain and style of tectonic deformation on fissility-ratios are also discussed. Fissility-ratios provide a rapid means of evaluating the effects of regional variations of total fabric and deformation intensity in a given rock type in low- to very low-grade metamorphic environments; they also represent a new tool that may assist in the study of weak deformations, incipient cleavage, sensitivity of different rock types to cleavage development, deformational or tectonic regimes (as reflected by fissility-fragment shape fields) and fabrics in undeformed mudrocks.

Introduction

Different terms have been used to describe rock cleavages. Various descriptions place emphasis on different factors, such as scale of observation or genesis, which make comparisons difficult. Qualifiers like "weak" and "strong", "continuous" and "spaced" have different meanings to different workers, and are mostly not uniquely defined. A more formal approach to nomenclature would, therefore, assist documentation of cleavage phenomena and investigation of their significance in relation to geological factors and mechanisms of formation.

In the course of a study of the relationship between the stage of development of incipient slaty cleavage and the degree of very low-grade metamorphism (Kisch 1989, 1991), it was found that the published characterisations of the fabric—in areas on which data on very low-grade metamorphism are available—can be correlated with a standard cleavage scale only in a very crude way.

Many descriptions merely give very general indications of the fabric, without indicating the—presumably mesoscopic—scale of observation, and distinguish areas of "weak", "moderate" or "strong" fabric (Kemp et al. 1985; Merriman & Roberts 1985) or "non-planar and non-penetrative" and "planar and penetrative" schistosity (Fieremans & Bosmans 1982; after Richert 1974), which are not clearly defined and have different meanings to different workers. Sometimes, observations are given on features such as "development of micaceous sheen on cleavage surfaces", fissility of associated sandstones, and development of segregation lamellae (Turner 1935; Hutton & Turner 1936). Other papers give the percentage of flattening without further textural details other than "fracture cleavage" and "slaty cleavage" (Siddans 1977) or details of spacing of cleavage lamellae (Beutner 1978; Beutner & Diegel 1985). Still others give some details on the characteristics of the microfabric, including spacing of cleavage domains, degree of fabric in the microlithons, and percentage of the rock affected (e.g. Piqué et al. 1984; Piqué 1975, 1982), referring to some standard terminology of microfabric characteristics, such as Powell (1979; see also Borradaile et al. 1982). In some cases, the nature of the microfabric could be clarified by reference to photomicrographs in either the original papers or other papers dealing with cleavage in the same areas, but generally the characterisations are too variable to allow accurate establishment of the stages of cleavage development and, therefore, of their relationship to the degree of very low-grade metamorphism.

Some of the criteria presently used for cleavage description depend on lithology rather than intensity of cleavage development. Thus, a primary parameter in the classification of Powell (1979), the spacing of cleavage domains, appears to be conditioned by pre-existing heterogeneity in clastic rocks, particularly the predominant size of clastic grains of competent minerals, such as quartz, rather than by the intensity of cleavage development—at least until very advanced cleavage development. For instance, during the progressive development of cleavage in the Rheinische Schiefergebirge (Weber 1976, 1981) and the Damara orogen of Namibia (Ahrendt et al. 1977), marked by increasing phyllosilicate recrystallisation in cleavage planes, the cleavage domain spacing remains constant.

If the equivalence of cleavage types in different lithologies at the same degree of regional deformation were known in sufficient detail, we should, ideally, be able to predict the cleavage to be expected in other rock types. However, since this equivalence is known only in very general terms, it is important that descriptions of cleavage contain at least some description of cleavage morphology in one or two common rock types, which can then be used as a standard for comparison; these rock types should include a mudstone (without very pronounced primary bedding-parallel fissility) or clay-rich siltstone and, preferably, a wacke.

[1] School of Earth Sciences, Macquarie University, N.S.W. 2109, Australia.

[2] Department of Geology and Mineralogy, Ben-Gurion University of the Negev, P.O.B. 653, Beer-Sheva 84105, Israel.

Since most published descriptions of slaty cleavage are—and are likely to remain—field descriptions, and since an essential attribute of cleavage is the ability of the rock to split along preferred directions on the hand-specimen scale, it is both convenient and justified that classification of cleavage should be primarily based on field observation. Further correlation should then be attempted between these field categories and characteristics of the microfabric or other factors, such as strain.

Surprisingly, no accepted field classification of the stages of cleavage development in clastic rocks exists. Such a classification is needed to facilitate comparison and correlation of rock deformation fabrics with other geological variables, such as strain and relation to tectonic features, as well as degree of metamorphism. The scheme should, as far as possible, be internally consistent, with attributes logically grouped according to kind and not overlapping or having ambivalent meanings. One example of this type of approach is the classification of fold geometry by Fleuty (1964). To preserve objectivity in the classification, a clear distinction needs to be made between observation and interpretation. This is best done if the names given to classes or attributes are descriptive and morphological (Dennis 1972; Powell 1979) rather than genetic. The resulting classification will then provide an independent observational framework that should assist in developing ideas about relationships and origins. To serve in this way, the class categories should take into account natural groupings or associations of natural forms. One of these is the extensive variation which can occur as a result of differing lithologies, and another is the effect of varying intensity of any one fabric type. Finally, a classification scheme should be practical to implement. Therefore, it should incorporate concepts and terms that have been widely accepted and should not deviate appreciably from these except where consistency is at risk or where some new attribute is needed to complete a set of descriptors.

The need to encompass incipient cleavage

Cleavage structure proper is generally regarded as planar (e.g. Dennis 1972), and considerable attention has been given to the well-developed planar forms, both mesoscopically in relation to strain (e.g. Wood 1974) and microscopically (e.g. Powell 1979; Borradaile et al. 1982).

One of the purposes of proposing the present classification of cleavage is to recognise and encompass the incipient stages of cleavage formation prior to the development of an overall planar fabric. It is a curious and long-standing paradox that cleavage appears to be closely related to tectonic strain and yet only appears (as a planar structure) above some finite strain threshold: ~35% total strain (including compaction) for slaty cleavage in pelites (Wood 1974); ~25–30% tectonic strain for cleavage in arenites (Clendenen et al. 1988); and ~25% total strain in quartz pebbles (Norris & Bishop 1990). This raises the question as to whether the fabric is suddenly created at some strain threshold or builds up gradually from the earliest stages of deformation, as suggested by Kligfield et al. (1983) and Ramsay & Huber (1983, p.185), and has simply escaped notice in the field. To address questions such as this, it is necessary to have a framework for objective description of incipient cleavage intensity. A similar need arises in attempts to understand the relationship between cleavage fabric initiation and metamorphism (Kisch 1991); a meaningful comparison cannot be made without including the weakest members of the cleavage series.

Two structures which reflect very incipient cleavages are (1) pencil structure (Fig. 2a) and (2) 'pre-pencil structure'.

(1) *Pencil structure*. The pencil structure (Cloos 1946, p.8) produced upon weathering of weakly deformed mudrock reflects a linear bedding/cleavage intersection fabric, which may be associated with either (a) stretching normal to bedding or (b) stretching parallel to the pencils.

For the first type of pencil structure, Reks & Gray (1982) have shown that its development requires two independent fabric anisotropies approximately equal in magnitude and that this condition is met only in a certain range of strain values, where the minimum principal strain (Z) ranges between 9 and 26% shortening; the long axes of the "pencils" are parallel to the bedding/cleavage intersection and the inferred Y-axis of the tectonic deformation ellipsoid. With increasing strain within this range, microfabric changes in the mudrock include lengthening of cleavage-domain traces and reduction in the degree of anastomosing as cleavage-domain traces tend towards planarity; these changes produce pencils with higher length/width ratios.

Pencils of the second type found in the Wildhorn nappe of the Swiss Alps (Ramsay 1981) are elongate parallel to the X-direction of both total strain (Ramsay 1981, fig. 10a; also Ramsay & Huber 1983, fig. 10.26) and tectonic strain (Ramsay 1981, fig. 9, Wildhorn), which here coincides with the bedding/cleavage intersection direction. Pressure-shadow extensions in this region are intersection-parallel (Durney & Ramsay 1973, fig. 22; Dietrich 1989, fig. 6, or Dietrich & Casey 1989, fig. 7) and, therefore, these pencils owe at least part of their elongation to mechanical elongation. However, since the pencils described by Reks & Gray (1982) were tectonically extended normal to the intersection direction, their examples cannot be explained by this means.

As far as is known at present, pencil structure is restricted to areas with very low degrees of metamorphism, with illite 'crystallinity' values of $>0.35°\Delta 2\Theta$ (Kisch 1991) indicative of low anchimetamorphic and "diagenetic" grades. For the area they studied, Reks & Gray (1982) gave the temperatures inferred from conodont colour alteration (Epstein et al. 1977) as 250–350°C; i.e. a CAI of 4–5. In the Paleozoic of the Yass area, New South Wales, pencil structure occurs in rocks with illite "crystallinity" values of $0.44–0.54°\Delta 2\Theta$.

(2) *'Pre-pencil' structure or embryonic cleavage*. Incipient cleavage-fissility so weak that it is subordinate to bedding-fissility—what may be called the 'pre-pencil' or embryonic type—is commonly overlooked in structural field investigations. It has been alluded to in some studies, mainly under the name of "fracture cleavage" (e.g. Siddans 1977; Price & Cosgrove 1990, p.447), also "pencil cleavage" (Engelder & Geiser 1979), but has otherwise been largely neglected as a serious structural entity. However, it displays a consistent geometrical relation to folds and is accompanied by weak fabric modification (Oertel et al. 1989; Weaver 1984, p.14) and layer-parallel shortening (Engelder & Geiser 1979). Limited regional study carried out for this paper suggests that it is much more widespread than is generally realised.

The need to consider cleavage types

Part of the difficulty, up to now, in defining a workable intensity scale for cleavage fabrics has been uncertainty

about whether some variables are functions of deformation, or are characteristic of different kinds of cleavage, or depend only on the lithology of the rock. Consequently, it is not possible to erect an intensity scheme without first distinguishing the factors that define different kinds of cleavage from those that define cleavage intensity. Even the question of what is, and what is not, a cleavage has to be settled before further progress can be made; especially, whether or not "fracture cleavage" is a real cleavage and/or a real fracture. Factors such as spacing of domains, composition and texture of the parent rock, and how fractures fit into the picture must all be addressed.

Accordingly, the first part of this paper reviews observations that previous workers have made about cleavage characteristics and their relationships, and uses this information as a basis for identifying morphological groupings of cleavage types. The chief considerations here are, first, logical consistency of the proposed scheme and, second, divisions that will be practical to use in the field.

In the second part of the paper we use the related concept of mechanical anisotropy—expressed as natural breakage phenomena—to develop a new, field-based, intensity scale, especially for slaty cleavages and related kinds in clastic sedimentary rocks.

Aims and restrictions of the classification

(1) The classification is restricted to rock cleavages; i.e. planar tectonic fabric elements (Dennis 1967), excluding fracture phenomena.

An important aim is to distinguish between the fabric (cleavage) and the ability of the rock to subsequently fracture along fabric planes (fissility). The former constitutes a basis for defining cleavage types, while the latter, especially cracking caused by weathering, provides a useful criterion for field assessment of cleavage intensity.

(2) The classification is intended primarily for application to first-generation penetrative cleavages in low-grade and very low-grade metamorphic clastic rocks. All types of cleavage are, however, considered.

(3) There is no restriction on rock type, but emphasis is mainly on clastic sedimentary rocks.

(4) The primary classification is based on descriptive characteristics which are observable in the field.

(5) The class attributes are:

(a) *type of cleavage* (penetrativeness and lithological dependance), and

(b) intensity (degree of preferred orientation of fissility-cracks).

(6) As far as possible, natural cleavage groupings are preserved (such as slaty cleavage in mudrocks), and existing descriptive terms and concepts are used whenever possible.

Rock type nomenclature

In naming the clastic sedimentary rocks that have been affected by cleavage development, we follow mainly Folk's (1980) sedimentological nomenclature (as far as can be determined from published information and field observations), especially at the lower grades of metamorphism, to emphasise the nature of the parent rocks. Examples are *mudrock* (comprising *claystone*, *mudstone*, *siltstone* or other varieties composed of clay and silt-size particles) and *sandstone* (dominated by sand-size particles of quartz, feldspar, mica and/or lithic fragments). Terms with particular textural significance are *wacke* (poorly sorted, muddy or matrix-rich sandstone) and *shale* (as opposed to mudstone, for a mudrock with pronounced bedding-fabric or lamination). In the latter part of the paper we use *"argillite"* for a dark, indurated lithic-composition mudrock (a laminated lithic siltstone) which can be distinguished in outcrop from more easily weathered "mudstone" and "shale". Where only a grain-size connotation is intended, irrespective of clast composition and roundness, we use *arenite* and *rudite*. To denote mudrocks and sandstones whose grain-size and mineralogy may have been significantly altered by regional or burial metamorphism, we use *pelite* and *psammite*, respectively.

Main cleavage type groupings

Some observations from previous work: a basis for main groupings

A number of important observations have been made about cleavage morphology over the last twenty years or so, which should be taken into account in any cleavage-nomenclature scheme.

(1) "Rock cleavage"

The definition of "rock cleavage" proposed by Dennis (1972, p.179; 1987b, p.172) is that it comprises "secondary planar fabric elements which impart mechanical anisotropy to the rock without apparent loss of cohesion". A consequence of this definition is that the existence of a cleavage can always be verified by the hammer test: an initially coherent sample will tend to split or "cleave" in a preferred direction, usually transverse to bedding. Nevertheless, Dennis emphasised that the planar fabric elements are planes of "potential parting" as opposed to planes which have been, or are now, actual partings (see also Dennis 1967, 1987a, b). The key distinction here is that rock cleavage results from a coherent rearrangement and realignment of the constituent minerals and is therefore essentially ductile rather than brittle in origin. This is supported by a wealth of modern microscopic and geometric observations. In particular, cleavage fabrics do not show the microstructural characteristics of brittle deformation mechanisms, such as split-and-displaced grains and open-space mineral precipitation (though cracks may occur either at a high angle to the fabric within constituent grains or incidentally parallel to the fabric, owing to subsequent cracking). Cleavage planes are also, for the most part, oriented normal to, or at a high angle to, the direction of maximum shortening strain and are, therefore, incorrectly oriented for extensional or brittle shear failure at the time of their development (for example, Dennis 1972; Siddans 1972; Groshong 1975a; Alvarez et al. 1978; Gray 1979; Gray & Durney 1979; Cosgrove 1989). Terms which imply a brittle origin, such as "fracture cleavage" (Leith 1905) and "close-joints cleavage" (Sorby 1857), which are still used in some structural textbooks are consequently inappropriate and should be abandoned (e.g. Dennis 1987b, p.182). It is necessary to carefully distinguish incidental partings and cracks which follow a pre-existing planar fabric—for example, partings brought about by weathering—from the fabric or "cleavage" itself. These features can be important field indicators of cleavage, as will be discussed below

under the heading of "fissility", but they do not constitute the actual cleavage, which is here understood to mean the internal rock fabric.

(2) Domainal character of common cleavages

The majority of cleavages, if observed at sufficiently small scale, are *domainal* in character (Williams 1972; Hobbs et al. 1976; Powell 1979; Borradaille et al. 1982). That is, the new alignment of minerals is most pronounced in regions called "cleavage domains" that are interwoven with parts of the rock having a weaker new alignment or remnants of an earlier fabric, called "microlithons" at the microscale and 'lithons' at the mesoscale. The cleavage domains are thin subplanar regions which are also sites of secondary concentration of platy minerals, so that rocks having this fabric tend to split readily along those domains. This is the chief cause of cleavage as a mechanical anisotropy in deformed sedimentary rocks and includes many cases in which the domainal character is observable only at the microscale; for example, common forms of slaty cleavage.

(3) Cleavages in mudrocks and clay-bearing sandstones/calcarenites

Cleavages in mudstones and marls and in clay-bearing sandstones and calcarenites (including poorly sorted varieties or wackes)—the "slaty" and "rough" cleavages, respectively, of Dennis (1972, 1987b)—represent a coherent group of cleavage types showing close spatial associations, micro-morphological similarities and complete transitions with one another (Bakewell 1815 *in* Siddans 1972, p.207; Powell 1969; Dennis 1972, 1987b; Means 1975; Gray 1978; Gibson & Gray 1985]. Both types typically display microscale cleavage domains, called "folia", "mica films", "seams", "cleavage laminae" or "cleavage lamellae", which run around and between the coarser clastic grains. A corollary of this behaviour, noted by Yoshida (1969) and measured by Gray (1978, fig. 17) and Reks & Gray (1982, fig. 11), is that the spacing of the cleavage domains is directly related to the width of the larger clastic grains. This has been further confirmed by Norris & Rupke (1986), who showed that the stratigraphically downward increase in slaty-cleavage intensity in a 200 m thick mudstone—as evident from a closer spacing (decreasing from ca. 250 to 20 μm) and increased continuity and coarsening of the initially anastomosing cleavage domains—correlates with a decrease in the mean grain size, average bed thickness, and quartz/mica ratio.

(4) Role of lithology and initial fabric

Cleavage development is strongly dependent on lithology and initial fabric, both with regard to the type of cleavage developed and its intensity. For example, "slaty" cleavage tends to occur in mudrocks, whereas mesoscopic "spaced" types are most common in impure limestones (e.g. Mitra & Yonkee 1985). These two types of cleavage are also most often developed in rocks with a low initial- or earlier-fabric anisotropy. When the rock has a strong previous fabric, such as an earlier slaty cleavage, the distinctive "crenulation"-cleavage type is usually the one which develops (Cosgrove 1976; Gray 1977c).

Within the pelitic to psammitic group of rocks, it has long been known that cleavage at any one locality is stronger in the pelitic than in the psammitic layers, a feature which is obvious in strata that have graded bedding. Fine argillaceous matrix also has an important influence on the type and strength of cleavage in psammites. In a study of low-grade psammitic (sandy) rocks from southeastern Australia, Gray (1978, p.580 and fig. 6) found that S_1 rough cleavage in silty sandstones (Type A, 50–80% matrix) is typically weak and irregular, due to short, discontinuous cleavage seams around random to weakly oriented grains, whereas in wackes (Type B, 80–90% matrix) it is stronger and more regular, due to continuous cleavage seams around S_1-oriented detrital grains.

The development of spaced cleavage in carbonate rocks of low to very low metamorphic grade appears also to be strongly influenced by clay content: for example, penetrative cleavage in pure limestone, but spaced cleavage in impure dolomite (Tapp & Wickham 1987), and isolated tectonic stylolites in pure limestone, but widespread cleavage only in limestones with more than 10% clay–quartz matrix (Marshak & Engelder 1985). In addition, Schweizer & Simpson (1986, p.781) found both a decrease in the spacing of cleavage domains and a change in their shape from planar to anastomosing with increasing clay content in dolomite; in limestone, domain spacing is similarly affected, but the domain shape in this rock changes from stylolitic to planar with increasing clay content (Alvarez et al. 1978).

(5) Cleavage zones or 'stripes'

Cleavage domains are commonly concentrated in roughly planar 'super-domains'. These structures are generally visible at the mesoscale and are marked by variation in both composition and fabric intensity: usually a concentration of platy minerals and dark opaque matter, together with a stronger cleavage fabric, in the more cleaved zones as compared with the less-cleaved zones. Descriptions which emphasise the compositional variation include "metamorphic layering", "metamorphic differentiation" or "differentiated layering" (Talbot & Hobbs 1968; Williams 1972; Cosgrove 1976), "litages tectoniques" (Soula & Debat 1976), "striping" (Beach 1974), "Pseudoschichtung" (Langheinrich 1977), "mica bands" (Boulter 1979; Boyer 1984), "P and Q domains" (Stephens et al. 1979; Waldron & Sandiford 1988), and "M and Q domains" (Gregg 1985). Those that emphasise the fabric enhancement include "cleavage zones" (Nickelsen 1972), "alignment zones" (Geiser 1974), "cleavage bands" (Means 1975), "isolated cleavage zones" (Gray 1978, p.580), "pressure solution cleavage", "cleavage stripes" or "pressure solution stripes" (Beach 1979; Siddans 1979), "compound tectonic fabrics" or "coplanar spaced cleavage" (Gray 1981), and "spaced cleavage zones" (Clifford et al. 1987).

These zones most commonly occur in impure psammites. A similar effect occurs in pelites—"layering parallel to cleavage" (Talbot & Hobbs 1968), "cleavage bundles" (Southwick 1987), "splaying" (Murphy 1990) or "coalesced slaty cleavage" (Erslev & Ward 1994)—although these are often special cases that are spatially tied to competence variations such as multilayer folds (Cosgrove 1976; Langheinrich 1977), contacts between coarser and finer lithologies (Talbot & Hobbs 1968, pl. 1; Nickelsen 1972; Langheinrich 1977; Southwick 1987), and margins of competent objects (Durney 1972a, 1976a; Cosgrove 1976; Gray 1981; Gratier 1979; Prior 1987). Cases which more closely resemble the free-ranging stripes in psammites include mesoscopic stripy zones in laminated low-grade pelites composed of mudstone, siltstone and very fine sandstone laminae (Soula & Debat 1976; Cox

et al. 1991; Gray & Willman 1991). Limestones may also display this effect as a clustering of fine anastomosing spaced cleavage domains called "diffuse-", "compound-" (Geiser & Sansone 1981, fig. 9) or "wispy-" (Koepnick 1985, fig. 1) "seams".

The phenomenon is not a purely mechanical "transposition of bedding", as proposed by Turner & Weiss (1963) and Bishop (1972, figs. 1 and 7), since it involves a pervasive loss or gain of selected minerals superimposed on previous layering. Indeed, the mesoscopic "differentiation" or segregration of minerals can occur in rocks, such as coarse wackes, that lack a primary internal layering. We also distinguish it from crenulation-cleavage differentiation (Cosgrove 1976; Gray 1977b) or metamorphic layering associated with crenulations (Glen 1982a), which is restricted to a fundamental domainal structure. It is essentially a modulation or "second order" (Durney 1972b, 1976b) variation of smaller scale, cleavage domain, differentiation and not strictly a separate type of cleavage in its own right. Although it is often called "spaced cleavage" (Gray 1981; Roberts 1989) or "disjunctive cleavage" (Murphy 1990), these are terms used for single-domain structures (Dennis 1972, p.180; Powell 1979). The zones referred to here comprise groupings of many individual cleavage domains, and the intervening zones also usually include some cleavage domains (Gray 1978, p.580). Extreme cases can arise where the concentration of cleavage domains is so great that they merge to form a single wide cleavage domain (Gray 1981; Murphy 1990, fig. 7). But even these cases typically display at least a weak cleavage throughout the rock, as shown by its ability to split parallel to cleavage anywhere in the specimen.

The difference between cleavage and cleavage zones (or bundles, differentiated bands, etc.) is perhaps clearest where the two are at an angle to each other (Boulter 1979; Boyer 1984; Powell & Rickard 1985, fig. 2; Murphy 1990). In this case, the rock splits oblique to the compositional layering, demonstrating that the latter is not *the* cleavage. In this paper, we distinguish *cleavage* (cleavage domains), as elementary-domain structures, from many-domain *cleavage zones*. The cleavage-type divisions which follow are based on the cleavage domains, if present. Cleavage zone development is considered to be a modification of the basic cleavage type.

(6) Shear zones

The previously described "cleavage zones" or "stripes" should be distinguished from heterogeneous zonal structures dominated by shearing rather than by loss of non-flaky minerals: namely, "shear zones" or "ductile shear zones" (e.g. Carreras et al. 1980; Simpson 1986; Lloyd et al. 1992) (see fig. 1B). The appearance and kinematics of these structures are very different from the "cleavage zones" of the preceding section. And, although they may contain domainal cleavages (Nickelsen 1986; Casas & Sàbat 1987), the type of cleavage or fabric within them is often different as well. The chief characteristics of shear zone fabrics in metamorphic rocks and their differences from cleavage zone fabrics are as follows:

(a) In constrast with domainal cleavage and cleavage zones, which are confined mainly to fine phyllosilicate-bearing rock types, shear zones are not restricted as to rock type and frequently occur in medium to coarse-grained, medium to high metamorphic grade or igneous parent rocks that lack fine phyllosilicates, especially schists, gneisses, granulites, granites, metadolerites, quartzites, coarsely crystalline vein quartz and so forth. At very low metamorphic grades, they may occur in relatively pure and fine-grained limestones.

(b) There is usually a reduction in grain size of all minerals in shear zones, leading to the formation of fine recrystallised "mylonite" and "mylonitic foliation" (Bell & Etheridge 1973; White et al. 1980), whereas grain size in domainly cleaved rock shows little or no variation between domains except for reductions in width of specific minerals, such as quartz, related to the local associated compositional variations.

(c) Initially coarse-grained quartz and mica, if present, becomes involved in the deformation of shear zones, whereas deformation in domainly cleaved low-grade sedimentary rocks appears to be concentrated in cleavage domains and, sometimes, beard structures, which run around and between the larger detrital grains of quartz and mica.

(d) Grain alignment in shear zones is commonly oblique to the zone, indicating shear parallel to the zones (Ramsay & Graham 1970), whereas in cleavage zones it is commonly parallel to the zone, indicating shortening normal to the zones (Gray 1981).

(e) A special type of meso- to microscale domainal structure is known only or mainly in shear zones: "S and C structure" (Berthé et al. 1979; Lister & Snoke 1984), and similar structures described as "extensional crenulation cleavage" (Platt & Vissers 1980), "shear bands" (Harris & Cobbold 1985) and "normal kink-bands" (Cosgrove 1989). It is characterised by very planar "C" or "C′" ("cissaillement" or "shear") bands, with a strong asymptotic fabric, that alternate with "S" ("schistosité" or "foliation") bands that contain a weaker, oblique and often sigmoidal fabric. Composition is usually about the same and can be identical in the two types of band or domain. This is in sharp contrast to the wavy, phyllosilicate-rich and sometimes 'conjunctive' (p. 265) domains that make up most types of domainal cleavage.

(f) Bulk compositional change may or may not (Beach 1980; Kerrich et. al. 1980) accompany shear zone fabric development. When present, it commonly involves both inward and outward migration of different chemical components in varying proportions with little apparent systematic pattern (Tobisch et al. 1991, table 3) and may occur in zones up to tens of kilometres wide (hydrated shear zones described by Grocott & Watterson 1980). In contrast, compositional variation always accompanies cleavage zone development; it consistently involves a relative loss of specific components such as carbonate (Gratier 1979) and silica (Clifford et al. 1987; Waldron & Sandiford 1988; Erslev & Ward 1994) from the cleavage zones; there is no obvious variation in degree of hydration of minerals; and cleavage zone widths fall within a restricted range of up to about 10 mm (e.g. Soula & Debat 1976; Waldron & Sandiford 1988).

Thus, it is clear that there are often fundamental differences between the fabrics developed in these two types of zonal structure. These differences involve considera-

tions of deformation mechanisms and deformation environments which are beyond the scope of this paper (cf. Groshong 1988, for an extensive review of those topics) and which may be difficult to resolve in some cases (e.g. Burg & Iglesias Ponce de Leon 1985). From an observational point of view, however, their respective occurrences are evidently conditioned to a large extent by lithology, especially by grain size, grain-size distribution and presence or absence of fine phyllosilicates, and by the ability of the rock to undergo mass transfer at the cleavage-domain scale. The nature of the parent lithology and type of zonal structure, therefore, provide clues to the existence of two distinct natural groups of penetrative cleavage. One displays a compositionally differentiated domainal fabric, while the other shows a more throughgoing deformation and alignment of the grains, with little or no domain-scale differentiation.

Proposed divisions of cleavage type: penetrative and non-penetrative

Our principal divisions of mesoscale cleavage types are what we term *penetrative* and *non-penetrative*, based on the known or inferrable relationship of the cleavage fabric to the size of the coarser constituent particles (see Fig. 1A).

"Penetrative", as ordinarily understood and as used here, is not equivalent to "uniform" (Oertel 1962, p.326); nor is it exactly equivalent to "continuous" as *defined* by Dennis (1972, after Chidester 1962), though it includes both of these as particular cases. It is the quality of 'permeating' or 'passing through' something to a fairly intimate level in the way that water, for instance, may pass through a porous rock. Thus, we define *penetrative cleavage* as a mineral alignment which 'penetrates' or 'passes through' the rock, down to the dominant grain or clast size. The mineral alignment may occur in all grains of the rock or, as more commonly happens, it may occur especially within domains which pass around and between the larger grains or clasts of the rock. It therefore includes the "slaty" and "rough" types referred to in (3) above as two particular examples ("continuous" as *used* by Dennis 1972). From the field observational point of view, the rock appears capable of splitting in the plane of cleavage anywhere between the coarser competent grains (such as quartz grains). In the case of a mudrock, the rock literally appears able to split anywhere. *Non-penetrative cleavage*, on the other hand, is defined as that in which domains of mineral alignment occur at intervals significantly greater than the size of the dominant grains or clasts.

Ideally, the penetrative/non-penetrative division depends on the relationship of cleavage spacing to grain size and does not occur at any particular cleavage domain spacing. But for practical reasons, a lower limit of 1.0–0.5 mm spacing must apply to the recognition of the non-penetrative type as a field-based term. Fortunately, the majority of these cleavages do appear to be spaced at intervals greater than 1.0–0.5 mm and can be readily identified in the field (e.g. the mesoscopic spaced cleavages of Alvarez et al. 1978).

Conversely, some "penetrative cleavages", according to the definition above, can be spaced at considerably more than the 1.0–0.5 mm field resolution limit (e.g. cleavage seams which weave between limestone pebbles and cobbles at spacings of more than 10 mm in Ramsay & Huber 1983, fig. 7.24B). These cases are morphologically analogous to "rough" cleavages in impure sandstones and calcarenites and therefore belong naturally within the penetrative group. The only difference is that cleavage domains in the conglomeratic type are clearly visible in the field, whereas, in the finer-grained varieties, they are inferred to exist from the way the rock splits.

Types of penetrative cleavage

As most "penetrative cleavages" are not further resolvable by direct observation in the field, and also because these cleavages tend to show close natural associations with particular lithologies (point 3 above), our major subdivision of this group is based on lithology. Accordingly, we recognise

(1) *penetrative type 1* cleavage fabrics in relatively fine-phyllosilicate-poor and usually well-sorted clastic and chemical sediments, and most igneous rock types; and

(2) *penetrative type 2* cleavage fabrics in clastic rocks containing significant proportions of fine phyllosilicate or other platy minerals (Fig. 1A).

We assign the numbers "1" and "2" to these types on the basis of relative fabric complexity. Type 1 fabrics are simpler in that they are typically undifferentiated uniform grain-shape fabrics. Except in cases where they are well developed, they impart little or even no capacity for directional splitting. Type 2 fabrics are more complex, in that they are typically, though not universally, domainal at the microscale. Rocks with type 2 fabric thus tend to split easily; the cleavage domains offer paths of easy parting through the rock.

(1) *Penetrative 1 or grain cleavage* occurs in rocks with little or no fine platy mineral fraction: relatively 'pure' and often well-sorted calcareous and siliceous sediments, many igneous rocks, and recrystallised metamorphic rocks with a medium to coarse-grained platy mineral fraction (schists, gneisses: see "schist fabric" of Gray 1977c). Fissility may occur anywhere within the rock, but is generally much harder to induce than in mudrocks and some poorly sorted arenites; in some cases, fissility may be lacking, although a poor fabric is present. Fissility in this type of cleavage is due to an alignment of all or most of the minerals present, whether of fine or coarse overall grain size (e.g. Dietrich & Song 1984).

Penetrative 1 cleavage may be heterogeneously developed in mesoscale shear zones (Fig. 1B). "Differentiation" or "striping", as seen in mudrocks and wackes, is generally absent except in some schists and gneisses.

(2) *Penetrative 2 cleavage* is pervasive in the sense that it penetrates at least part of the matrix of the rock between the coarser clastic grains, which means that the cleavage domains, if present, are spaced at about the width of the coarse grains: the rock splits anywhere except through the coarser competent clastic grains. Microscopically, the platy mineral orientation in the microlithons between cleavage domains may be largely unrelated to the cleavage domains (disjunctive in the terminology of Powell 1979) or it may be largely oriented parallel to the cleavage domains, what we propose to call a "conjunctive" or simply

"parallel" relationship.

Two principal divisions of penetrative 2 cleavage are recognised, according to the degree of lithification and metamorphism of the rock:

(a) *Clay type*—an undifferentiated preferred orientation of clay flakes known to occur in some unlithified and unmetamorphosed clay-rich fault gouges ("P-foliation" of Rutter et al. 1986; "clay foliation" of Chester & Logan 1987).

"Clay type" penetrative 2 cleavage is commonly accompanied by scaly cleavage, with which it forms a small angle, analogous to S-structure in ductile shear zones (Chester & Logan 1987) (Fig. 1B).

(b) *Slaty type*—which is by far the more common, including slaty cleavage and its incipient forms and related fabric types in poorly sorted coarser clastic rocks. The slaty type occurs in lithified fine-platy-mineral-bearing rocks of very low to low metamorphic

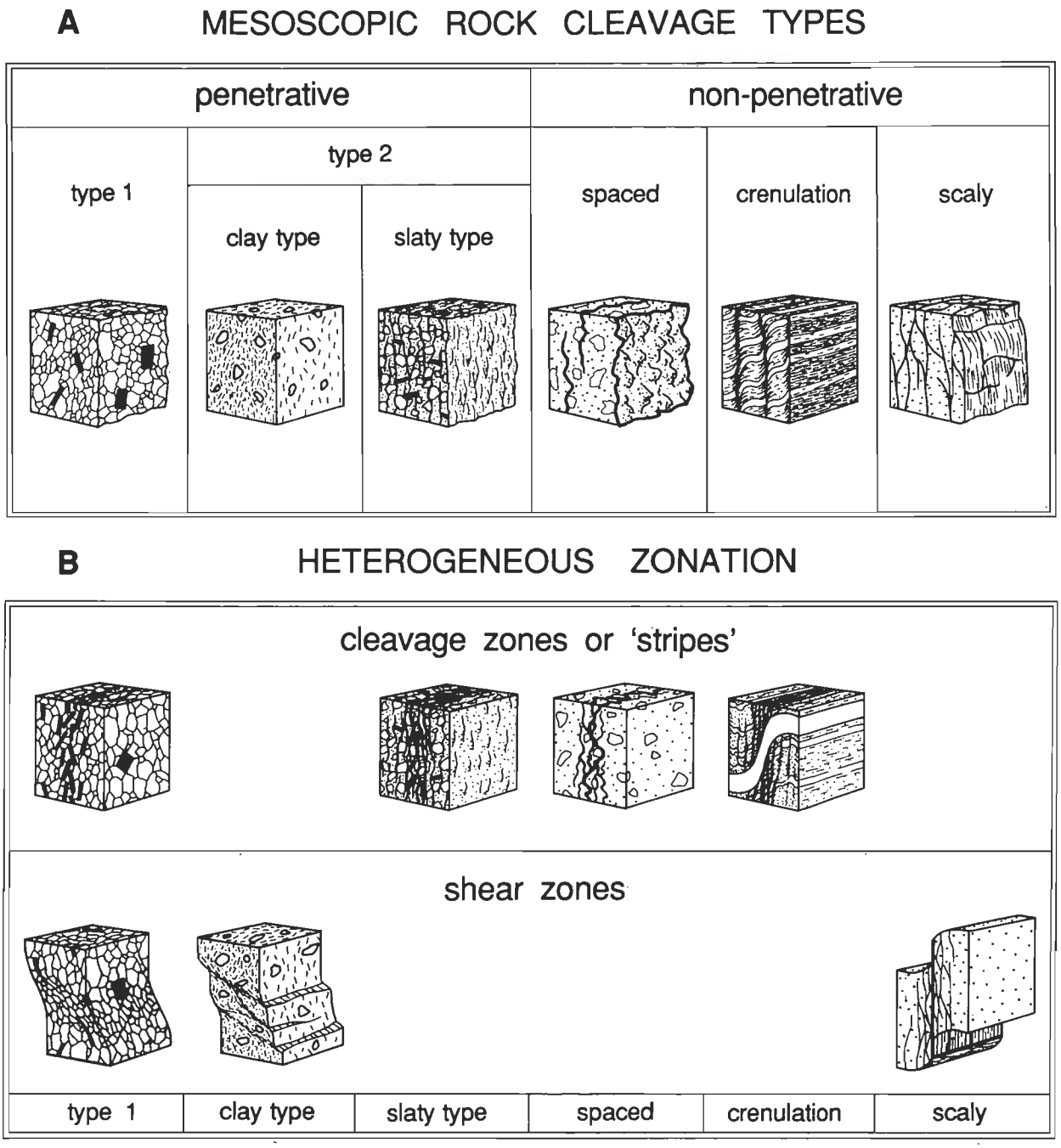

Figure 1. A—Schematic representation of *cleavage types* observable in the field. *Penetrative:* mineral alignment down to the dominant grain or clast size, comprising non-domainal fine-phyllosilicate poor (*type 1*) and domainal and non-domainal fine-phyllosilicate rich (*type 2*) types. *Non-Penetrative:* domainal mineral alignment spaced wider than the dominant grain or clast size, usually mesoscopic.

B—Schematic varieties of mesoscale zonation of the six cleavage types. *Cleavage zones:* Compositional differentiation into bands of greater and lesser concentration of cleavage domains and immobile minerals. *Shear zones:* Fabric intensification in bands of high shear strain without necessary compositional differentiation.

grade. Mineralogically differentiated domainal structure is typically present at the microscale (or, in rudaceous rocks, at the mesoscale).

"Slaty type" penetrative 2 cleavage domains may be heterogeneously developed at the mesoscale in usually gradational and cleavage-parallel zones of greater and lesser cleavage intensity (Fig. 1B). These are commonly marked by darker and lighter appearances, respectively, as a result of differences in mineral composition—differentiated "stripes" and mesoscopic "cleavage zones". In the more weakly developed stages, the enhanced cleavage may be restricted to isolated zones. Zonation may occur both in impure psammites or wackes (e.g. Gray 1978) and in pelites (e.g. the cleavage bundles of Southwick 1987). The dominant fabric orientation in the less-cleaved zones may be either disjunctive or conjunctive, as in microscale microlithons.

Two sub-types of "slaty type" penetrative 2 cleavage can be distinguished on the basis of clastic grain size (Dennis 1987b). The terms are derived from Powell (1979, p.34) and Dennis (1987b, p. 172) and are applied as field names to the major grain-size divisions of slaty type penetrative 2 fabrics in low and very low-grade metamorphic rocks (at higher grades of metamorphism, the fabric tends towards penetrative 1 type):

(i) *Smooth*—fissility has a smooth or smoothish feel. It occurs in rocks up to about coarse silt size and includes *slaty cleavage* and its incipient forms.

(ii) *Rough*—fissility has a rough feel, owing to wrapping of cleavage around coarse clastic grains. It occurs in coarser grained rocks with a predominance of sand sizes, including arenites and rudites with a notable phyllosilicate mineral fraction and wackes.

Types of non-penetrative cleavage

Non-penetrative cleavages are subdivided into three distinctive types (Fig. 1A):

(1) *spaced cleavage*—tectonic stylolites and more planar equivalents in initially isotropic to weakly anisotropic rocks (Davis 1984, p.407; Engelder & Marshak 1985);

(2) *crenulation cleavage*—fold-limb-related types in harmonically folded, initially strongly anisotropic, rocks (Rickard 1961; Cosgrove 1976; Gray 1977a); and

(3) *scaly cleavage*, otherwise known as "scaly foliation" and "scaly clay fabric" (Moore et al. 1986), "phacoidal cleavage" (e.g. Bosworth 1984), "microscopic shear bands" (Chester & Logan 1987), and "hydroplastic microfaults" (Guiraud & Séguret 1987), comprising a mineralogically poorly differentiated to undifferentiated, slickensided, phenomenon in a group on its own (this paper).

(1) *Spaced cleavage.* Differentiated cleavage domains, and portions of uncleaved rock with many clasts or grains which we call "lithons", can be distinguished in hand-specimen (Engelder & Marshak 1985, p.327). Cleavage is generally restricted to relatively narrow and distinct cleavage domains showing concentration of dark or phyllosilicate minerals; exposed cleavage surfaces generally show dark coatings with a sheen due to very strong platy mineral alignment. Domain spacing may range from about 1 mm to decimetres and may be regular (Fig. 1A) or clustered (Fig. 1B). The intervening rock is generally little changed. This type corresponds to mesoscopic "discrete" and "disjunctive" cleavage.

Spaced cleavage occurs mainly in rocks with a minor proportion of fine platy minerals and a major proportion of other fine mineral grains, such as carbonates, quartz, and feldspar. The morphology of the cleavage surfaces may range from subplanar through wavy to dentate or stylolitic forms. The surfaces are commonly axial planar (Alvaro & Capote 1973) and symmetrical with respect to extension veins and minor faults (Arthaud & Mattauer 1969), but may be striated due to oblique convergence (Ramsay & Huber 1987, pp.648–658).

(2) *Crenulation cleavage.* For crenulation cleavage, we use the morphological definition of Gray (1977a)—"zones of mineral differentiation coincident with the limbs of microfolds in crenulated rock fabrics"—which follows essentially the earlier definition of Rickard (1961, his section II, iii). Essential features are its strict dependence on "crenulations" or harmonic microfolds, its restriction to microfold limbs and its constitution as axial planar cleavage domains marked by a concentration of dark or platy minerals. Thus, it differs from, for example, stripy differentiated slaty cleavage in folded laminated mudrocks (Hills 1965, his fig. VIII–29; Cox et al. 1991 fig. 9a; Gray & Willman 1991 fig. 6c) in not existing in the related microfold hinges and always being coincident with fold limbs.

Although sometimes visible only under the microscope, the crenulations commonly range from "a fraction of an inch (~1 mm?) up to about 1 inch (25 mm) across" (Rickard 1961, p.325; see also Dennis' 1972 examples). Hence there is usually little difficulty in distinguishing them in the field.

Mesoscale concentration of cleavage domains, similar to that associated with slaty cleavage, is common in the vicinity of competency contrasts and larger mesoscopic folds (Fig. 1B).

(3) Scaly cleavage. Scaly cleavage is a distinctive structure with smooth and highly polished/slickensided discrete surfaces which intersect or merge with one another to yield lensoid flakes, scales or chips (Fig. 2b). The fresh rock is coherent, but breaks with extreme ease along the scaly cleavage surfaces. The cleavage occurs in rocks with a high proportion of weak or platy minerals, such as claystones, mudstones, marls, carbonaceous rocks, serpentinites and talcstones. An analogous structure called "web structure" (Cowan 1982; Witschard & Dolan 1990) has been found in sandstones and consists of polished, striated and discoloured intersecting seams of cataclasis. In highly argillaceous rocks, such as clay-rich fault gouges, a penetrative clay-mineral alignment is sometimes present in the domains between the surfaces of scaly cleavage (Rutter et al. 1986; Chester & Logan 1987). In marls, similar structures may be accompanied by a sigmoidally distorted, smooth to stylolitic, spaced cleavage (Casas & Sàbat 1987).

Scaly cleavage appears to result chiefly from slip along the surfaces; the surfaces are spaced, but usually lack obvious mineral differentiation or new mineral

concentration in hand specimen. Unlike other cleavages, it is essentially a shearing phenomenon rather than a flattening phenomenon or axial-planar cleavage. Its orientation relative to the axial planes of folds is variable, ranging from "subparallel" in some cases (Witschard & Dolan 1990, p.801) to grossly discordant in others (Fig. 2c). It typically forms a small angle with any other associated cleavage, often in obtuse angle sets displaying conjugate shear motion symmetrical with respect to the associated cleavage (Casas & Sàbat 1987). It is often associated with fault movement, particularly thrust faults, and may be concentrated within fault zones (Bosworth 1984; Behrmann et al. 1988; Maltman et al. 1993) or "scaly deformation bands" (Labaume et al. 1991) (Fig. 1B). A similar structure, marked by films of strong particle alignment, has been produced by engineering shear tests and surficial landslip movement in unlithified clays (Skempton 1964; Morgenstern & Tchalenko 1967a, b) and in laboratory analogue materials (Williams & Price 1990; Wilson & Will 1990), all in relation to known shear displacements. The fact that dilational features and cataclasis are often scarce or absent, whereas thin, gently curved films of highly oriented platy minerals with undoubted shear displacement are present, suggests that it is not, in the main, brittle in origin, but a true fabric rearrangement analogous to C-surfaces of ductile shear zones (Moore et al. 1986; Chester & Logan 1987 p.631; cf. p. 261).

As far as known, the occurrence of scaly cleavage in argillaceous rocks is restricted to "soft" (Guiraud & Séguret 1987) and "partially lithified" (Behrmann et al. 1988; Maltman et al. 1993) sediments, and to lithified mudstones and greywackes with low ('diagenetic') degrees of very low-grade metamorphism (cf. Kisch 1989, p.181). Because it does not appear to develop into a penetrative slaty cleavage, it cannot be considered an intermediate stage in the development of slaty cleavage, but represents a variety of non-penetrative cleavage in a class of its own.

Relationships to earlier cleavage classifications

Our penetrative and non-penetrative groups correspond directly to Dennis' (1972, 1987b) *usage,* in practice, of the terms "continuous" and "spaced". Dennis (1972 after Chidester 1962; Dennis 1967, p.19 and 22) *defined* these terms as applying to both mesoscale and microscale observations: "continuous"—"dimensional parallelism of all platy minerals present" (Dennis 1972, p.179;1987b, p.172); and "spaced"—"all types of cleavage which by visual or microscopic examination reveal discretely spaced surfaces of discontinuity, but do not affect intervening spaces" (Dennis 1972, p.180). However, the examples that he described (Dennis 1972, figs 9–1 to 9–5) seemed to be best distinguished on the basis of visual examination: "slaty" and "rough" "continuous" types (with domainal character at the microscale) and "crenulation" "spaced" types (with domain spacings of a few millimetres).

In terms of usage, Dennis' major divisions correspond to the older divisions of "flow" and "fracture" cleavage proposed by Leith (1905), which, though now rightly discredited, were at least eminently practical for application in the field. The attraction of Dennis' terms, however, is that they are purely descriptive.

A problem with Dennis' (1972) definition of "continuous" is that it stipulates a platy mineral alignment which is not always present, or not always present in the same direction as cleavage, in the microscopic domains between cleavage domains in slaty and rough cleavages. This point was recognised in the classification of Powell (1979), who suggested, in fact, that all slaty and rough cleavages show a discordant or "disjunctive" relationship between microlithon and cleavage domain platy mineral fabrics. Dennis (1987a, b) later revised the usage of his classification to reflect this to some degree, recognising cases of disjunctive relationship as "spaced". Both parallel and disjunctive types of platy mineral relationship are, however, known to exist in these cleavages: for example, microlithons with cleavage-parallel "mica beards" in some rough cleavages (Means 1975) and microlithons with clearly discordant mica fabric in some slates (Weber 1982). Consequently, neither of the two categories, "continuous" or "disjunctive", or for that matter "continuous" or "spaced", appears applicable by definition to all slaty and rough cleavages. If they were to be applied strictly, they would introduce a major division within this important and naturally associated group of fabrics (e.g. Dennis 1987b, p.172, with reference to slaty cleavage). It has also never been very clear exactly how one distinguishes between "continuous" and "spaced", in Dennis' definitions, in a rock with domainal cleavage and a parallel microlithon fabric. Chidester (1962, figs 8,9,10, p.21), in describing domainal slate fabrics of this kind from Vermont, stated that "the sericite flakes between surfaces of spaced schistosity have a continuous schistosity", clearly indicating that he intended these terms as descriptors of fabric attributes which could coexist within the one fabric. Therefore, it may be that "continuous" and "spaced" were never entirely appropriate as a basis for defining mutually exclusive cleavage types.

For these reasons, we suggest the simple term "penetrative" (as defined here) for the members of the slaty cleavage and rough cleavage group. Because "penetrative" is not defined in terms of absolute dimensions, this usage also avoids, on the whole, description conflicts which arise from the scale-dependence inherent in the Chidester–Dennis–Powell classifications, as in 'continuous' at the mesoscale, but 'disjunctive' at the microscale. Any need to convey grain-scale heterogeneity of the fabric should be covered adequately by the now common and self-explanatory term "domainal".

Powell (1979, p.29) applied the term "disjunctive" to what he called "spaced cleavages" which "lack sense of continuity or relationship between the pre-existing rock fabric and the new fabric in the cleavage domains". "Disjunctive" therefore describes a type of interdomainal relationship in a domainal fabric. Since our "penetrative type 2" and "non-penetrative" groups are domainal, we adopt and extend the use of the term "disjunctive" for these groups. For rocks showing largely parallel orientation of platy minerals in the microlithon domains, we use the term parallel or *conjunctive* (the opposite of "disjunctive"). "Conjunctive" is equivalent to a "continuous" (as defined by Dennis 1972, p.179; 1987b, p.172) domainal fabric. But we prefer not to use that term in view of the divergent use made of it by Powell (1979) and Borradaile et al. (1982: "continuous 1"), who used it as the opposite of "spaced", and by Borradaile et al. (1982: "continuous 2"), who modified Dennis' (1972, p.179) and Chidester's (1962) "continuous" by adding the stipulation that "cleavage domains do not exist in the sample" (p. 5, and p. 34ff).

The classification scheme suggested by Borradaile et al. (1982) follows, to some extent, the earlier scheme of Powell (1979). Unfortunately, this new scheme incorporates wholesale re-definitions of previously well-established terms ("continuous", "spaced", "rough", "zonal", "foliation", "schistosity") as well as some resurrected terms of genetic or very doubtful connotation ("cracks", "crack-like", "slices", "conjugate" and "differentiated"—as a 'variety' of "mineral concentration"), and has not been widely adopted in the literature. Nevertheless, our type 1 and type 2 penetrative cleavages correspond approximately with their "continuous 2" and "continuous 1"

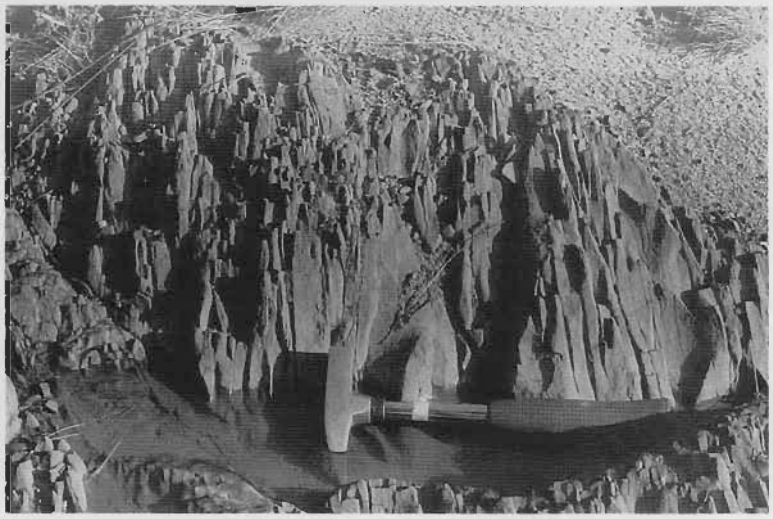

a. pencil structure

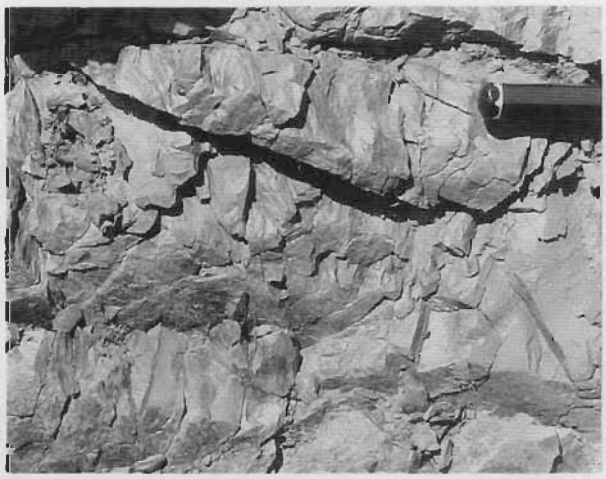

b. scaly cleavage

c.

d. weathering

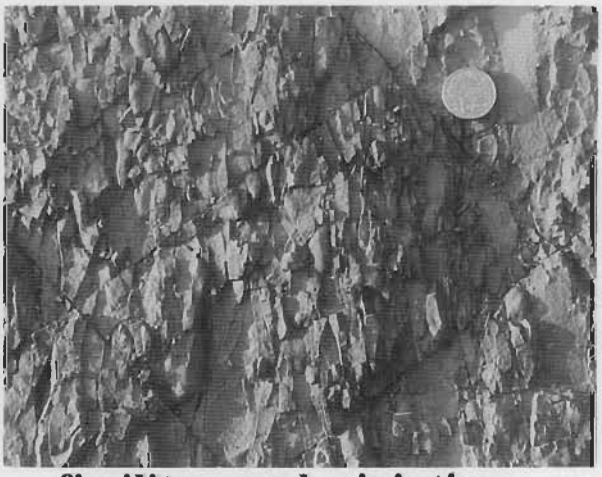

fissility and jointing e.

types, respectively.

The term "spaced" which was used by Dennis (1972) has found a place as an umbrella for 'non-continuous' (or non-penetrative) types in many idealised classification schemes, including Dennis' own scheme. But it is rarely used in such a broad sense in practice. For example, most writers refer to "crenulation cleavage" as just that and apparently do not find a need for the more formal 'crenulation spaced cleavage'. Also, many writers in recent times have referred to stylolites and more planar mesoscopic equivalents simply as "spaced cleavages" or alternatively as "disjunctive cleavage", rather than the more formal 'stepped (spaced) cleavage' and '(quasi-stylolitic?/mesoscopic?) disjunctive (spaced) cleavage'. Some writers have suggested "solution cleavage" or "pressure solution cleavage" for these (Alvarez et al. 1978; Cosgrove 1976; Geiser & Sansone 1981; Ramsay 1981). But this introduces the dimension of genesis into what should be an objective descriptor and suggests, perhaps not correctly, that microscopic domainal cleavages and non-domainal cleavages have a different origin. Groshong (1975b), Geiser & Sansone (1981) and Guzzetta (1984) have suggested including the more planar, unsutured varieties under the name "stylolite", but this is not consistent with the etymology and usually accepted meaning of "stylolite" as a "columnar" (Stockdale 1922) or at least "very uneven" (Park & Schot 1968, p.175) structure.

There is clearly a need to identify the natural fabric group of stylolites and more planar equivalents with a simple, non-genetic, term. Current usage of "spaced" (Alvarez et al. 1976; Durney 1984, p.A2; Engelder & Marshak 1985; Mitra & Yonkee 1985) seems to satisfy this requirement. The alternative term disjunctive" has been used in a wider sense to include slaty cleavages and, therefore, seems less distinctive. So we adopt the usage of "spaced" suggested for this group by Engelder & Marshak (1985).

Where we differ from the Engelder & Marshak (1985) scheme is in the primary division into penetrative and non-penetrative. We believe that a primary division based solely on spacing is arbitrary and unnatural, just as a division between joints and spaced cleavages on the basis of spacing is arbitrary and unnatural [cf. the "jointes stylolitiques" of Arthaud & Mattauer (1969) or "joints with stylolites" of Ramsay & Huber (1987) of the central European Jura Mountains, in which some stylolites are considered to have a joint-like character and vice versa]. Our primary division is based on the relation of cleavage to grain size, acknowledging that there will be some overlap in the domain spacing of the two main divisions.

We have also not adopted an intensity scale for cleavage based on domain spacing, though it may be a useful technique for spaced cleavages in certain types of limestones (Alvarez et al. 1978). Our reservations in this regard stem from the known grain-size dependence of domain spacing in penetrative type 2 cleavages (Gray 1978) and the influence of rock composition on the spacing of some spaced cleavages in carbonate rocks (Alvarez et al. 1978; Schweizer & Simpson 1986; Ferrill & Dunne 1989, p. 427). Considering the highly variable nature of spaced cleavages, intensity estimates for these structures may require measurements of relative thickness (Simon & Gray 1982) and continuity (length) of cleavage domains, as well as domain spacing, and should probably be considered unique for each lithology in which the spaced cleavage occurs. An alternative that might circumvent some of the problems associated with lithological variation would be to use a cleavage/bedding ratio-scale based on the relative spacing of bedding and cleavage clay seams. Later in this paper, this type of approach will be adopted in a different way, using cracks rather than domains, to establish an intensity-scale for penetrative cleavages.

Some authors have suggested that fabrics in many slates, particularly in the early stages of development, are in fact varieties of crenulation cleavage (Knipe & White 1977; White & Johnson 1981; Weber 1982). Whether or not the fabrics described are true "crenulations" in the sense of Rickard (1961) is perhaps a matter for debate. But the different naming of the fabric on microscopic grounds presents a nomenclatural problem that requires special attention, particularly where a potential for conflict of terms exists. The present scheme can include first-generation cleavages in strongly oriented primary fabrics under the "crenulation cleavage" grouping. But because of its field-based nature, the scheme only allows this as a mesoscopically recognisable form distinct from slaty cleavage (c.f. penetrative/non-penetrative division, p. 262). If a first-generation crenulation fabric occurs in a slate or an embryonic equivalent, it will be recognised only under the microscope and will not alter the primary naming of the rock as a "slate" nor of the cleavage as a "slaty cleavage". If required, we suggest that microstructural observations could be incorporated in the naming of the cleavage by means of qualifying adjectives to clarify cases of possible ambiguity, as in "crenulation pencil cleavage" (Ferrill 1989) and "domainal slaty cleavage".

Cleavage field intensity divisions based on fissility

Relationships of fissility to cleavage

Many writers have referred to the fact that tectonically deformed rocks, particularly low to very low-grade metamorphosed mudrocks, tend to occur in a naturally cracked or fractured state in outcrop, with cracks spaced a few centimetres or less and aligned parallel either to an obvious plane of cleavage or to directions which behave geometrically as though they were cleavages in relation to strain indicators and the axial planes of folds. The effect has been noted particularly in weakly deformed mudrocks: "pencil cleavage" or "pencil structure"

Figure 2. a—Pencil structure, view normal to bedding. Upper Silurian Booroo Ponds Gp, Bowning Creek, Bowning, New South Wales (NSW). b—Detail of fault-related scaly cleavage surfaces showing polish and striations. Lower Devonian Elmsdale Fm. mudstone, Black Range Rd, Yass, NSW. c—Scaly cleavage in steep limb of a kink fold, view parallel to cleavage and fold axis. The cleavage is mostly confined to, and subparallel to bedding in, the steep limb (right), and runs for a short distance discordantly over the hinge plane (dipping left). Upper Silurian Cowridge Siltstone mudstone, Boorowa Rd, Bowning, NSW. d—Disaggregation of a roadside block into pencils by modern weathering processes. Lower Devonian Kirawin Shale, Wee Jasper Rd, Wee Jasper, NSW. e—Fissility-cracks (close, discontinuous cracks running from 'top to bottom' of photo) contrasted with joints (widely spaced, planar, continuous factures in three oblique sets). View normal to bedding. Termination of fissility-cracks at joints shows that the cracks post-date regional stress relief and uplift associated with jointing. Upper Devonian Noumea Beds mudstone, Byrnes Gap Rd, Manilla, NSW.

(Engelder & Geiser 1979; Reks & Gray 1982; Wilson with Cosgrove 1982; Ramsay & Huber 1983, p.185–188; Nickelsen 1986), "reticulate cleavage" (Crook 1964; 1982), examples of "cleavage fracture" (Weiss 1972, plates 1 to 5), and so-called "fracture cleavage" in mudrocks (Price & Hancock 1972; Siddans 1977; Price & Cosgrove 1990). Also, the degree of alignment of the cracks is generally understood to increase towards the more deformed parts of fold belts, suggesting a probable correlation with either strain or strength of internal fabric. At outcrop scale, the relationship has been demonstrated qualitatively by Nickelsen (1986, figs. 10 & 11) and Price & Cosgrove (1990, p. 447–448) as a continuous change of the structure from bedding-parallel cracks to a cleavage-parallel platy structure in relation to expected strain gradients around concretions and folds.

As is evident from the names given to these structures, they have often been regarded as actual cleavages (especially "fracture cleavage"). However, none of them is, properly speaking, a cleavage in the sense of Dennis (see discussion p. 259), since the described feature is an incidental pattern of cracks and not the cleavage fabric itself. This is confirmed by recent microscopic observations showing that the structure is a form of natural open cracking which approximately follows the internal tectonic and bedding-parallel fabrics of the rock (Durney 1982; Reks & Gray 1982; Ferrill 1989). The cracks are actual separations, usually with no cementation, and there is no evidence of tangential movement on them. Thus, although they are directionally analogous to a cleavage, they are morphologically quite unlike any of the cleavage types reviewed earlier in this work. Accordingly, the crack patterns should be referred to as "structures", not "cleavages"—especially *pencil structure* (Reks & Gray 1982; Ramsay & Huber 1983) for elongate, subuniaxial, crack clusters and *reticulate structure* (renamed here after Crook 1964) for the more stubby, subuniaxial, crack clusters (see also pp. 281–282 for further discussion).

Crook (1964, p.527) noted that incipient forms of the structure in mudstone are "barely distinguishable from the irregular fracture that results from weathering". The irregular variety referred to by Crook is typical of undeformed mudstones and has been acknowledged to be a weathering product in engineering studies of weathering: viz. centimetrically spaced and randomly oriented "stress relief fissures" transverse to bedding, regarded as an indicator of the first stage of weathering in the mudstone-weathering-zone classification of Hawkins & Pinches (1992).

We suggest that all of these forms—random, incipient, and the more closely spaced planar cracks which follow an obvious slaty fabric—are products of weathering in the surface environment. Evidence for this is:

(a) the similarities in surface morphology (curviplanar), spacing, parent rock and mode of occurrence of all types, with complete gradations between them, suggesting a common origin, and differing only in degree of alignment of the cracks and strength of tectonic fabric;

(b) the general absence or very much greater rarity of the structure in fresh surface excavations, fresh drill-core specimens and underground exposures;

(c) greatest intensity of crack development at the weathered surface, decreasing rapidly with a depth of only a few centimetres below the surface (e.g. relatively uncracked bedding beneath a highly cracked veneer, Fig. 2e);

(d) instances where road development work or quarrying has mechanically dumped large blocks of mudrock, which are now pervaded by a delicate network of the structure and could not conceivably have been transported in that condition (Fig. 2d): in other words, development in a matter of years on exposure to the atmosphere; and

(e) a structural timing for the structures post-dating jointing (Fig. 2e).

A general name to describe this effect is *fissility* (Wilson with Cosgrove 1982 pp. 35, 37). "Fissility" is a word commonly used to describe bedding-parallel partings in mudrocks and has served as a field criterion for distinguishing shale ("fissile") from mudstone (considered as "massive") (Pettijohn 1975, p. 261). The effect of bedding anisotropy is physically similar to that of a tectonic fabric in mudrocks; the splitting is parallel to, and depends on the degree of alignment of, clay particles, organic matter and lamination (Ingram 1953; Curtis et al. 1980). Like the transverse cracks discussed in (c) above, bedding-parallel fissility is also restricted to surface environments (Lewan 1978, p. 748) and for this reason has been called a "weathering phenomenon" (Lundegard & Samuels 1980, p. 781).

Thus, the term "fissility" is applicable to both bedding and cleavage structures: *bedding-fissility* for partings guided by bedding fabric, and *cleavage-fissility* for partings guided by tectonic fabric. This meaning is consistent with a literal interpretation of Van Hise's (1896, p. 450) definition for fissility as "a structure in some rocks by virtue of which they are already separated in parallel laminae in a state of nature", as distinct from "cleavage proper" which he regarded as a "capacity to part" rather than an actual parting. A similar definition was given in a related paper by Hoskins (1896, p. 872): "actual separation of the rock along certain planes".

The definition of "fissility" given by Van Hise (1896) was subsequently confused by many writers, including Van Hise himself (1896), Leith (1905), Knopf & Ingerson (1938), and Shaw (1957), who included under this term cleavages that were believed to form by fracturing ("fracture cleavage") or even a "capacity to part". However, there is a practical need to distinguish the two things. With the decline in use of the term "fracture cleavage" in modern writings, there is no longer a reason to confuse "fissility" or "actual separation ..." with "cleavage" as a fabric element having "a potential to part" (Dennis 1972) and Van Hise's "cleavage proper". So, we suggest using the term "fissility" in this sense as an incidental parting that follows a pre-existing tectonic fabric. This conforms with the way that the term is currently applied to undeformed mudrocks by sedimentary petrologists: partings that follow a bedding fabric or lamination (e.g. Pettijohn 1975).

Because it is the same phenomenon in slates as in shales, we propose an expanded role for the term fissility as a *fabric-dependent parting* that predominantly follows a tectonic fabric, or a bedding fabric, or both. Fissility, then, is a form of present-day open-crack structure that

is guided by internal anisotropy and occurs naturally in surface outcrops as a result of, or through enhancement by, weathering. Cleavage, on the other hand, represents a potential for the rock to part on certain planes, as manifest, for example, when the rock is struck by a hammer.

Distinction between fissility and jointing

Joints may display a surface texture similar to fissility-cracks and, like them, some joints may be closely spaced (Priest & Hudson 1976), i.e. "extremely close" or < 2 cm in engineering parlance (Brown 1981, p. 18). Fissility-cracks nevertheless appear to originate in quite a different way and are distinct from joints in several respects.

(a) Fissility-cracks are less regular than joints, being characterised by curviplanar surfaces and seemingly unsystematic T-intersections in a 3D-network, producing a generally flat or elongate pattern of interlocking, irregular polygonoids. In contrast, joints in all rock types, including mudrocks, are usually very planar and parallel. (See Hancock 1982 for an analogous distinction between jointing and cracked spaced cleavage; also Siddans 1977; Price & Cosgrove 1990, fig. 9.31, and Figs. 2E and 14B here, for illustrations of joints in mudrocks.) Joints therefore appear in distinct orientational sets and tend to produce flat-sided angular blocks, often parallelepipeds and prisms.

Crack irregularity and crack length (discussed in the next point) are probably the most useful criteria for distinguishing the two types of fracture when the fragments are similar in size and shape. For example, the small parallelepipeds in Foster & Hudleston (1986, fig ??) are clearly joint-controlled, whereas the irregular chips and discontinuous cracks in our Figure 10 are fissility structures.

(b) Joints are much more continuous ("persistent"—Brown 1981, p. 19) in length, being commonly decimetric (Engelder 1987, fig. 2.15) to kilometric (Zhao & Johnson 1992, fig. 2), as opposed to the centimetric lengths that are typical of fissility-cracks. Thus, joints tend to traverse minor lithological junctions without interruption or deflection (Fig. 14b) and commonly produce boulder-size blocks, long slivers (e.g. Ramsay & Huber 1987, fig. 27.3) or long chains of blocks (e.g. Rawnsley et al. 1992). These properties presumably reflect relatively regular stress fields during the formation of many joints, particularly systematic joints, as would occur when a pre-existing regional tectonic stress is modified by removal of overburden pressure (Price & Cosgrove 1990), though local perturbations may occur (Rawnsley et al. 1992). In contrast, the stresses responsible for fissility-cracks are evidently more disordered, considering their small-scale variability. (It is possible that they are of internal origin associated with heterogeneous hydration and oxidation reactions during weathering.)

(c) Statistically, fissility-cracks develop parallel to tectonic and sedimentary fabric anisotropy planes, as observed microscopically (Durney 1982; Hancock 1982), mesoscopically, or by directions of preferred splitting on impact of a hammer. Joints, on the other hand, enjoy no such exclusive relationship, except that they may preferentially develop orthogonal to bedding (Hancock 1985) or cleavage (Siddans 1977, fig. 4).

(d) The frequency of fissility-cracks decreases very rapidly with depth below the earth"s surface, whereas joints, except for exfoliation structure and sheeting joints (Suppe 1985), persist well into the subsurface.

Fissility as a field basis for interpretation of cleavage intensity

Since fissility is the prominent attribute of cleavage on a mesoscopic scale, the scale of cleavage-intensity proposed here, at least as applied to penetrative-cleavage types, is based on fissility.

Fissility is a property which lends itself to quantitative description, because the degree of fissility in any one plane can be gauged from the spacing of the cracks. However, earlier attempts to define fissility scales on the basis of 1-dimensional spacing of bedding-plane partings (Lewan 1978, table 3; Potter et al. 1980, table 1.3; and, in part, Ingram 1953, p. 871) are limited by the fact that absolute spacing of the cracks depends on degree of weathering (see Lewan, 1978, for bedding-fissility, and p. 268 here, for tectonic fissility) and on rock and clay-mineral composition (Pettijohn 1975, p. 263–264; Blatt et al. 1980, p. 398) as well as on internal fabric and lamination.

The fundamental property that we seek a relationship to is the anisotropy of the parent-rock fabric. So it is more meaningful for this purpose to consider the anisotropy of fissility. The 3-dimensionally connected nature of fissility-cracks means that connecting cracks exist across the dominant fabric-plane as well as cracks along this plane. Hence the total network of cracks defines a statistical orientation-density tensor capable of possessing anisotropy: i.e. form, symmetry and orientation. It is easy to estimate all three attributes of the fissility-tensor in the field from the shapes and orientation of the split pieces of rock. Thus, different degrees of one fissility (say, a bedding fissility) in different directions can be judged from the width-to-thickness ratio of the platy fragments. Or two different fissilities in the same specimen can be compared from the cross-sectional shapes of the fragments.

Here, we use the latter property to define a relative-intensity scale for slaty cleavage and related structures compared with bedding. The assumption is that the shapes of the fragments reflect the relative strengths of the two fabrics. Hence, in any one rock type with a uniform initial bedding fabric, the shapes should represent an absolute strength of the cleavage fabric.

An advantage of this method is that it can be applied almost instantly in the field and does not require sophisticated microscopic or analytical procedures. It is furthermore unique in being a clearly observable and estimable index of fabric development over the entire range of fabric intensities and grain scales, and it is especially sensitive in precisely those areas where direct observation of fabric so often fails: in mudrocks and in the low-intensity fabric ranges.

Cleavage/bedding fissility ratio or relative cleavage-fissility scale

The intensity scale that we propose for cleavage-fissility is the relative intensity of tectonic-fissility compared with bedding-fissility in the same sample. We call this the *cleavage/bedding fissility ratio* or *relative cleavage-fissility*.

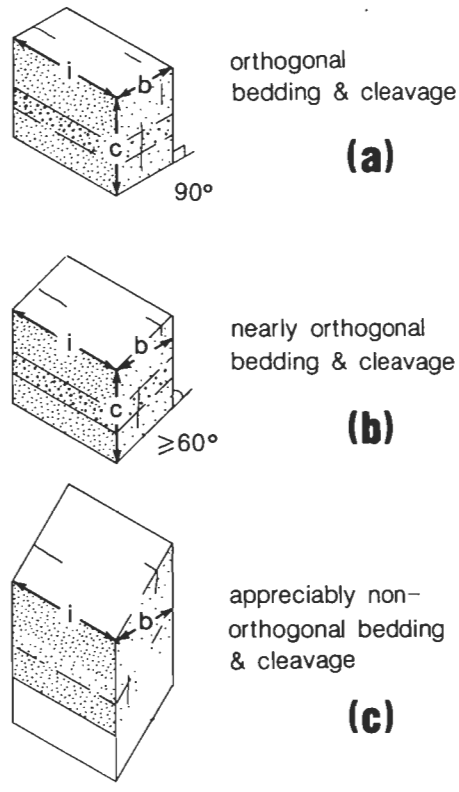

Figure 3. Fissility-fragment dimension measurements. Cleavage is vertical and trends '10 o'clock'; bedding is horizontal and shown by top surface and stippled band.
(a) & (b)—*orthogonal and nearly orthogonal cracks: c, b* and *i* may be measured as fragment lengths and widths parallel to 'cleavage', 'bedding' and 'intersection' directions, respectively.
(c)—*appreciably non-orthogonal cracks: c, b* and *i* are normal spacings of bedding, cleavage and transverse cracks, respectively.

To be recognisable as such, the fracture that we call "cleavage-fissility" should display a detectable, though not always strong, preferred direction transverse to bedding. It follows that cleavage-fissility cannot be directly distinguished when cleavage coincides with bedding; for purposes of measuring cleavage/bedding fissility ratios, the cleavage should be at a moderate to high angle to bedding (for example, near the hinges of folds).

A suitable index for this scale is the relative spatial frequency of cleavage-fissility cracks and bedding-fissility cracks, c/b, in the plane normal to the bedding/cleavage intersection. c/b may be measured simply as the aspect ratio of the fissility-fragments in the cleavage direction relative to the bedding direction in this plane (see Fig. 3 and further explanation in Appendix A). The order of the ratio (i.e. c/b rather than b/c) is significant; therefore it is necessary to know the directions of cleavage and bedding in the samples, preferably from observations of in-situ material. Where only a bedding-fissility exists, an analogous parameter to c/b is the thickness-to-width ratio of the fragments (c_0/b_0 or $b\perp/b$). This represents the inverse of bedding-fissility anisotropy (see eqn. 2, p. 275, and **Lithology effects— shaliness**, p. 280 for further discussion).

Being dimensionless, the quantity c/b may be applied to rocks with different absolute crack spacings and different weathering histories. In practice, we have found it to be consistent among fragments of different size; that is, smaller fragments preserve similar c/b ratios to larger ones, and larger fragments break up into smaller fragments of approximately similar shape.

In any one statistically homogeneous outcrop, the shape ratios of individual fragments nevertheless vary within a certain range. For measurements reported below, we estimated mean fissility-ratios by visual selection of mean-shape and extreme-shape fragments from representative samples comprising many fragments. Where greater precision is required, the mean of several such estimates has been taken. In all cases, we assume logarithmic mean values for "fissility-ratios" discussed here.

Cleavage/bedding fissility ratio or relative slaty-cleavage fissility categories

Fissility-fragments with predominant bedding-fissility and subordinate cleavage-fissility ($c/b < 1$) and those with intersection pencil structure (c/b 1), represent incipient forms of cleavage development. Fragments with predominant cleavage-fissility ($c/b > 1$) are manifestations of true cleavage in the sense that they reflect a planar tectonic direction of potential rupture of the rock (Dennis 1972).

These broad divisions may be further subdivided into a series of quantitative categories based on approximately binary logarithmic divisions of the c/b ratio (Fig. 4), thereby permitting greater descriptive precision than was possible previously when formal divisions did not exist. In earlier writings, it was common to call all obvious incipient forms of slaty cleavage, and some barely developed true slaty cleavages, "pencil cleavage" or "pencil structure". The categories presented below allow this broad field to be separated into more truly equidimensional cross-section "pencils" (0.7 to 1.4 aspect ratio), and structures having varying degrees of relative cleavage-fissility both stronger and weaker than this. In this way, the scheme extends and refines earlier ideas that originated from the study of pencil structure (esp. Ramsay 1982 or Ramsay & Huber 1983, p. 185–188; Reks & Gray 1982).

(a) *Cleavage-fissility absent* (c/b generally small)—rock does not split in any preferred direction transverse to

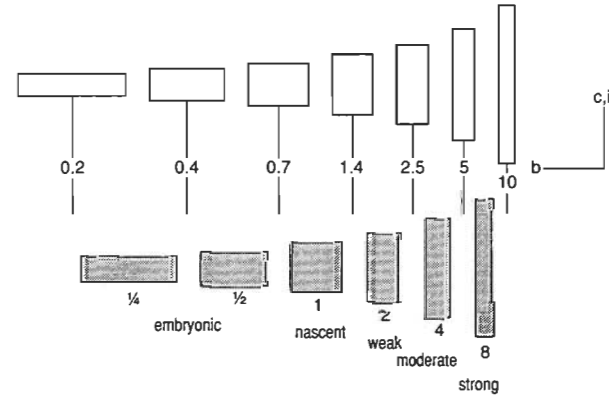

Figure 4. Fissility-crack ratio categories. *Open rectangles:* decimal divisions corresponding to a nearly binary progression. *Shaded rectangles:* approximate median values of categories. Ranges are: $0 < c/b < \infty$ and $0.7 < i/b < \infty$.

bedding. Bedding-fissility, ordered sets of subplanar joints, and (in mudrocks) irregular polygonal transverse cracks are the only fractures present. In some cases, the rock is known to be tectonically deformed from field relations or deformation of primary structures, but no preferred fissility can be found. This case is mainly of interest for penetrative 1 "grain" cleavage types.

(b) *Embryonic cleavage-fissility* ($c/b < 0.7$)—rock splits with comparative difficulty in the tectonic direction: bedding-plane fissility is dominant, though may be widely spaced in arenites. Mudrocks yield a bedding-parallel 'platy', 'blade' or 'matchbox' structure, though with a recognisable elongation in the tectonic direction; the fracture is often curviplanar, subconchoidal or ragged; oval corestone or spheroidal weathering may occur in mudrocks in weathered environments: *pre-pencil structure* (especially when markedly elongate in the intersection direction) and *pre-reticulate structure* (weakly to moderately elongate).

(c) *Nascent cleavage-fissility* (c/b 0.7–1.4)—rock splits roughly equally in bedding and tectonic directions. Mudroks yield irregular polygonal to rhomboidal cross-section, curviplanar, prismatic fragments elongate in the intersection direction: bedding-parallel *pencil structure* (when strongly to very strongly elongate) and *reticulate structure* (when weakly to moderately elongate).

Well-sorted arenites show a distinct though weak grain flattening.

(d) *Weak cleavage-fissility* (c/b 1.4–2.5)—the first appearance of true cleavage structure: the rock splits more readily, though weakly, in the tectonic direction; matchbox-like and slightly flattened prisms elongate in the intersection direction are typical ("intersection pencil structure" of Ramsay & Huber 1983, p. 186).

(e) *Moderate cleavage-fissility* (c/b 2.5–5)—rock splits readily and preferentially in the tectonic direction; bedding-fissility is subordinate, but usually distinct. The tectonic fissility tends to be somewhat curviplanar and disconnected. Mudrocks normally yield truncated lensoid fragments.

Poorly sorted arenites mainly show weak grain flattening and grain impingement; well-sorted arenites show clear grain flattening.

(f) *Strong cleavage-fissility* (c/b 5–10)—rock splits almost invariably in the tectonic direction; bedding fracture is uncommon except at lithological junctions. Cleavage fracture tends to be planar and closely spaced. Yields sharply ended flakes and sheets; an intersection lineation may be observed on the cleavage surface, but general alignment of the minerals on this surface is not obvious, except possibly in arenites.

Poorly sorted arenites display distinct grain flattening, while well-sorted arenites show strong flattening and elongation.

(g) *Very strong cleavage-fissility* (c/b 10–20)—rock splits in a manner similar to strong fissility, but cleavage flakes are more highly planar, and all lithologies may display a distinct elongation of constituent minerals or of cleavage flakes on the cleavage surface: a mineral lineation. This lineation may be expressed as an elongation of coarser grains, of augen or beard structures around coarser grains, of corrugations or of cleavage flakes; to be clearly recognisable as a mineral lineation it should usually be observed at an angle to the intersection lineation or to the known direction of the bedding/cleavage intersection lineation.

Poorly sorted arenites display strong flattening of grains parallel to cleavage.

(h) *Extremely strong cleavage-fissility* ($c/b > 20$)—a further development beyond category (g), $c/b = 40$ being a probable practical upper limit for cleavage/bedding fissility measurements because of a tendency for interference from later structures in highly deformed material.

Effect of lithology

For comparable results, cleavage/bedding fissility observations should be restricted to a particular lithology, since lithology will affect the strength of the initial bedding fabric (Spears 1980) and hence the stage of deformation at which a planar cleavage fabric first begins to appear. For example, a shale with "nascent relative cleavage-fissility" (pencil structure) is likely to possess a stronger tectonic fabric than a mudstone with "nascent relative cleavage-fissility" (reticulate structure), since it balances a stronger bedding fabric. Similarly, in mudstones with only weakly developed bedding-fissility, 'absolute' cleavage-fissilities similar to those formed in associated shales (with a strong bedding-fissility) should result in much higher c/b ratios.

The cleavage/bedding fissility scale is intended primarily for rocks with poor initial bedding anisotropy, such as mudstones, marls and wackes. It may also be applied to shales and other rocks with strong initial bedding fabric, such as finely laminated shale–siltstone composites and sandstones with closely spaced carbonaceous partings. But, in this case, no direct equivalence with mudrock fissility can be assumed. Therefore, it is advisable to supplement the observations with measurements of fissility-fragment aspect ratio in the bedding plane to define more fully the respective influence of bedding and cleavage fabrics.

Relative intersection fissility scale

In order to incorporate the effect of lithology in the relative slaty-cleavage-fissility scale, and to indicate the extent of tectonic fabric development in rocks of different initial bedding anisotropy, the relative length of the fissility-fragments measured in the direction of the cleavage/bedding intersection lineation (i) has to be considered.

This can be done using the i/b ratio of fissility-fragments in the bedding plane: the length (i) of fissility of fragments in the cleavage/bedding intersection direction over their width (b) normal to i in the bedding. This ratio, which we call the *intersection fissility-ratio*, is similar to the l/w shape factor used by Reks & Gray (1982, p. 163) to describe pencil shapes, except that i is taken as the actual length of the fragments, whereas l is the projected taper length. An alternative procedure, which is convenient for rocks with a strong cleavage, is to measure the ratio of the length of cleavage fractures in the intersection direction over their height, i/c (Fig. 3), and to compute i/b from this and from c/b .

As noted for the "cleavage-fissility absent" category in

the relative slaty-cleavage-fissility scale, cases where a tectonic fabric appears to be absent are represented by equidimensional polygonal fragment shapes in the bedding plane, or $i/b = 1$. Increasing unidirectional or planar tectonic fabric development should therefore produce fissility-fragments of increasing slenderness in the intersection direction, or $i/b > 1$. This should occur in both shales and massive lithologies. Thus, whereas c/b measures degree of cleavage development, i/b represents an index for degree of directional tectonic fabric development which begins at the most incipient stages. For this reason, it should be closely related to the degree of tectonic deformation and is necessary for interpreting deformation as against just cleavage development.

However, because fissility-ratios are only secondarily related to fabric and strain, they may be (and are) both numerically different from tectonic stretch-ratios and capable of bearing different relationships to stretch-ratio in different rock types. Also, the proviso of a unidirectional (or plane) tectonic fabric modification is necessary for tectonic intensity interpretations of i/b, because two or more weak tectonic fabrics transverse to bedding may combine to produce what we call "transverse pencil structure" and "transverse reticulate structure" with i/b 1, but $c/b > 1$. This case may show little or even no anisotropy in the bedding plane, but may nevertheless have a distinct linear fabric at an angle to bedding, signifying a significant deformation. A similar effect could be produced by a single, well-developed "stretching" deformation (Cloos 1946, p. 18) or "grain" (Wilson with Cosgrove 1982, p. 63–64) oblique to bedding. The simple interpretation of i/b as a tectonic index thus requires observations to be restricted to regions with single- (first-) generation structures with a single axis of tectonic shortening—for example, a system of straight horizontal folds—as well as to a single rock type and deformational regime.

Three-dimensional fissility-fragment shape

Combined measurements of i/b and c/b define a 3-dimensional (3D) fissility-fragment shape, which can be shown on a 3-axis diagram similar to that adopted for 3D natural strains by Owens (1974) after Hsu (1966). This diagram shows deviation in shape of an object, say a rectangular parallelepiped, from an equant body of the same volume (a cube), along three fixed principal axes. The axes have a logarithmic scale with zero at their common origin. Each shape plots as a single point on this diagram, with cubes at the origin and increasingly slender shapes farther out. Points on the diagram can be visualised physically as approximately the offset positions of the upper front corner of rectangular objects relative to the lower rear corner, when viewed in isometric projection (compare dot positions on objects and plot in Fig. 5). In addition to representing invariant shape, the diagram also shows which of the three reference axes the object"s longest and shortest axes are aligned with.

Special features of the fissility-ratio system and the way it represents shapes are described here. As reference axes, we choose directions C, B and I of the cleavage, bedding and intersection fissility dimensions c, b and i (Fig. 3), respectively. The C-axis is drawn in a 'vertical' position to represent the reference bedding orientation as a 'horizontal' plane (tilted slightly towards the observer). Axes C and I contain the plane of dominant cleavage, which has a 'vertical' reference orientation striking '10 o'clock'

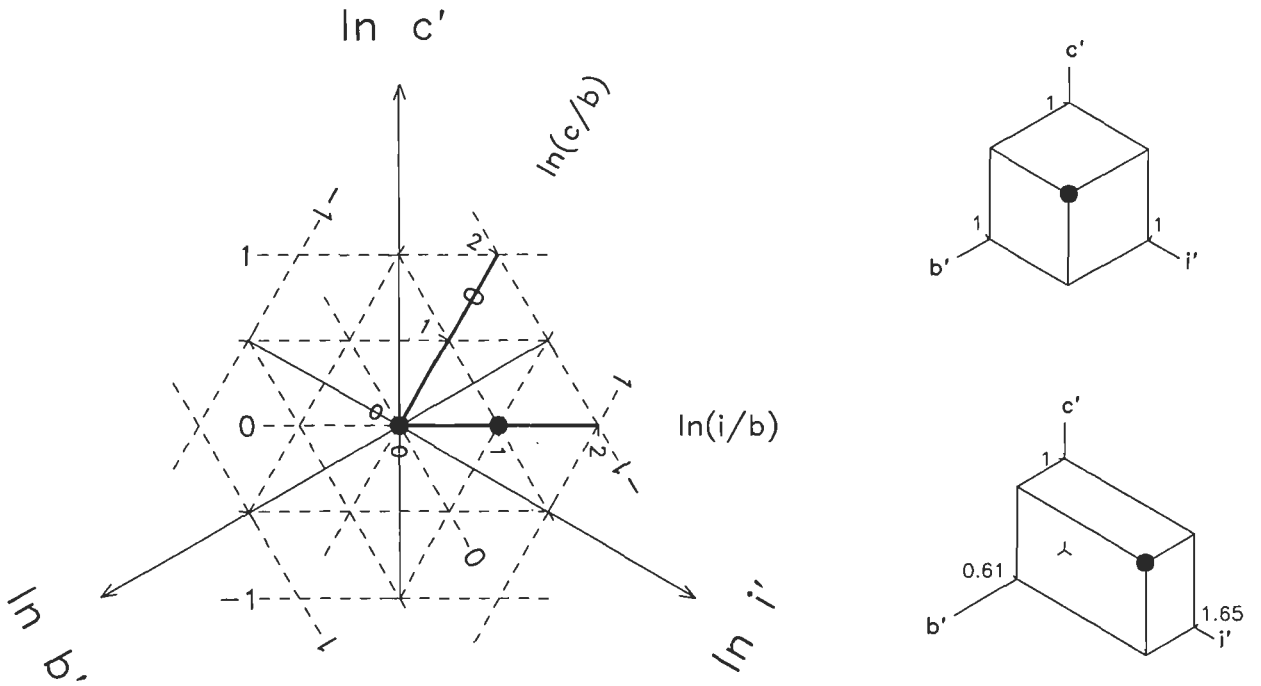

Figure 5. Relationship of axes on a logarithmic 3-axis shape/orientation diagram. Principal axes (ln c', ln b' and ln i') define prolateness of axisymmetric shapes in fixed directions C, B and I respectively. Axial ratio axes (ln(c/b) and ln(i/b)) define 2D shapes seen on specific principal planes. Slenderness of shapes increases outwards from the centre of the plot while shape type and orientation varies with polar direction. At each point, ln c' + ln b' + ln i' = 0, ln(c/b) = ln c' − ln b' and ln(i/b) = ln i' − ln b'. The example cube (upper right) plots at the centre of the diagram. The example blade (lower right) plots at the point ln c' = 0, ln i' =½, ln b' =−½, and hence at ln(i/b) = 1. (See text for further explanation.)

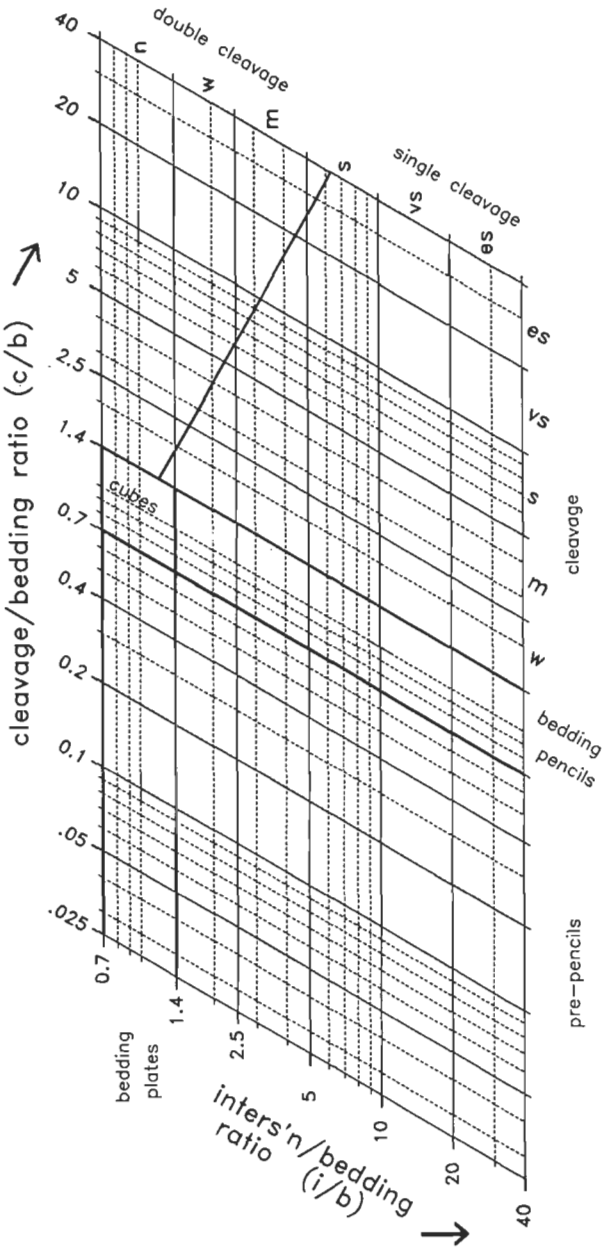

Figure 6. Logarithmic 3-axis grid for plotting *c/b* and *i/b* fissility-ratios or categories. Category divisions are shown by solid lines. The suggested relative strength categories are: *n* ('absent'), *w* ('weak'), *m* ('moderate'), *s* ('strong'), *vs* ('very strong') and *es* ('extremely strong'). Only the right hand field is shown, corresponding to one dominant cleavage and increasing *i/b* values.

to '4 o'clock'. Principal axis dimensions are ln *c'*, ln b' and ln i', respectively, where c', b' and i' are the measured fissility dimensions normalised against the cube root of their product ($c' \equiv c/(cbi)^{1/3}$, etc.).

The fissility-ratios *c/b* and *i/b* are shown as natural logarithms, $\ln c/b = \ln c' - \ln b'$ and $\ln i/b = \ln i' - \ln b'$, along a pair of subsidiary axes 30° from the C (ln *c'*) and I (ln *i'*) axes, respectively. Contour lines drawn normal to any principal axis or subsidiary axis show the value of the logarithmic quantity along that axis. However, the subsidiary axes, derived vectorially from the principal axes by the above equations, have a different scale, as shown in Figure 5. Contours and descriptive categories for direct plotting of c/*b* and *i/b* ratios in logarithmic 3-axis format are shown in Figure 6. If normalised principal values are required, they can be obtained from ratios most conveniently by expressions of the type: $i' \equiv i/(cbi)^{1/3} = [(i/b)^2/(c/b)]^{1/3}$.

Assuming there is only one dominant cleavage direction, all shapes can be represented in one half of the 3-axis diagram, as shown in Figure 7. Distance from the centre represents degree of slenderness, while angular position around the centre shows the type of shape and its orientation in the *C*, *B* and *I* coordinate directions. Thus, *bedding plates* and *cleavage plates* lie in the *–C* and *–B* directions, respectively, whereas *pencil structures* may be elongate either in the *+I* (*bedding*) or in the *+C* (*transverse*) direction. Intermediate polyaxial shapes are called *laths* or *blades*, with a distinction between *broad* and *narrow* forms according to whether they lie closer in shape to plates or pencils, respectively. Blades that are halfway between plates and pencils (with intermediate normalised dimension equal to 1) are called *biaxial*. The three possible orientations of blades are distinguished according to the dominant plane (*bedding* or *cleavage*) and, in the case of cleavage blades, the long-axis direction (*bedding-elongate* or *transversely elongate*): for example, "biaxial bedding-elongate cleavage blades" along the *I–B* (ln *i/b*) axis.

From a structural point of view, the most meaningful divisions are between:

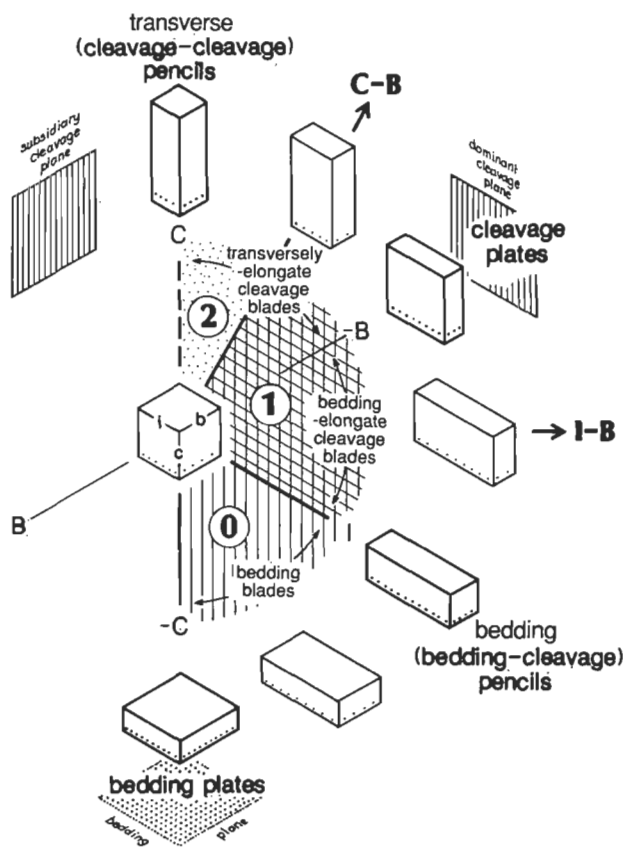

Figure 7. 3D fissility-fragment *shape fields* on a 3-axis diagram. Dimensions and orientations are shown relative to fixed fabric principal directions: *C*, *B* and *I*, as shown in Fig. 3. *Field 0:* bedding-dominant. *Field 1:* single-cleavage dominant. *Field 2:* multiple- or linear-cleavage dominant.

- bedding-dominant structures—*Field 0*: $c/b < 1$;
- single-cleavage dominant structures—*Field 1*: $c/b > 1$ and $i > \sqrt{(c'b')}$; and
- multiple transverse cleavage structures—Field 2: $i' < \sqrt{(c'b')}$ (see Fig. 7).

For practical purposes, we recognise bedding plates, bedding pencils and cubes as distinct groups of structures with finite c/b and i/b ranges (see Fig. 6). Therefore, these groups, in effect, represent transitions between Field 0 and adjoining fields. The basis for the Field 1 to 2 division is discussed further in connection with multiple deformation at the end of the paper.

The 3-axis fissility diagram shows most directly the shapes of orthorhombic fragments. Moderately monoclinic and triclinic shapes can be plotted and classified in the same way, insofar as c, b and i are independent quantities (Appendix A) and thus algebraically orthogonal. However, the axes on the plot do not then correspond physically to axes of oblique-fissility samples, and predictions based on orthogonally superposed fabrics (outlined in the next section) probably will not apply in precisely the same way.

Models of fissility intensity and style on a 3-axis diagram

It is useful to consider ways in which a tectonic fabric might be superimposed on an initial bedding fabric and how this would be expressed in the resulting fissility-fragment shapes.

In the absence of a suitable theory for oblique-coaxial superposition of fabrics, we consider combinations of orthogonal-coaxial superposition. In particular, we explore the consequences of assuming that:

(1) fissility-fragment shape is directly related to total fabric;
(2) the total fabric comprises an initial bedding-parallel oblate part and an orthogonal coaxially superposed tectonic part;
(3) the tectonic part of the total fabric is directly related to tectonic deformation; and
(4) relations between the sets of principal ratios for fissility, fabric and deformation are of a power-law type and are unique for each rock type and each pair of ratio sets; e.g.

$$c/b = p\ (s_c/s_b)^n; \quad (1a)$$

$$i/b = q\ (s_i/s_b)^n; \quad (1b)$$

for relations between fissility and deformation, where the s parameters are stretches parallel to fissility axes and p, q and n are constants).

It can be shown that fissility-fragment shapes that vary in a regular way in one rock type would then fall on a locus in the same relative positions and with the same gradient on a logarithmic plot as the relative positions and loci of fabric variation and deformation variation in that rock, though all three loci would generally be different in length and different from loci in other rocks. (The *loci*, or *fields* if they occupy areas on a logarithmic plot, refer here to variations of final states through space.) These correspondences would therefore allow deductions to be drawn about the *relative intensities* (relative plot positions) and *style* (plot gradient) of fabric and total deformation variations in a region from the relative intensities and style of the fissility variations.

An important property of the logarithmic 3-axis diagram is that multiples of the same shape transformation, applied coaxially in the same way to any initial shape, plot as equally spaced points on a *straight line* locus. This results from the logarithmic conversion of shape multiples to simple vector sums. The direction of the line indicates the type of shape change, while the starting point represents the initial shape. On a natural strain plot (Hsu 1966), such lines would correspond to loci of increasing distortional strain of a particular 3D type superimposed on some initial object shape. On a fissility-fragment shape plot, the lines represent increasing degrees of tectonic fissility intensity of a particular type superimposed in a particular way on a notional initial bedding-fissility anisotropy. Quantitatively, this is expressed by a relation between fissility ratios:

$$\ln c/b = \ln A + B \ln i/b, \text{ or} \quad (2a)$$

$$c/b = A\ (i/b)^B, \quad (2b)$$

where A is the intercept of c/b for the undeformed state ($i/b = 1$), equal to the inverse of bedding-fissility anisotropy ratio, and B is the gradient:

$$\Delta \ln (c/b) \ / \ \Delta \ln (i/b)$$

of the line on a $\ln c/b$ versus $\ln i/b$ plot, representing the local deformational style (tectonic axial ratio type

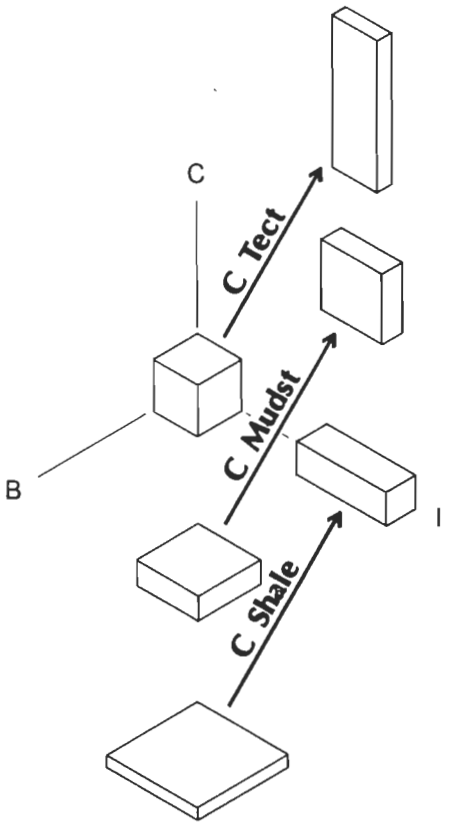

Figure 8A. Effect of *bedding-fissility strength* on fissility-fragment shape locus in a single tectonic regime. Cleavage-fissility in this example is assumed to be directly related to a biaxial, layer-parallel shortening and layer-normal extension (a contraction locus). *C Tect:* no bedding-fissility. *C Mudst:* notionally 'moderate' bedding-fissility, as in a mudstone. *C Shale:* notionally 'strong' bedding bedding-fissility, as in a shale.

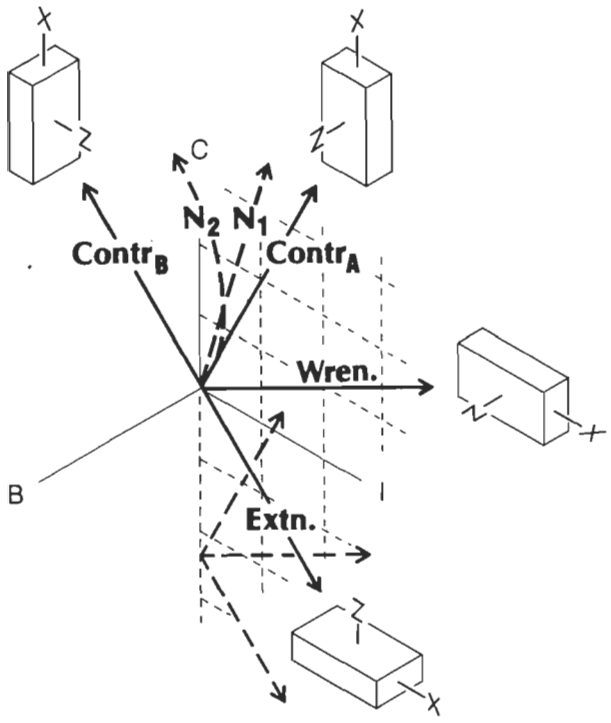

Figure 8B. Effect of *tectonic deformation style* on fissility-fragment shape locus, beginning with an isotropic (unbedded) material. *Contr, Wren* and *Extn* are biaxial fissility-fragment shape loci assumed to correspond to biaxial, bedding-parallel, 'contraction-', 'wrench-' and 'extension-' tectonic deformations, respectively. Principal directions of tectonic elongation (X) and shortening (Z) with respect to bedding (IB plane) as shown. N_1 and N_2 are non-plane loci. N_1 has a constant style and N_2 a changing style. $Contr_B$ shows a locus which is horizontally orthogonal to (the mirror of) $Contr_A$.

and its orientation with respect to bedding).

Figure 8A illustrates this idea for one type of fissility locus superimposed on three materials of different initial anisotropy. The loci start at different positions on the $-C$ axis, because of differing initial bedding platiness, and they trend upwards at the same angle for the same distance, as a result of experiencing identical tectonic fissility modifications. The locus for the initially isotropic material is not influenced by the initial state and so shows the tectonic changes directly. The initially anisotropic materials, however, show complex shape series resulting from interplay of the two factors. Also, the more anisotropic the starting material (e.g. a 'shale' compared with 'mudstone': Fig. 8A), the greater is the change in fissility intensity required to reach a shape of any particular type, say, pencils.

The kinds of alternatives expected when different types of locus or tectonic modification are superimposed on any one material are shown in Figure 8B. The straight lines are loci of constant shape-change type, whereas curved lines are loci of varying shape-change type.

Three biaxial straight-line loci (loci for which there is no change in the intermediate normalised fissility dimension) are of special interest as analogues of constant-volume plane-strain deformation on a deformation plot. We call these *contraction-*, *wrench-*, and *extension-loci* by geometric analogy with the "contraction" and "extension" fault kinematic categories proposed by Norris in relation to bedding (Hancock 1985, p. 440; Hatcher 1990, p. 213). They represent three different ways of coaxially superimposing an ideal plano-linear cleavage fabric on a planar bedding fabric. In the contraction type ($B = 2$), cleavage is superposed normal to bedding, while the beds undergo shortening and thickening. In the wrench type ($B = ½$), cleavage is also normal to bedding, but there is elongation in the plane of bedding instead of thickening of the beds. In the extension type ($B = -1$), cleavage is bedding-parallel and accompanied by thinning of the beds and extension in one direction in the plane of bedding.

These three loci concern local cleavage/bedding relations in the field. Because the way that strains are superposed on bedding varies according to position within folds (Mazzoli & Carnemolla 1993), the corresponding fissility states will generally vary from one part of a fold to another, particularly between the limbs and hinges of open to tight folds (Mazzoli & Carnemolla 1993, figs 14–17). Hence, to investigate variations of fissility state on a regional scale, it is necessary to select measurement sites with comparable deformation histories and comparable positions within folds, such as in the middle of incompetent layers in fold hinge zones.

If, after allowing for local variation within folds, there is a consistent linear locus of fissility across a region, it suggests there is probably a corresponding consistent deformation style at the regional scale. To distinguish these regional styles or "tectonic regimes" from the *cbi* bed-related loci discussed above, the three simplest biaxial regimes will be called *contraction-tectonic*, *wrench-tectonic* and *extension-tectonic*, according to whether the particular section of crust under study has been shortened and thickened, shortened and orthogonally extended, or thinned and extended, respectively. These categories are equivalent to the "thrust", "wrench" and "gravity" regimes, respectively, of Harland & Bayly (1958), except that they are expressed here in terms of deformation rather than stress. When bedding is subhorizontal (as in the hinges of upright folds), the *c*, *b* and *i* fissility coordinates may correspond to the *V*, *H* and *L* tectonic coordinates of Harland & Bayly (1958), in which case the fissility data may be interpreted directly in terms of the regional tectonic regime.

Our final section discusses some field examples illustrating the use of the fissility-ratio technique and applications of the concepts that have been outlined in this section.

Field examples of relative fissility intensity

The following sections illustrate applications of the two scales of relative fissility to quantification of cleavage and tectonic fabric intensity in the field.

The *c/b* (cleavage/bedding) ratio and, especially, the *i/b* (fissility-ratio in the plane of bedding) ratio, provide sensitive indicators for the early stages of fabric development. A simple way of describing a progression of cleavage development states is to measure the *c/b* fissility-ratio in a fixed rock type. Our first set of examples shows such a progression of *c/b* in mudstones, from undeformed bedding-fissility to a well-developed slaty cleavage. However, for a more complete picture it is necessary to include also measurements of *i/b* at the same outcrops. We have therefore included illustrations of *i/b* in this series. The photographs and ratio data for this series thus form a reference set which serves as a guide

to the way we envisage the method can be applied in the field.

Subsequent examples deal with several further and also little-investigated effects: effects of lithology (grain size, initial anisotropy, and ability to crack) and effects resulting from the apparent superposition of two cleavage fabrics at a high angle to each other. Both of these can have a significant influence on fissility-ratios and on the interpretation of these ratios in terms of tectonic deformation and structural evolution. To infer a particular style of deformation from fissility measurements, it is necessary to isolate the possible influence of variable initial bedding anisotropy and, if possible, to conduct measurements in regions which have just a single cleavage fabric. To do this, measurements of both *c/b* and *i/b* are required. In addition, these ratios can be used to identify regions where cryptic multiple deformation occurs; we give an example of this little-documented, but fairly widespread phenomenon, from the Lachlan Fold Belt of New South Wales (NSW).

Progression of relative cleavage-fissility and intersection-fissility, Manilla district of the Tamworth Belt, NSW

The Tamworth Belt (Fig. 9A) is a west-verging fold-and-thrust belt belonging to the western margin of the Late Permian–Triassic New England Fold Belt in northern NSW (Korsch 1977). It is an essentially linear belt, some 60 km wide, comprising Devonian to Permian arc-derived volcaniclastics, volcanics and minor limestones, that is affected by colinear, NNW-trending, gentle to tight upright folding and is bounded by major thrust faults (Pedder 1967; Chesnut et al. 1973; Leitch 1974; Leitch et al. 1988, p. 12–15; Liang 1991; Brown et al. 1992). Some thrusting or reverse faulting also occurs within the belt.

A dominant lithology over much of the region is a turbiditic grey-green mudstone, having a litharenite composition with a mainly andesitic volcanic provenance (Morris 1988; Chappell 1968). It occurs in four main formations: the Noumea Beds, Lowana Formation and Mandowa Mudstone (all Upper Devonian), and the Namoi Formation (Lower Carboniferous) (Brown et al. 1992). These formations include arenaceous and rudaceous members and are capped by a thick succession of fluvial sediments and volcanics deposited in partly glacigene conditions.

"Reticulate cleavage" (reticulate structure) was first described by Crook (1964, 1982) from mudstones of this fold belt in a region south of Tamworth in the Goonoo Goonoo Mudstone, a unit equivalent to the Mandowa Mudstone and Namoi Formation farther north. Packham & Crook (1960) also described several stages of incipient metamorphism in the Tamworth Belt, interpreted as a burial metamorphism.

A reconnaissance study at about the latitude of Manilla, some 50 km north of Tamworth, indicates the presence of incipient reticulate structure over the gently folded western three-quarters of the Belt (Fig. 9B). Near the eastern boundary of the Fold Belt it rapidly increases in intensity and locally becomes a strong slaty cleavage associated with tight upright folds (Fig. 9C). For most of the region, up to a few kilometres from the Peel Fault, the trace of the fissility on bedding is concordant with the NNW-trending regional folds and thrusts. As shown by the photographs, the optimum material for study is *in-situ* material that has been strongly disaggregated, but not significantly disoriented, by weathering processes.

No examples of completely undeformed mudstone were found in the western section of the belt, but one is present in the centre of the Manilla Syncline (Voisey 1957), where it is presumed to have been protected by underlying arenite members of the Lowana Formation (Fig. 9C). This example, sample 1 of the series, is shown in Figures 10a and b. The *c/b* ratio at this location is estimated to be about 0.3 (Fig. 10a). As in other examples of this series, this ratio was estimated visually in the following manner: identification of the most slender fragments, identification of the least slender fragments, then estimation of the mean or most common dimensional ratio as the cited figure. Typically, the extreme values vary by a factor of one category interval (x2 to x½) from the mean. Fissility on the bedding plane (Fig. 10b) is a completely random network of polygonal cracks, having no preferred direction, apart from locally in the neighbourhood of transecting joints, and no visible relation to the known fold-axis direction, which here runs upwards across the photograph.

Sample 2 of the series is a typical "embryonic cleavage-fissility" or "pre-reticulate" structure from the western half of the fold belt near Keepit Dam (Fig. 10c, d). S_0 (bedding) fissility is dominant in most of the outcrop. However, the view parallel to fold axis (horizontal, Fig. 10c) shows a weak but distinct preferred orientation of steep S_1 (embryonic cleavage) fissility-cracks in the approximate orientation expected for the axial plane of major folding at this location. The existence of a tectonic fabric anisotropy in the mudstone is confirmed by a clear alignment of fissility-cracks on the bedding surface (Fig. 10d) with *i/b* about 2.5.

Examples of roughly equidimensional *c/b* "reticulate structure" in mudstone are found in a major anticline immediately east of the Manilla Syncline (sample 3 in Figure 10e, f). *i/b* here is noticably greater than the previous example—around 3 to 4—consistent with it having a stronger tectonic imprint (Fig. 10f). Although pencil-like in form, the structure is too short to be called pencil-structure; therefore, we use the term reticulate structure to describe these. (This is a slightly more restricted usage than Crook's (1964) original, which he applied to examples with a marginally dominant S_1 fissility.)

The first stage of true, planar, cleavage-fissility (sample 4) is observed on the eastern limb of the previously mentioned anticline. (Crook 1964, plate 1, shows a similar example from a locality south of Tamworth.) Figure 11a shows this fissility in profile with a reasonably good planar preferred orientation of S_1 cracks at 40° to bedding. This case is closely related to the previous example of reticulate structure *sensu stricto*, but has a noticably more pronounced development of S_1 fissility over S_0 fissility, which we call "post-reticulate structure" or "weak slaty cleavage-fissility". As the bedding/cleavage angle is less than 60°, the observed length/orthogonal width ratio in profile ($c/c\perp$ = 2.5, where $c\perp$ is normal to c) requires a downward adjustment by sin 40° to give a true crack-spacing ratio of *c/b* = 1.6 (cf. Fig. 3). The *i/b* ratio (4) is viewed down-cleavage in Figure 11b and so shows the true crack spacings. These ratios define "narrow bedding-elongate cleavage blades" (Fig. 7), typical of the beginning stages of a true cleavage in many fold belts (e.g. Ramsay & Huber 1983, fig. 10.27).

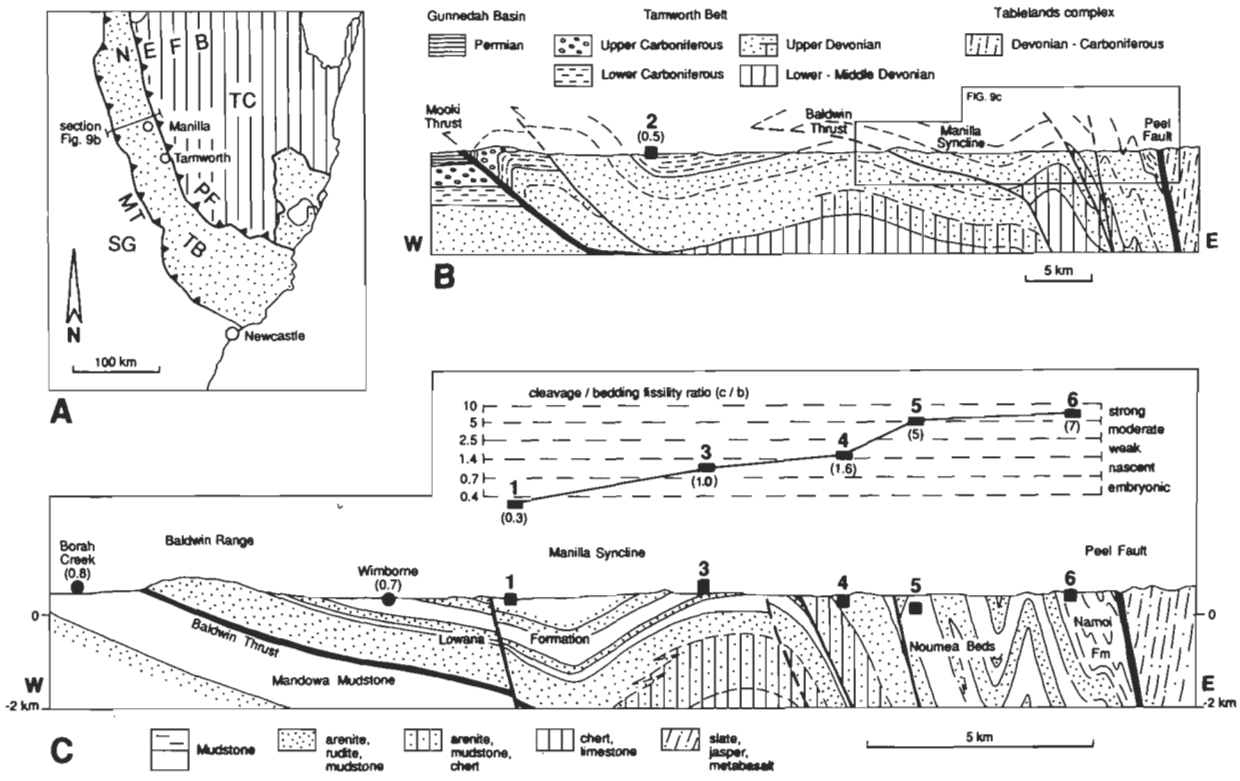

Figure 9. Location of mudstone fissility progression samples, Manilla, NSW, shown in Figs 10 & 11. A—Location of area. *MF*: Mooki Fault. *NEFB*: New England Fold Belt. *PF*: Peel Fault. *SG:* Sydney–Gunnedah Basin. *TB*: Tamworth Belt. *TC*. Tablelands Complex. B—Section through Tamworth Belt, Keepit to Manilla (modified after Liang 1991). Includes location of sample 2. C—Section and *c/b* fissility-ratio profile through eastern margin of Tamworth Belt along Namoi River, Manilla, NSW (based on field studies by D.Durney, P.Conaghan and students) showing sample locations 1 and 3–6. Section coordinates (AMG): 669045 (W), 807075, 848092, 921117 (E).

The remaining two examples are from the region of close to tight folds in the far eastern part of the Tamworth Belt.

Sample 5 (Fig. 11c, d) we categorise as having a "moderate to strong" slaty cleavage-fissility. Although not what most observers would call a "slate", it displays a clear and dominant S_1 fissility in profile. The *i/b* ratio here is similar to *c/b* (5), defining an oblate "cleavage plate" morphology in 3D.

Sample 6 (Fig. 10e, f) shows the strongest planar cleavage observed in this Belt, about 1 km from the bounding Peel Fault. It is definitely a "strong" slaty-cleavage-fissility, and approaches oblate "cleavage plate" morphology, though still with a greater length in the intersection direction and no sign of stretching lineation on the cleavage surfaces.

3D interpretation of Manilla mudstone fissility series

The 3D fissility-fragment shapes of the preceding cleavage-fissility series are plotted on a 3-axis logarithmic ratio diagram in Figure 12. We refer to the field of points in Figure 12 as the *Manilla mudstone field* (see Table 1, Appendix B, for sample descriptions).

The most striking feature of this distribution is its confinement to an *I*-constant band parallel to the *c/b* axis. *c/b* ratios correlate well with *i/b* according to a mean relation represented by

$$c/b = A\ (i/b)^B,$$

(eqn. 2b) where $A = 0.16$ and $B = 1.86$. The constant A is the mean initial cleavage/bedding fissility ratio, where the projected mean trend of the distribution intersects the $i/b = 1$ axis. From A we may calculate $i' = (1/A)^{1/3} = 1.84$.

With minor variations, and despite increasing tectonic modification, other samples from this series show similar values of i'. Since the samples are all of similar mudstone lithology, it seems reasonable to conclude that initial bedding fabric is responsible for this feature and has been preserved in the uniform i' values. Consequently, the inverse of A (or $b_0/c_0 = 1/A$, the projected bedding/cleavage fissility ratio) represents a measure of this initial anisotropy. It has a value of 6.3 or is "strong" according to the category divisions of Figure 4.

At the same time, the distribution runs very close to the expected fabric modification locus for increasing plane "contractional" fabric modification, having a value for B equal to 1.86 compared with 2 for the model locus 'C–Mudst' in Figure 8A. This type of data field and deformation style has been demonstrated previously for 3D total strain measurements in other areas; e.g. the Sudbury Basin of Canada (Clendenen et al. 1988) and the Alpine foreland of Southern France (Siddans et al. 1984; Hanna & Graham 1988). In the Tamworth Belt, supporting evidence is found in associated structural patterns—upright folds with reverse faults, and consistently oriented, fold belt parallel, fold axes and bedding/cleavage intersection lineations—suggesting simple horizontal contraction with vertical extension on a regional scale.

a. ABSENT cleavage fissility b.

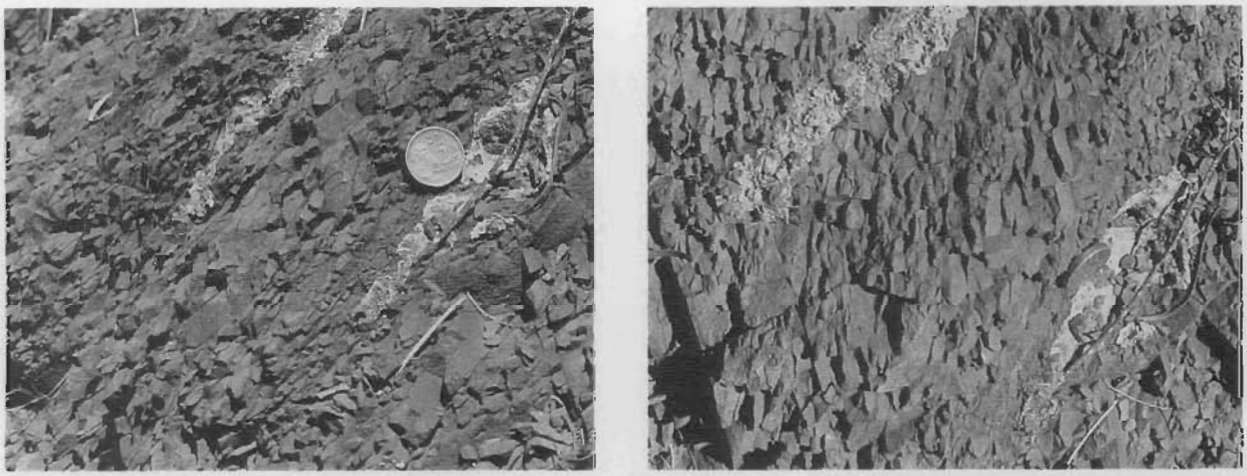

c. EMBRYONIC cleavage fissility d.

e. NASCENT (reticulate) cleavage fissility f.

Figures 10 and 11. Progression of cleavage-fissility states in slaty-type penetrative 2 cleaved mudstone, Manilla, NSW. Left hand photos (a, c & e) view the outcrops looking along the bedding/cleavage intersection direction and show cleavage cracks and bedding cracks (*c*/*b* ratios). Right hand photos (b, d & f) view the same outcrops looking down cleavage onto bedding planes and show cleavage cracks in the intersection direction and linking cracks (*i*/*b* ratios). Cleavage traces run 'top to bottom'; bedding traces and linking cracks run approximately 'left to right'. Figure 10 a & b: Sample 1, uncleaved. c–f: Samples 2 & 3, incipiently cleaved. Figure 11 a–f: Samples 4 to 6, weakly to strongly cleaved.

a. **WEAK cleavage fissility** b.

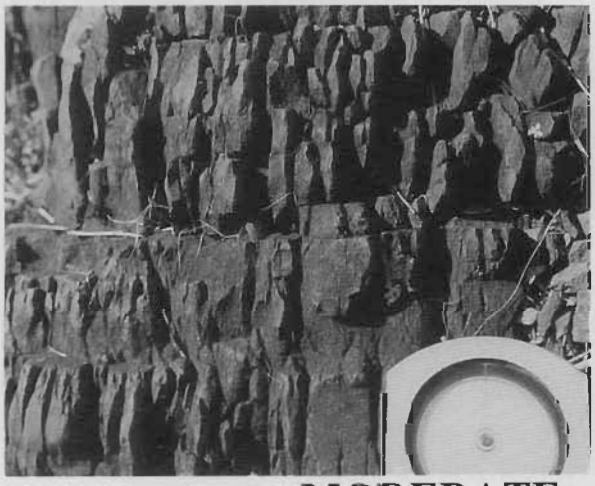

c. **MODERATE cleavage fissility** d.

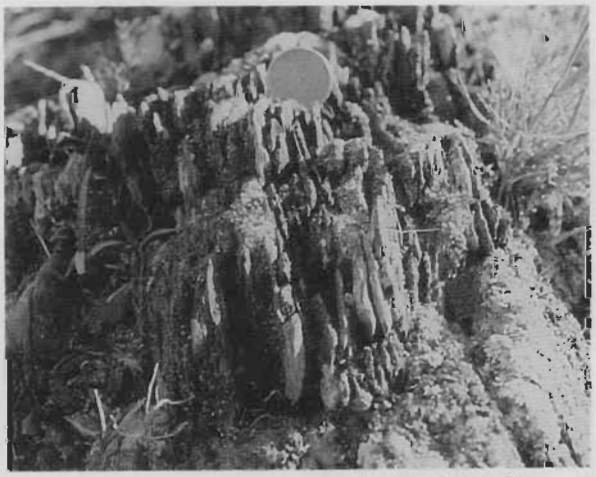

e. **STRONG cleavage fissility** f.

Strain in incipiently cleaved Manilla mudstones

Ideally, 3D measurements of both fissility-ratio and strain should be combined to establish the precise relationship between these two variables. In the previous section, we showed how the type of imposed tectonic deformation can be qualitatively determined from a fissility progression. Previously, Reks & Gray (1982) reported measurements demonstrating that there is also a quantitative relation to strain in the case of nascent cleavage-fissility in shaly rock. In this section, we present some initial measurements for embryonic cleavage-fissility in mudstones from Manilla which support this view.

2D measurements in the plane of bedding are possible at some locations in the Manilla area using specimens of

the deformed plant fossil *Leptophloeum australe* (Gould 1975 fig. 2f; previously *"Lepidodendron australe"*, David & Browne 1950, pl.26d). This lycopod stem displays a bilaterally symmetric pattern of diamond-shaped leaf cushions which can be analysed for distortional strain by Breddin"s method (Ramsay & Huber 1983) (Fig. 13A, B, C). In single specimens, the stretch-ratio on bedding, $R(S_0)$, is found assuming the trace of cleavage to be a principal axis of strain. Multiple specimens yield, in addition, independent confirmation that the principal axis of strain, $\phi(S_0)$, is close to the trace of cleavage, plus some information on statistical uncertainty.

Table 2 (Appendix B) summarises the results, together with fissility measurements and structural data for the three localities. These data show an increase in i/b with increase of $R(S_0)$, as foreseen previously on p. 271(Relative intersection fissility scale), although i/b increases more rapidly than $R(S_0)$. The limited data available could fit either a power function (like that proposed in eqn. 1b and as proposed for magnetic anisotropy ratio/stretch-ratio correlation by Rathore & Henry 1982, eqn. 1):

$$i/b = R^n(S_0), \quad (3)$$

where $n = 2.4$ (Fig. 13D), or the linear approximation to equation (3)

$$i/b - 1 = m\,(R(S_0) - 1), \quad (4)$$

where $m = 3.3$ (Fig. 13E).

Lithology effects — sandstone vs. mudstone

From the point of view of cleavage-fissility development, sandstones fall into two distinct categories: (1) muddy sandstones or wackes and (2) well-sorted sandstones (also, well-sorted siltstones) (Gray 1978, fig. 1).

Our observations at a number of different localities generally indicate that the c/b and i/b fissility-ratios for rough penetrative cleavage in thin beds of wacke are similar to, or lower than, those of interbedded mudstones (Fig. 14a).

The situation in thickly bedded and especially well-sorted sandstones is very different, however; these lithologies tend to be dominated by diagonal joints and display no evidence whatever of any fissility at low associated mudstone i/b values (Fig. 14b). Only when moderately strained do they begin to display a crude form of fissility, and even then it is subordinate to jointing (e.g. deformed micro cross-lamination in fine quartz sandstone, and moderate to strong S_1 cleavage in associated mudstone, observed in the Lower Devonian Majurgong Formation, Taemas Synclinorium, near Yass, NSW).

Lithology effects—shaliness

To illustrate how fissility-ratios vary as a function of bedding anisotropy, we examined a location in the Lachlan Fold Belt of NSW where two muddy lithologies of contrasting initial anisotropy have undergone the same amount of strain. For these examples, we use the same numerical ratio categories to describe strength of the initial anisotropy as for the relative cleavage-fissility scale: "weak" anisotropy (b_0/c_0 1.4–2.5), "moderate" anisotropy (b_0/c_0 2.5–5), and so on.

The area referred to is the uniformly dipping eastern limb of the Yass Syncline at Derringullen Creek, Yass, in NSW, where Upper Silurian shaly limestone and dark-grey calcareous mudstone lie in close proximity to each other (Fig. 14c & d). The structure here is uncomplicated; the beds dip gently, there are no faults or bedding-plane detachments in the vicinity, and incipient cleavage lies at a high (60°–70°) angle to bedding. Therefore the two rock units would have experienced the same layer-parallel shortening and similar layer-parallel shear strain. The fissility-ratios in the mudstone are typical of those found in the Manilla mudstones, notwithstanding the contrasting compositions and tectonic histories of these two rock units (see Yass mudstone in Fig. 15). The shaly rock, however, is distinguished from the mudstone by having a much smaller c/b ratio while having nearly the same i/b (Yass shaly limestone in Fig. 15). If these samples are projected back to the $-C$ axis along a contractional fabric locus, the mudstone shows a "strong" initial bedding anisotropy (b_0/c_0), while the shaly limestone shows a "very strong" to "extremely strong" anisotropy. This confirms the previous observation that c/b is strongly bedding-dependent. It also shows that i/b is relatively independent of the initial bedding anisotropy in these rocks.

An example of bedding anisotropy in undeformed shale is shown by Upper Ordovician black paper shale (Llanffawr Mudstone) at Llandrindod Wells in central Wales, UK. The beds here directly display the initial bedding anisotropy: b_0/c_0 = 30 to 50, which is at the limit of our "extremely strong" category. This is similar to the 50:1 ratio for various undeformed "flaggy shales" studied by Ingram (1953). Thus the Yass shaly limestone and undeformed shales suggest a grouping for some rocks at significantly higher bedding anisotropies than mudstone (Fig. 15). We call this group the *shale field* (in accordance with the meaning of "shale" as used by Pettijohn 1975).

With increasing tectonic modification of the fabric, lithologies belonging to the "shale" group should lie increasingly distant from the bedding-dominant group shown at the bottom of Figure 15. If the fabric locus is contractional, c/b and i/b ratios should both increase in a locus parallel to the Manilla mudstones, but below this field, and will eventually reach and continue beyond the category of structures we have called "bedding/cleavage (or bedding) pencil structure" (that is, fragments which are equidimensional in c/b but strongly elongate in i/b).

Most published examples of 'pencil' structure (*sensu lato*) in fact lie approximately in this position (Fig. 15). They lie in a higher i' (or I) band than mudstone and occupy the same i' range as undeformed and weakly deformed "shales". These facts are consistent with these pencils having been derived from shaly lithologies by a contractional tectonic locus. But further evidence is required to corroborate this conclusion.

Some 'pencils' from the Appalachian fold and thrust belt of the USA (Reks & Gray 1982; Ferrill & Dunne 1989) appear to fit this interpretation well; they commonly have a "black shale" or "shale" parent lithology, and pressure-shadow fibres show extensional strain normal to bedding signifying a contractional tectonic deformation.

Pencil structure observed in thin section in grey mudrock of the Booroo Ponds Group on the west limb of the Yass Syncline in NSW (e.g. Figs 2A and 15) shows relict bedding-parallel differentiated microdomains, similar to slaty cleavage domains, and/or a higher than usual detrital mica content (silt-size flakes of clear white mica sert in

a dark illitic matrix of very low metamorphic grade: cf. p. 258 "Pencil structure"). The S_1 cleavage microdomains themselves are moderately well-developed, suggesting that they would have been capable of forming a weak to moderate slaty-cleavage-fissility had they been present in a mudstone. Small chlorite pressure-shadows on pyrite grains are oriented at a high angle to bedding in the plane of cleavage and thus indicate a true contractional deformation. In addition, fissility-fragments from the same horizon exposed on the limb of a gentle cleavage-congruent fold have a form which is intermediate between

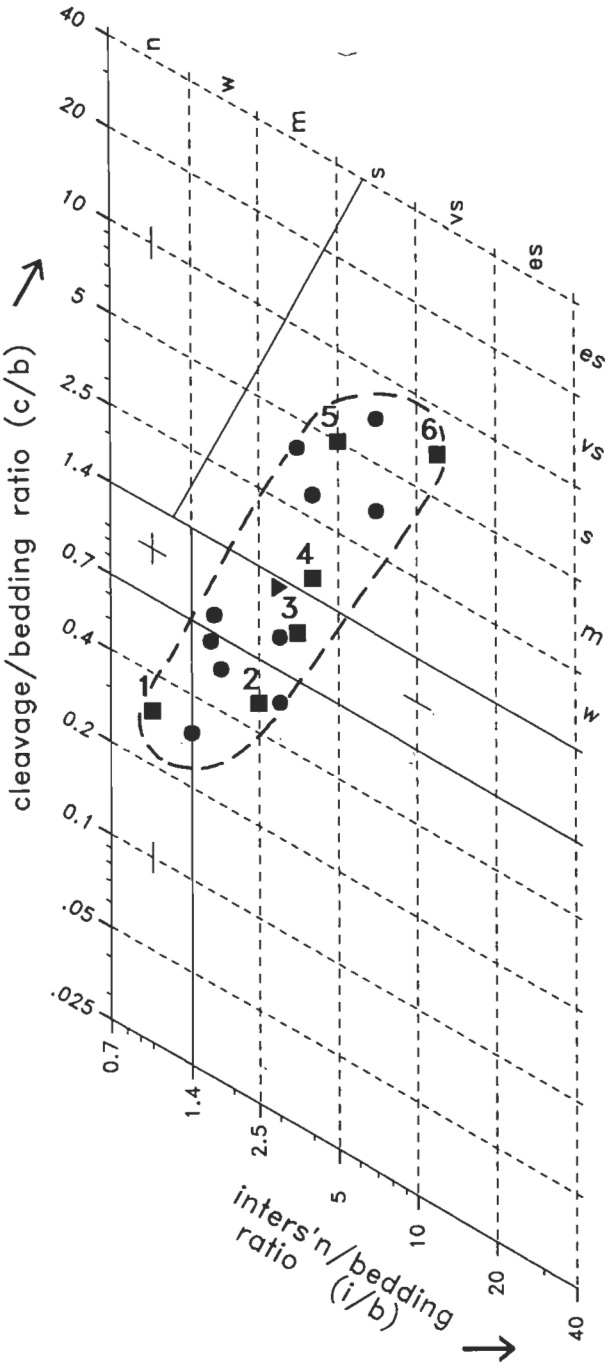

Figure 12. 3-axis plot of 3D fissility-ratio measurements for mudstones of the Manilla area, NSW. *Squares:* progression series samples illustrated in Figures 10 & 11. *Dots:* other locations in the Manilla area. *Triangle:* Tamworth Council Quarry sample.

that of the pencils and bedding plates of the "shale field": namely, "strong bedding blades" ("blades" on Fig. 15).

Our interpretation of this example is therefore twofold. First, the initial bedding anisotropy in these pencils is stronger than that of mudstones; in other words, these rocks are more shaly in character than ordinary mudstones. This is further confirmed by the contractional type of deformation locus by which the pencils would have been reached, and by the observed intermediate fissility forms. Second, the degree of tectonic fabric modification required to balance the initial bedding anisotropy in the pencils is greater than that required for mudstones.

These examples suggest that the shale field and what we call the "para-pencil field", on Figure 15, may be linked to form an important second lithological grouping on 3-axis plots having a boundary with the Manilla mudstone field at approximately $i' = 2.7$, $b_0/c_0 = 20$ or i/b (true pencil/reticule division) = 5. Observations that the more stubby fissility forms from "mudstones" (Crook 1964; Engelder & Geiser 1979) fall within our mudstone fissility field (Fig. 15) further support this interpretation. On the other hand, the pencil structure described by Ramsay (1981) is associated with a "wrench" deformation (see p.258) and hence more logically derived from a mudstone parent fabric than from a shale (cf. "Wren" path in Fig. 8B). So, although the fields outlined in Figure 15 may be common, they are dependent on the style of deformation and, consequently, are by no means unique for particular lithologies.

The conclusion we reached concerning a greater fabric modification in pencils than in mudstone reticules suggests that *c/b* ratios are probably not a reliable guide to intensity of tectonic strain. For a given deformation style, the *i/b* ratio should be a more appropriate deformation index in view of its independence of bedding anisotropy. However, as the next example demonstrates, *i/b* is not totally independent of lithology and in fact may display considerable variation in its response to strain in different rock types.

Lithology effects—sensitivity to strain

At the Borah Creek strain measurement location at Manilla, NSW, three distinct rock types are interbedded with one another in the same outcrop of uniformly and gently dipping beds: a mudstone, a fine to medium muddy sandstone (both slightly weathered) and an argillite of fresh, very dark green to black, splintery, appearance. Figures 14E and F show contrasting development of intersection fissility, *i/b*, in the argillite and sandstone seen on bedding planes: a "moderate to strong" *i/b* ratio in the argillite but only "nascent to weak" in the mudstone and sandstone. The *c/b* ratio is also higher for the argillite than the sandstone (Table 3, Appendix B, and Fig. 17); however, the mudstone is comparable to the sandstone in both *c/b* and *i/b*.

These differences cannot be explained by variable deformation, because layer-parallel shortening strain should be identical in the three lithologies and the cleavage/bedding angle (related to layer-parallel shear strain) in the argillite is similar to that of the sandstone. The reason for the difference in behaviour is not clear, other than that it is a function of lithology. We call it simply the *sensitivity* of cleavage-fissility development to tectonic strain: high in argillite, and moderate in mudstone and sandstone. The consequences for fissility-ratio measurements are

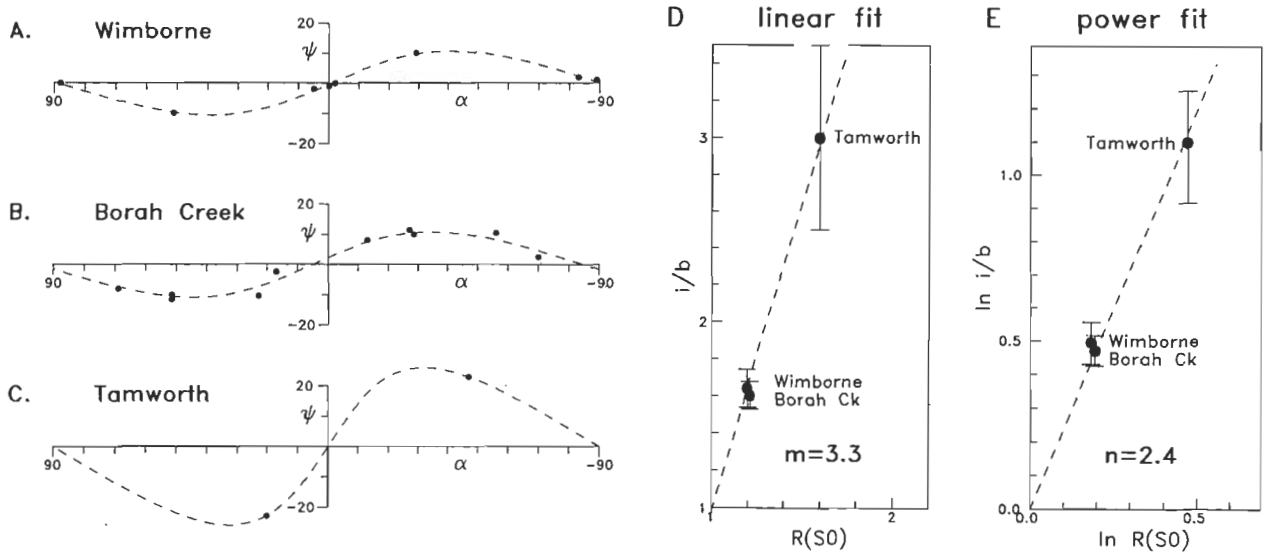

Figure 13. Stretch-ratios in the Manilla–Tamworth area from deformed *Leptophloeum* plant stems. A–C: Breddin plots (angular shear strain, ψ, vs. line orientation, α) and best-fit curves; see Table 1 for results. Angle conventions are as described in Ramsay & Huber (1983). The angles are measured in the plane of bedding, viewed downwards, relative to the average trace of cleavage on bedding at each location. D & E: Intersection-fissility ratio vs. stretch-ratio plots for the above localities; vertical error-bars are standard errors on *i/b* means. D—linear-law interpretation; E—power-law interpretation.

nevertheless clear. Neither *c/b* nor *i/b* may be assumed to be universal indicators of deformation intensity in all rock types; the value of these measurements lies chiefly in their use for characterising deformation and fabric intensity in a single lithology. For any one lithology, whether mudstone, shale, sandstone or argillite, we predict that an ordered relationship will exist between the fissility anisotropy, initial bedding anisotropy and tectonic strain, but that the relationships will be different for the different lithologies.

Figure 16 summarises the currently available data for sensitivity in three rock types in contractional deformation environments: Manilla-Tamworth mudstone, Borah Creek argillite and Appalachian "shale". We use the exponent *n* in equation 3, the *sensitivity exponent*, as a quantitative measure of sensitivity in these examples. Reks & Gray"s (1982, fig. 14) pencil data are plotted as *i/b* ratios using the conversion given in our Table 4 (Appendix B). Their *Y/Z* (intermediate to least principal tectonic stretch-ratio) is taken to mean effectively the same as our $R(S_0)$ (bedding plane stretch-ratio, where cleavage is at a high angle to bedding).

The Reks and Gray 'pencils', which we believe represent the behaviour of a "shale", clearly show the greatest sensitivity of tectonic fissility development to deformation: $n = 11$, or a power 8.6 greater than that of the Manilla–Tamworth mudstones ($n = 2.4$). The single measurement for argillite lies intermediate between these two rock types with an *n* value 6 powers greater than mudstone. Thinly bedded muddy sandstone (Table 3) appears to have a sensitivity similar to or slightly lower than that of mudstone.

These results demonstrate:

(1) very much greater numerical values of *i/b* compared with stretch-ratios and hence their appreciable sensitivity for registering small variations of deformation;

(2) widely varying fissility sensitivities to deformation in some rock types, ranging over 8.6 powers of $R(S_0)$; and

(3) considerably greater fabric modification, for a given amount of tectonic strain, in shales compared with mudstones and sandstones. Note that property (3) has the effect of balancing, to some extent, the opposed influence of high bedding anisotropy on *c/b* ratios in shales.

Effects of multiple deformation?: transverse blades

The samples that we have discussed so far all lie below the *c/b* or *C–B* axis on the 3-axis diagram (Figs 12 and 15); that is, within Fields 0 and 1 of Figure 7. This is the behaviour expected when a single, plano-linear, tectonic fabric is superimposed on an initial bedding-parallel fabric. As shown in Figure 8B, all initially isotropic and bedding-parallel anisotropic materials will fall on or below the *c/b* axis if modified by any of the three straight biaxial loci. The *c/b* axis therefore defines the theoretical upper limit of samples that are dominated by a single, planar, cleavage. The small sector above the *c/b* axis represents constrictional or linear, non-plane, fissility-fragment shapes at a high angle to bedding called "transverse pencils" and "narrow, transversely elongate, cleavage blades" (Fig. 7). This distinctive group is defined as Field 2. Using the correspondence principles (1) to (4) postulated on p.274, the style of tectonic fabric and total deformation required to produce Field 2 fissility would also be constrictional non-plane.

Fissility-fragment shapes which belong to Field 2 have only rarely and very briefly been reported in the literature; e.g. "forma astillosa" (splinters) due to "two cleavages almost perpendicular to bedding" (translated from Meléndez & Fúster 1978, fig. 19-4), and perhaps pencils that are due to "intersection of two cleavages" (translated from Mattauer 1973, fig. 5.48). However, we have found them at several places in the Lachlan Fold Belt of NSW, where Devonian strata have been affected by NW to NNE-trending upright folds and reverse faults of the Early

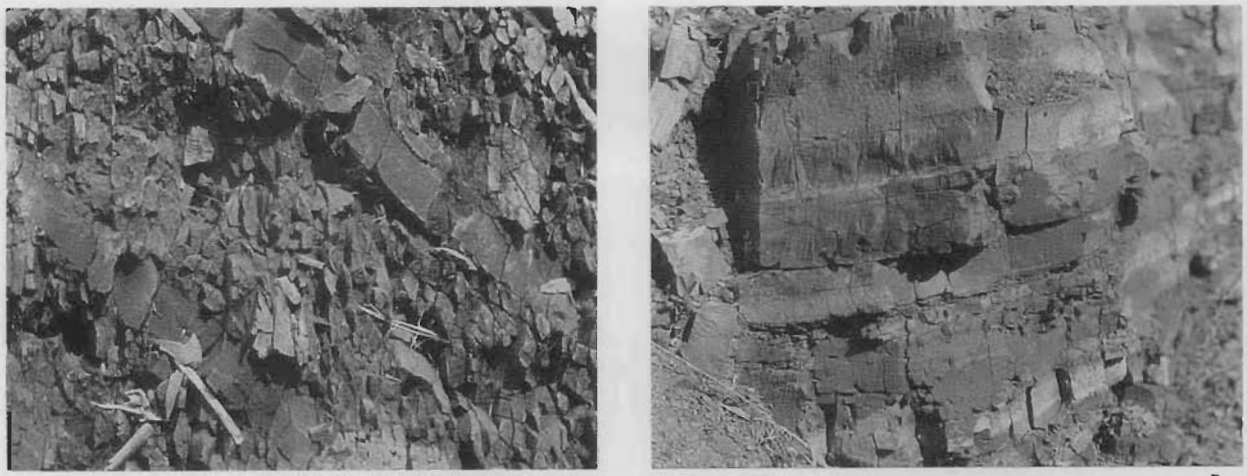

a. sandstone vs. mudstone b.

c. shale vs. mudstone d.

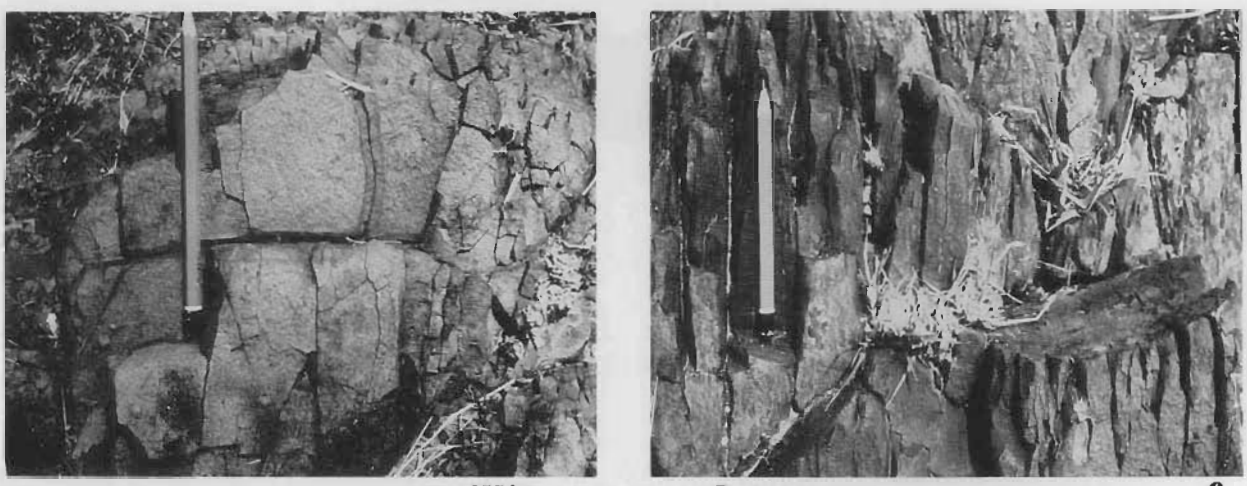

e. argillite vs. sandstone f.

Figure 14. Effects of lithology on fissility. a & b: Contrasting *fracture types in sandstone*, viewed parallel to bedding/cleavage intersection. a—Nascent cleavage-fissility in deformed litharenite sandstone and weak cleavage-fissility in associated mudstone layers (Lower Carboniferous Namoi Fm, Glamorgan homestead, Manilla, NSW). b—Joint-dominated fracture in weakly deformed litharenite sandstone (Upper Devonian Mandowa Mudstone, with nascent relative cleavage in associated mudstone layers, Tamworth Council Quarry, NSW). c & d: Contrasting *strength of bedding-fissility* in two Upper Silurian muddy calcareous rocks, 100 m apart in uniformly dipping strata, viewed parallel to bedding: Derringullen Creek, Yass, NSW. c—Grey calcareous mudstone (Booroo Ponds Gp) with absent to weak bedding-fissility (b_0/c_0 = 1.4). d—shaly limestone (Silverdale Fm) with strong to very strong bedding-fissility (b_0/c_0 = 10). e & f: Contrasting *cleavage intersection fissility* at one location in Upper Devonian Mandowa Mudstone, Borah Creek, NSW. View normal to bedding. Beds dip gently and uniformly; relative cleavage-fissility in associated mudstone layers is nascent. e—Absent to weak intersection fissilty in tuffaceous sandstone layers (i/b = 1.5). f—moderate to strong intersection fissility in siliceous argillite (i/b = 5).

Carboniferous Kanimblan Orogeny (Powell et al. 1976; Glen 1982b). Below we describe an example from the Merimbula area on the South Coast of NSW where Rixon et al. (1983) first noted the related phenomenon of prismatic cleavage lithons transverse to bedding.

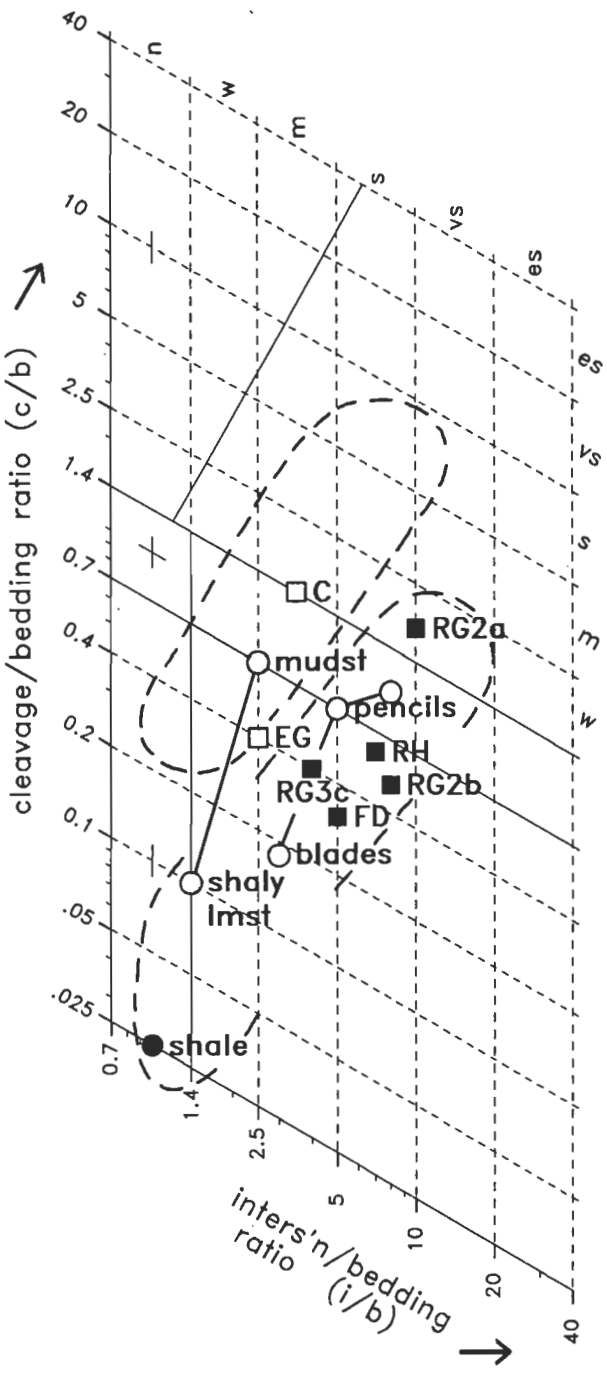

Figure 15. Comparison of bedding-anisotropy fissility effects in shaly rocks and Manilla mudstones (upper outlined field); 3-axis plot. *Solid squares*—para-pencil and deformed shale fissility-ratios measured from published illustrations: *FD* (Ferrill & Dunne 1989, fig. 7b, "pencil cleavage"), *RG* (Reks & Gray 1982, figs 2a, 2b & 3c, "pencil structure"), *RH* (Ramsay & Huber 1983, fig. 10.26, "pencil structure"). *Open squares*—mudstone fissility-ratios measured from published illustrations: *C* (Crook 1964, pl.1, "reticulate cleavage"), *EG* (Engelder & Geiser 1979, figs 3 & 4, "pencil cleavage"), *Circles*—Yass mudrocks: mudstone and shaly limestone, Derringullen Creek (Figs 14c, d); pencils (Fig. 2a); bedding blades, Bowning Creek, NSW. *Dot*—Paper shale, Llandrindod Wells, Wales.

At Merimbula Point, a strong slaty-type cleavage is locally developed in Upper Devonian Worange Point Formation fluvial red mudrocks in the steep limb of a horizontal monocline. Fissility in the cleaved mudrocks shows a distinctive "narrow transversely elongate blade" morphology (Fig. 17) characteristic of Field 2 (cf. Fig. 7). The blades display a well-defined steep plunge at 40° to 60° to bedding, but the strike of fissility cracks fluctuates up to 30° about the fold-axis direction, defining fragments that are crudely rhombic in horizontal section. The structure thus displays properties of both a single cleavage (the mean fabric plane) and two or more intersecting cleavages (the tendency to split at angles to the mean direction).

The associated fabric could be explained in one of two ways:

(1) The fabric is a single plano-linear cleavage of an anastomosing nature (Rixon et al. 1983; M. Rickard pers. comm. 1993), possibly produced by a continuous constrictional, non-plane deformation (straight path in Fig. 17).

(2) It is a compound fabric resulting from discretely or progressively superposed contractional biaxial deformations acting in different or changing directions with time in the plane of bedding (kinked and curved paths, respectively, in Fig. 17).

There is a singular lack of obvious overprinting relation between the different cleavage and fold trends that are

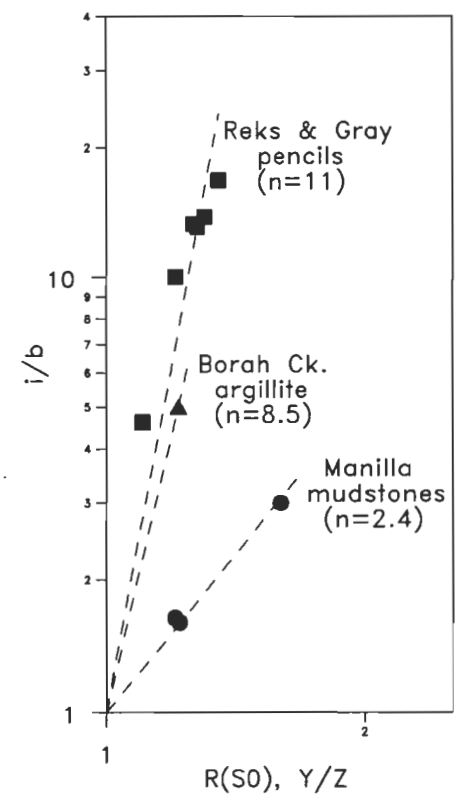

Figure 16. Comparison of *i/b* vs. stretch-ratio relations for Reks & Gray pencils (Table 4) and Manilla mudstones and argillite (Tables 2 & 3). Log-log plot with reduced ordinate scale; gradients of best-fit lines through (1,1) give sensitivity exponents (*n*).

present in the area; therefore the question cannot be easily resolved by conventional structural means.

Observations which suggest that the fissility morphology and related cleavage morhology here are not typical of single-generation structures are:

(a) Transverse-blade structure is unknown in regions where there is a single fold direction, such as the Tamworth Belt (cf. 'mudstone field' in Fig. 12).

(b) The circa 60° azimuth range of weak cleavage-stripe intersection traces on bedding in flat-lying sandstones (Rixon et al. 1983, fig. 6) is much larger than the norm for such cleavages in other areas (see outcrop illustrations of stripy and spaced cleavage in Borradaile et al. 1982: plates 53 (Granath), 65 (Alvarez & Engelder), 71 (Hancock), 89 (Cook), 91 (Sansone), 92 (Pfiffner), 97–98 (Beach) and 229 (Williams)).

(c) At low strain, a greater fluctuation of cleavage traces across bedding than in the bedding-plane would be expected as a result of lithological variation across the beds, but the situation at Merimbula is opposite to this (compare Rixon et al. 1983, figs 6 & 11).

(d) Contractional-style *en echelon* vein arrays and locally associated cleavage stripes in nearby sandstones show gently plunging σ_1 axes ranging over 80° in azimuth (Powell 1983, fig. 44; Rixon et al. 1983, fig. 18b) suggesting non-coaxial layer-parallel shortening during at least part of the cleavage-forming history.

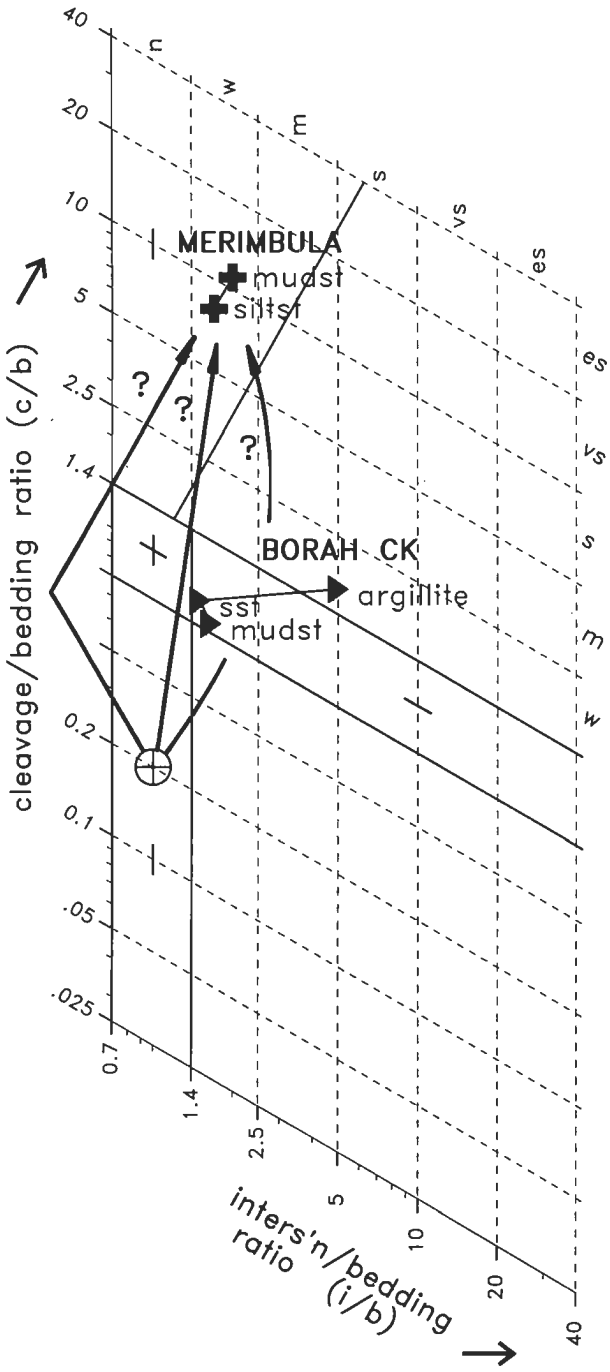

Figure 17. 3-axis plot illustrating sensitivity and cryptic multiple deformation effects. *Triangles*—Comparative sensitivity of Borah Creek lithologies, NSW: mudstone, sandstone (Fig. 14E) and argillite (Fig. 14F). See Table 3 for data. *Crosses*—Transverse cleavage blades, Merimbula Point, NSW: mudstone and siltstone. *Arrowed paths*—some possible deformation paths that may give rise to Merimbula transverse blades: 2-stage contraction (left); constant non-plane (centre) and changing non-plane (right). *Circle with cross*—presumed initial anisotropy of Merimbula sediments.

The lack of clear overprinting in the cleavage might be due to an insensitivity of the fabric to changing directions of strain at low strain; i.e. a *cryptic multiple or non-coaxial deformation* where early stages of the fabric are insufficiently advanced to respond to later oblique increments by crenulation. Field 2 fissility structures may, therefore, warrant further investigation as indicators of polydeformation and cleavage-strain behaviour in weakly deformed rocks.

Conclusions

(1) Characteristic fabric attributes which distinguish or relate different varieties of cleavage are reviewed and lead to a revised morphological classification for first-generation cleavages based on field characteristics. The classification applies mainly to clastic sedimentary rocks, where the cleavage is at a moderate to high angle to bedding, and encompasses rocks showing evidence of incipient slaty cleavage, such as pencil structure. Structures formed by purely brittle deformation processes are not included as categories within this *cleavage-type scheme*.

The primary field division is into *penetrative* and *non-penetrative* cleavages, penetrative being defined on the basis of grain size as a mineral alignment penetrating the rock down to the dominant grain or clast size; this distinction corresponds to Dennis' (1972) usage (rather than his definition) of the terms "continuous" and "discontinuous". A practical lower limit of 0.5 mm spacing applies to the mesoscopic recognition of the non-penetrative type.

Two types of "penetrative" cleavages are distinguished:

- *penetrative type 1*, a non-domainal or grain cleavage in relatively phyllosilicate-poor and relatively well-sorted clastic and chemical sediments and most igneous and coarse-grained metamorphic rocks; and
- *penetrative type 2*, a commonly though not exclusively differentiated domainal type typified by *slaty type* cleavage in lithified clastic rocks with significant

proportions of phyllosilicate or other platy minerals.

The *non-penetrative* cleavages, which are all domainal, are divided into three kinds:

- *spaced cleavage*, tectonic stylolites and more planar differentiated domainal non-penetrative cleavage in initially isotropic to weakly anisotropic rocks);
- *crenulation cleavage*, microfold-dependent differentiated domainal cleavage in initially strongly anisotropic rocks; and
- *scaly cleavage*, a largely non-differentiated slip phenomenon consisting of microscopic C-surfaces analogous to ductile shear zones.

Two kinds of heterogeneous mesoscopic intensity banding of the basic cleavage types are recognised:

- differentiated *cleavage zones* or *stripes*, and
- largely mechanical ductile *shear zones* in type 1 penetrative and scaly cleaved rocks.

(2) The main attribute of cleavage on a mesoscopic scale being fissility, we propose a *cleavage-intensity scale* based on this property. *Fissility* is distinguished as an actual parting (Dennis' 1972 "incidental partings") guided by the mechanical anisotropy of an existing cleavage or bedding fabric, especially small-scale fissility-cracks produced by present-day weathering processes in type 2 penetrative cleavage and bedding fabrics.

The intensity scale uses two aspect ratios of fissility-fragments:

- the *cleavage/bedding fissility ratio c/b* in the plane normal to the bedding/cleavage intersection, defining the *relative slaty-cleavage fissility scale*; the *c/b* ratio incorporates effects due to initial bedding anisotropy and shows the relative degree of cleavage development compared with bedding fabric; and
- the relative fissility in the cleavage/bedding intersection and bedding direction *i/b*, defining the *relative intersection fissility scale*; the *i/b* ratio indicates the extent of tectonic fabric development in any one lithology and structural/tectonic regime.

Class names are given to these ratios using approximately binary divisions of the *c/b* and *i/b* scales: *weak* (1.4–2.5), *moderate* (2.5–5), and so on. The categories cover a complete range of usefully measurable forms, from very incipient pre-pencil types to rocks with strongly developed slaty cleavage. The divisions thus lead to more precise definitions of cleavage-fragment shape, one of the consequences of which is a more restricted usage of the terms "cleavage structure" and "pencil structure".

Undeformed *bedding-fissility anisotropy* is also describable under this scheme, using the width-to-thickness ratio (b_0/c_0) of morphologically platy bedding-parallel fragments and the same class intervals as *c/b* and *i/b* ratios.

(3) The two fissility-ratios are shown on a 3-axis diagram in bedding–cleavage–intersection coordinate space, with the natural logarithms of b', c' and i' [b, *c* and *i* normalised against $(ibc)^{1/3}$] as axes; this diagram gives contours of both the *c/b* and the *i/b* ratio for plotting and description purposes. The diagram displays:

- the type of *fissility-fragment shape* or *structure* ("plate" or "blade" or "pencil", with qualifications "narrow", "biaxial" and "broad" for blades);
- its *orientation* with respect to the bedding and cleavage axes (cleavage-parallel or bedding-parallel for planes of flatness, and "bedding-elongate" or "transversely elongate" with respect to bedding for long axes); and
- its *slenderness*.

Three structural groups of are distinguished according to whether the dominant fissility is:

- bedding (*Field 0*), or
- a single cleavage at high angle to bedding (*Field 1*), or
- a constrictional or intersecting dual cleavage fabric at a high angle to bedding (*Field 2*).

(4) Methods for interpreting data fields on the logarithmic 3-axis diagram are outlined in terms of *initial bedding anisotropy* and its modification by spatially variable coaxial *tectonic deformations* ("fissility loci"). These methods include a new general relation for constant shape-type (straight line) loci:

$$c/b = A\ (i/b)B,$$

where *A* is inverse initial bedding anisotropy ratio (intercept) and *B* defines the type of shape locus or style of tectonic deformation with respect to bedding (slope). Three kinds of biaxial fissility locus are distinguished:

- $B = 2$ or *contractional*, involving shortening and thickening of beds,
- $B = ½$ or *wrench*, involving shortening and orthogonal elongation in the plane of bedding, and
- $B = -1$ or *extensional*, involving thinning and elongation of beds.

(5) Possible *applications of the fissility intensity scales* to problems of cleavage development and regional deformation in the field are illustrated with examples of penetrative type 2 cleavage fabrics from New South Wales (NSW), Australia, and the Northern Hemisphere.

- A *series of mudstones* showing progressively increasing cleavage-fissility intensity from the Tamworth Belt, NSW ('Manilla mudstones') is presented as a kind of standard for comparison of other cases. A complete progression is recorded, from apparently undeformed samples to samples which possess a strong slaty cleavage. These changes define a linear spread with mean slope $B = 1.86$ on the 3-axis diagram and are related to a regionally increasing, single-generation, contractional-tectonic, episode of folding and reverse faulting. A persistent influence of generally "moderate to strong" initial bedding anisotropy is also noted and characterises the *c/b* to *i/b* relationship as being of a "mudstone" type. Mudstones from other areas mostly fall within this fissility field. Deformed plant remains in the same samples indicate a relationship between the *i/b* fissility-ratio and the bedding plane tectonic stretch-ratio in the order of 3.3:1.
- Fissility-ratios in muddy sandstones or *wackes* are comparable to those in the mudstones; no fissility

observations could be made on deformed, well sorted sandstone due to its poor development and a dominating influence of joints.

- Undeformed to weakly deformed *shaly rocks* define part of a separate lithological field on the 3-axis diagram, called the "shale" field, characterised by "very strong" to "extremely strong" initial bedding anisotropy. Many of the structures from the Appalachian fold-and-thrust belt, USA, described in the literature as 'pencils', and pencils from Upper Silurian shallow-marine sediments in the Yass area, Australia, define a linear contractional spread of data, called the "para-pencil" field, which appears to be contiguous with the shale field.

- *Cleavage/bedding pencils* of the 'Ramsay'-type (Ramsay 1981), formed from mudstone in a wrench deformational setting, may be morphologically indistinguishable from 'Reks & Gray'-type pencils (Reks & Gray 1982), formed from shale in a contractional setting. Structural indicators of tectonic elongation direction are required to differentiate these two types.

- Differing responses of relative cleavage-fissility (*c/b*) and relative intersection fissility (*i/b*) to uniform layer-parallel deformation in different rock types are attributed to a property that we call the *sensitivity* of fissility development to tectonic strain. Available correlations of *i/b* with bedding plane stretch-ratio show shale and argillite to be highly sensitive, whereas mudstone and muddy sandstone are significantly less sensitive.

- A *new kind of pencil and narrow blade structure*, with steep plunge at a high angle to bedding and a slaty-type cleavage or incipient cleavage, is recognised as a probable product of multiple tectonic deformation. Cryptic cleavage-cleavage intersection structures of this kind plot in field 2 of the fissility 3-axis diagram and represent the type of response expected from weak, non-coaxially superimposed, contractional (layer-parallel shortening) events.

(6) In view of the dependence of fissility-ratios on bedding anisotropy, sensitivity and orientation of the imposed deformation, their use as indicators of cleavage development and tectonic strain is best restricted to a specified rock type and structural setting, such as mudstone in a mudstone-dominant formation near hinges of folds.

Acknowledgements

Fieldwork in Australia was supported by Research Grants from Macquarie University and a Travel Grant from Ben Gurion University of the Negev (1989 and 1990). D.W.D. also acknowledges assistance from organisers of The John Ramsay Meeting, Zürich, 1991, which enabled a summary of the work to be presented there, and facilities at Barcelona University (1993), where part of the manuscript preparation was carried out.

An article of this nature inevitably draws upon the work of many individuals over a period of time, to whom we are indebted for information and stimulus. In particular, reviews by Pat Conaghan, John Cosgrove, Keith Crook, Mike Rickard, Brinley Roberts, Ron Vernon, Karl Wolf and two anonymous reviewers led to improvements in the manuscript. We also thank David Gray and Xingnan Cao for discussion; Brinley Roberts and Dick Merriman for comments on the fissility-ratio technique during a field trial in Wales; and structural staff of the Department of Dynamic Geology, University of Barcelona, and CISC Institute, Barcelona, for comments during a similar trial in the Eastern Pyrenees. Students and staff in the Macquarie University field unit 'Field Geology' contributed information which assisted preparation of the cross-section (Fig. 9C). We thank Ken Rousell for preparing Figure 9.

References

Ahrendt, H., Hunziker, J.C. & Weber, K., 1977. Age and degree of metamorphism and time of nappe emplacement along the southern margin of the Damara orogen/Namibia (SW-Africa). *Geologische Rundschau,* 67, 719–742.

Alvarez, W., Engelder, T. & Geiser, P.A., 1978. Classification of solution cleavage in pelagic limestones. *Geology*, 6, 263–266.

Alvarez, W., Engelder, T. & Lowrie, W., 1976. Formation of spaced cleavage and folds in brittle limestone by dissolution. *Geology*, 4, 698-701.

Alvaro, M. & Capote, R., 1973. Las estructuras menores de las calizas jurásicas de un anticlinal de la Sierra de Altomira (Cuenca, España). *Estudios Geológicos*, 29, 467–478.

Arthaud, F. & Mattauer, M., 1969. Exemples de stylolites d'origine tectonique dans le Languedoc, leurs relations avec la tectonique cassante. *Bulletin de la Société géologique de France* (7), 11, 738–744.

Beach, A., 1974. A geochemical investigation of pressure solution and the formation of veins in a deformed greywacke. *Contributions to Mineralogy and Petrology,* 46, 61–68.

Beach, A., 1979. Pressure solution as a metamorphic process in deformed terrigenous sedimentary rocks. *Lithos,* 12, 51–58.

Beach, A., 1980. Retrogressive metamorphic processes in shear zones with special reference to the Lewisian complex. *Journal of Structural Geology,* 2, 257–263.

Behrmann, J.H., Brown, K., Moore, J.C., Mascle, A., Taylor, E. et al., 1988. Evolution of structures and fabrics in the Barbados Accretionary Prism. Insights from Leg 110 of the Ocean Drilling Program. *Journal of Structural Geology,* 10, 577–591.

Bell, T.H. & Etheridge, M.A., 1973. Microstructure of mylonites and their descriptive terminology. *Lithos,* 6, 337–348.

Berthé, D., Choukrone, P. & Jegouzo, P., 1979. Orthogneiss, mylonite and non-coaxial deformation of granites: the example of the South Armorican Shear Zone. *Journal of Structural Geology,* 1, 31–42.

Beutner, E.C., 1978. Slaty cleavage and related strain in Martinsburg slate, Delaware Water Gap, New Jersey. *American Journal of Science,* 278, 1–23.

Beutner, E.C. & Diegel, F.A., 1985. Determination of fold systematics from syntectonic fibers in pressure shadows, Martinsburg slate, New Jersey. *American Journal of Science,* 285, 16–50.

Bishop, D.G., 1972. Transposition structures associated with cleavage formation in the Otago schists. *New Zealand Journal of Geology and Geophysics,* 15, 360–371.

Blatt, H., Middleton, G.V., & Murray, R.C., 1980. *Origin of sedimentary rocks*. Prentice-Hall, Englewood Cliffs, 782 pp.

Borradaile, G.J., Bayly, M.B. & Powell, C.McA., (editors),

1982. *Atlas of deformational and metamorphic rock fabrics*. Springer-Verlag, Berlin, 551 pp.

Bosworth, W., 1984. Foreland deformation in the Appalachian Plateau, central New York: the role of small-scale detachment structures in regional overthrusting. *Journal of Structural Geology*, 6, 73–81.

Boulter, C.A., 1979. On the production of two inclined cleavages during a single folding event. *Journal of Structural Geology*, 1, 207–219.

Boyer, S.E., 1984. Origin and significance of compositional layering in Late Precambrian sediments, Blue Ridge Province, North Carolina, U.S.A. *Journal of Structural Geology*, 6, 121–133.

Brown, E.T., (editor), 1981. *Rock characterization testing and monitoring: ISRM suggested methods*. Pergamon, Oxford, 211 pp.

Brown, R.E., Krynen, J.P. & Brownlow, J.W., 1992. Manilla–Narrabri 1:250 000 Metallogenic Map. Geological Survey of New South Wales, Sydney.

Burg, J.P. & Iglesias Ponce de Leon, M., 1985, Pressure-solution structures in a granite. *Journal of Structural Geology*, 7, 431–436.

Carreras, J., Cobbold, P.R., Ramsay, J.G. & White, S.H., (editors), 1980. Shear zones in rocks. *Journal of Structural Geology*, 2 (special issue 1/2), 287 pp.

Casas, J.M. & Sàbat, F., 1987. An example of three-dimensional analysis of thrust-related tectonites. *Journal of Structural Geology*, 9, 647–657.

Chappell B.W., 1968. Volcanic greywackes from the Upper Devonian Baldwin Formation, Tamworth–Barraba District, New South Wales. *Journal of the Geological Society of Australia*, 16, 87–102.

Chesnut, W.S., Flood, R.H., & McKelvey, B.C., 1973. Manilla 1:250 000 geological sheet, SH 56–9. New South Wales Department of Mines, Sydney.

Chester, F.M. & Logan, J.M., 1987. Composite planar fabric of gouge from the Punchbowl Fault, California. *Journal of Structural Geology*, 9, 621–634.

Chidester, A.H., 1962. Petrology and geochemistry of selected talc-bearing ultramafic rocks and adjacent country rocks in North–Central Vermont. *United States Geological Survey Professional Paper*, 345, 207 pp.

Clendenen, W.S., Kligfield, R., Hirt, A.M. & Lowrie, W., 1988. Strain studies of cleavage development in the Chelmsford Formation, Sudbury Basin, Ontario. *Tectonophysics* ,145, 191–211.

Clifford, P.M., Rice, M.C., Pryer, L.L & Fueten, F., 1987. Mass transfer in unmetamorphosed carbonates and during low-grade metamorphism of arenites. *In* Jones, M.E. & Preston, R.M.F., (editors), Deformation of sediments and sedimentary rocks. *Geological Society Special Publication*, 29, 197–209.

Cloos, E., 1946. Lineation—a critical review and annotated bibliography. *Geological Society of America Memoir*, 18, 122 pp. (reprinted 1957 with Supplement).

Cosgrove, J.W., 1976. The formation of crenulation cleavage. *Journal of the Geological Society (London)*, 132, 155–178.

Cosgrove, J.W., 1989. Cleavage, folding and the finite strain ellipsoid. *Proceedings of the Geologists' Association*, 100, 461–479.

Cowan, D.S., 1982. Origin of "vein structure" in slope sediments on the inner slope of the Middle America Trench off Guatemala. *In* Aubouin, J., Huene, R. et al., *Initial Reports of Deep Sea Drilling Project*, 67, 645–650.

Cox, S.F., Etheridge, M.A., Cas, R.A.F. & Clifford, B.A., 1991. Deformational style of the Castlemaine area, Bendigo–Ballarat Zone: implications for evolution of crustal structure in central Victoria. *Australian Journal of Earth Sciences*, 38, 151–170.

Crook, K.A.W., 1964. Cleavage in weakly deformed mudstones. *American Journal of Science*, 262, 523–531.

Crook, K.A.W. 1982. Reticulate cleavage in the Goonoo Goonoo Mudstone, Australia. *In* Borradaile, G.J., Bayly, M.B. & Powell, C.McA., (editors), *Atlas of deformational and metamorphic rock fabrics*. Springer-Verlag, Berlin, plate 72, 190–191.

Curtis, C.D., Lipshie, S.R., Oertel, G. & Pearson, M.J., 1980. Clay orientation in some Upper Carboniferous mudrocks, its relationship to quartz content and some inferences about fissility, porosity and compactional history. *Sedimentology*, 27, 333–339.

David, T.W.E. & Browne, W.R., 1950. *The geology of the Commonwealth of Australia. vol 1*. Arnold, London, 747 pp.

Davis, G.H., 1984. *Structural geology of rocks and regions*. Wiley, New York, 492 pp.

Dennis, J.G., 1967. International tectonic dictionary. *American Association of Petroleum Geologists Memoir*, 7, 196 pp.

Dennis, J.G., 1972. *Structural geology*. Ronald, New York, 532 pp.

Dennis, J.G., 1987a. Cleavage and schistosity. *In* Seyfert, C.K., (editor), *Encyclopedia of structural geology and plate tectonics*. Van Nostrand Reinhold, New York, 48–53.

Dennis, J.G., 1987b. *Structural geology—an introduction*. W.C. Brown, Dubuque, 448 pp.

Dietrich, D., 1989. Axial depressions and culminations in the evolution of the Helvetic chain. *Schweizerische Mineralogische und Petrographische Mitteilumgen*, 69, 183–189.

Dietrich, D. & Casey, M., 1989. A new tectonic model for the Helvetic nappes. *In* Coward, M.P., Dietrich, D. & Park, R.G., (editors), Alpine tectonics. *Geological Society, Special Publication*, 45, 47–63.

Dietrich, D. & Song, H., 1984. Calcite fabrics in a natural shear environment, the Helvetic nappes of western Switzerland. *Journal of Structural Geology*, 6, 19–32.

Durney, D.W., 1972a. Solution-transfer, an important geological deformation mechanism. *Nature*, 235, 315–317.

Durney, D.W., 1972b. Deformation history of the Western Helvetic nappes, Valais, Switzerland. Unpublished PhD thesis, University of London, 326 pp.

Durney, D.W. 1976a. Pressure-solution and crystallization deformation. *Philosophical Transactions of the Royal Society (London), A*, 283, 229–240.

Durney, D.W., 1976b. Solution-transfer primary differentiation and cleavage-forming processes. *25th International Geological Congress (Sydney), Abstracts*, 1, 120–121.

Durney, D.W., 1982. Slaty cleavage in flysch (I). *In* Borradaile, G.J., Bayly, M.B. & Powell, C.McA., (editors), *Atlas of deformational and metamorphic rock fabrics*. Springer-Verlag, Berlin, plate 108, 268–269.

Durney, D.W. 1984. *Taemas excursion, field guide (provisional)*. Geological Society of Australia, Specialist Group in Tectonics and Structural Geology, Sydney, 15 pp.

Durney, D.W. & Ramsay, J.G., 1973. Incremental strains measured by syntectonic crystal growths. *In* De Jong, K.A. & Scholten, R., (editors), *Gravity and tectonics*. Wiley-Interscience, New York, 67–96.

Engelder, T., 1987. Joints and shear fractures in rock. *In* Atkinson, B.K., (editor), *Fracture mechanics of rock*.

Academic Press, London, 27–69.
Engelder, T. & Geiser, P., 1979. The relationship between pencil cleavage and lateral shortening within the Devonian section of the Appalachian Plateau, New York. *Geology*, 7, 460–464.
Engelder, T. & Marshak, S., 1985. Disjunctive cleavage formed at shallow depths in sedimentary rocks. *Journal of Structural Geology*, 7, 327–343.
Epstein, A.G., Epstein, J.B. & Harris L.D., 1977. Conodont color alteration — an index to organic metamorphism. *United States Geological Survey, Professional Paper*, 995, 27 pp.
Erslev, E.A., & Ward, D.J., 1994. Non-volatile element and volume flux in coalesced slaty cleavage. *Journal of Structural Geology*, 16, 531–553.
Ferrill, D.A., 1989. Primary crenulation pencil cleavage. *Journal of Structural Geology*, 11, 457–461.
Ferrill, D.A. & Dunne, W.M., 1989. Cover deformation above a blind duplex: an example from West Virginia, U.S.A. *Journal of Structural Geology*, 11, 421–431.
Fieremans, M. & Bosmans, H., 1982. Colour zones and the transition from diagenesis to low-grade metamorphism of the Gedinnian shales around the Stavelot Massif (Ardennes, Belgium). *Schweizerische Mineralogische und Petrographische Mitteilungen*, 62, 99–112.
Folk, R.L., 1980. *Petrology of sedimentary rocks*. Hemphill, Austin, 185 pp.
Foster, M.E. & Hudleston, P.J., 1986. "Fracture cleavage" in the Duluth complex, northeastern Minnesota. *Geological Society of America Bulletin*, 97, 85–96.
Fleuty, M.J., 1964. The description of folds. *Proceedings of the Geologists' Association*, 75, 461–492.
Geiser, P.A., 1974. Cleavage in some sedimentary rocks of the Central Valley and Ridge Province, Maryland. *Geological Society of America Bulletin*, 85, 1399–1412.
Geiser, P.A. & Sansone, S., 1981. Joints, microfractures, and the formation of solution cleavage in limestone. *Geology*, 9, 280–285.
Gibson, R.G. & Gray, D.R., 1985. Ductile-to-brittle transition in shear during thrust sheet emplacement, Southern Appalachian thrust belt. *Journal of Structural Geology*, 7, 513–525.
Glen, R.A., 1982a. Component migration patterns during the formation of a metamorphic layering, Mount Franks area, Willyama Complex, N.S.W., Australia. *Journal of Structural Geology*, 4, 457–467.
Glen, R.A., 1982b. Nature of the late-Early to Middle Devonian tectonism in the Buckambool area, Cobar, New South Wales. *Journal of the Geological Society of Australia*, 29, 127–138.
Gould, R.E., 1975. The succession of Australian pre-Tertiary megafossil floras. *Botanical Review*, 41, 453–481.
Gratier, J.P., 1979. Mise en évidence de relations entre changement de composition chimique et intensité de déformation dans les roches à schistosité. *Bulletin de la Société géologique de France* (7), 21, 95–104.
Gray, D.R., 1977a. Morphological classification of crenulation cleavage. *Journal of Geology*, 85, 229–235.
Gray, D.R., 1977b. Differentiation associated with discrete crenulation cleavages. *Lithos*, 10, 89–101.
Gray, D.G., 1977c. Some parameters which affect the morphology of crenulation cleavages. *Journal of Geology*, 85, 763–780.
Gray, D.R., 1978. Cleavages in deformed psammitic rocks from southeastern Australia: their nature and origin. *Geological Society of America Bulletin*, 89, 577–590.
Gray, D.R., 1979. Microstructure of crenulation cleavages: an indicator of cleavage origin. *American Journal of Science*, 279, 97–128.
Gray, D.R., 1981. Compound tectonic fabrics in singly folded rocks from Southwest Virginia, U.S.A. *Tectonophysics*, 78, 229–248.
Gray, D.W. & Durney, D.W., 1979. Investigations on the mechanical significance of crenulation cleavage. *Tectonophysics*, 58, 35–79.
Gray, D.R. & Willman, C.E., 1991. Deformation in the Ballarat Slate Belt, central Victoria, and implications for the crustal structure across southeast Australia. *Australian Journal of Earth Sciences*, 38, 171–201.
Gregg, W.J., 1985. Microscopic deformation mechanisms associated with mica film formation in cleaved psammitic rocks. *Journal of Structural Geology*, 7, 45–56.
Grocott, J. & Watterson, J., 1980. Strain profile of a boundary within a large ductile shear zone. *Journal of Structural Geology*, 2, 111–117.
Groshong, R.H., 1975a. "Slip" cleavage caused by pressure solution in a buckle fold. *Geology*, 3, 411–413.
Groshong, R.H., 1975b. Strain, fractures, and pressure solution in natural single-layer folds. *Geological Society of America Bulletin*, 86, 1373–1376.
Groshong, R.H., 1988, Low-temperature deformation mechanisms and their interpretation. *Geological Society of America Bulletin*, 100, 1329–1360.
Guiraud, M. & Séguret, M., 1987. Soft-sediment microfaulting related to compaction within the fluvio-deltaic infill of the Soria strike-slip basin (northern Spain). *In* Jones, M.E. & Preston, R.M.F. (editors), Deformation of sediments and sedimentary rocks. *Geological Society Special Publication*, 29, 123–136.
Guzzetta, G., 1984. Kinematics of stylolite formation and physics of the pressure-solution process. *Tectonophysics*, 101, 383–394.
Hancock, P.L., 1982. Distinction between cleavage and joints using morphology. *In* Borradaile, G.J., Bayly, M.B. & Powell, C.McA. (editors), *Atlas of deformational and metamorphic rock fabrics*. Springer-Verlag, Berlin, plate 71, 188–189.
Hancock, P.L., 1985. Brittle microtectonics: principles and practice. *Journal of Structural Geology*, 7, 437–457.
Hanna, S.S. & Graham, R.H., 1988. A structural context of strain measurements on reduction spots in the Alpes Maritimes and the Hercynian fold belt of Southern Britain. *Annales Tectonicae*, 2, 71–83.
Harland, W.B. & Bayly, M.B., 1958. Tectonic regimes. *Geological Magazine*, 95, 89–104.
Harris, L.B. & Cobbold, P.R., 1985. Development of conjugate shear bands during bulk simple shearing. *Journal of Structural Geology*, 7, 37–44.
Hatcher, R.D., 1990. *Structural geology*. Merrill, Columbus, 531 pp.
Hawkins, A.B. & Pinches, G.M., 1992. Engineering description of mudrocks. *Quarterly Journal of Engineering Geology*, 25, 17–30.
Hills, E.S., 1965. *Elements of structural geology*. Science Paperbacks & Methuen, London, 483 pp.
Hobbs, B.E., Means, W.D. & Williams, P.F., 1976. *An outline of structural geology*. Wiley, New York, 571 pp.
Hoskins, L.M., 1896. Flow and fracture of rocks as related to structure. *United States Geological Survey, 16th Annual Report (1894-1895)*, pt.I, 845–874.
Hsu, T.C., 1966. The chararacteristics of coaxial and non-coaxial strain paths. *Journal of Strain Analysis*, 1, 216–222.
Hutton, C.O. & Turner, F.J., 1936. Metamorphic zones in north-west Otago. *Transactions of the Royal Society of New Zealand*, 65, 405-406.

Ingram, R.L., 1953. Fissility of mudrocks. *Geological Society of America Bulletin*, 64, 869–878.

Kemp, A.E.S., Oliver, G.H.J. & Baldwin, J.R., 1985. Low-grade metamorphism and accretion tectonics: Southern Uplands terrain, Scotland. *Mineralogical Magazine*, 49, 335–344.

Kerrich, R., Allison, I., Barnett, R.L., Moss,S. & Starkey, J., 1980. Microstructural and chemical transformations accompanying deformation of granite in a shear zone at Mieville, Switzerland: with implications for stress corrosion cracking and superplastic flow. *Contributions to Mineralogy and Petrology*, 73, 221–242.

Kisch, H.J., 1989. Discordant relationship between degree of very low-grade metamorphism and the development of slaty cleavage. *In* Daly, J.S., Cliff, R.A. & Yardley, B.W.D., (editors), Evolution of metamorphic belts. *Geological Society Special Publication*, 43, 173–185.

Kisch, H.J., 1991. Development of slaty cleavage and degree of very-low-grade metamorphism: a review. *Journal of Metamorphic Geology*, 9, 735–750.

Kligfield, R., Lowrie, W., Hirt, A. & Siddans, A.W.B., 1983. Effect of progressive deformation on remanent magnetization of Permian redbeds from the Alpes Maritimes (France). *Tectonophysics*, 97, 59–85.

Knipe, R.J. & White, S.H., 1977. Microstructural variation of an axial plane cleavage around a fold—a H.E.V.M. study. *Tectonophysics*, 39, 355–380.

Knopf, E.B. & Ingerson, E., 1938. Structural petrology. *Geological Society of America Memoir*, 6, 270 pp.

Koepnick, R.B., 1985. Distribution and permeability of stylolite-bearing horizons within a Lower Cretaceous carbonate reservoir in the Middle East. *60th Annual Technical Conference & Exhibition of the Society of Petroleum Engineers, Las Vegas, Sept. 1985*, SPE 14173, 1–7.

Korsch, R.J., 1977. A framework for the Palaeozoic geology of the southern part of the New England Geosyncline. *Journal of the Geological Society of Australia*, 24, 339–355.

Labaume, P., Berty, C. & Laurent, Ph., 1991. Syn-diagenetic evolution of shear structures in superficial nappes: an example from the Northern Appenines (NW Italy). *Journal of Structural Geology*, 13, 385–398.

Langheinrich, G., 1977. Zur Terminologie der Schieferungen. *Geologische Rundschau*, 66, 336–352.

Leitch, E.C., 1974. The geological development of the southern part of the New England Fold Belt. *Journal of the Geological Society of Australia*, 21, 133–156.

Leitch, E.C., Iwasaki, M., Honma, H., Watanabe, T., Iizumi, S., Ishiga, H. & Kawachi, Y., 1988. The structure of the southern part of the New England Fold Belt. In *Preliminary report on the geology of the New England Fold Belt, Australia,* 1, Cooperative Research Group of Japan and Australia, pp. 9–31.

Leith, C.K., 1905. Rock cleavage. *United States Geological Survey Bulletin*, 239, 153 pp.

Lewan, M.D., 1978. Laboratory classification of very fine grained sedimentary rocks. *Geology*, 6, 745–748.

Liang, T.C.K., 1991. Fault-related folding : Tulcumba Ridge, western New England. *Australian Journal of Earth Sciences*, 38, 349–355.

Lister, G.S. & Snoke, A.W., 1984. S-C mylonites. *Journal of Structural Geology*, 6, 617–638.

Lloyd, G.E., Law, R.D., Mainprice, D. & Wheeler, J., 1992. Microstructural and crystal fabric evolution during shear zone formation. *Journal of Structural Geology*, 14, 1079–1100.

Lundegard, P.D. & Samuels, N.D., 1980. Field classification of fine-grained sedimentary rocks. *Journal of Sedimentary Petrology*, 50, 781–786.

Maltman, A.J., Byrne, T., Karig, D.E. & Lallement, S., 1993. Deformation at the toe of an active accretionary prism: synopsis of results from ODP Leg 131, Nankai, SW Japan. *Journal of Structural Geology*, 15, 949–964.

Marshak, S. & Engelder, T., 1985. Development of cleavage in limestones of a fold-thrust belt in eastern New York. *Journal of Structural Geology*, 7, 345–359.

Mattauer, M., 1973. *Les Déformations des Matériaux de l'Écorce terrestre.* Hermann, Paris, 493 pp. or: 1980. *Les Déformations des Matériaux de l'Écorce terrestre,* 2me édition. Hermann, Paris, 512 pp.

Mazzoli, S. & Carnemolla, S., 1993. Effects of the superposition of compaction and tectonic strain during folding of a multilayer sequence—model and observations. *Journal of Structural Geology*, 15, 277–291.

Means, W.D., 1975. Natural and experimental microstructures in deformed micaceous sandstones. *Geological Society of America Bulletin*, 86, 1221–1229.

Meléndez, B. & Fúster, J.M., 1978. *Geología.* 4a. edn., Paraninfo, Madrid, 911 pp.

Merriman, R.J. & Roberts, B., 1985. A survey of white mica crystallinity and polytypes in pelitic rocks of Snowdonia and Llyn, North Wales. *Mineralogical Magazine*, 49, 305–319.

Mitra, G. & Yonkee, W.A., 1985. Relationship of spaced cleavage to folds and thrusts in the Idaho–Utah–Wyoming thrust belt. *Journal of Structural Geology*, 7, 361–373.

Moore, J.G., Roeske, S., Lundberg, N., Schoonmaker,J., Cowan, D.S., Gonzales, E., Lucas, S.E., 1986. Scaly fabrics from Deep Sea Drilling Project cores from forearcs. *In* Moore, J.C. (Editor), Structural fabric in Deep Sea Drilling Project cores from forearcs. *Geological Society of America Memoir*, 166, 55–73.

Morgenstern, N.R. & Tchalenko, J.S., 1967a. Microstructural observations on shear zones from slips in natural clays. *Proceedings of the Geotechnical Conference, Oslo*, 1, 147–152.

Morgenstern , N.R. & Tchalenko, J.S., 1967b. The optical determination of preferred orientation in clays and its application to the study of microstructure in consolidated kaolin. *Proceedings of the Royal Society (London)*, A, 300, 218–250 (parts I & II).

Morris, P.A., 1988. A geochemical approach to the characterization of a hidden magmatic arc: the source of the Goonoo Goonoo Mudstone, eastern Australia. *Australian Journal of Earth Sciences*, 35, 81–92.

Murphy, F.X., 1990. The role of pressure solution and intermicrolithon-slip in the development of disjunctive cleavage domains: a study from Helvick Head in the Irish Variscides. *Journal of Structural Geology*, 12, 69–81.

Nickelsen, R.P., 1972. Attributes of rock cleavage in some mudstones and limestones of the Valley and Ridge province, Pennsylvania. *Proceedings of the Pennsylvania Academy of Science*, 46, 107–112.

Nickelsen, R.P., 1986. Cleavage duplexes in the Marcellus Shale of the Appalachian foreland, *Journal of Structural Geology*, 8, 361–371.

Norris, R.J. & Bishop, G., 1990. Deformed conglomerates and textural zones in the Otago Schists, South Island, New Zealand. *Tectonophysics*,174, 331–349.

Norris, R.J. & Rupke, N.A., 1986. Development of cleavage in a mudstone unit from the Cantabrian Mountains, northern Spain. *Journal of Structural Geology*, 8, 871–878.

Oertel, G., 1962. Extrapolations in geologic fabrics. *Geological Society of America Bulletin*, 73, 325–342.

Oertel, G., Engelder, T. & Evans, K., 1989. A comparison of the strain of crinoid dolmnals with that of their enclosing silty and shaly matrix on the Appalachian Plateau, New York. *Journal of Structural Geology*, 11, 975–993.

Owens, W.H., 1974. Representation of finite strain state by three-axis planar diagrams. *Geological Society of America Bulletin*, 35, 307–310.

Packham, G.H. & Crook, K.A.W., 1960. The principle of diagenetic facies and some of its implications. *Journal of Geology*, 68, 392–407.

Park, W.C. & Schot, E.H., 1968. Stylolites: their nature and origin. *Journal of Sedimentary Petrology*, 38, 175–191.

Pedder, A.E.H., 1967. The Devonian System of New England, New South Wales, Australia. *In* Oswald, D.H., (editor), *International symposium on the Devonian System*. Alberta Society of Petroleum Geology, Calgary, 2, 135–142.

Pettijohn, F.J., 1975. *Sedimentary rocks*. 3rd. edn., Harper & Row, New York, 628 pp.

Piqué, A., 1975. Répartition des zones d'anchimétamorphisme dans les terrains dinantiens du Nord-Ouest du Plateau central (Meseta marocaine). *Bulletin de la Société géologique de France* (7), 7, 416–420.

Piqué, A., 1982. Relations between stages of diagenetic and metamorphic evolution and the development of a primary cleavage in the northwestern Moroccan Meseta. *Journal of Structural Geology*, 4, 491–500.

Piqué, A., Huon, S. & Clauer, N., 1984. La schistosité hercynienne et la métamorphisme associé dans la vallée de la Meuse, entre Charleville–Mézières et Namur (Ardennes franco-belges). *Bulletin de la Société belge de Géologie*, 93, 55–70.

Platt, J.P. & Vissers, R.L.M., 1980. Extensional structures in anisotropic rocks. *Journal of Structural Geology*, 2, 397–410.

Potter, P.E., Maynard, J.B. & Pryor, W.A., 1980. *Sedimentology of shale*. Springer-Verlag, New York, 306 pp.

Powell, C.McA., 1969. Intrusive sandstone dikes in the Siamo Slate near Negaunee, Michigan. *Geological Society of America Bulletin*, 80, 2585–2594.

Powell, C.McA., 1979. A morphological classification of rock cleavage. *Tectonophysics*, 58, 21–34.

Powell, C.McA., 1983. Geology of the N.S.W. South Coast and adjacent Victoria with emphasis on the pre-Permian structural history. *Geological Society of Australia, Specialist Group in Tectonics and Sructural Geology, Field Guide*, 1, 118 pp.

Powell, C.McA. & Rickard, M.J., 1985. Significance of the early foliation at Bermagui, N.S.W., Australia. *Journal of Structural Geology*, 7, 385–400.

Powell, C.McA., Edgecombe, D.R., Henry, N.M. & Jones, J.G., 1976. Timing of regional deformation of the Hill End Trough: a reassessment. *Journal of the Geological Society of Australia*, 23, 407–421.

Price, N.J. & Cosgrove, J. W., 1990. *Analysis of Geological Structures*. Cambridge University Press, Cambridge, 502 pp.

Price, N.J. & Hancock, P.L., 1972. The development of fracture cleavage and kindred structures. *24th International Geological Congress (Canada) Proceedings*, section 3, 584–592.

Priest, S.D. & Hudson, J.A., 1976. Discontinuity spacings in rock. *International Journal of Rock Mechanics, Mining Science and Geomechanics Abstracts*, 13, 135–148.

Prior, D.J., 1987. Syntectonic porphyroblast growth in phyllites: textures and processes. *Journal of Metamorphic Geology*, 5, 27–39.

Ramsay, J.G., 1981. Tectonics of the Helvetic nappes. *In* McClay, K. & Price, N.J. (Editors). Thrust and nappe tectonics. *Geological Society Special Publication*, 9, 293–309.

Ramsay, J.G., 1982. Variations in linear and planar fabrics in the Western Helvetic nappes, Switzerland. *Mitteilungen aus dem Geologischen Institut der Eidgenossischen Technischen Hochschule und der Universität Zürich, Neue Folge*, 239a, 230–232 & 231a.

Ramsay, J.G. & Graham, R.H., 1970. Strain variation in shear belts. *Canadian Journal of Earth Sciences*, 7, 786–813.

Ramsay, J.G. & Huber, M.I., 1983. *The techniques of modern structural geology, vol 1: strain analysis*. Academic Press, London, 307 pp.

Ramsay, J.G. & Huber, M.I., 1987. *The techniques of modern structural geology, vol. 2: folds and fractures*. Academic Press, London, 309–700 pp.

Rathore, J.S. & Henry, B., 1982. Comparison of strain and magnetic fabrics in Dalradian rocks from the southwest Highlands of Scotland. *Journal of Structural Geology*, 4, 373–384.

Rawnsley, K.D., Rives, T., Petit, J.-P., Hencher, S.R. & Lumsden, A.C., 1992. Joint development in perturbed stress fields near faults. *Journal of Structural Geology*, 14, 939–951.

Reks, I.J., & Gray, D.R., 1982. Pencil structure and strain in weakly deformed mudstone and siltstone. *Journal of Structural Geology*, 4, 161–176.

Richert, J.P., 1974. Les relations entre les niveaux supérieurs de la schistosité et l'anchimétamorphisme (abstract). *2e Réunion annuelle de Sciences de la Terre*, Nancy 1974, p.327.

Rickard, M.J., 1961. A note on cleavages in crenulated rocks. *Geological Magazine*, 98, 324–332.

Rixon, L.K., Bucknell, W.R. & Rickard, M.J., 1983. Mega kink folds and related structures in the Upper Devonian Merrimbula Group, south coast of New South Wales. *Journal of the Geological Society of Australia*, 30, 277–293.

Roberts, J.L., 1989. *A field guide to geological structures*. Macmillan, London, 250 pp.

Rutter, E.H., Maddock, R.H., Hall, S.H. & White, S.H., 1986. Comparative microstructures of natural and experimentally produced clay-bearing fault gouges. *Pure & Applied Geophysics*, 124, 3–30.

Schweizer, J. & Simpson, C., 1986. Cleavage development in dolomite of the Elbrook Formation, southwest Virginia. *Geological Society of America Bulletin*, 97, 778–786.

Shaw, D.M. 1957. Some recommendations regarding metamorphic nomenclature. *Geological Association of Canada, Proceedings*, 9, 69–81.

Siddans, A.W.B., 1972. Slaty cleavage—a review of research since 1815. *Earth-Science Reviews*, 8, 205–232.

Siddans, A.W.B., 1977. The development of slaty cleavage in a part of the French Alps. *Tectonophysics*, 39, 533–557.

Siddans, A.W.B., 1979. Deformation of muddy rocks at low metamorphic grade. *In* Easterling, K.E., (editor), *Mechanisms of deformation and fracture*. Pergamon, Oxford, 195–202.

Siddans, A.W.B., Henry, B., Kligfield, R., Lowrie, W., Hirt, A. & Percevault, M.N., 1984. Finite strain patterns and their significance in Permian rocks of the Alpes Maritimes (France). *Journal of Structural Geology*, 6, 339–368.

Simon, R.I. & Gray, D.R., 1982. Interrelations of mesoscopic structures and strain across a small regional fold, Virginia Appalachians. *Journal of Structural Geology*, 4, 271–289.

Simpson, C., 1986. Fabric development in brittle-to-ductile shear zones. *Pure & Applied Geophysics*, 124, 269–288.

Skempton, A.W., 1964. Long-term stability of clay slopes. *Geotechnique*, 14, 77–01.

Sorby, H.C., 1857. On some facts connected with slaty cleavage. *Report of the 27th meeting of the British Association for the Advancement of Science,* (27th meeting 1857, published 1858), 92–93.

Soula, J.C. & Debat, P., 1976. Développement et caractères des litages tectoniques. *Bulletin de la Société géologique de France* (7), 18, 1515–1537.

Southwick, D.L., 1987. Bundled slaty cleavage in laminated argillite, north-central Minnesota. *Journal of Structural Geology*, 9, 985-993.

Spears, D.A., 1980. Towards a classication of shales. *Journal of the Geological Society (London)*, 137, 125–129.

Stephens, M.B., Glasson, M.J. & Keays, R.R., 1979. Structural and chemical aspects of metamorphic layering development in metasediments from Clunes, Australia. *American Journal of Science*, 279, 129–160.

Stockdale, P.B., 1922. Stylolites: their nature and origin. *Indiana University Studies*, 9, 1–97.

Suppe, J., 1985. *Principles of structural geology.* Prentice-Hall, New Jersey, 537 pp.

Talbot, J.L. & Hobbs, B.E., 1968. The relationship of metamorphic differentiation to other structural features at three localities. *Journal of Geology*, 76, 581–587.

Tapp, B.J. & Wickham, J., 1987. Relationships of rock cleavage fabrics to incremental and accumulated strain in the Conococheague Formation, U.S.A. *Journal of Structural Geology*, 9, 457–472.

Tobisch, O.T., Barton, M.D., Vernon, R.H. & Paterson, S.R., 1991. Fluid-enhanced deformation: transformations of granitoids to banded mylonites, western Sierra Nevada, California, and southeastern Australia. *Journal of Structural Geology*, 13, 1137–1156.

Turner, F.J., 1935. Metamorphism of the Te Anau Series in the region north-west of Lake Wakatipu. *Transactions of the Royal Society of New Zealand*, 65, 329–349.

Turner, F.J. & Weiss, L.E., 1963. *Structural analysis of metamorphic tectonites.* McGraw-Hill, New York, 545 pp.

Van Hise, C.R., 1896. Deformation of rocks—III. Cleavage and fissility. *Journal of Geology*, 4, 449–483.

Voisey, A.H., 1957. The Manilla Syncline and associated faults. *Journal & Proceedings of the Royal Society of New South Wales*, 91, 209–214.

Waldron, H.M. & Sandiford, M., 1988. Deformation volume and cleavage development in metasedimentary rocks from the Ballarat slate belt. *Journal of Structural Geology*, 10, 53–62.

Weaver, C.E., (editor), 1984. *Shale-slate metamorphism in Southern Appalachians.* Elsevier, Amsterdam, 239 pp.

Weber, K., 1976. Gefügeuntersuchungen an transversalgeschieferten Gesteinen aus dem östlichen Rheinischen Schiefergebirge (Ein Beitrag zur Genese der transversalen Schieferung). *Geologische Jahrbuch, Reihe D*, 15, 99 pp.

Weber, K., 1981. Kinematic and metamorphic aspects of cleavage formation in very low-grade metamorphic slates. *Tectonophysics,* 78, 291–306.

Weber, K., 1982. Microfabric of slates from the Rheinische Schiefergebirge. *In* Borradaile, G.J., Bayly, M.B. & Powell, C.McA., (editors), *Atlas of deformational and metamorphic rock fabrics.* Springer-Verlag, Berlin, plates 47–48, 136–139.

Weiss, L.E., 1972. *The minor structures of deformed rocks.* Springer-Verlag, Berlin, 431 pp.

White, S.H., Burrows, S.E., Carreras, J., Shaw, N.D. & Humphreys, F.J., 1980. On mylonites in ductile shear zones. *Journal of Structural Geology*, 2, 175-187.

White, S.H. & Johnston, D.C., 1981. A microstructural and microchemical study of cleavage lamellae in a slate. *Journal of Structural Geology*, 3, 279–290.

Williams, P.F., 1972. Development of metamorphic layering and cleavage in low grade metamorphic rocks at Bermagui, Australia. *American Journal of Science*, 272, 1–47.

Williams, P.F. & Price, G.P., 1990. Origin of kinkbands and shear-band cleavage in shear zones: an experimental study. *Journal of Structural Geology*, 12, 145–164.

Wilson, C.J.L. & Will, T.M., 1990. Slickenside lineations due to ductile processes. *In* Knipe, R.J. & Rutter, E.H., (editors), Deformation mechanisms, rheology and tectonics. *Geological Society Special Publication*, 54, 455–460.

Wilson, G., with Cosgrove, J.W., 1982. *Introduction to small-scale geological structures.* Allen & Unwin, London, 128 pp.

Witschard, M. & Dolan, J.F., 1990. Contrasting structural styles in siliciclastic and carbonate rocks of an off-scraped sequence: The Peralla accretionary prism, Hispaniola. *Geological Society of America Bulletin*, 102, 792–806.

Wood, D.S., 1974. Current views of the development of slaty cleavage. *Annual Review of Earth and Planetary Sciences,* 2, 369–401.

Yoshida, S., 1969. Structural analysis of the Paleozoic system in northeastern Tamba mountainous district, with special reference to folds and and cleavage. *Japanese Journal of Geology and Geography,* 40, 25–40.

Zhao, G. & Johnson, A.M., 1992. Sequence of deformations recorded in joints and faults, Arches National Park, Utah. *Journal of Structural Geology*, 14, 225–236.

Appendix A: Fissility dimension/crack -frequency relations

Because physical dimensions of fissility fragments are more directly measured and conceptualised than crack frequencies, we have adopted dimension as the preferred basis for describing fissility-ratios in this paper. However, in certain cases, such as where cleavage and bedding are oblique to one another, it is necessary to appreciate that the intensity of a particular set (parallel group) of cracks is more fundamentally described by its spatial frequency, a parameter which increases with increasing numbers of cracks of a particular set in a given volume of material. When two or more distinct sets of fractures exist, it is assumed that intensity measurements based on crack frequency of each set are independent of the intensity of other crack sets in the rock. Two other parameters related directly or indirectly to crack frequency are: (1) crack spacing and (2) fragment edge length. Of these two, crack spacing is the more fundamental and forms the basis of the *c-b-i* dimension system. This appendix presents notation for and relations between the different measurement systems so that conversions may freely be made one to the other, especially when the fissility planes are oblique to each other, as shown in Figure 3c.

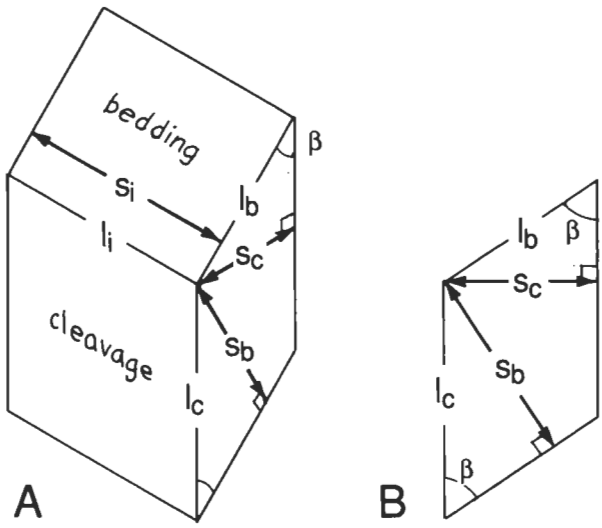

Figure A1. A—Edge lengths (l) and crack normal spacings (s) for a monoclinic fissility-fragment of bedding/cleavage angle β. B—Relationships between l and s in the plane normal to the bedding/cleavage intersection.

Let the *frequency* (f) of a set of subparallel cracks be the number of cracks of that set per unit distance normal to the cracks over some representative distance interval. Then the average *normal spacing* (s) of consecutive cracks over the same interval is the inverse of the crack frequency: $s = 1/f$.

Consider now a notional monoclinic parallelepiped bounded by pairs of cracks belonging to three crack sets where the crack pairs have normal spacings equal to the average normal spacings of the respective sets. In a physical sense, this solid represents the average three-dimensional morphology of fissility fragments in a particular outcrop. The three crack sets considered are:

(1) cleavage plane cracks (denoted by subscript c),

(2) bedding plane cracks (denoted by subscript b), and

(3) cross cracks normal to the cleavage-bedding intersection (subscript i), as shown in Figure A1A. Then

$$f_c = 1/s_c,$$
$$f_b = 1/s_b,$$
$$f_i = 1/s_i. \quad \text{(A1)}$$

Let the *edge lengths* (l) of the parallelepiped normal to the cleavage-bedding intersection be l_c and l_b in the cleavage and bedding planes, respectively, and let l_i be the edge length in the intersection direction. The edge lengths are related to normal spacings as shown in Figures A1A and B and by the relations:

$$s_c = l_b \sin\beta,$$
$$s_b = l_c \sin\beta,$$
$$s_i = l_i, \quad \text{(A2)}$$

where β is the angle between the bedding and cleavage planes.

Defining relative crack frequency (R) as the fundamental measure of relative crack intensity, the relative *crack frequency ratios* of the three crack systems are

$R_{cb} \equiv f_c / f_b$, (cleavage/bedding frequency ratio)

$R_{ci} \equiv f_c / f_i$, (cleavage/cross-intersection frequency ratio)

$R_{bi} \equiv f_b / f_i$.
(bedding/cross-intersection frequency ratio) (A3)

We introduce the following simplified notation for measurement purposes:

$$c \equiv s_b,$$
$$b \equiv s_c,$$
$$i \equiv s_i, \quad \text{(A4)}$$

the ratios of which are the *fissility dimension-ratios* referred to in the paper. Combining A1 to A4 yields equivalencies for these ratios as follows:

$c/b = Rcb = sb / s_c = l_c / l_b$,
(cleavage/bedding dimension-ratio)

$i/b = R_{ci} = s_i / s_c = l_i / l_b \sin\beta$,
(intersection/bedding dimension-ratio)

$i/c = R_{bi}\ s_i / s_b = l_i / l_c \sin\beta$.
(intersection/cleavage dimension-ratio) (A5)

Hence, c/b can be measured directly as the ratio of edge lengths in the cleavage and bedding directions. i/b and i/c, however, require either trigonometrically adjusted edge lengths or projections of edge lengths as seen when the fragment is viewed in the direction of the third edge. An example of projected edge length ratio would be the ratio (i/b) of the edges seen when simultaneously looking down the cleavage and cross crack planes; the resulting measurement is equivalent to the ratio of the normal spacings of the cross cracks and cleavage cracks.

When the angle β in Figure A1A is 90°, the dimension-ratios (A5) are reduced to

$$c/b = l_c / l_b,$$
$$i/b = l_i / l_b,$$
$$i/c = l_i / l_c, \quad \text{(A6)}$$

as shown in Figure 3a.

When 60° < β < 90°, (A6) may be assumed as approximations since the trigonometric adjustments are then no more 13%.

When 0° < β < 30° approximately, the bedding and cleavage fabrics may no longer be independent and so interpretation becomes problematical.

Finally, when β = 0°, cleavage no longer exists as a fabric separate from bedding; therefore c does not exist and fragment shape must be represented with the aid of edge length normal to bedding instead of c.

Appendix B: Tables

Table 1. Data for "Manilla mudstone field" fissility samples in Figure 12.

Series no.	*Sample*	*Grid ref.*[1]	*Formation*	*Rock type*[2]	*Fissility c/b*	*Ratios i/b*	*Structure*[3] S_0	I_1	S_0^S_1
Progression series samples (Figs. 10, 11)									
1	K89–19	2763566126	Lowana	M	0.3	1	160 15W	—	—
2	K89–10.2	2578 65867	Namoi	Z	0.5	2.5	150 45E	338 8	60
3	M90–12.1	2815 66077	Lowana	M	1	3.5	025 8E	178 3	90
4	M90–20.2	2840 66090	Noumea	M	1.6	4	130 42E	000 40	40
5	M90–17.7	2857566093	Noumea	mfS	5	5	102 62N	345 60	85
6	K89–26.2	2903566081	Namoi	Z	7	12	085 70S	218 65	70
Strain samples (Table 2)									
Wim.	M91–14	2742 66070	Lowana	M	0.7	1.6	042 6E	166 2	85
Bor.	M90–1	2691 66100	Mandowa	M	0.8	1.6	025 15E	163 10	65
Tam.	K89–2	2965 65560	Mandowa	Z	1.3	3	140 12E	340 4	75
Other samples									
	K89–10.1	2578 65867	Namoi	M	0.3	1.4	150 40E	350 16	—
	K89–5.1a	2668 65740	Namoi	M	0.6	1.8	160 13W	160 0	70
	K89–5.1b	,,	,,	,,	0.9	3	,,	,,	,,
	K89–20	2732566197	Noumea	Z/M	0.6	3	000 12E	165 4	88
	K89–21a	2849 66123	Noumea	mS	3	4	015 40E	162 25	50
	K89–24	2859 66065	Lowana	Z	4	3.5	145 60E	338 25	45
	K89–26.1	2902566080	Namoi	Z	3.5	7	095 53S	193 52	66
	K89–22	2848 66149	Noumea	sM	7	7	170 20E	150 10	40

[1] Australian Map Grid, Zone 56J.

[2] Field-identified rock types: M — mudstone, Z — siltstone, S — sandstone, m — muddy, s — sandy, fs — fine sandy (c.f. Folk, 1980, p.25–28).

[3] Structural data (degrees): S_0 — bedding (strike, dip), I_1 — bedding/cleavage intersection (azimuth, inclination), S_1 — cleavage, ^ — "angle from" (in mudstone).

Table 2. Correlation of mudstone fissility-ratios and stretch-ratios in the plane of bedding, Manilla–Tamworth district, NSW. Stretch-ratios determined by Breddin method from *Leptophloeum australe*.

Location: sample:		*"Wimborne" M91–14*		*Borah Creek M90–1*		*Tamworth Council Quarry K89–2*	
Fissility–ratios							
c/b ± s.e.	(*n*)	0.66 ± 0.01	(2)	0.79 ± 0.13	(2)	1.3 ± 0.27	(2)
i/b ± s.e.	(*n*)	1.64 ± 0.23	(5)	1.60 ± 0.16	(5)	3.0 ± 0.68	(5)
Stretch–ratios							
$R(S_0)$ ± s.e.	(*n*)	1.20	(1)	1.21 ± 0.03	(5)	1.6	(4)
$\phi(S_0)$^I_1		+1° ± 2°		+5° ± 5°		assumed 0°	

I_1: bedding/cleavage intersection. $R(S_0)$: stretch-ratio on bedding. $\phi(S_0)$: major principal strain axis on bedding, measured anticlockwise positive relative to locality average cleavage trace. *n*: number of mean estimates (of fissillity-ratio) or specimens (for stretch-ratio). s.e.: standard error. ^: "angle from". (See Table 1 for further information.)

Table 3. Comparison of fissility-ratios in three rock types, Borah Creek, Manilla, NSW. (See Table 2 for symbols.)

		Mudstone		*Muddy sandstone*		*Argillite*	
c/b ± s.e.	(*n*)	0.79 ± 0.13	(2)	0.85 ± 0.17	(4)	1.69 ± 0.21	(5)
i/b ± s.e.	(*n*)	1.60 ± 0.16	(5)	1.52 ± 0.33	(5)	5.0 ± 0.8	(6)
S_0^S_1		65°		85°		75°–90°	

Table 4. Correlation of fissility-ratios with dimensional ratio and stretch-ratio data for "pencil structure" in Reks & Gray (1982, Figs 2, 3 & 14).

Reks & Gray data				*Our estimates*		*R & G.*
Figure	*View*	*Locality*	*l/w ratio*	*i./b*	*c/b*	*Y/Z*
i/b — l/w correlation from outcrop photographs						
2a	↑↑ I_1	158	15.6	10	2	
2b	⊥ S_0	17 (2)	13.4	7.5	0.5 ?	
2c	⊥ S_0	21	19.8	12		
3a	loose	21	19.8	15		
3b	loose	17 (2)	13.4	10		
3c	⊥ S_0	57	10.4	4	0.4 ?	
	(linear best-fit correlation: i/b = 0.92 *l/w* — 4.4, corr. coeff. = 0.92)					
i/b — Y/Z correlation from best-fit relation						
14		66	9.8	4.6		1.10
14		158	15.6	10.0		1.20
14		35	19.0	13.1		1.27
14		36 (2)	19.2	13.3		1.26
14		21	19.8	13.8		1.30
14		53	23.0	16.8		1.35

I_1: intersection lineation direction. S_0: bedding. *l/w*: Reks & Gray projected intersection length/width parameter. *i/b:* Durney & Kisch intersection/bedding parameter. *Y/Z*: intermediate/least principal stretch-ratio, approx. parallel to bedding (inferred from pressure-shadow extension strains normal to bedding).

Editorial invitation: Supporting comments or counter-arguments relating to the above paper would be welcome for publication as *Discussion*.

AGSO Journal of Australian Geology & Geophysics, 15 (3), 297–312 © Commonwealth of Australia 1994

Early, methane-rich fluids and their role in Archaean gold mineralisation at the Sand King and Missouri deposits, Eastern Goldfields Province, Western Australia

T.P. Mernagh[1] & W.K. Witt[2]

The Sand King and Missouri lode gold deposits in the Siberia district of the Eastern Goldfields Province are situated within an amphibolite-facies metamorphic aureole in deformed greenstones flanking a monzogranitic batholith, which crops out less than 1 km to the west. The Missouri deposit was mined from 1899 to 1912 and again in 1987–1988 and produced approximately 921 kg of gold. The Sand King mine has produced about 4000 kg of gold since 1980. Gold occurs in the margins of the quartz (–biotite–pyrite) veins and in the alteration assemblage adjacent to the vein systems. Fluid inclusions in quartz and carbonate veins from both deposits have been studied by microthermometry and Raman spectrometry and have been classified into six types according to their chemical composition. The vapour phase of Type I inclusions contains pure or nearly pure CH_4 and the liquid-rich inclusions which appear least likely to have leaked contain up to 5 mole% CH_4 and 95 mole% H_2O. Rare Type II inclusions are multiphase and contain approximately equal amounts of CO_2 and CH_4 in the vapour phase. They may also contain up to four solid phases, of which muscovite and carbonate have been identified by Raman spectroscopy. Type III inclusions may also contain a muscovite daughter crystal, but have highly variable vapour contents and CO_2/CH_4 ratios. Type IV inclusions are CO_2-rich and may be either monophase or occur as liquid + vapour CO_2 ($\pm H_2O$) at room temperature. Type V inclusions are aqueous inclusions with an average salinity of 5.8 equiv. wt.% NaCl, and Type VI are high salinity inclusions (~27 equiv. wt.% $CaCl_2$) that may contain halite and two other unidentified solids.

The textural evidence suggests that Type I inclusions were trapped in the early phases of mineralisation at both the Sand King and Missouri deposits, around 500 to 600°C and 3–4 kbar. The fluid inclusions also provide evidence for mixing of the CH_4-rich Type I fluid with a CO_2-rich fluid. The latter may be related to a pervasive synmetamorphic fluid responsible for regional carbonation of the deformed metavolcanic rocks. Heterogeneous trapping is thought to be largely responsible for the variation in vapour content and CO_2/CH_4 ratio in inclusion Types II and III. The presence of muscovite as a daughter mineral in Types II and III links them to a potassic alteration event which is evident at both deposits. Type IV inclusions contain little or no detectable CH_4, which indicates that CO_2-rich fluids continued to circulate after most of the CH_4 and H_2 in the system had been consumed. The aqueous Types V and VI inclusions are thought to represent, respectively, late influx of meteoric waters and connate brines.

The early methane-bearing fluids indicate low fO_2 conditions, which may have been generated during the serpentinisation of nearby ultramafic rocks or, alternatively, could have been derived from a deep source in the crust or lower mantle. The addition of methane to the CO_2-rich ore-bearing fluid by fluid mixing greatly increases the field of fluid immiscibility over that of the conventional CO_2–H_2O–NaCl system. Thus, the fluid unmixes over a larger range of P–T conditions when methane is present and the sulphur content of the fluid diminishes as H_2S is strongly partitioned in the vapour phase during subsequent phase separation. These effects destabilise the auriferous sulphide ligands in solution and, hence, trigger gold precipitation. They may thus be important factors controlling gold precipitation under greenschist and amphibolite facies conditions.

Introduction

In recent years, it has become evident that Archaean lode-style gold deposits have formed over a wide temperature range and metamorphic grades from prehnite-pumpellyite to granulite facies. These observations have led to the suggestion of a continuum of gold deposit styles from shallow to deep crustal levels (Colvine et al. 1988; Foster 1989; Groves et al. 1992). Fluid inclusion and thermodynamic studies have documented a low-salinity H_2O–CO_2 fluid in many deposits hosted by greenschist-facies rocks (Smith et al. 1984; Robert & Kelly 1987; Ho et al. 1990), but data from higher grade rocks are relatively sparse. This paper presents the results of microthermometric and Raman microprobe analyses of fluid inclusions from amphibolite-facies-hosted deposits at Missouri and Sand King, in the Siberia district of the Eastern Goldfields Province, Western Australia. We have used these and other geological data to interpret the P–T–X evolution of the fluids from these two deposits and, in particular, present evidence for the existence of early methane-rich fluids.

Methane-bearing inclusions have been reported from a number of Archaean gold deposits of various metamorphic grades. $CO_2 \pm CH_4$ inclusions with rare thin water rims have been reported from the Wiluna deposit (Hagemann et al. 1992), which is a high crustal level deposit in prehnite-pumpellyite facies metamorphic terrain. Deposits in greenschist terrains which contain methane-bearing fluid inclusions include Lancefield, the Golden Mile, Mount Charlotte, Water Tank Hill and Granny Smith in the Yilgarn Block, Western Australia (Ho et al. 1990; Hagemann & Ridley 1993) and the McIntyre-Hollinger (Smith et al. 1984) and Sigma (Robert & Kelly 1987) mines in the Abitibi greenstone belt in Canada. Some very CH_4-rich ($X_{CH_4} \leq 0.8$) fluid inclusions have been observed in recent studies of the Corinthia-Hopes Hill, Marvel Loch, Three Mile Hill and Griffins Find deposits, which occur in amphibolite to granulite facies domains in the Yilgarn Block in Western Australia (Hagemann & Ridley 1993). It is also interesting to note that methane-bearing fluid inclusions and the widespread occurrence of graphite have been reported (Lapointe & Chown 1993) from the metamorphosed iron-formation of the Lac Lilos gold prospect in the Eastern Superior Province of the Canadian Shield. This prospect is in a granulite terrain and is thought to represent a deep-level expression of the crustal-scale mineralising systems documented for the late Archaean.

Regional geologic setting

The Sand King and Missouri deposits are in the Siberia district of the Eastern Goldfields Province (Fig. 1). The metavolcanic rocks in this district record four stages of deformation (Witt 1993a). The age of mineralised struc-

[1] Australian Geological Survey Organisation, GPO Box 378, Canberra ACT 2601, Australia.

[2] Geological Survey of Western Australia, 100 Plain Street, Perth, WA 6000, Australia.

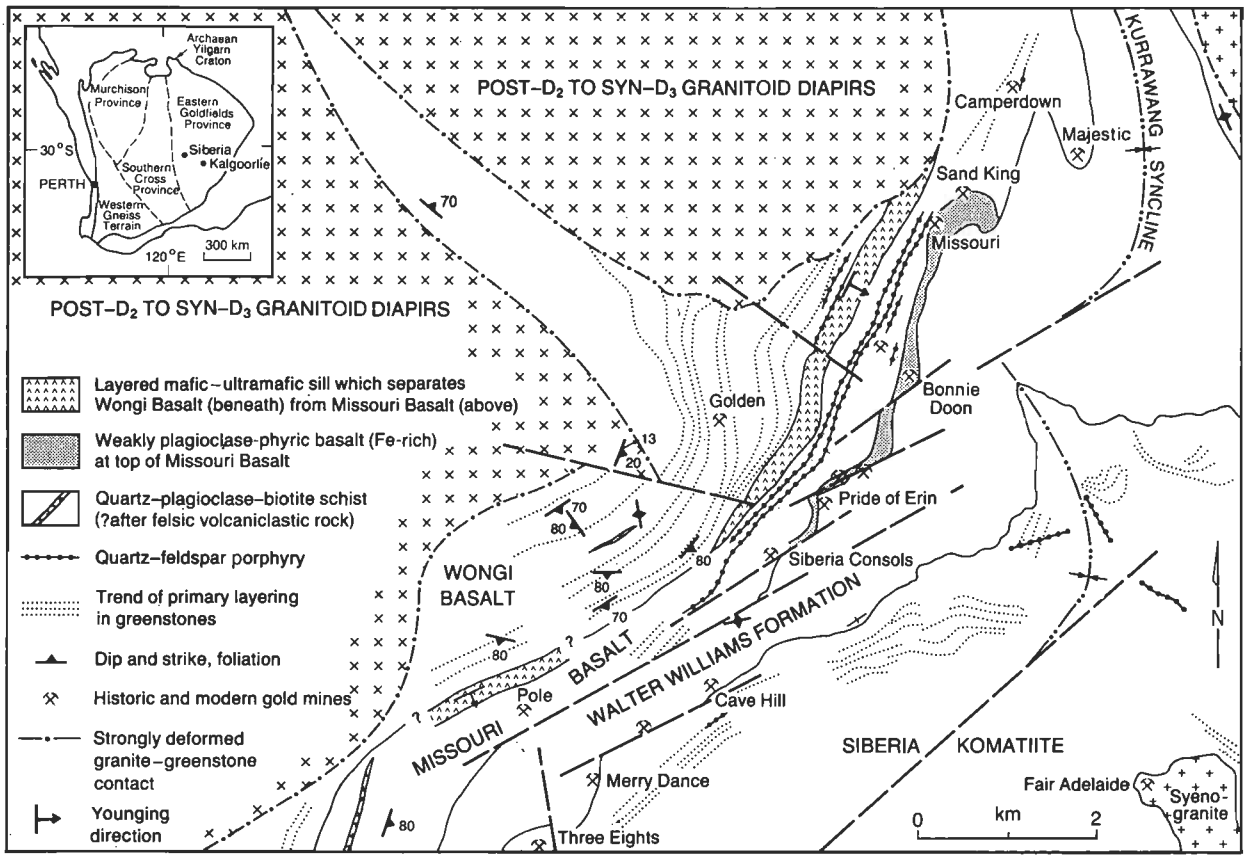

Figure 1. Geology and mines in the Siberia district, Eastern Goldfields Province.

tures is given by the timing of emplacement of the associated granitoid intrusion. The intrusion of monzogranitic diapirs to within 0.6 km of the deposits during D3 caused uplift and deformation of the metavolcanic rocks and generated the ductile to veined brittle-ductile shear zones which host the gold at Missouri and Sand King. Textural evidence from the mineralised structures and associated metasomatised host rock (Witt 1993a) indicates that auriferous fluids were introduced during this stage of deformation, and that high fluid pressures actively contributed to the formation of these structures.

Both deposits are hosted by fractionated Fe-rich tholeiitic basalt with small plagioclase phenocrysts. This pillowed basalt unit forms the uppermost part of the Missouri Basalt, which is locally interbedded with biotite–quartz–plagioclase schist with feldspar porphyroclasts. The Missouri Basalt is separated by a layered mafic/ultramafic sill from the underlying Wongi Basalt, and is overlain by olivine cumulates of the Walter Williams Formation and the Siberia Komatiite (Wyche & Witt 1992). The mafic rocks are strongly foliated in zones parallel to the monzogranite/greenstone contacts and a broad amphibolite-facies metamorphic aureole is developed over several kilometres adjacent to the contact. Small quartz–feldspar porphyry intrusions are generally conformable with primary layering in the greenstones and may be genetically related to late monzogranite intrusions (Witt 1992). An undeformed 080°-trending dolerite dyke south of the Missouri deposit forms part of the Proterozoic Widgiemooltha Dyke Suite (Myers 1990).

Most epigenetic lode gold deposits in the Eastern Goldfields Province with associated sericite–ankerite alteration are interpreted to have formed at 250–350°C and 1.5–2.5 kbar (Groves 1993). Deposits of this type include those along strike from the Siberia deposits (e.g. Ora Banda, Grants Patch, and Mount Pleasant), which formed more or less contemporaneously with Sand King and Missouri, during the final stages of regional deformation (Witt 1993a). Sand King and Missouri occur 3–5 km stratigraphically below these typical 'epigenetic' deposits, and at slightly deeper structural levels. Therefore, the Sand King and Missouri deposits are estimated to have formed at approximately 3–4 kbar. Biotite-dominant alteration assemblages at Siberia record temperatures between 440 and 600°C (Witt 1991). The relatively high alteration temperatures are considered to reflect proximity to the adjacent synmetamorphic monzogranite intrusions as well as deeper structural levels. The available geochronological data indicate that most granitoids were emplaced by the time of peak metamorphism at about 2.66 Ga, but that gold mineralisation did not occur until 2.63 Ga (McNaughton et al. 1993).

A prolonged period of post-cratonisation weathering has led to the development of a thick laterite profile, typically consisting of ferruginous, mottled and saprolite zones (Smith 1983), in parts of the Siberia district. Although the modern open pits at Missouri and Sand King have won gold from unweathered Archaean rocks, much of the historic mining in the Siberia district exploited supergene gold in the laterite profile.

Missouri

The Missouri deposit (Fig. 2) produced 20.8 kg of gold between 1899 and 1912 in workings to a depth of

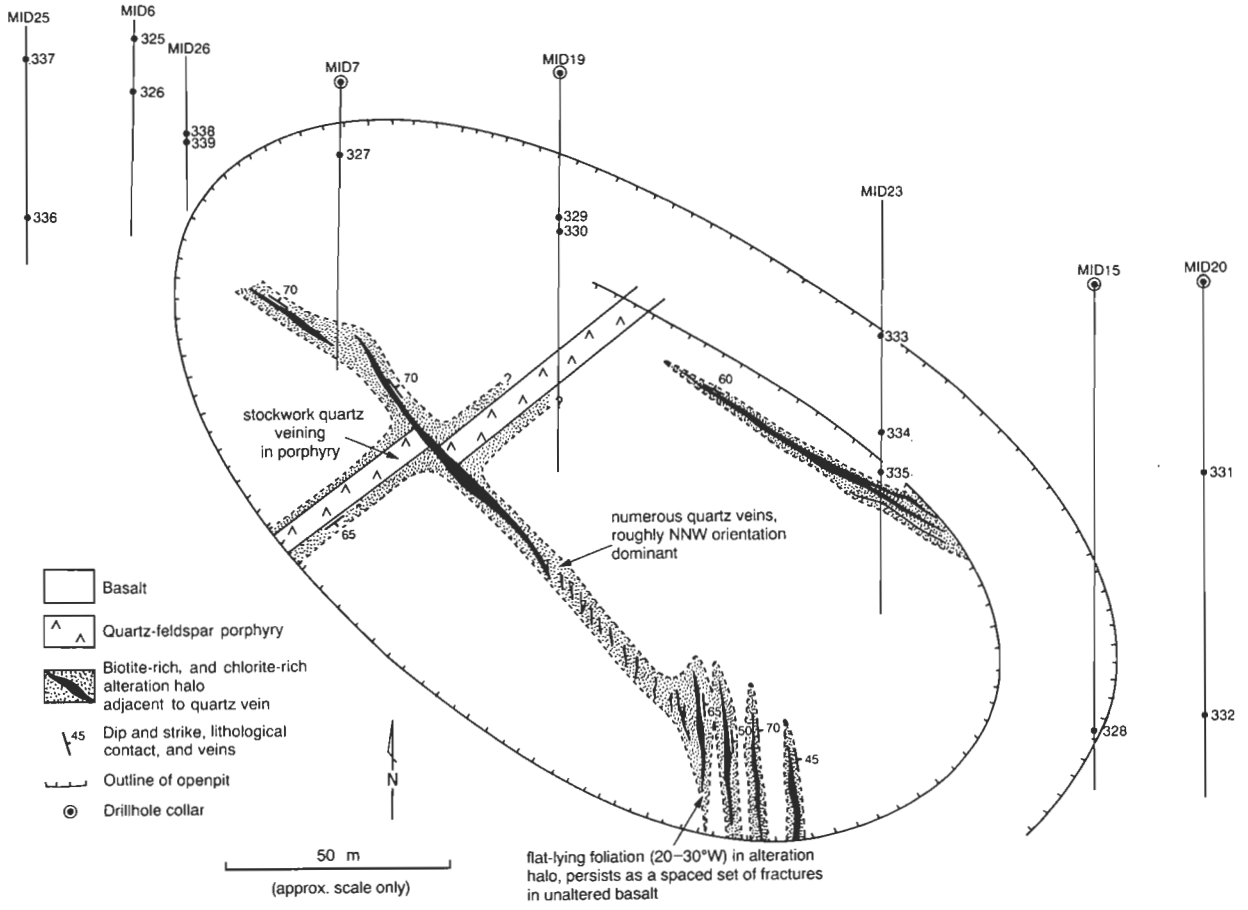

Figure 2. Geological plan of the Missouri open pit, showing the position of drill-holes and samples projected to the surface. Most drill-holes are inclined ~60° S.

approximately 100 m (Montgomery 1909). Further open pit mining during 1987 and 1988 produced approximately 900 kg Au (Witt 1993b). The mineralisation occurs in a 0.5–2 m wide, northwest-trending zone of quartz veins with minor ductile deformation and hydrothermal alteration in the adjacent host rocks. The mineralised zone dips approximately 70° northeast, but breaks up into several en echelon veins at the southeastern end of the open pit. These en echelon veins strike 345–355° and dip 45–70° northeast, consistent with dextral displacement and northeast-side-up movement.

Quartz(–plagioclase)–biotite–carbonate–pyrite alteration assemblages are developed adjacent to quartz veins. Oriented biotite grains locally define a weak shear fabric parallel to the quartz veins. Pyrite occurs as coarse (≤2 mm), idioblastic grains with small biotite-rich pressure shadows. The biotite-rich alteration assemblage is enveloped by a mildly chloritic outer alteration halo of a similar width, and minor late chlorite overprints biotite and the shear fabric in the inner alteration zone.

Sand King

The Sand King deposit (Fig. 3) has produced about 4000 kg of gold since 1980, but contains an underground resource, as yet unmined, of approximately 4500 kg of gold (Witt 1993b). Quartz–feldspar porphyry dykes, varying in width from 0.5 to 5 m, intrude the basalt and are flanked by barren, sulphide-absent biotitic alteration (Hill & Bird 1990). Sinistral north–south faults, 1 to 6 m wide, offset some of the porphyry dykes and are cross-cut by the mineralised vein system. A northeast-trending and northwest-dipping fault (not shown in Fig. 3) along the southern wall of the open pit appears to have controlled formation of the mineralised veins (Hill & Bird 1990).

The ore is hosted by zones of quartz (–biotite–pyrite) veins and breccias, which trend 090–060° and dip 70–80°N. Individual quartz veins vary from 1 mm to >5 m wide and the en echelon arrangement of the quartz veins defines a broad 050° trend. Best gold grades (up to 11 g/t) occur in the basaltic rocks adjacent to the porphyry intrusions and at intersections of the mineralised zone with north–south faults. Gold occurs at the margins of the quartz(–biotite–pyrite) veins and in the 0.5–2 m wide biotite–plagioclase–pyrite(–pyrrhotite) alteration assemblage adjacent to the vein systems. Gold occurs mainly as inclusions and in fractures within pyrite. Other sulphides (galena, chalcopyrite, sphalerite) and tellurides (hessite, petzite, altaite, tellurobismuthite, melonite), freibergite, and scheelite occur in minor quantities (Hill & Bird 1990). Minor fuchsite occurs in some quartz veins, and quartz–amphibole veins with amphibole-rich alteration selvages occur locally. Grossularite garnet has been observed in veins and alteration selvages towards the western end of the system, which lies close to the contact with one of the monzogranite plutons.

Analytical procedures

All analytical work was carried out at the Australian

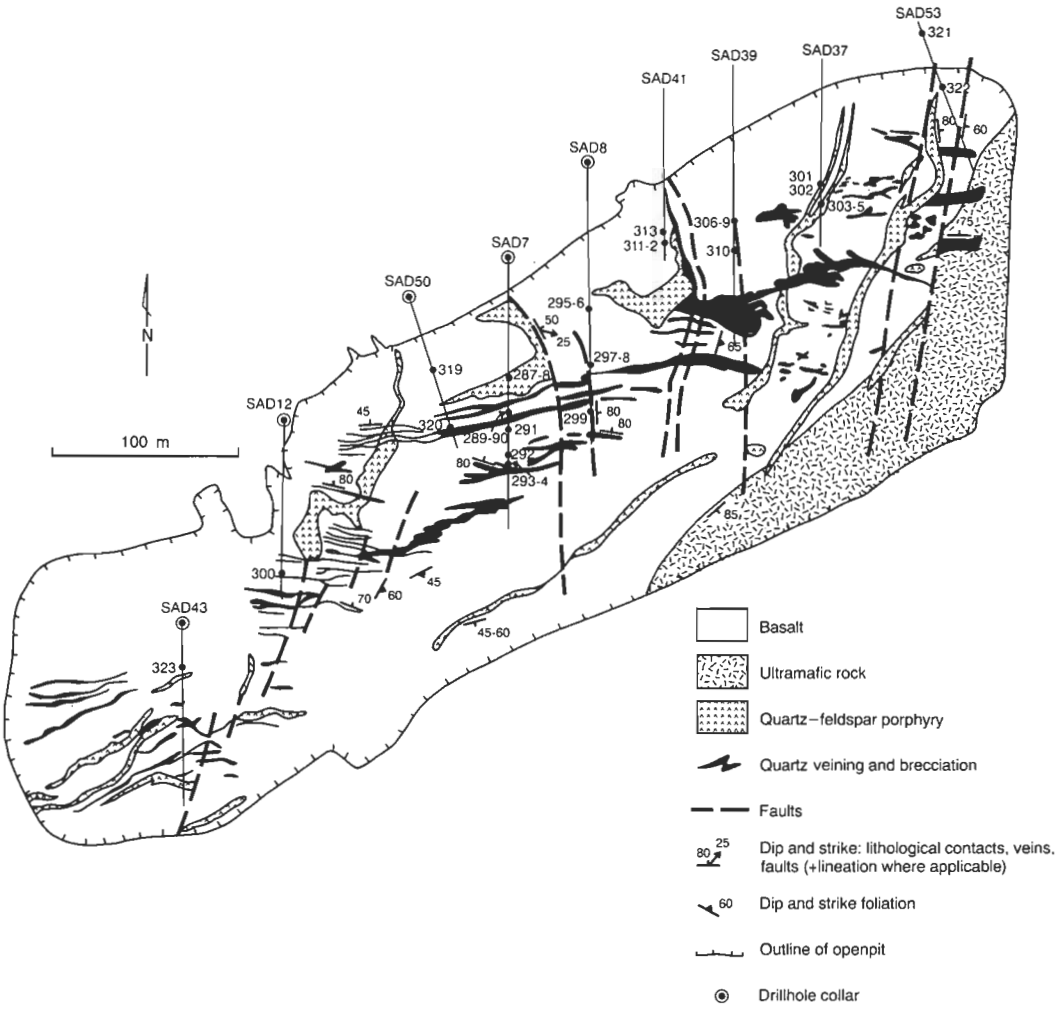

Figure 3. Geological plan of the Sand King open pit mine (after Bird & Pilapil 1988), showing the position of drill-holes and samples projected to the surface. Most drill-holes are inclined ~60° S.

Geological Survey Organisation's fluid-inclusion laboratories. Thermometric data were obtained from a Fluid Inc.-adapted USGS gas-flow system (Woods et al. 1981; Shepherd et al. 1985) and also from a Linkam heating–freezing stage (Shepherd et al. 1985) fitted to the microscope stage of the Raman microprobe. Both systems were calibrated with the same set of synthetic fluid inclusions (manufactured by Synflinc Ltd). Freezing measurements are estimated to be accurate to ± 0.5°C, while homogenisation temperatures have an estimated accuracy of ± 5°C.

Raman microprobe analyses were obtained from a Microdil 28 spectrometer (Liu & Mernagh 1990), using 40 mW (at the sample) of 514.5 nm laser excitation from a Spectra Physics 2020 5W Ar^+ laser. Spectra were typically obtained after 10 accumulations with a 5 second integration time and an approximately 5 cm^{-1} spectral bandpass. The Raman spectra were calibrated using Ar^+ plasma and neon emission lines; wave numbers were measured from the position of the peak maximum and are accurate to ± 1 cm^{-1}. The ratios of gases in the vapour phase were calculated using the method described by Dubessy et al. (1989) and the following 'quantification factors' were calculated as outlined in Pasteris et al. (1988): CO_2 = 1.3; N_2 = 1.0; H_2S = 6.4; CH_4 = 7.6 and C_2H_6 = 13.0. Raman detection limits are dependent on instrumental sensitivity and the partial pressure of each gas, but are estimated to be about 0.15 MPa for CO_2, O_2, N_2 and 0.03 MPa for H_2S and CH_4 under the conditions of this study. The salinity of carbonic inclusions was determined from the Raman spectra of the aqueous phase, using the skewing parameter method of Mernagh & Wilde (1989), which allows salinities to be determined to within ± 2 equivalent weight per cent NaCl.

Nature and occurrence of fluid inclusions

Fluid inclusions were examined in 20 doubly polished sections of quartz (± carbonate) veins selected from 38 samples of drill core from the Sand King deposit and in 8 doubly polished sections chosen from 15 samples of drill core from Missouri. Drill holes from which samples were collected are projected onto near-surface pit geology in Figures 2 and 3.

Two types of quartz are distinguished in the mineralised veins. The first and apparently earliest type of quartz shows undulose extinction, indicating limited amounts of ductile deformation. This 'relic' quartz contains dense populations of dominantly vapour-rich fluid inclusions. The second type occurs as sub-grains, mainly around the margins of the larger 'relic' grains of quartz and near the margins of the veins with wall rock. This recrystallised quartz is relatively unstrained. Most pre-existing fluid

inclusions were probably degraded during dynamic recrystallisation (Wilkins & Barkas 1978) and this later generation of quartz is characterised by relatively few small inclusions (generally <5 μm) near grain boundaries, except for grains with inclusions trapped in late secondary fractures.

Short, discontinuous, healed fractures, typically outlined by vapour-rich fluid inclusions, are observed in both types of quartz. They are generally parallel or subparallel to the vein walls and may cut across grain boundaries. In some samples, a second set of healed fractures with generally smaller aqueous inclusions is observed to intersect the other fractures at approximately 90°. A series of late secondary aqueous inclusions forms relatively continuous, cross-cutting trails. The relationships described suggest alternating periods of brittle and ductile deformation in a dynamic tectonic environment (cf. Robert & Brown 1986), although the mineralised vein system formed in a predominantly brittle deformation regime (Witt 1993b).

The fluid inclusions have been classified according to their composition, determined by microthermometry and Raman microprobe analyses (Table 1).

Type I inclusions (CH_4–H_2O)

These inclusions have negative crystal to irregular shapes and contain CH_4 as the dominant constituent of the vapour phase. Sizes vary up to about 20 μm, but most are only a few micrometres across. Trace amounts of CO_2 (<5 mole%) were detected by Raman spectroscopy in a small number of vapour-rich inclusions from this group. Some inclusions contain between 50 and 90 volume per cent liquid water, but others appear to contain only methane at room temperature (Figs 4A and 5). The range of observed H_2O/CH_4 ratios could be accounted for by invoking post-entrapment changes (Hollister 1990; Bakker & Jansen 1990), resulting in the loss of H_2O via mechanisms similar to those proposed for CO_2 rich inclusions (see below).

The CH_4-rich phase in these inclusions homogenised to liquid or by critical behaviour at temperatures from −87.9 to −71.8°C (Fig. 6A). The majority of inclusions showed homogenisation temperatures for the CH_4-rich phase which were slightly above the critical temperature of CH_4 (−82.6°C), indicative of the presence of minor amounts of CO_2. However, the data of Donnelly & Katz (1954) indicate that X_{CO_2} lies in the range 0 to 0.05 and the CO_2/CH_4 ratio could be even lower as CH_4 is selectively partitioned into the clathrate phase (Ramboz et al. 1985; Seitz et al. 1987), which was present or assumed to be present in all Type I inclusions at the temperature of homogenisation of the carbonic phase.

The small size of the inclusions made it difficult to observe the final melting temperature of clathrate, but several water-rich inclusions showed clathrate melting between 14 and 16°C. The final melting point of ice could not be observed, owing to the presence of clathrate in the water-rich inclusions. However, the salinities determined from the Raman spectra of the aqueous phase were generally below 3 equivalent wt % NaCl in the liquid at room temperature (Fig. 7). Inclusions that were not monophase at room temperature generally decrepitated before total homogenisation, but a few were observed to

Table 1. Summary of fluid-inclusion properties.

Deposit	*Inclusion Type*	*Size Range (μm)*	*Volume % Vapour*	*Mole % CO_2 in the Vapour*	*Mole % CH_4 in the Vapour*	*Mole % H_2S in the Vapour*	*Tm [a] (°C)*	*Tm [b] Clath.*	*Salinity [c]*	*Th [d] Carb.*	*Th [e] Total*
Missouri	I	<1–20	10–50	n.d. [f]	100	n.d.			1.1±0.4	−82.7±0.5	338±48
Missouri	I	<1–20	90–100	<5	95–100	n.d.					
Sand King	I	<1–20	10–20	n.d.	100	n.d.		15±1	1.3±0.5	−79±4	
Missouri	II	<1–40	50–100	41–65	35–59	0.4	−64.5±1.3		14±7	−4.6±5.8	302±22
Sand King	II	<1–12	50–90	41–73	27–59	n.d.	−63.0±0.4	13±4	15±6		316±26
Missouri	III	<1–20	40–100	10–88	12–90	n.d.	−66.1±2.9	13±1	4.8±1.4	−3.2±6.2	305±18
Sand King	III	<1–22	20–100	5–94	6–95	n.d.	−65.3±2.2	11±3	3.5±0.9		286±44
Missouri	IV	<1–40	40–95	88–100	0–12	n.d.	−56.9±0.4	8.6±0.5	1.1±0.8	21±4	289±29
Sand King	IV	<1–20	40–95	79–100	0–21	n.d.	−59.1±1.8	11.5±1.4	1.9±0.9	10±10	323±27
Missouri	V	<1–50	5–10	n.d.	n.d.	n.d.	−2.4±1.2	n.d.	4.0±1.5	n.d.	191±25
Sand King	V	<1–20	5–10	n.d.	n.d.	n.d.	−3.3±1.2	n.d.	5.8±1.5	n.d.	132±56
Missouri	VI	<1–50	5–10	n.d.	n.d.	n.d.	−28.7±9.1	n.d.	28.4±10.8	n.d.	105±24
Sand King	VI	<1–30	5–10	n.d.	n.d.	n.d.	−30.9±8.5	n.d.	29.8±9.6	n.d.	85±23

[a] Melting temperature of solid CO_2 in Types I–IV and the melting temperature of ice in Types V–VI. The results are given as an average followed by the standard deviation.

[b] CO_2±CH_4 clathrate melting temperature (°C).

[c] Fluid salinity in equivalent weight per cent NaCl, determined by Raman spectroscopy.

[d] Homogenisation temperature (°C) of the carbonic (CH_4 or CO_2 or both) phase.

[e] Total homogenisation temperature of the fluid inclusion (°C).

[f] n.d. = not detected.

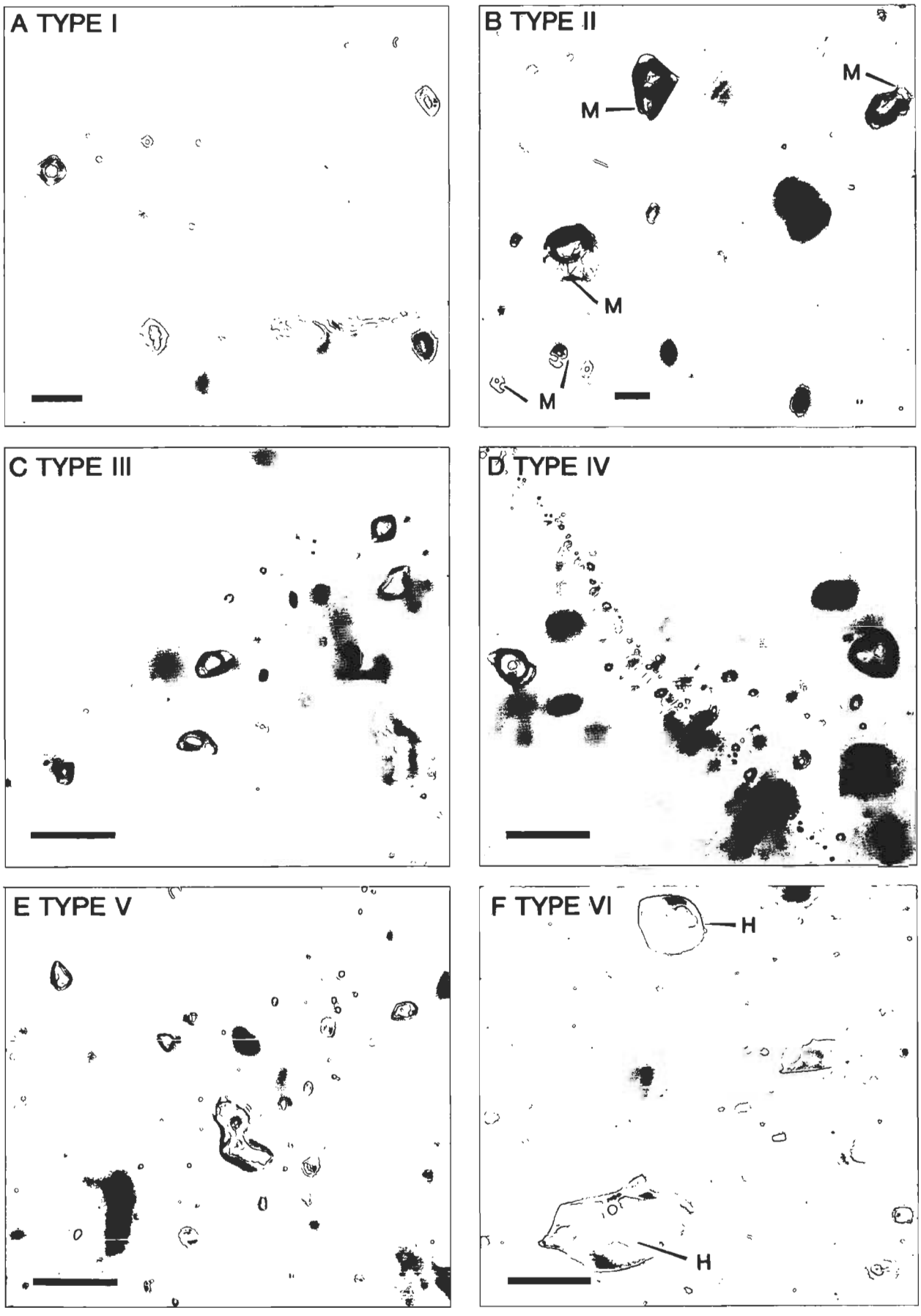
A TYPE I
B TYPE II
M
M
M
M
C TYPE III
D TYPE IV
E TYPE V
F TYPE VI
H
H

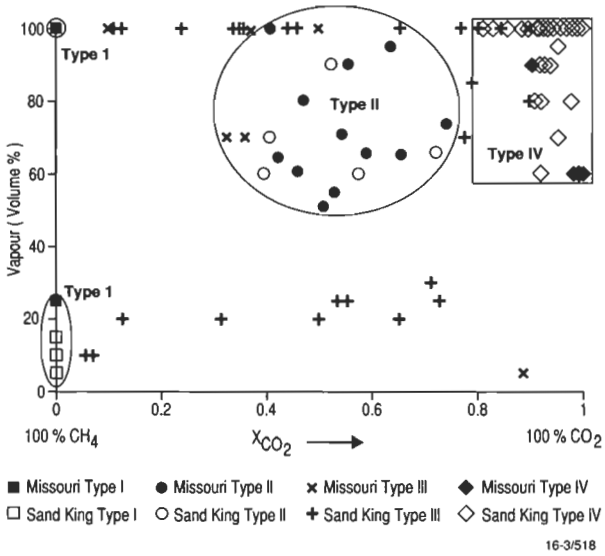

Figure 5. A plot of X_{CO_2} in the vapour phase versus vol.% vapour of inclusions for Raman microprobe analyses of inclusion Types I–IV.

homogenise over the temperature range 296–402°C with an average value of 338°C (Fig. 8A).

Type II (multiphase inclusions)

Multiphase inclusions containing up to four solid phases, an aqueous phase and greater than 50 vol. % vapour (Figs 4B and 5) have been classified as Type II. These inclusions are quite rare and have only been observed in 'relic' quartz surrounded by thin veins of sulphide or fuchsite (identified by Raman spectroscopy). Raman spectroscopy has also identified muscovite and carbonate in some of these inclusions. Sizes range from 40 μm or less and most have rounded or negative crystal morphology.

As shown in Figure 6B, melting of the carbonic phase in these inclusions occurs over a range from –68 to –60°C with a distinct mode near –64°C. Because CH_4 is strongly partitioned into the vapour phase and $Tm(CO_2)$ is only a function of the amount of CH_4 in the coexisting liquid phase, inclusions containing significant volumes of vapour are more CH_4-rich than indicated by $Tm(CO_2)$. Therefore, although the $Tm(CO_2)$ mode indicates 38 mole % CH_4 in the vapour phase (Swanenberg 1979), the Raman microprobe analyses (Fig. 5) indicate that the vapour phase in these inclusions contains an average of 49 mole % CO_2 and 51 mole % CH_4. Hydrogen sulphide (0.4 mole %) was also detected in the vapour phase of Type II inclusions from Missouri (Table 1) which were in relic quartz grains surrounded by thin veins of arsenopyrite.

Clathrate formation could only be observed in a few inclusions and their final melting temperatures ranged from 9 to 14°C, the majority melting between 13 and 14°C. The Raman spectra indicate that the aqueous phase has a salinity between 13 and 24.8 equiv. wt % NaCl (Fig. 7) with an average of 15 equiv. wt % NaCl. Although the salinity of these inclusions is considerably higher than any of the other carbonic inclusions, the aqueous phase appears to be undersaturated and thus these inclusions do not contain any solid chlorides, but only solid silicate and carbonate phases. These solid phases did not dissolve before decrepitation occurred at temperatures

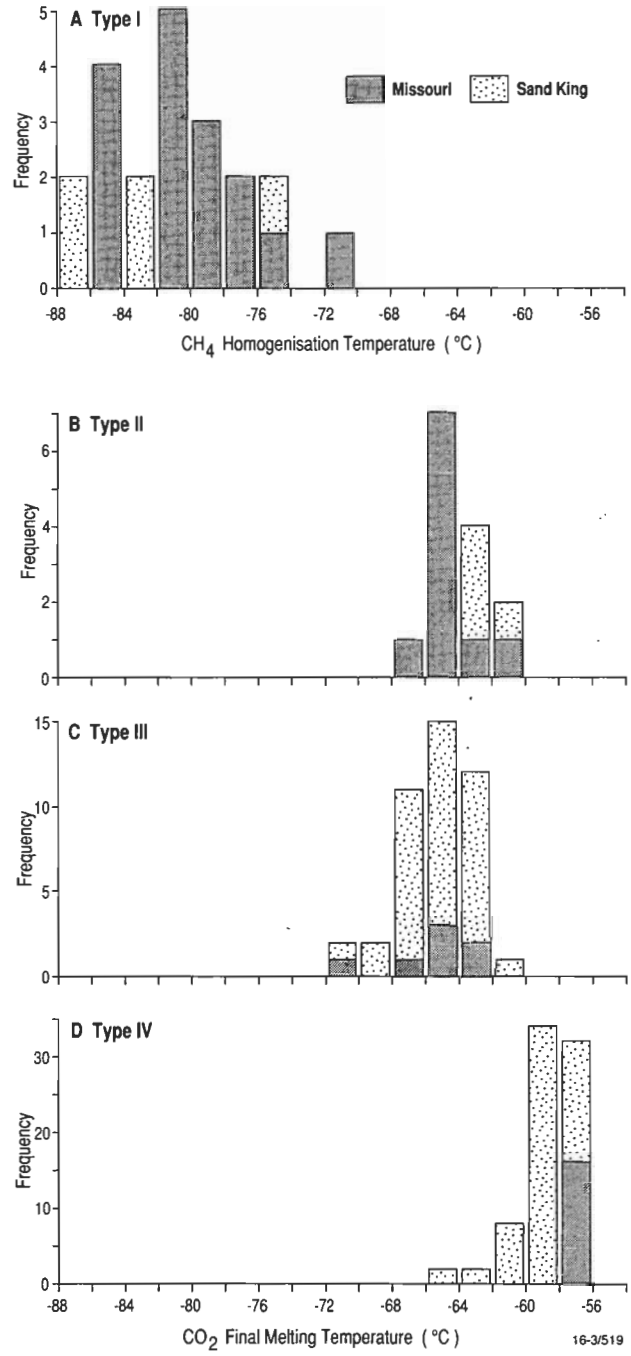

Figure 6. Homogenisation temperatures for the CH_4-rich vapour phase in (A) Type I inclusions, and final melting temperatures for CO_2 in (B) Type II, (C) Type III, and (D) Type IV inclusions.

Figure 4. Photomicrographs showing the nature of fluid inclusions at Missouri and Sand King. (A) Relatively isolated, vapour-rich Type I inclusions with only CH_4 detected in the vapour phase; (B) Multiphase, Type II inclusions in 'relic' quartz surrounded by fuchsite veins, 'M' denotes crystals of muscovite; (C) Type III inclusions containing both CO_2 and CH_4 in the vapour phase; (D) CO_2-rich Type IV inclusions, containing both liquid and vapour CO_2 cut by a trail of secondary aqueous inclusions; (E) low-salinity, Type V aqueous inclusions in quartz; (F) high-salinity, Type VI inclusions in calcite, some of which contain a halite daughter crystal, denoted by 'H'. Scale bars = 10 μm.

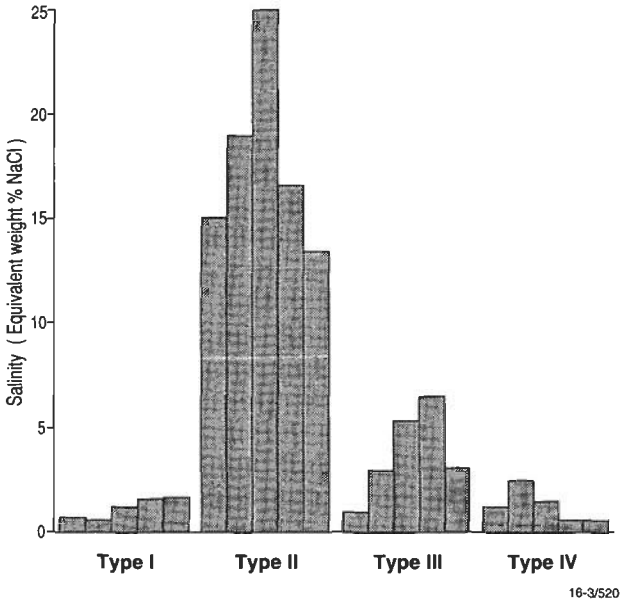

Figure 7. Salinity in equiv. wt % NaCl, as determined from Raman microprobe spectra of the aqueous phase of fluid inclusions, using the skewing parameter method described by Mernagh & Wilde (1989).

above 200°C. Homogenisation of aqueous and carbonic phases to a carbonic phase was observed in a few inclusions and covered the range from 287 to 335°C (Fig. 8B).

Type III inclusions (H_2O–CO_2–CH_4)

These inclusions consist of either one phase or two phases (an aqueous liquid + carbonic vapour) at room temperature (Fig. 4C). The carbonic phase contains both CO_2 and CH_4 and a few of these inclusions also contain a small daughter mineral, identified as muscovite by Raman spectroscopy. Individual fractures or clusters may have relatively constant or highly variable phase proportions.

Final CO_2 melting temperatures for Type III inclusions ranged from −71 to −61°C with an average value of −65.2°C (Fig. 6C), which indicates the presence of significant amounts of CH_4. The Raman microprobe analyses also confirmed a wide variation in $X(CO_2)$ in the vapour phase, which ranged from 0.86 to 0.09 (Fig. 5). The CO_2 content of the vapour phase is generally lower than that in Type II inclusions.

Homogenisation (l+v→v) of the carbonic phase was only observed in a few inclusions and varied from −8.7 to 7.6°C. These values are generally lower than those of Type II inclusions (see Fig. 6) and result from the higher CH_4 content of Type III inclusions. Clathrate melting was observed between 5.8 and 13.4°C with an average value of 11.2°C. The Raman spectra of the aqueous phase indicate that the salinity of the fluid is less than 7 equiv. wt % NaCl (Fig. 7). Most inclusions decrepitated before homogenisation, but a few were observed to homogenise into the carbonic phase between 220 and 338°C (Fig. 8C).

Type IV inclusions (CO_2–H_2O)

In many of these inclusions, only CO_2 is observed at room temperature, either as a single phase or as both liquid and vapour. Other CO_2-rich inclusions also contained an aqueous phase with the volumetric proportions of CO_2 ranging from 40 to 95%, but typically greater than 50% (Fig. 4D). Rare Type IV inclusions also contain a small carbonate daughter mineral. Inclusions up to a maximum size of about 40 μm have been observed and shapes vary from irregular to negative crystal forms.

Microthermometric studies show that solid CO_2 melts over the range −66 to −56.6°C with a mode around −58°C

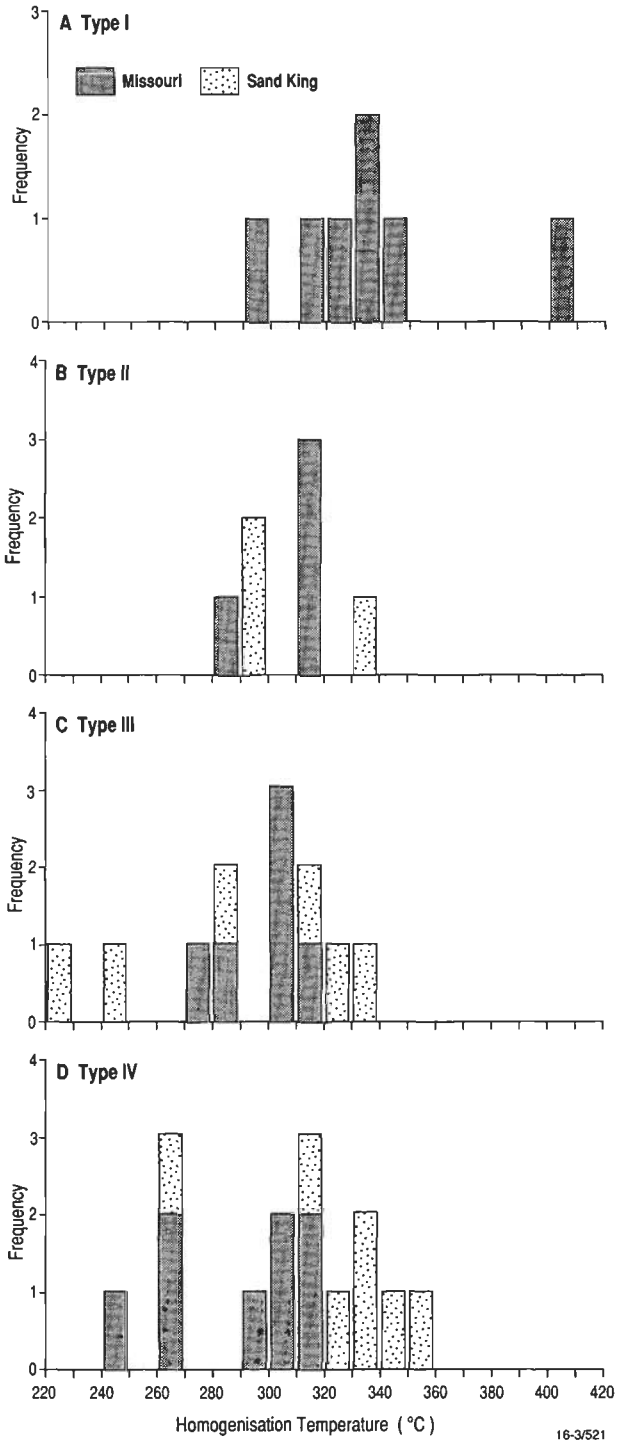

Figure 8. Total homogenisation temperatures for (A) Type I, (B) Type II, (C) Type III, and (D) Type IV inclusions. Note that the solids present in Types II and III inclusions generally did not dissolve before homogenisation of the liquid and vapour phases.

(Fig. 6D), and Raman microprobe analysis has shown that the depression in the melting point of CO_2 is caused by the presence of CH_4. The compositions of the vapour phase, as determined by Raman spectroscopy, are shown in Fig. 5. The CO_2 content of the vapour phase varies from 100 mole % down to 79 mole % with an average value of 93.8 mole % and the corresponding X_{CO2} of the inclusions varies from 0.10 to 0.85.

The CO_2 phases homogenise into the liquid phase at temperatures ranging from –8 to 31°C with a mode around 22°C. The spread of CO_2 homogenisation temperature indicates a wide range of densities (0.47–0.93) and it was noted that fluid inclusions from single grains or even single micro-fractures seldom had identical densities. Elsewhere, similar observations have been interpreted as resulting from heterogeneous trapping or as a result of volume changes after entrapment (cf. Robert & Kelly 1987; Santosh et al. 1991). The formation of clathrate was only observed in inclusions which exhibited an aqueous phase at room temperature. Clathrate melting temperatures ranged from 9 to 15°C, the majority melting around 9°C. However, a significant number of inclusions showed clathrate melting above 10°C (the invariant melting point of clathrate in the salt-free H_2O–CO_2 system) and hence, reflect the presence of minor CH_4 in these inclusions. Raman spectra indicated that the salinity was less than 3 equiv. wt % NaCl in these inclusions (Fig. 7).

Type IV inclusions which contained an observable aqueous phase typically decrepitated before total homogenisation, but a small number were observed to homogenise into the carbonic phase. Final homogenisation temperatures ranged from 240 to 360°C (Fig. 8D). Inclusions from Missouri generally had slightly lower homogenisation temperatures, with an average of 289°C, while inclusions from Sand King had an average of 323°C. These relatively high homogenisation temperatures further support the presence of a minor NaCl component in Type IV inclusions, since the critical curve for the salt-free H_2O–CO_2 system reaches a maximum of around 270°C at the inferred trapping pressures of 3–4kbar.

Type V (aqueous inclusions)

These are secondary, low-salinity, aqueous inclusions, some of which contain a vapour bubble of about 5 vol. % (Fig. 4E). The Raman microprobe did not detect any species in the vapour phase and, hence, H_2O is assumed to be the only volatile species. Individual inclusions are typically irregular, jagged or rounded, and vary in size up to approximately 50 μm. The irregularly shaped inclusions are generally flat-lying along the plane of the fracture and many show evidence of necking down. They represent relatively late fluids, as they generally outline healed fractures traversing the entire crystal, and have been observed to cross-cut trails of carbonic inclusions. Final melting temperatures of ice range from –5 to 0°C with a mode at –3.5°C, giving an average salinity of 5.8 equiv. wt % NaCl (Fig. 9A). Total homogenisation to the liquid phase occurred from 78 to 253°C, and there appears to be a bimodal distribution with modes around 100°C and 190°C (Fig. 10A), possibly representing the existence of two generations of low-salinity fluids.

Type VI (high-salinity aqueous inclusions)

Type VI inclusions typically contain 5–10 vol. % vapour and are relatively saline (Fig. 4F). They are rounded to irregular in shape and vary in size up to 50 μm. Most Type VI inclusions in quartz contained only vapour and brine. However, some inclusions in late calcite vein-fill contained a single halite crystal or, more rarely, up to three daughter minerals. The Raman microprobe could not detect any species in the vapour phase of Type VI inclusions and H_2O is assumed to be the only volatile species.

Inclusions in quartz have initial ice melting temperatures between –86 and –59°C and final ice melting temperatures

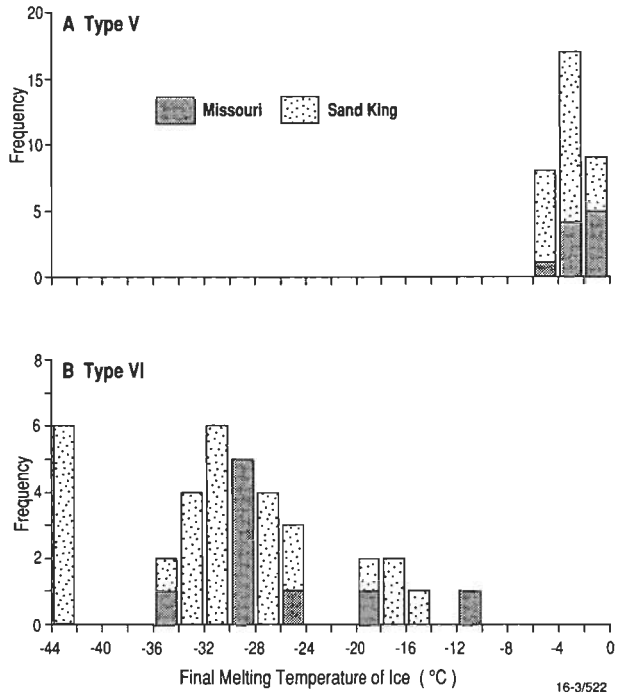

Figure 9. Final melting temperatures of ice in (A) Type V and (B) Type VI inclusions.

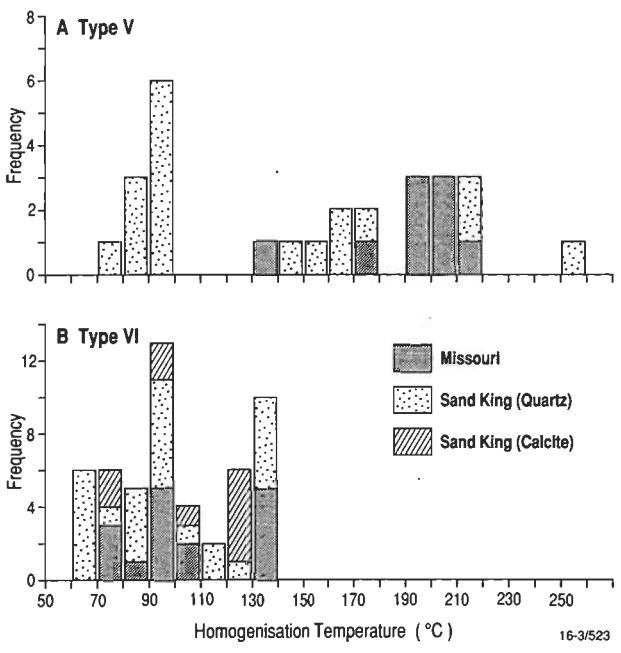

Figure 10. Total homogenisation temperatures for (A) Type V and (B) Type VI inclusions.

ranging from −44 to −11.5°C (Fig. 9B) with an average of −30.9°C or 26 equiv. wt % $CaCl_2$. The depression of the final ice melting temperature to as low as −44°C suggests that these fluids are $MgCl_2$-rich or $CaCl_2$-rich, as the eutectic melting temperature of $CaCl_2$ is −49.8°C (Crawford 1981). The very low eutectic melting temperatures observed in these inclusions may be due to the presence of metastable $MgCl_2$ x nH_2O or $CaCl_2$ x nH_2O complexes, which have reported first melting temperatures as low as −70°C (Davis et al. 1990). Homogenisation (l+v→l) temperatures range from 61 to 129°C (Fig. 10B), consistent with a late-stage influx of very saline fluids.

Inclusions in calcite have initial melting temperatures of −48 to −11°C, with an average of −32.2°C. This suggests that they may contain a brine similar to that in the quartz-hosted inclusions, but the presence of halite daughter crystals indicates a much higher Na^+ content in these fluids. Halite daughter crystals melted between 122 and 123°C, giving a salinity of 28.5 equiv. wt % NaCl (or 27 equiv. wt % $CaCl_2$). Total homogenisation to liquid occurred at temperatures between 76 and 139°C, which is again similar to those of Type VI inclusions in quartz.

Discussion

The CH_4-rich fluids

Methane-rich inclusions are rare, but their presence in early (relic) quartz and in quartz associated with biotite–carbonate–pyrite–wall rock alteration assemblages and their relatively high homogenisation temperatures suggest that they represent the earliest generation of fluid trapped in these deposits. Although the origin of the CH_4–H_2O fluid is not clear, possible sources for the fluid are evaluated below.

Methane-bearing fluids have been detected in a number of igneous (Konnerup-Madsen et al. 1985; Thomas et al. 1990; Larsen et al. 1992) and metamorphic environments (Hollister & Burrus 1976; Poutiainen 1990). Rumble & Hoering (1986) proposed that CH_4-rich fluids may form during greenschist to amphibolite facies grade metamorphism of graphitic pelites at 'low fO_2'. In fact, any rock plus fluid bulk composition that lies within the CH_4–H_2O–graphite field has an fO_2 very close to that defined by the quartz–fayalite–magnetite (QFM) buffer (Holloway 1984). Calculations by Ohmoto & Kerrick (1977) have shown that for fluid in equilibrium with graphite + pyrite + pyrrhotite at 2 kbar and 500°C, CH_4 becomes the dominant carbonic species at one log unit or more below the QFM buffer and at QFM−2, fluids on the graphite boundary consist of ~85 mol. % CH_4 and ~15 mol. % H_2O (Holloway 1981). However, there are few metapelitic rocks in the immediate mine area. The nearest metasedimentary rocks are several kilometres from the deposits and they have a quartzofeldspathic composition. Low fO_2 conditions favourable for the generation of methane could, however, occur during the serpentinisation of nearby ultramafic rocks (cf. Frost 1985).

Methane-bearing fluids may be stable to considerable depths within the Earth's crust, as a variety of heterogeneous equilibria (Buddington & Lindsley 1964; Eggler 1983; Haggerty & Tompkins 1985; Mattioli & Wood 1986) and intrinsic fO_2 measurements (Arculus & Delano 1981; Arculus et al. 1984) indicate that portions of the upper mantle and lower crust have values of fO_2 within ±2 log units of the QFM buffer. Therefore, the CH_4-bearing fluids could also be generated from a deep high-temperature source in the lower crust or mantle, where the fO_2 may be very close to QFM−2.

The vapour (CH_4)-rich Type I inclusions appear to result from post-entrapment modification of CH_4–H_2O inclusions rather than from phase separation. At high temperatures the CH_4–H_2O fluid will form a homogeneous supercritical fluid and this fluid will not unmix until the temperature falls below 325°C in the salt-free system (Holloway 1984). The addition of NaCl to the system will extend the two-phase region to higher temperatures (cf. Krader & Franck 1987); however, the Raman microprobe analyses indicate fairly low salinities (Fig. 7). Thus, it is unlikely that the CH_4–H_2O fluid would have unmixed at the temperatures recorded by mineralised alteration assemblages (i.e. >450°C).

The CO_2-bearing fluids

There is widespread evidence for the existence of a synmetamorphic, CO_2-bearing, aqueous fluid in all gold deposits of the Eastern Goldfields Province (Ho et al. 1990). This relatively oxidised fluid introduced massive amounts of carbonate into deformed metavolcanic rocks and formed hematite, epidote, titanite and green biotite in the granitoids (Witt & Davy in prep.; Libby et al. 1990). The particularly strong carbonation of mafic and ultramafic rocks in regional shear zones suggests a deep source for the CO_2-bearing fluids (Perring et al. 1990), but the ultimate source of these fluids is controversial (Burrows et al. 1986; Groves & Phillips 1987; Cameron 1988; reviewed by Kerrich 1990, and Perring et al. 1990).

Inclusions containing only CO_2 have been observed in some Archaean gold deposits (e.g. Robert & Kelly 1987), but these observations are at odds with thermodynamic calculations, which predict that significant amounts of water should also be present if the carbonic phase coexisted with an aqueous CO_2–H_2O fluid (e.g. Hall & Bodnar 1990). Kreulen (1987) has demonstrated that, in many cases, a significant volume of water (20–40 mole %) may remain undetected. Phase separation of an originally homogeneous fluid at the temperatures recorded by alteration assemblages at Sand King and Missouri (~500°C) could only occur with the addition of 10–12 wt % NaCl (Takenouchi & Kennedy 1964), much higher than the salinities of Type IV inclusions indicated by Raman microprobe analyses. Alternatively, strain-induced leakage of H_2O from inclusions (Hollister 1990; Bakker & Jansen 1990) may have led to CO_2 enrichment after entrapment. The latter process could account for the observed variations in the density of CO_2 in different inclusions, even within a single microfracture.

Mixed CO_2–CH_4–H_2O±NaCl fluids

At low fluid/rock ratios there would be redox exchange with iron in the upper crustal rocks, which may reduce the fO_2 of the fluid and convert some of the CO_2 to CH_4 via reactions such as:

$$6\,Fe_2SiO_4 + 7\,H_2O = 3\,Fe_3Si_2O_5(OH)_4 + Fe_3O_4 + H_2 \quad (1)$$

fayalite fluid serpentine magnetite

$$CO_2 + 4\,H_2 = CH_4 + 2\,H_2O \quad (2)$$

However, these reactions do not necessarily require a high hydrogen fugacity (Frost 1985) and this process is unlikely to generate the high CH_4/CO_2 ratios observed in some Type II and III inclusions. Therefore, other

processes such as fluid mixing or post-entrapment modification must be invoked. Evidence of fluid mixing between the CH_4-rich and CO_2-rich end-member fluids is given in Figure 11(A), which shows inclusions trapped in a microfracture parallel to the plane of the section. Large vapour-rich inclusions, some of which contain a muscovite crystal, grade into smaller, liquid-rich inclusions. Bulk compositions derived by the methods outlined in Ramboz et al. (1985) for the numbered inclusions in Figure 11(A) are given in Table 2. Figure 11(B) shows that the inclusions in the lower left of Figure 11(A) are CO_2-rich, while those in the upper right contain only CH_4 in the vapour phase, with mixed CO_2/CH_4 compositions being recorded from intermediate inclusions.

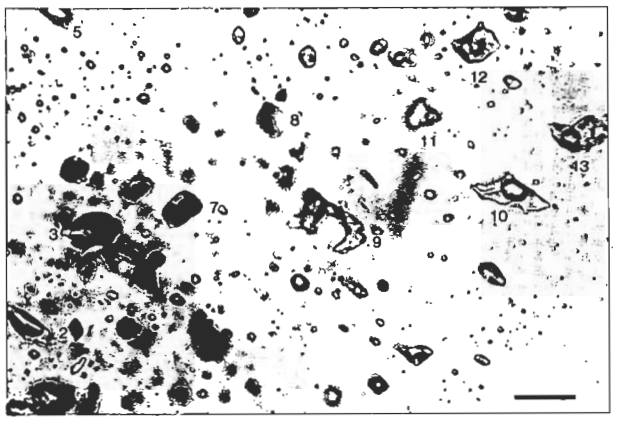

Figure 11(A). Photomicrograph of fluid inclusions in a single microfracture parallel to the plane of the page. There is a gradual progression from CO_2-rich, vapour-rich inclusions at the lower left to liquid-rich inclusions in the top right which contain only CH_4 in the vapour bubble, and this is interpreted as evidence for mixing between CO_2-rich and CH_4-bearing fluids. Analyses of the vapour phase of numbered inclusions are given in Table 2 (Nos 4, 6, and 14 are outside the field of view). Scale bar = 10μm.

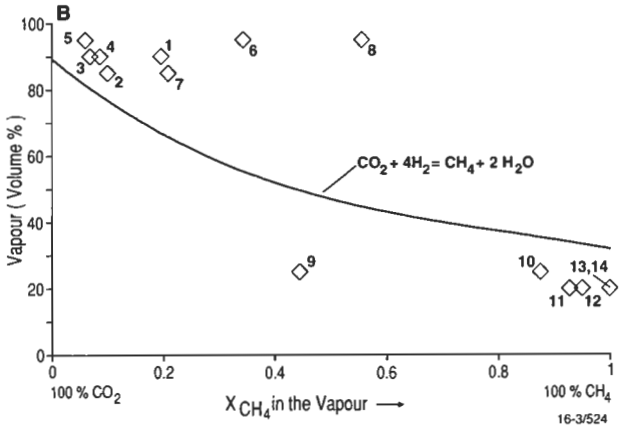

Figure 11(B). Plot of volume per cent vapour versus mole fraction of methane in the vapour bubble for the inclusions shown in Figure 11(A) and Table 2. The solid curve represents the predicted change in volume of the vapour bubble (assuming a constant vapour density) as a result of hydrogen diffusion into an inclusion initially containing 90 vol.% vapour. The CO_2 will be converted into CH_4 according to equation 2 (see text).

Addition of CH_4 to the CO_2–H_2O(±NaCl) system further expands the two-phase field to the conditions implied for mineralisation at Missouri and Sand King (cf. Duan et al. 1992). Phase separation of this complex fluid may have occurred over a range of pressures, owing to transient decreases in pressure, related to vein formation, yielding mixed CO_2+CH_4, vapour-rich inclusions and corresponding water-rich inclusions with varying vapour contents. Mixed CO_2+CH_4, vapour-rich inclusions are the most abundant Type III inclusions, but a few water-rich, Type III inclusions with a CO_2+CH_4 vapour phase have also been observed.

Table 2. Interpreted bulk composition derived from Raman microprobe analytical data for selected fluid inclusions from Figure 11.

Inclusion No.	*Vol. % vapor*	X_{CO_2}	X_{CH_4}	X_{H_2O}
1	90	0.667	0.158	0.175
2	85	0.623	0.073	0.304
3	90	0.762	0.063	0.175
4	90	0.737	0.070	0.193
5	95	0.853	0.039	0.108
6	95	0.597	0.299	0.104
7	85	0.588	0.155	0.257
8	95	0.403	0.503	0.094
9	25	0.023	0.021	0.956
10	25	0.003	0.017	0.970
11	20	0.001	0.022	0.977
12	20	0.001	0.022	0.977
13	20	0.000	0.017	0.983
14	20	0.000	0.017	0.983

Type II inclusions, on the other hand, display a more constant chemical composition than do Type III inclusions. They may represent the vapour-rich end-members generated by phase separation of an initially homogeneous CH_4–CO_2–H_2O fluid. Ubiquitous muscovite in these inclusions may have been soluble in this supercritical fluid or may have been accidentally trapped. Type II inclusions may also have been further modified by post-entrapment changes.

The aqueous fluids

The morphology of the low-salinity Type V inclusions indicates that they are relatively low-temperature, secondary inclusions. The low homogenisation temperatures (≤253°C) are in accord with the late influx of this fluid, which is possibly of meteoric origin. The saline fluids trapped by Type VI inclusions are similar to those observed by Robert & Kelly (1987) from the Sigma mine in the Abitibi Greenstone Belt, Canada. Calcium-dominated, saline formation waters are common in many sedimentary basins (e.g. Wilson & Long 1992), and are believed to originate from either diagenetic or modified connate brines (Land 1992). Overlapping homogenisation temperatures for Type V and Type VI inclusions (Fig. 10) suggest a broad contemporaneity between the two fluids. The higher homogenisation temperatures of some Type V inclusions may indicate their early entry into the still warm host rocks or, alternatively, may simply result from necking down. The higher Na^+ content of the saline fluid inclusions in calcite may reflect changes in the cation ratios which occurred as the Ca^{2+} ions were removed from the fluid under conditions favourable for the precipitation of carbonate minerals.

Fluid evolution

The textural evidence suggests that Type I inclusions were trapped in the early phases of mineralisation at both Sand King and Missouri. The Type I fluid inclusions indicate the presence of an initially low fO_2 fluid, which may have resulted from serpentinisation of the ultramafic units near these deposits. The widespread occurrence of native metals in many serpentinites indicates that they may form under conditions of extremely low fO_2 where the activity of hydrogen is relatively high. Frost (1985) has shown that, even under amphibolite-grade metamorphic conditions, there is a considerable gradient in fO_2 across a serpentinite body from a partially serpentinised core to a carbonatised margin. Oxygen fugacity progressively decreases towards the centre of the body until it reaches a minimum at the serpentinisation front, which may be up to four or five log units below the QFM buffer. Owing to the zone of strong reduction at the serpentinisation front, X_{CO_2} in this region will also fall and CO_2 will be converted to CH_4. The water-rich inclusions shown in Figure 11(A) are assumed to represent the end-member composition for Type I fluids. The calculated density of methane in these inclusions varies from 0.14 to 0.25 g.cm^{-3} and the average bulk density is estimated to be 0.78 g.cm^{-3}. Isochores calculated from the equation of state derived by Jacobs & Kerrick (1981) for CH_4–H_2O fluids with densities of 0.5–0.8 g.cm^{-3} are shown in Figure 12. Type IV inclusions contain only minor amounts of CH_4 and, although they show some evidence of necking or partial decrepitation, they do not appear to have been greatly affected by other post-entrapment changes or fluid mixing. Thus, they represent a CO_2–H_2O fluid which was generated or circulating after the system became more oxidised. The small amount of methane in the Type IV inclusions was taken into account by expressing the density of the carbonic phase in terms of 'equivalent CO_2' density and by using the data from Swanenberg (1979) and Heyen et al. (1982). This gives densities between 0.80 and 0.93 for Type IV inclusions, as shown by the 'equivalent CO_2'–H_2O isochores in Figure 12. The densities of CH_4-bearing and CO_2-bearing fluids are consistent with both having been trapped at the P–T conditions (450–600°C, 3–4 kbar) implied for the hydrothermal alteration and gold mineralisation.

The CO_2–H_2O fluids may have accompanied relatively oxidised I-type magmas during their ascent through the crust (Holloway 1976) and subsequent emplacement in the Siberia metavolcanic rocks. The CO_2-rich fluid appears to have been present before and during formation of the auriferous structures and gold-related metasomatism of the wallrocks. Thus, it seems most likely that the CH_4-rich fluid was locally generated in mafic or ultramafic units which may have been carbonated at their margins during interaction with the CO_2-rich fluid, but have retained a very low fO_2 at the serpentinisation front (Frost 1985), as described above.

The presence of muscovite and carbonate in Types II and III also provides a link with the potassic alteration event associated with gold mineralisation in both deposits. As shown in Figure 5, Type III inclusions exhibit a wide range of compositions and degree of fill. These variations may be the result of mixing between CO_2-rich and CH_4-rich fluids, as evident in Figure 11. The higher salinity of Type II inclusions (Fig. 7) suggests that they may be linked to the intrusion of the granitic magma. Additionally, Type II and some Type III inclusions may represent the products of phase separation from a mixed

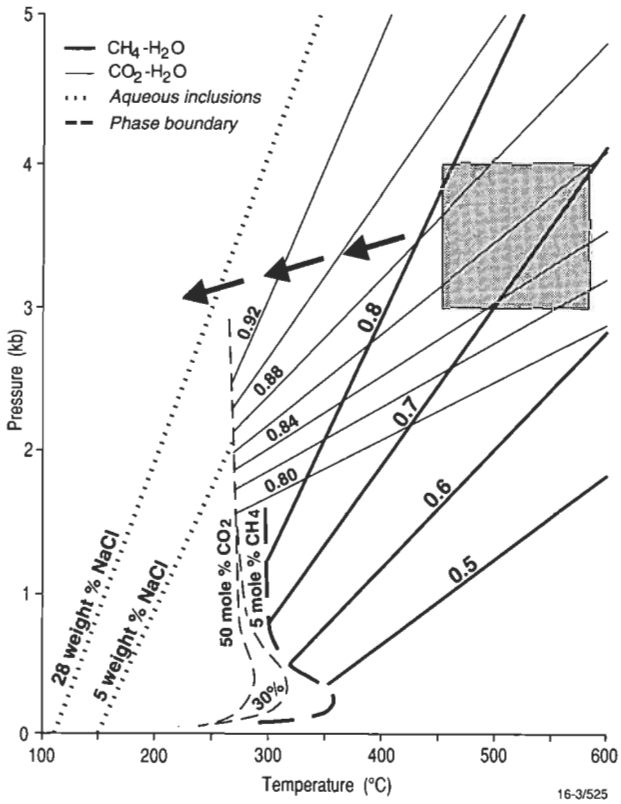

Figure 12. P–T diagram showing selected isochores representing the range of inclusions encountered at the Missouri and Sand King deposits. CH_4–H_2O (Type I) isochores are shown as thick lines, CO_2–H_2O (Type IV) as thin lines, and aqueous solutions containing 5 wt% NaCl (Type V) and 28 wt% NaCl (Type VI), respectively, as dotted lines. The mixed CH_4–CO_2–H_2O isochores for Types II and III have been omitted for clarity, but Duan et al. (1992) have shown that these are generally steeper than the corresponding CO_2–H_2O isochores. The numbers on the isochores represent fluid densities in g.cm^{-3}. Isoplethic phase boundary curves for H_2O systems with 5 mole % CH_4, 30 mole % CO_2 and 50 mole % CO_2 are also shown. The shaded region represents the approximate P–T conditions of gold deposition and potassic alteration as indicated by alteration assemblages and other geological relationships, and the arrows indicate a possible, close to isobaric, cooling path.

CO_2–CH_4–H_2O fluid. The range of CO_2/CH_4 ratios and liquid/vapour ratios defined by Type II and III inclusions could be generated if a compositionally variable, mixed CO_2–CH_4–H_2O fluid underwent phase separation over a range of transient pressures related to vein formation. However, necking-down and other post-entrapment changes (see below) may also have contributed to the range of vapour contents and CO_2/CH_4 ratios.

The P–T path during the latter stages of cooling is unknown, but is likely to have been essentially isobaric. Figure 12 indicates that the influx of low-salinity fluids, possibly of meteoric origin, was the next event, followed by the late influx of saline, $CaCl_2$-bearing brines.

The effect of post-entrapment changes to fluid inclusions

Recently, Hall et al. (1991) examined the evidence for hydrogen mobility at amphibolite to granulite facies conditions and have provided evidence for diffusion of

hydrogen into peak metamorphic fluid inclusions. This has been verified experimentally by Morgan et al. (1993), who re-equilibrated CO_2-rich inclusions in quartz and olivine at controlled fH_2 conditions at 718–728°C and 2 kbar. The experiments on isolated inclusions in quartz produced binary CO_2 (47–63 mol. %)–CH_4 (37–53 mol. %) gas mixtures, and even higher CH_4 contents were noted along secondary trails. The diffusion of H_2 into CO_2-rich inclusions leads to the formation of methane and water via reaction (2). The effect of this reaction on an inclusion which initially contains 90 vol. % CO_2 vapour is shown by the line in Figure 11(B). Although this line may be displaced either up or down, according to the initial vapour content of the inclusion, it is clear that, in all cases, most inclusions in Figure 11(B) do not plot close to this line. Therefore, hydrogen diffusion has not had a significant effect on these inclusions, and fluid mixing is thus the major mechanism controlling the compositional variation in Types II and III inclusions at Missouri and Sand King.

Inclusions which contain mixtures of CO_2 and CH_4 are also expected to precipitate graphite by the following reaction:

$$CO_2 + CH_4 = 2H_2O + 2C \quad (3)$$

However, graphite was not detected with the Raman microprobe in any of the fluid inclusions examined in this study. The nucleation of graphite from fluids is known to involve a high activation energy (Ziegenbein & Johannes 1980) and will also be affected by slower nucleation kinetics and metastability at lower temperatures. Ramboz et al. (1985) suggested that CH_4-rich fluids may be produced at temperatures below the blocking temperature (approximately 370°C for the H_2O–CO_2–CH_4–graphite system). Furthermore, Morgan et al. (1993) noted that all their re-equilibration experiments in quartz resulted in a decrease in the pressure of the carbonic fluids and they calculated that the minimum density required for the stable formation of graphite is near 0.74 $g.cm^{-3}$. Therefore, the lower density of Types II and III inclusions from Sand King and Missouri may explain the absence of graphite in these inclusions.

The mechanisms for gold deposition

Low-salinity, H_2O–CO_2 fluids have been implicated as the ore-bearing fluid in many of the world's Archaean greenstone belts (Colvine et al. 1988; Roberts 1989; Ho et al. 1990), including the Eastern Goldfields Province, and it is probable that Type IV inclusion fluids had an important role in ore genesis at Missouri and Sand King. Methane is less ubiquitous in Archaean lode gold deposits, but its presence at Missouri and Sand King, as well as in many other deposits in the Eastern Goldfields (Ho et al. 1990; Mernagh & Witt 1993; Hagemann & Ridley 1993), has important implications for depositional models, especially where chemical reaction between hydrothermal fluids and Fe-rich host rocks (Groves & Phillips 1987) is not an appropriate mechanism.

The mixing of CO_2-rich and CH_4-rich fluids may result in large changes in the oxidation potential of the ore-bearing fluid. Figure 13 shows the major sulphur species expected at conditions similar to those of mineralisation at Missouri and Sand King. A high total-sulphur concentration has been adopted in accord with the suggestion by Mikucki & Ridley (1993) that fluids in amphibolite facies deposits may contain from 1–10 molal total sulphur.

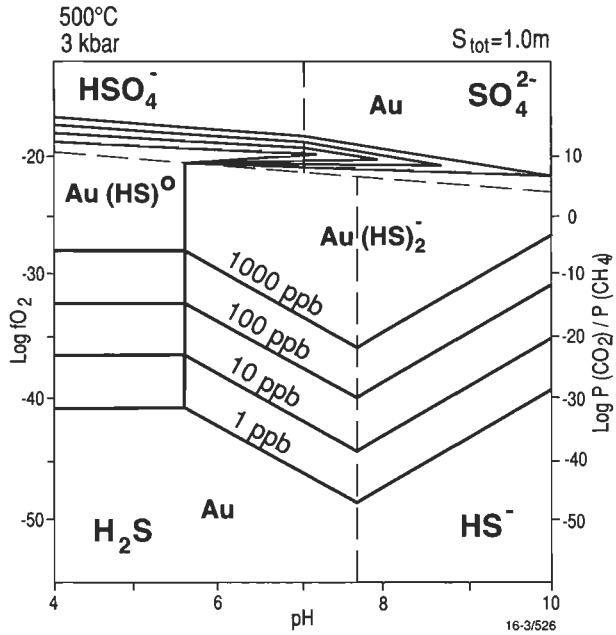

Figure 13. Log fO_2 versus pH diagram, showing solubility contours for the gold thio-complexes (ΣS = 1.0m) at 500°C and 3 kbar. Note that the stabilities of the thio-complexes have been extrapolated from the data of Hayashi & Ohmoto (1991), and remain speculative until they are experimentally verified. The corresponding CO_2/CH_4 ratios under the same conditions are shown on the right ordinate.

Note that Figure 13 is highly speculative, and was produced by extrapolating the data of Hayashi & Ohmoto (1991), which was obtained at or below 350°C. Nevertheless, it does show clearly that gold is probably transported either as the $Au(HS)^0$ or $Au(HS)_2^-$ complex under these conditions, and that relatively high concentrations of gold may be transported in methane-dominated fluids or fluids near the CO_2/CH_4 buffer. Gold will be precipitated as the fluid is oxidised and CO_2 becomes the dominant gaseous species.

However, the consequences of fluid mixing in these amphibolite-grade, lode-gold deposits should not be overlooked, as even minor increases in the CH_4 concentration of the ore-bearing fluid will greatly increase the immiscibility field in the CO_2–CH_4–H_2O–NaCl system. Duan et al. (1992) have shown that even the addition of a few mole per cent of CH_4 to the CO_2–H_2O system greatly increases the field of immiscibility and generally steepens the corresponding isochores. Addition of NaCl to the CO_2–H_2O system also increases the two-phase field (Bowers & Helgeson 1983), and Krader & Frank (1987) have shown that this effect is even greater in the CH_4–H_2O–NaCl system. In the latter case, the addition of 8 wt % NaCl extended the two-phase field from just over 300°C up to 500°C.

Hydrogen sulphide will be strongly partitioned into the (CH_4+CO_2)-rich vapour phase during phase separation, and gold will be deposited as a direct consequence of destabilisation of the aqueous auriferous sulphide complexes. Thus, the loss of sulphur as H_2S during phase separation and the resulting decrease in a_{H_2S} are important factors which may control gold precipitation under greenschist and amphibolite facies conditions. Fluids which contain methane will unmix over a wider range of

pressures and temperatures than for the corresponding CO_2–H_2O system and, thus, would enable this mechanism to operate to considerable depths within the crust.

Conclusions

From the distribution of fluid inclusions in quartz and carbonate from the Sand King and Missouri deposits and microthermometric and Raman microprobe data, we conclude that the earliest fluid (Type I) was trapped at a temperature of 500–600°C and a pressure of at least 3 kbar.

At approximately the same time as peak metamorphism and the intrusion of the nearby syn-D_3 granitoids there was an influx of CO_2-rich fluid. Mixing of this fluid with a CH_4–H_2O fluid from a possible ultramafic source and heterogeneous entrapment generated inclusions with a wide range of densities and CO_2/CH_4 ratios. The muscovite crystals observed in a number of Type II and Type III inclusions indicate a link between these fluids and the potassic alteration event evident in both deposits. The presence of CO_2-rich (Type IV) inclusions unaffected by the above processes suggests that CO_2-rich fluids continued to circulate after consumption of the CH_4-bearing fluid and the decrease in the activity of H_2 in the system. These events were followed by the influx of a low-salinity (meteoric?) fluid and, later, by a $CaCl_2$-rich (connate?) brine.

The prevalence of CO_2-bearing fluids in gold deposits in Archaean greenstone belts throughout the world suggests that mineralisation was associated with the influx of the CO_2-rich fluids. Methane enrichment of these fluids greatly increases the P–T range of fluid immiscibility, and H_2S, CH_4 and CO_2 would all be strongly partitioned into the vapour phase during unmixing of the ore fluid, leading to a decrease in the sulphur content of the residual fluid and, ultimately, gold precipitation. These mechanisms may operate over a wider range of pressures and temperatures than for the corresponding CO_2–H_2O system, thus enabling gold precipitation to occur at considerable depths within the crust.

Acknowledgments

We wish to thank Kalgoorlie Gold Operations for access to samples from Sand King and Missouri, and Christoph Heinrich, Greg Ewers and Brian Oversby for helpful discussions and comments. Thanks also to the referees, Robert Kerrich, Phillip Brown and Kenneth McQueen, for constructive reviews which helped improve this manuscript. W.K.W. publishes with permission of the Director of the Geological Survey of Western Australia.

References

Arculus, R.J. & Delano, J.W., 1981. Intrinsic oxygen fugacity measurements: techniques and results for spinels from upper mantle peridotite and megacryst assemblages. *Geochimica et Cosmochimica Acta*, 45, 899–913.

Arculus, R.J., Dawson, J.B., Mitchell, R.H., Gust, D.A. & Holmes, R.D., 1984. Oxidation states of the upper mantle recorded by megacryst ilmenite in kimberlite and type A and B spinel lherzolites. *Contributions to Mineralogy and Petrology*, 85, 85–94.

Bakker, R.J. & Jansen, B.H., 1990. Preferential water leakage from fluid inclusions by means of mobile dislocations. *Nature*, 345, 58–60.

Bird, P. & Pilapil, L., 1988. Description of mining operations at Sand King and Theil Well, Siberia. Unpublished report, Western Mining Corporation.

Bowers, T.S. & Helgeson, H.C., 1983. Calculation of the thermodynamic and geochemical consequences of nonideal mixing in the system H_2O–CO_2–NaCl on phase relations in geologic systems: Equation of state for H_2O–CO_2–NaCl fluids at high pressures and temperatures. *Geochimica et Cosmochimica Acta*, 47, 1247–1275.

Buddington, A.F. & Lindsley, D.H., 1964. Iron-titanium oxide minerals and synthetic equivalents. *Journal of Petrology*, 5, 310–357.

Burrows, D.R., Wood, P.C. & Spooner, E.T.C., 1986. Carbon isotope evidence for a magmatic origin for Archaean gold-quartz vein ore deposits. *Nature*, 321, 851–854.

Cameron, E.M., 1988. Archaean gold: relation to granulite formation and redox zoning in the crust. *Geology*, 16, 109–112.

Colvine, A.C., Fyon, J.A., Heather, K.B., Marmont, S., Smith, P.M. & Troop, D.G., 1988. Archaean lode gold deposits in Ontario. *Ontario Geological Survey Miscellaneous Paper*, 139.

Crawford, M.L., 1981. Phase equilibria in aqueous fluid inclusions. In Hollister, L.S. & Crawford, M.L. (editors). *Fluid inclusions, applications to petrology.* Mineralogical Association of Canada, 75–100.

Davis, D.W., Lowenstein, T.K. & Spencer, R.J., 1990. Melting behaviour of fluid inclusions in laboratory-grown halite crystals in the systems NaCl–H_2O, NaCl–KCl–H_2O, NaCl–$MgCl_2$–H_2O, and NaCl–$CaCl_2$–H_2O. *Geochimica et Cosmochimica Acta*, 54, 591–601.

Donnelly, H.G. & Katz, D.L., 1954. Phase equilibrium in the carbon-dioxide–methane system. *Industrial Engineering Chemistry*, 46, 511–517.

Duan, Z., Møller, N. & Weare, J.H., 1992. An equation of state for the CH_4–CO_2–H_2O system: II. mixtures from 50 to 1000°C and 0 to 1000 bar. *Geochimica et Cosmochimica Acta*, 56, 2619–2631.

Dubessy, J., Poty, B. & Ramboz, C., 1989. Advances in C–O–H–N–S fluid geochemistry based on micro-Raman spectrometric analysis of fluid inclusions. *European Journal of Mineralogy*, 1, 517–534.

Eggler, D.H., 1983. Upper mantle oxidation state: evidence from olivine–orthopyroxene–ilmenite assemblages. *Geophysical Research Letters*, 10, 365–368.

Frost, B.R., 1985. On the stability of sulfides, oxides, and native metals in serpentinite. *Journal of Petrology*, 26, 31–63.

Foster, R.P., 1989. Archaean gold mineralization in Zimbabwe: implications for metallogenesis and exploration. *In* Keays, R.R., Ramsay, W.R.H. & Groves, D.I. (editors). The geology of gold deposits: the perspective in 1988. *Economic Geology Monograph*, 6, 54–70.

Groves, D.I., 1993. An integrated model for genesis of Archaean gold mineralisation within the Yilgarn Block, Western Australia. *In* Williams, P.R. & Haldane, J.A. (compilers). An international conference on crustal evolution, metallogeny and exploration of the Eastern Goldfields, Extended Abstracts, *Australian Geological Survey Organisation, Record,* 1993/54, 115–121.

Groves, D.I., Barley, M.E., Barnicoat, A.C., Cassidy, K.F., Fare, R.J., Hagemann, S.G., Ho, S.E., Hronsky, J.M.A., Mikucki, E.J., Mueller, A.G., McNaughton, N.J., Perring, C.S., Ridley, J.R. & Vearncombe, J.R., 1992. Sub-greenschist to granulite-hosted Archaean lode-gold deposits of the Yilgarn Craton: a depositional contin-

uum from deep-sourced hydrothermal fluids in crustal-scale plumbing systems. *Geology Department (Key Centre) & University Extension, The University of Western Australia Publication*, 22, 325–337.

Groves, D.I. & Phillips, G.N., 1987. The genesis and tectonic controls on Archaean gold deposits of the Western Australian Shield: a metamorphic replacement model. *Ore Geology Reviews*, 2, 287–322.

Hagemann, S.G., Groves, D.I., Ridley, J.R. & Vearncombe, J.R., 1992. The Archaean lode-gold deposits at Wiluna, Western Australia: high level brittle-style mineralisation in a strike-slip regime. *Economic Geology*, 87, 1022–1053.

Hagemann, S.G. & Ridley, J.R., 1993. Hydrothermal fluids in epi- and katazonal crustal levels in the Archaean: implications for P–T–X–t evolution of lode-gold mineralisation. *In* Williams, P.R. & Haldane, J.A. (compilers). An international conference on crustal evolution, metallogeny and exploration of the Eastern Goldfields, Extended Abstracts, *Australian Geological Survey Organisation, Record*, 1993/54, 123–130.

Haggerty, S.E. & Tompkins, L.A., 1985. The redox state of the Earth's upper mantle from kimberlitic ilmenites. *Nature*, 303, 295–300.

Hall, D.L. & Bodnar, R.J., 1990. Methane in fluid inclusions from granulites: a product of hydrogen diffusion. *Geochimica et Cosmochimica Acta*, 54, 641–651.

Hall, D.L., Bodnar, R.J. & Craig, J.R., 1991. Evidence for postentrapment diffusion of hydrogen into peak metamorphic fluid inclusions from the massive sulfide deposits at Ducktown, Tennessee. *American Mineralogist*, 76, 1344–1355.

Hayashi, K. & Ohmoto, H., 1991. Solubility of gold in NaCl- and H_2S-bearing aqueous solutions at 250–350°C. *Geochimica et Cosmochimica Acta*, 55, 2111–2126.

Heyen, G., Ramboz, C. & Dubessy, J., 1982. Simulation des equilibres de phases dans le system CO_2–CH_4 en dessous de 50°C et de 100 bar. Application aux inclusions fluides. *Comptes rendus de Academie des Sciences, Paris*, 294, Serie II, 203–206.

Hill, B.D. & Bird, P., 1990. Sand King gold deposit. *In* Hughes, F.E. (editor). *Geology of the mineral deposits of Australia and Papua New Guinea.* The Australasian Institute of Mining and Metallurgy, Melbourne, 377–381.

Ho, S.E., Bennett, J.M., Cassidy, K.F., Hronsky, J.M.A., Mikucki, E.J. & Sang, J.H., 1990. Nature of ore fluid, and transportational and depositional conditions in sub-amphibolite facies deposits. In Ho, S.E., Groves, D.I. & Bennett, J.M., (editors). Gold deposits of the Archaean Yilgarn block, Western Australia: nature, genesis and exploration guides. *The University of Western Australia, Geology Department and University Extension, Publication,* 20, 198–211.

Hollister, L.S., 1990. Enrichment of CO_2 in fluid inclusions in quartz by removal of H_2O during crystal-plastic deformation. *Journal of Structural Geology*, 12, 895–901.

Hollister, L.S. & Burrus, R.C., 1976. Phase equilibria in fluid inclusions from the Khtada Lake metamorphic complex. *Geochimica et Cosmochimica Acta*, 40, 163–175.

Holloway, J.R., 1976. Fluids in the evolution of granitic magmas: Consequences of finite CO_2 solubility. *Geological Society of America Bulletin*, 87, 1513-1518.

Holloway, J.R., 1981. Compositions and volumes of supercritical fluids in the Earth's crust. *In* Hollister, L.S., & Crawford, M.L. (editors). *Fluid inclusions: applications to petrology.* Mineralogical Association of Canada, 13–38.

Holloway, J.R., 1984. Graphite–CH_4–H_2O–CO_2 equilibria at low-grade metamorphic conditions. *Geology*, 12, 455–458.

Jacobs, G.K. & Kerrick, D.M., 1981. Methane: an equation of state with application to the ternary system H_2O–CO_2–CH_4. *Geochimica et Cosmochimica Acta*, 45, 607–614.

Kerrich, R., 1990. Carbon-isotope systematics of Archaean Au–Ag vein deposits in the Superior Province: *Canadian Journal of Earth Sciences*, 27, 40–56.

Konnerup-Madsen J., Dubessy, J. & Rose-Hansen, J., 1985. Combined Raman microprobe spectrometry and microthermometry of fluid inclusions in minerals from igneous rocks of the Gardar province (south Greenland). *Lithos*, 18, 271–280.

Krader, T. & Franck, E.U., 1987. The ternary systems H_2O–CH_4–NaCl and H_2O–CH_4–$CaCl_2$ to 800K and 250 MPa. *Berichte der Bunsengesellschaft fuer Physikalische Chemie*, 91, 627–634.

Kreulen, R., 1987. Thermodynamic calculations of the C–O–H system applied to fluid inclusions: are fluid inclusions unbiased samples of ancient fluids? *Chemical Geology*, 61, 59–64.

Land, L.S., 1992. Saline formation waters in sedimentary basins: connate or diagenetic? *In* Kharaka, Y. & Maest, A.S., (editors). *Water–rock interaction.* Balkema, Rotterdam, 865–868.

Lapointe, B. & Chown, E.H., 1993. Gold-bearing iron-formation in a granulite terrane of the Canadian Shield: a possible deep-level expression of an Archean gold-mineralizing system, *Mineralium Deposita*, 28, 191–197.

Larsen, R.B., Brooks, C.K. & Bird, D.K., 1992. Methane-bearing, aqueous, saline solutions in the Skaergaard intrusion, east Greenland. *Contributions to Mineralogy and Petrology*, 112, 428–437.

Libby, J.W., Barley, M.E., Eisenlohr, B.N., Groves, D.I., Hronsky, J.M.A., Vearncombe, J.R., 1990. Structural setting of gold deposits: craton-scale deformation zones. *In* Ho, S.E., Groves, D.I. & Bennett, J.M., (editors). Gold deposits of the Archaean Yilgarn block, Western Australia: nature, genesis and exploration guides. *University of Western Australia, Geology Department and University Extension, Publication,* 20, 30–37.

Liu, L. & Mernagh, T.P., 1990. Phase transitions and Raman spectra of calcite at high pressures and room temperature. *American Mineralogist*, 75, 801–806.

Mattioli, G.S. & Wood, B.J., 1986. Upper mantle oxygen fugacity recorded by spinel lherzolites, *Nature*, 322, 626–628.

McNaughton, N.J., Groves, D.I. & Witt, W.K., 1993. The source of lead in Archaean lode gold deposits of the Menzies–Kalgoorlie–Kambalda region, Yilgarn Block, Western Australia, *Mineralium Deposita*, 28, 495–502.

Mernagh, T.P. & Wilde, A.R., 1989. The use of the laser Raman microprobe for the determination of salinity in fluid inclusions. *Geochimica et Cosmochimica Acta*, 53, 765–771.

Mernagh, T.P. & Witt, W.K., 1993. The relationship between gold mineralisation and metamorphic grade in the Menzies–Kambalda area, Eastern Goldfields, W.A.: evidence from fluid inclusions. *Australian Geological Survey Organisation, Record*, 1993/27.

Mikucki, E.J. & Ridley, J.R., 1993. The hydrothermal fluid of Archaean lode-gold deposits at different

metamorphic grades: compositional constraints from ore and wallrock alteration assemblages. *Mineralium Deposita*, 28, 469–481.

Montgomery, A., 1909. Report on the Waverly or Siberia District, Western Australia. *Department of Mines Western Australia, Annual Report.*

Morgan, G.B., Chou, I-M., Pasteris, J.D. & Olsen, S.N., 1993. Re-equilibration of CO_2 fluid inclusions at controlled hydrogen fugacities. *Journal of Metamorphic Geology*, 11, 155–164.

Myers, J.S., 1990. *In* Geology and Mineral Resources of Western Australia. *Western Australia Geological Survey, Memoir* 3, 126–127.

Ohmoto, H. & Kerrick, D., 1977. Devolatilization equilibria in graphitic systems. American Journal of Science, 277, 1013–1044.

Pasteris, J.D., Wopenka, B. & Seitz, J.C., 1988. Practical aspects of quantitative laser Raman microprobe spectroscopy for the study of fluid inclusions. Geochimica et Cosmochimica Acta, 52, 979–988.

Perring, C.S., Barley, M.E., Groves, D.I., McNaughton, N.J. & Ridley, J.R., 1990. Fluid and metal sources. *In* Ho, S.E., Groves, D.I. & Bennett, J.M., (editors). Gold deposits of the Archaean Yilgarn block, Western Australia: nature, genesis and exploration guides. *University of Western Australia, Geology Department and University Extension, Publication,* 20, 285–291.

Poutiainen, M., 1990. Evolution of a metamorphic fluid during progressive metamorphism in the Joroinen-Sulkava area, southeastern Finland, as indicated by fluid inclusions. *Mineralogical Magazine*, 54, 207–218.

Ramboz, C., Schnapper, D. & Dubessy, J., 1985. The P–V–T–X–fO_2 evolution of H_2O–CO_2–CH_4-bearing fluid in a wolframite vein: reconstruction from fluid inclusion studies. *Geochimica et Cosmochimica Acta*, 49, 205–219.

Robert, F. & Brown, A.C., 1986. Archean gold-bearing quartz veins at the Sigma mine, Abitibi greenstone belt, Quebec. Part I. Geologic relations and formation of the vein systems. Economic Geology, 81, 578–592.

Robert, F. & Kelly, W.C., 1987. Ore-forming fluids in Archean gold-bearing quartz veins at the Sigma mine, Abitibi greenstone belt, Quebec, Canada. *Economic Geology*, 82, 1464–1482.

Roberts, R.G., 1989. Archean lode gold deposits. In Roberts, R.G. & Sheahan, P.A. (editors). Ore Deposit Models, *Geoscience Canada, Reprint Series*, 3, 1–19.

Rumble, D., III & Hoering, T.C., 1986. Carbon isotope geochemistry of graphite vein deposits from New Hampshire, U.S.A. *Geochimica et Cosmochimica Acta*, 50, 1239–1247.

Santosh, M., Jackson, D.H., Harris, N.B.W. & Mattey, D.P., 1991. Carbonic fluid inclusions in South Indian granulites: evidence for entrapment during charnockite formation. *Contributions to Mineralogy and Petrology*, 108, 318–330.

Seitz, J.C., Pasteris, J.D. & Wopenka, B., 1987. Characterization of CO_2–CH_4–H_2O fluid inclusions by microthermometry and laser Raman microprobe spectroscopy: inferences for clathrate and fluid equilibria. *Geochimica et Cosmochimica Acta*, 51, 1651–1664.

Shepherd, T.J., Rankin, S.H. & Alderton, D.H.M., 1985. *A practical guide to fluid inclusion studies*. Blackie, London, 235 pp.

Smith, B.H., 1983. Siberia and Ora Banda laterites. *In* Smith, B.H., (Editor). *Geochemical exploration in the Eastern Goldfields region of Western Australia, Tour Guide.* The Association of Exploration Geochemists.

Smith, T.J., Cloke, P.L. & Kesler, S.E., 1984. Geochemistry of fluid inclusions from the McIntyre–Hollinger gold deposit, Timmins, Ontario, Canada. *Economic Geology*, 79, 1265–1285.

Swanenberg, H.E.C., 1979. Phase equilibria in carbonic systems, and their application to freezing studies of fluid inclusions. *Contributions to Mineralogy and Petrology*, 68, 303–306.

Takenouchi, S. & Kennedy, G.C., 1964. The binary system H_2O–CO_2 at high temperatures and pressures. *American Journal of Science*, 262, 1055–1074.

Thomas, A.V., Pasteris, J.D., Bray, C.J. & Spooner, E.T.C., 1990. H_2O–CH_4–NaCl–CO_2 inclusions from the footwall contact of the Tanco granitic pegmatite: estimates of internal pressure and composition from microthermometry, laser Raman spectroscopy, and gas chromatography. *Geochimica et Cosmochimica Acta*, 54, 559–573.

Walshe, J.L., 1986. A six-component chlorite solid solution model and the conditions of chlorite formation in hydrothermal and geothermal systems. *Economic Geology*, 81, 681–703.

Wilkins, R.W.T. & Barkas, J.P., 1978. Fluid inclusions, deformation and recrystallization in granite tectonites. *Contributions to Mineralogy and Petrology*, 65, 293–299.

Wilson, T.P. & Long, D.T., 1992. Evolution of $CaCl_2$ brine in Silurian aged formations of the Michigan basin, USA: the role of mineralogic reactions and evaporite diagenesis. *In* Kharaka, Y. & Maest, A.S., (editors). *Water-rock interaction*. Balkema, Rotterdam, 1213–1216.

Witt, W.K., 1991. Regional metamorphic controls on alteration associated with gold mineralization in the Eastern Goldfields province, Western Australia: implications for the timing and origin of Archean lode-gold deposits. *Geology*, 19, 982–985.

Witt, W.K., 1992. Porphyry intrusions and albitites in the Bardoc–Kalgoorlie area, Western Australia, and their role in Archean epigenetic gold mineralization. *Canadian Journal of Earth Sciences*, 29, 1609–1622.

Witt, W.K., 1993a. Lithological and structural controls on gold mineralization in the Archaean Menzies–Kambalda area, Western Australia. *Australian Journal of Earth Sciences*, 40, 65–86.

Witt, W.K., 1993b. Gold deposits of the Mount Pleasant Ora Banda areas, Western Australia—Part 1 of a systematic study of the gold mines in the Menzies–Kambalda region, Western Australia. *Western Australia Geological Survey, Record*, 1992/14, 104 pp.

Witt, W.K. & Davy, R., in prep. Granitoids of the southwest Eastern Goldfields Province, W.A. *Western Australian Geological Survey, Report.*

Woods, T.L., Bethke, P.M., Bodnar, R.J. & Werre, R.W., 1981. Supplementary components and operation of the U.S. Geological Survey gas-flow heating/freezing stage. *U.S. Geological Survey Open-file Report*, 81–954, 12 pp.

Wyche, S. & Witt, W.K., 1992. Geology of the Davyhurst 1:100 000 sheet, Western Australia. *Western Australia Geological Survey, Record* 1991/3, 48 pp.

Ziegenbeim, D. & Johannes, W., 1980. Graphite in C–H–O fluids: an unsuitable compound to buffer fluid composition at temperatures up to 700°C. *Neues Jahrbuch für Mineralogie: Abhandlungen*, 7, 289–305.

AGSO Journal of Australian Geology & Geophysics, 15 (3), 313–328 © Commonwealth of Australia 1994

Integrated geological and geophysical mapping of southwestern Western Australia

Alan J. Whitaker[1]

The major basement components within the Albany 1:1M Sheet area of southwestern Western Australia are defined from aeromagnetic anomalies and 10–40 km wavelength gravity anomalies, and are integrated with mapped geology to provide a geological model. Their structure (lithological banding), faults and dykes are determined from short-wavelength magnetic anomalies. The main tectonic elements are the Archaean Yilgarn Craton, the younger Albany Province to the south, and the Perth Basin with Proterozoic basement to the west.

The Yilgarn Craton comprises an eastern zone with strike-extensive sinuous anomalies, typical of granite–greenstone terrane, and a western zone with sparse, short anomalies, characteristic of granite–gneiss terrane. Highly magnetised granulites along the eastern margin of the western zone correlate with outcrop of the Jimperding Metamorphic Belt in the north of the sheet. The eastern boundary of these granulites is parallel to a weak gravity gradient, and corresponds with a significant change in structural style; it is inferred to be a major intra-cratonic discontinuity. A north-northwest-trending gravity gradient within the western zone coincides with the Southwest Seismic Zone, and defines the eastward extent of thick, relatively dense crust defined by earlier studies of seismic refraction data.

The Albany Province consists of a low-density southern zone with weakly sinuous magnetic banding, and a northern zone characterised by high-density, high-magnetisation, and linear magnetic banding. The southern margin of the Yilgarn Craton has been deformed for up to 50 km and demagnetised up to 20 km from the boundary. This deformation is inferred to have been caused by overthusting of the Albany Province during the Mid-Proterozoic. Subsequently, tectonism involving the Proterozoic crust beneath the Perth Basin deformed the western edge of the Yilgarn Craton and folded adjacent parts of the Albany Province southward.

Greenstone and metamorphic belts are highly prospective and host many of the region's mineral deposits. Both the composition and geophysical characteristics of these belts contrast with those of more widespread granite and granite–gneiss terrane, which are of considerably lower economic interest. Analysis of the regional geophysical data sets in conjunction with outcrop geology leads to a more complete model of the Precambrian geology of the region than that derived from outcrop mapping alone.

Introduction

The Albany 1:1M sheet area contains rocks of great antiquity (>3180 Ma for parts of the Yilgarn Craton; Nieuwland & Compston 1981), which have undergone high-grade metamorphism and host economic mineralisation. Despite relatively good access, both the location of significant lithologic boundaries and, thus, understanding of the regional geology are severely limited by poor outcrop, a result of extensive regolith. Previous geological studies include the 1:250 000 regional geological mapping (Chin 1986; Chin et al. 1984; Chin & Brakel 1986; Muhling & Brakel 1985; Thom & Chin 1984; Thom et al. 1984; Wilde & Low 1980; Wilde & Walker 1982; Wilde & Walker 1984). The regional geological framework is constrained by structural, metamorphic and isotopic investigations, but these data neither detail province boundaries nor the distribution of lithologies. This paper offers a model of the Precambrian geology of the southwest Yilgarn Craton and Albany Province[2] through the integration of geophysical and geological data. The geophysical data are invaluable to this model as they map major zones and regional structures and are little affected by regolith. This integrated model is based in particular on stacked profiles, contours, and images of the aeromagnetic data, published as a map at 1:1M scale (Whitaker 1992).

Previous aeromagnetic pixel maps (Tucker & D'Addario 1986) addressed the classification and distribution of textural patterns for the Albany 1:1M sheet, but did not refer to mapped geology, and consequently did not offer an understanding of the origin and significance of the main components of the crust.

Geological framework

The major geological components of the Albany 1:1M Sheet area are the Yilgarn Craton, Albany Province, and Perth Basin (Figs 1 and 2). Page et al. (1984) previously published granitoid crystallisation ages of between 4.2 and 2.6 Ga for the Yilgarn Craton, 1.7 and 0.9 Ga for the Albany Province, and 1.1 and 0.6 Ga for basement to the Perth Basin. McCulloch (1987) estimated Sm–Nd depleted-mantle derivation model ages, respectively, of between 3.7 and 2.6 Ga, 2.3 and 1.9 Ga, and 2.2 and 1.1 Ga for these components.

The southwestern Yilgarn Craton consists of the Southern Cross Province and Western Gneiss Terrane (Gee et al. 1981; fig. 1). The Southern Cross Province is composed of greenstone belts separated by large areas of granite. These belts are long and sinuous and comprise greenschist to amphibolite facies sediment, ultramafic rocks, basalts, and felsic volcanics (Binns et al. 1976). Conventional zircon U–Pb ages of approximately 2.7 Ga were obtained from felsic volcanic rocks and rhyolite in greenstone sequences of the Southern Cross Province to the northeast of the sheet (Pidgeon & Wilde 1990).

The Western Gneiss Terrane is generally regarded as being older than the other provinces of the Yilgarn Craton (Gee 1979). It is composed mainly of poorly layered amphibolite to granulite facies quartzo-feldspathic gneiss and granite, with enclaves of similarly metamorphosed interbedded sediments and volcanics. Meta-quartzite in the Jimperding Metamorphic Belt is thought to have formed between 3340 and 3180 Ma (Nieuwland & Compston 1981). The terrane encloses the greenschist facies Saddleback Greenstone Belt, which is probably a remnant of younger greenstone. This greenstone belt has given U–Pb isotopic ages (in the range 2670–2650 Ma; Wilde & Pidgeon 1986), which are comparable with ages for granite–greenstone terrane farther east.

[1] Australian Geological Survey Organisation, GPO Box 378, Canberra ACT 2601.

[2] Albany Province is used here to represent rocks thrust against the southern boundary of the Yilgarn Craton during the Mid-Proterozoic and is distinguished from the Albany Fraser Orogen, a name currently in use by the Geological Survey of Western Australia, which includes both the Albany Province, defined herein, and the deformed southern margin of the Craton.

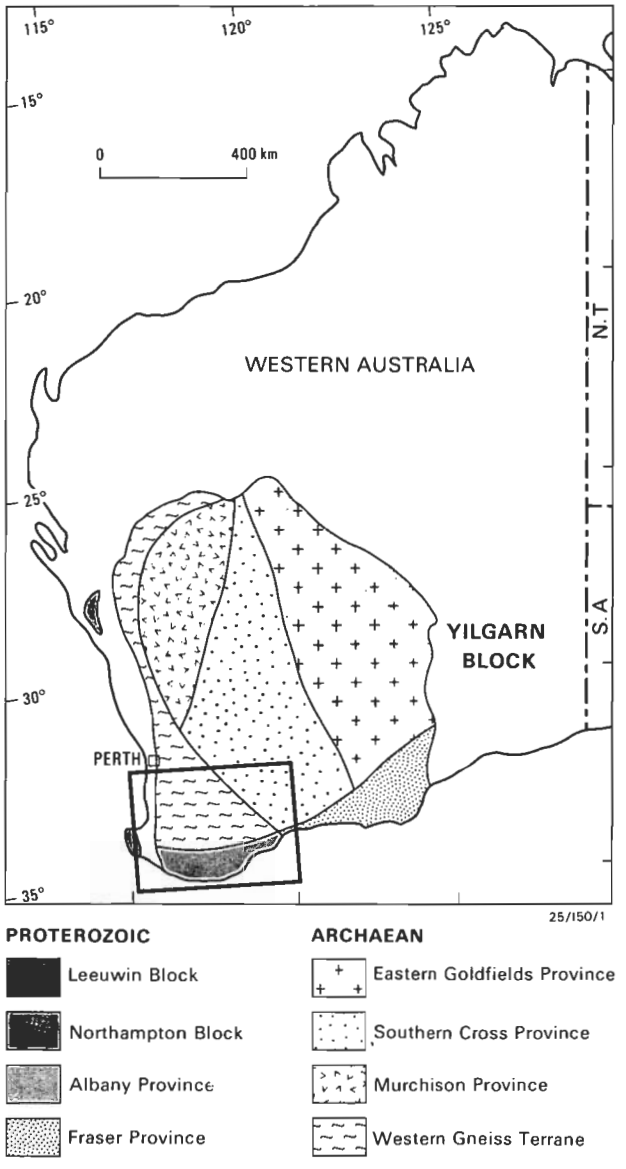

Figure 1. Location of the Albany 1:1M Sheet area and major subdivisions of the Yilgarn Craton (adapted from Gee et al. 1981, after Whitaker 1989). Figures 3, 5, 6, 9, 10 and 12 correspond with the outlined rectangular area. The term Yilgarn Block in this and subsequent figures equates with Yilgarn Craton used in the text.

The east–west-elongated Albany Province, to the south of the Yilgarn Craton, consists of highly deformed basic and acid gneiss of amphibolite to granulite facies, and granite (Wilde & Walker 1984; Muhling & Brakel 1985; Fig. 1). The province was metamorphosed at about 1300–1100 Ma, when it was transpressionally deformed (Beeson et al. 1988) against the Yilgarn Craton; its boundary with the Yilgarn Craton is almost totally obscured by regolith.

Unconformably overlying the southern Yilgarn Craton are weakly to moderately deformed, greenschist facies, sandstones, and shales of the Proterozoic Stirling Range Beds and Mount Barren Group. A whole-rock Rb–Sr age of 1150 Ma for the Stirling Range Beds (Turek & Stephenson 1966) probably dates the metamorphism. Also overlying the Craton are down-faulted remnants of Permian basins, which, at Collie, contain economic coal measures.

The Phanerozoic Perth Basin is in faulted contact (Darling Fault) with the western margins of the Yilgarn Craton and Albany Province. Proterozoic rocks underlying the basin crop out in the Leeuwin and Northampton Complexes. The Leeuwin Complex has north–south compositional layering, consisting of amphibolite–granulite facies quartzo-feldspathic and mafic gneiss (Myers 1990a).

Granites of the Albany 1:1M Sheet area have a wide range of compositions and textures; some are strongly foliated. Isotopic dating defines periods of intrusion in the Yilgarn Craton at 3100–2900 Ma, 2700–2550 Ma, and 2300–2200 Ma (Arriens 1971), and intrusion in the Albany Province at 1290–1070 Ma (Turek & Stephenson 1966; Rosman et al. 1980; Pidgeon 1990). Basic to intermediate dykes are abundant within the Yilgarn Craton. The east–northeast-trending Binneringie Dyke, part of the Widgiemooltha Dyke Suite, is the longest and broadest system in the area. Dykes are much less common in the

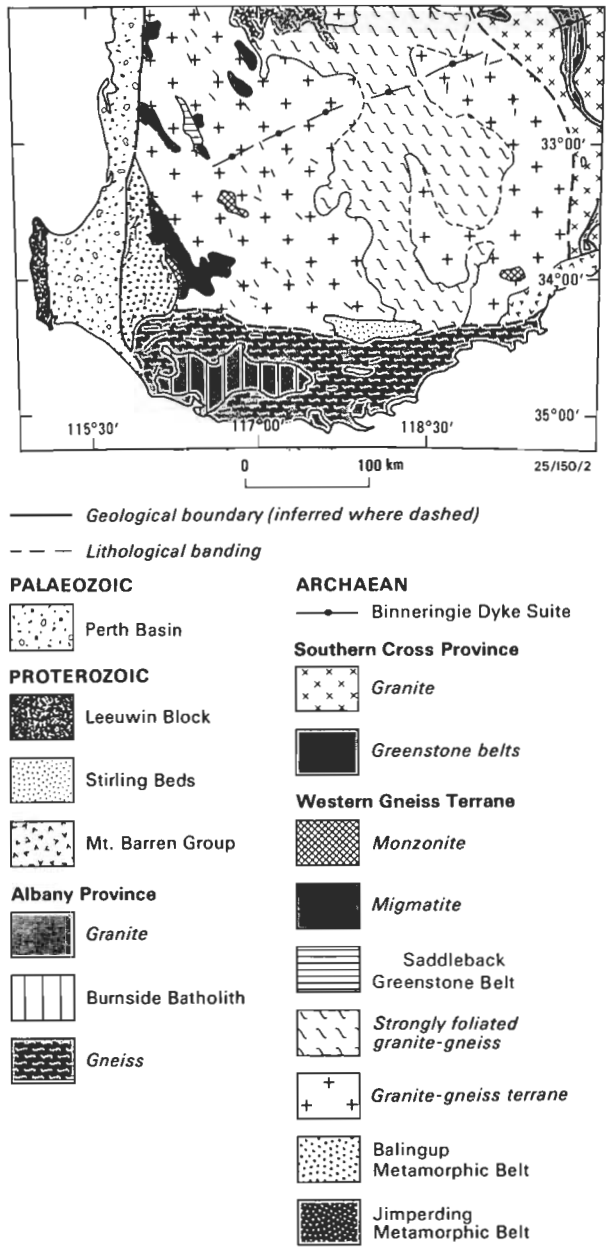

Figure 2. Geology (after Gee et al. 1986; and Myers 1989).

Albany Province. Outcrop throughout the sheet area is generally poor, owing to regolith.

Aeromagnetic data and interpretation methods

This study is based mainly on the aeromagnetic data because of the detailed information they provide on the distribution and structure of the Precambrian rocks of the sheet area, relative to the other regional geophysical data sets (gravity and gamma–ray data). Digital coverage acquired by the then Bureau of Mineral Resources (BMR, now Australian Geological Survey Organisation, AGSO) with 1.5 km line spacing covers both the Yilgarn Craton and onshore Albany Province. Much of the Perth Basin and onshore Leeuwin Complex is covered with analogue BMR aeromagnetic data flown at 1.6 km line spacing, some of which have been digitised. The offshore Leeuwin Complex is covered by surveys with line spacing of 1.5 to 6 km, as well as scattered shipborne traverses. The offshore Albany Province and its boundary with the Yilgarn Craton in the southeast of the sheet area are covered by scattered shipborne traverses and, between 115°E and 123°E, by a reconnaissance airborne survey (ESSO 1972).

The BMR aeromagnetic surveys of the Yilgarn Craton and Albany Province were flown at 150 m ground clearance, with a sample interval of 60 m. Resolution of the interpretation is constrained by the 1.5 km flightline spacing. Most anomalies were only mapped if they could be correlated between adjacent flightlines and, therefore, had to be at least 1.5 km long. Interpretation was based on computer-drawn maps of stacked flightline profiles at various amplitude scales, contour maps, and photographic prints of pixel images. Four types of images were used (Tucker et al. 1986):

- grey-scale total magnetic intensity (Fig. 3),
- pseudo-colour total magnetic intensity,
- east–west first horizontal derivative, and
- north–south first horizontal derivative.

Short-wavelength magnetic features attributed to either lithological layering or cross-cutting lineaments were largely mapped using stacked profiles of the data. The separation of these anomalies was based on their characteristics, relationship with adjacent magnetic anomalies, and correlation with geology. The stacked profiles display

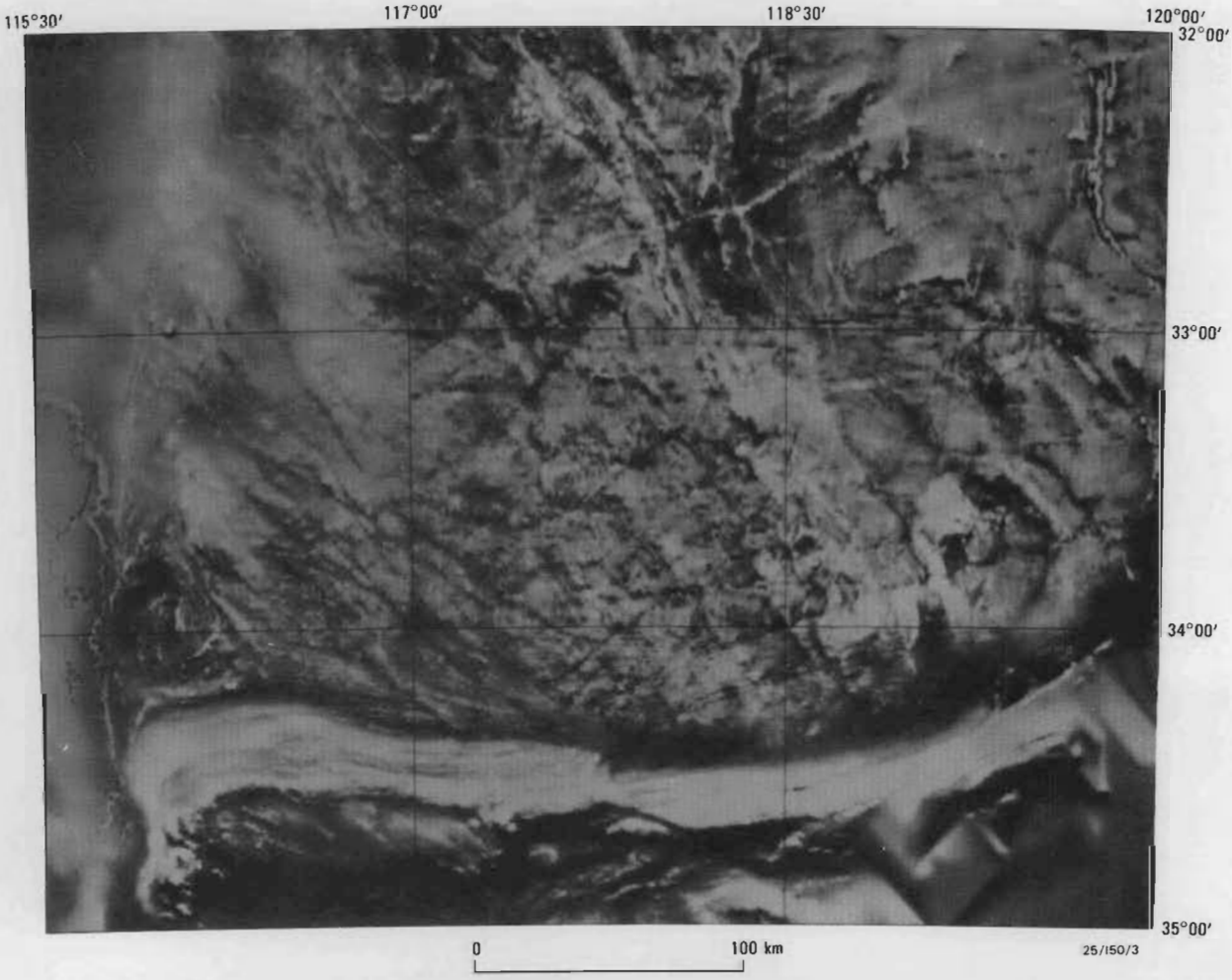

Figure 3. Total magnetic intensity grey-scale pixel image (after Whitaker 1989). The gradation from black to white represents a change from low to high magnetic anomaly values. The image was generated from a grid with cell dimensions representing approximately 450 m.

the shortest wavelength anomalies of any presentations of the aeromagnetic data with anomalies 250–350 m wide commonly correlated throughout the sheet area. Despite the necessity to relocate anomaly correlations using flight-path maps, the profile data were invaluable, providing 40–50% of structural detail; detail which was not available from other representations of the data.

Contour maps and pixel images used in the analysis were produced from grids of the data. For a flightline spacing of 1.5 km, a grid cell size of about 450 m has been found to be a reasonable compromise between interpolating values between the flightlines and representing the collected data. Anomalies more than 900 m wide (two grid cells) are well represented by grids of the data. Anomalies less than 450 m wide (one grid cell) are rarely evident in images and are not seen in contour presentations of the data. However, images and contours are more easily interpreted than the stacked profiles, and anomalies at acute angles to the flight-paths are more readily correlated in these presentations.

There is good correlation between magnetic trends related to lithological layering and adjacent (<1.5 km distant) mineral foliation mapped on 1:250 000 geological sheet areas. The correlation for PINJARRA (Wilde & Low 1980) and PEMBERTON (Wilde & Walker 1984) is shown in Figure 4. Mineral foliation is sub-parallel to lithologic layering, where observed in the Yilgarn Craton and Albany Province.

The interpretation involved two procedures: (1) anomaly separation—the identification and mapping of individual anomalies; and (2) anomaly grouping—the delineation of regions with similar anomalies or anomaly trends. Geological data were incorporated through the second of these procedures, enabling the mapping of outcrop of known affinity into areas of cover. Crustal zone boundaries were located at changes in magnetic pattern, least ambiguously where one set of lithological layering was truncated by another set. Crustal zone boundaries were

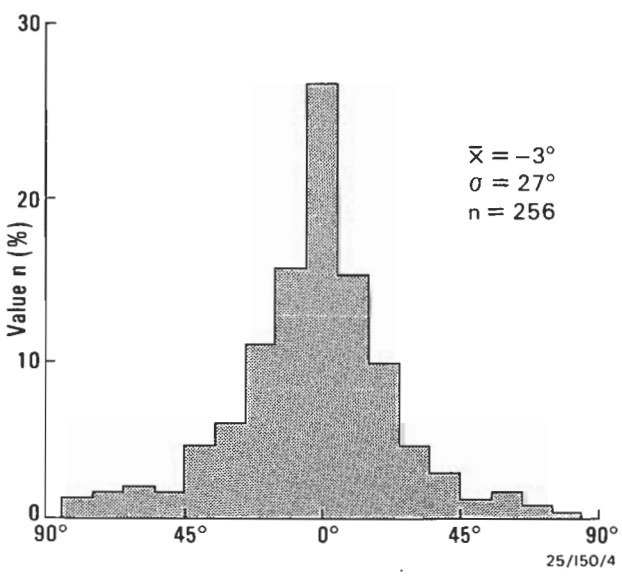

Figure 4. Histogram of the differences in direction between magnetic trend and mineral foliation. The magnetic trends are inferred to map lithological banding. Mineral foliation data for PINJARRA are from Wilde & Low (1980) and for PEMBERTON, from Wilde & Walker (1984).

also located on the steepest section of gradients between zones of different average magnetisation. The interpretative process was an iterative one, commencing with obvious correlations of either short or long-wavelength anomalies, and subsequently dealing with less-obvious correlations. The major crustal zones are:

(1) the Archaean Yilgarn Craton with common northwest to north trends;

(2) the Proterozoic Albany Province with largely easterly trends; and

(3) the Proterozoic Leeuwin Complex and basement to the Perth Basin, characterised by northerly trends. The southern margin of the Yilgarn Craton is marked by a zone of low magnetisation with few medium to high-amplitude, short-wavelength anomalies. All magnetisations are approximately in the direction of the Earth's present field, unless stated otherwise.

Interpretation of the aeromagnetic anomalies

Yilgarn Craton magnetic anomalies

The southwestern Yilgarn Craton coincides with two broad zones of relatively low magnetisation (Zones A to the east and C to the West, Fig. 5) with an intervening north-northwest to north-trending zone of high magnetisation (Zone B, Fig. 5). Zone A has many long sinuous anomalies attributed to lithological layering. In the east, bands of generally low magnetic amplitude correspond with outcrops of greenstone belts of metamorphosed sediment and mafic volcanic rocks. These eastern bands also commonly include long and narrow, very high-amplitude magnetic anomalies corresponding with outcrops of banded iron formation (BIF) and ultramafic rocks. Broad, weakly magnetised areas between the greenstone belts correlate with poorly exposed granite and gneiss. In these areas, the anomaly contrast is low and inferred compositional banding is either absent or poorly developed relative to adjacent greenstones. Zone A also contains moderate-amplitude, ovoid to elongate magnetic anomalies, caused by granite. One anomaly pattern is indicative of a zoned pluton with a rim of material more highly magnetised than the core (Fig. 5). The measured susceptibility is 600 to 2500 x 10^{-5} SI for highly magnetised granite, and 40 to 150 x 10^{-5} SI for weakly magnetised granite. In the west of Zone A, in areas of intermittent granite outcrop, long sinuous magnetic anomalies are also attributed to greenstone belts. The poorer definition of these belts and their lack of high-amplitude anomalies may reflect differences in lithology or mineralogy as a result of changes in metamorphic grade. Regardless of these subtle differences, the pattern of deformation is similar throughout Zone A.

Zone B_1 is a north-northwest-trending belt of high magnetisation (Figs 3 and 5) to the west of Zone A with weakly sinuous to linear magnetic/lithological banding. It is extensively cut by lineaments (Fig. 6). Convergent magnetic trends at its northern end may reflect large-scale folds. The belt occurs within a region of strongly deformed north-northwest-trending rocks which underwent granulite metamorphism at about 2640 Ma (fig. 2; Nemchin in press). B_2 is a more northerly trending belt (Fig. 5) of similar magnetisation and internal structure, thought to be a dislocated segment of Zone B_1. The eastern boundary of Zone $B_{(1+2)}$ corresponds with a change in structural

pattern from the sinuous lithological banding trends of Zone A to the largely linear trends of Zones B and C. This boundary is inferred to be a major intra-craton discontinuity, across which there is a change in both gross geology and structure.

Zone C of Figure 5 largely consists of sparse, weak to moderate-amplitude anomalies of short strike extent and dominant north-northwest trends. The zone coincides with widespread granite and quartzo-feldspathic gneiss of fairly uniform composition. Anomalies attributed to granite cover a larger area in the western third of the zone; a number of these bodies are angular in outline and bounded by lineaments. Along the western boundary of Zone C in a 2–4 km wide corridor adjacent and parallel to the Darling Fault, north-trending linear anomalies are unusually abundant. The northerly orientation of these anomalies

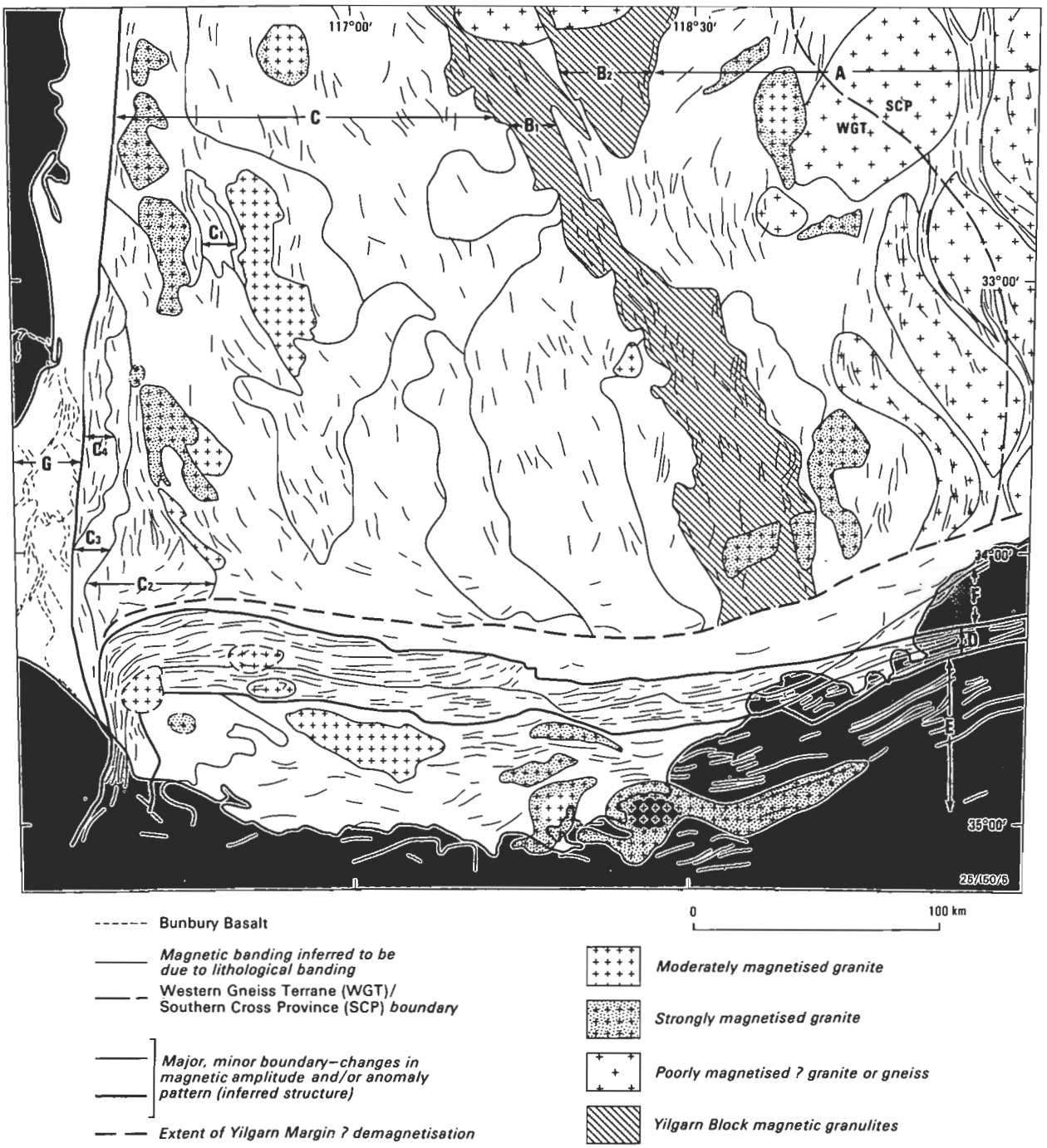

Figure 5. Major crustal components and their internal structure as determined from aeromagnetic data (after Whitaker 1989). The Yilgarn Craton is composed of zones A, B, and C. Zone A is granite–greenstone terrane and Zone C is dominantly granite–gneiss terrane. Zone $B_{1\&2}$ is a belt of highly magnetised granulites. Zone B_1 correlates with part of the Jimperding Metamorphic Belt in the north of the area. Sub-zone C1 correlates with the Saddleback Greenstone Belt and sub-zones C_2 to C_4 correlate with the Balingup Metamorphic Belt. The Albany Province is composed of zones D (northern zone) and E (southern zone). Zone F is an area of deformed Yilgarn Craton with trends imposed from thrusting of inferred Albany Province equivalents in the west of the Esperance 1:1M sheet area. Zone G is the Perth Basin.

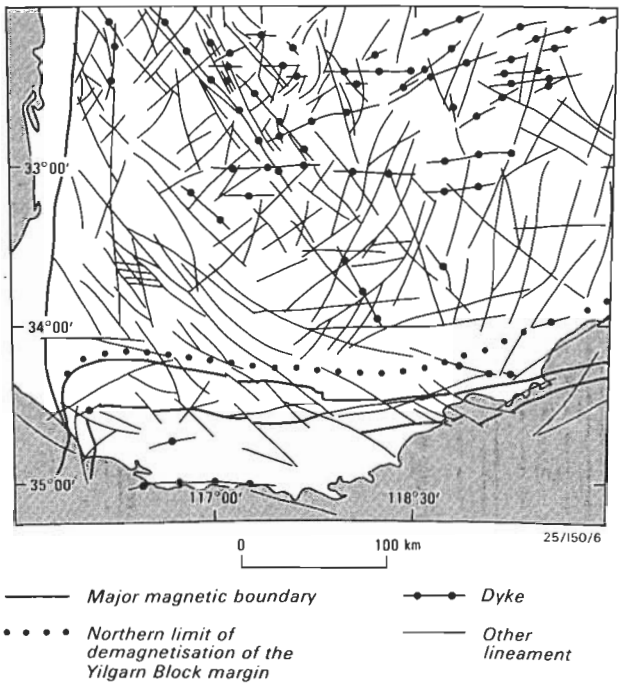

Figure 6. Major lineaments, including dykes, as mapped from the aeromagnetic data.

perhaps represents a structural overprint of the more general north-northwest compositional trends of Zone C through tectonism associated with the basement to the Perth Basin and the Darling Fault. Zone C encloses the small Saddleback Greenstone Belt (Fig. 2; C_1 in Fig. 5), which correlates with an area of relatively low magnetisation. It includes a long, thin magnetic high, which corresponds with an ultramafic unit. These characteristics of magnetisation are similar to those of larger greenstone belts to the east in Zone A.

The Balingup Metamorphic Belt in the southwest of Zone C (Fig. 2, C2 to C4 in Fig. 5) corresponds to a region of abundant, elongate, sub-parallel, short-wavelength anomalies, indicative of well-developed lithological layering. The belt can be subdivided on the basis of the abundance of inferred layering, with highest incidence in the east and west (parts C2 and C4, respectively). The intervening part (C3 in Fig. 5) corresponds with a north-northeast to north-trending, 10 km wide, band of low magnetic amplitude, relatively devoid of short-wavelength anomalies. Several long, high-amplitude anomalies in part C2 correspond with outcrops of BIF and ultramafic rocks. The western boundary of the Balingup Metamorphic Belt coincides with the Darling Fault. The eastern boundary is less well-defined and is interpreted as occurring where common sub-parallel layering is lost.

Zones A and B+C correspond approximately with the Southern Cross Province (SCP) and Western Gneiss Terrane (WGT) of Gee et al. (1986). The Province/Terrane boundary is placed by Gee et al. at the western edge of outcrop of large greenstone belts (Figs 2 and 5). However, this position does not correspond to a boundary in the aeromagnetic data (Fig. 3) and cuts across anomaly trends interpreted to be buried greenstone. In addition, the inferred deformation pattern of the western part of Zone A is identical to that in the area accepted as Southern Cross Province to the east. A different approximate southwestern boundary to the SCP, located in the west of Zone A, was used by Gee et al. (1981). This boundary cuts across Zone B in the north of the sheet. The most appropriate boundary between granite–greenstone terrane (SCP) and granite–gneiss terrane(WGT) is the boundary between Zones A and B, where gross changes in lithology and structural deformation are inferred.

Lineaments

Images of the aeromagnetic data show numerous lineaments cutting the area of the Yilgarn Craton (Figs 3 and 6). The most common result from irregularly shaped, low-amplitude magnetic lows. The cause of these lineaments is not certain, though it is speculated here that they are due to demagnetised fault and shear zones. In many instances, the lineaments truncate or dislocate inferred geological trends, as may be expected by faulting. The orientation and geometry of local dykes as mapped in the 1:250 000 geological maps do not readily explain these anomalies, nor are the anomaly shapes and their variation along strike typical of dyke associated-anomalies. Thus, faults and shears are thought to be a likely cause for most of the lineaments in the regional data.

Moderate to high-amplitude, normally polarised, and moderate to strongly reverse-polarised lineaments are much less abundant. These anomalies are attributed to, and in a number of instances correlate with, outcropping dykes. The longest and perhaps broadest group of dyke-related anomalies correlate with the Binneringie Dyke. The dyke is the largest in the region (McCall & Peers 1971) and is inferred from the magnetic data to traverse at least 250 km of the Yilgarn Craton within the Albany Sheet (Fig. 2) and a similar distance to the east-northeast. In the northeast of the sheet area, results of ground magnetic traverses (this study) indicate that a dyke swarm comprising the Binneringie Dyke is over 600 m wide. Most dykes in the Albany Sheet area, by comparison, are relatively narrow (Myers 1990b) and are not resolved in the regional aeromagnetic data. The susceptibility of measured outcropping dykes ranges from 40 to 6000 x 10^{-5} SI. Reverse-polarised dykes are not known to crop out within the Albany Sheet area.

Dominant directions of lineaments attributed to faults and shears differ across the Yilgarn Craton (Fig. 6): in Zone A trends are mainly north-northeast and east-northeast; in Zone C trends are mainly northwest and northeast; in Zone B, between Zones A and C, lineaments are abundant with most directional groupings well represented; and along the southern margin of the craton trends are mainly west-northwest in the west and east-northeast in the east, sub-parallel to the local boundary of the craton. Curvilineaments are particularly prevalent in the southwest of the craton. Lineaments attributed to dykes are mainly oriented in just three directions: north-northwest, east-northeast, and east–west.

Albany Province magnetic anomalies

The Albany Province, as defined from the aeromagnetic data, has easterly trending magnetic anomalies cutting across the general trends of the Yilgarn Craton. It consists of two main subdivisions: a larger southern zone of low magnetisation (E, Fig. 5), and a zone of very high magnetisation (D, Fig. 5) to the north and west.

The southern zone is characterised by weakly sinuous, east–west anomalies, attributed to compositional layering.

Drag folds are inferred adjacent to some of the larger cross-cutting faults, though lineaments generally are not common. The zone is intruded by several moderate to highly magnetised elongate to ovoid granites, with long axes parallel to adjacent lithological trends. Some of these granites are zoned, with relatively highly magnetised rims.

The very highly magnetised northern zone of the Albany Province is the most outstanding feature of the TMI pixel image (Fig. 3). The northern and southern boundaries are marked by steep magnetic gradients, and the northern boundary truncates internal lithological banding of the zone at an acute angle. The linear internal structure is distinctly different from sinuous banding of the southern zone. The northern zone can be subdivided for much of its length into two parts, with a southern part of higher average magnetisation relative to the northern part. North-west-trending lineaments, inferred to be faults, dislocate the northern zone at 10 to 25 km intervals (Fig. 7). The net transcurrent component of movement on these faults ranges from 5 to 15 km, and is consistently dextral (Fig. 7). Correlation of thin magnetic bands between fault blocks is difficult, owing to common east-northeast-trending magnetic lineaments, which intersect the banding at acute angles. A dextral sense of movement is also indicated in outcrop on east to east-northeast-trending thrust faults adjacent to and in the eastern portion of the zone (Beeson et al. 1988).

Magnetic susceptibility was measured on rocks exposed on a transect across the northern zone from the lower Pallinup River to Cape Riche (Fig. 8; Section V, Fig. 12). The transect was previously mapped in detail by Beeson et al. (1988). The northern zone is characterised by an abundance of mafic gneiss in layers of 1 cm to 40 m, which locally account for up to 30% of outcrop. Quartzo-feldspathic gneiss is the most common lithology exposed over the length of the transect. The highest susceptibility measured coincided with a section of two-pyroxene granulite in the northern zone (Fig. 8). Within this section susceptibility of quartzo-feldspathic rocks averages 1 x 10^{-2} SI and mafic rocks 6 x 10^{-2} SI. These susceptibilities are 10 to 100 times the average values of respective compositions at lower metamorphic grade to the north or south. Similar granulites in the Fraser Complex are considered to be up-thrust lower crustal material (Fountain & Salisbury 1981; Myers 1990c). Schlinger (1985) showed that rocks identified as exposed lower crust and of intermediate-pressure granulite facies contain abundant magnetite, and so have anomalously high magnetisation. Susceptibilities of felsic and mafic granulites of the northern zone of the Albany Province are comparable to those reported by Schlinger (1985; Table 1). Lower susceptibilities for retrogressive granulite in the northern part of the section across the northern zone are also consistent with experimental work, which shows that magnetite is consumed at lower grades of metamorphism (Schlinger 1985). Lower average magnetisation in the northern part of the northern zone may, therefore, be more a result of retrogressive metamorphism rather than differences in lithology. High average mag-

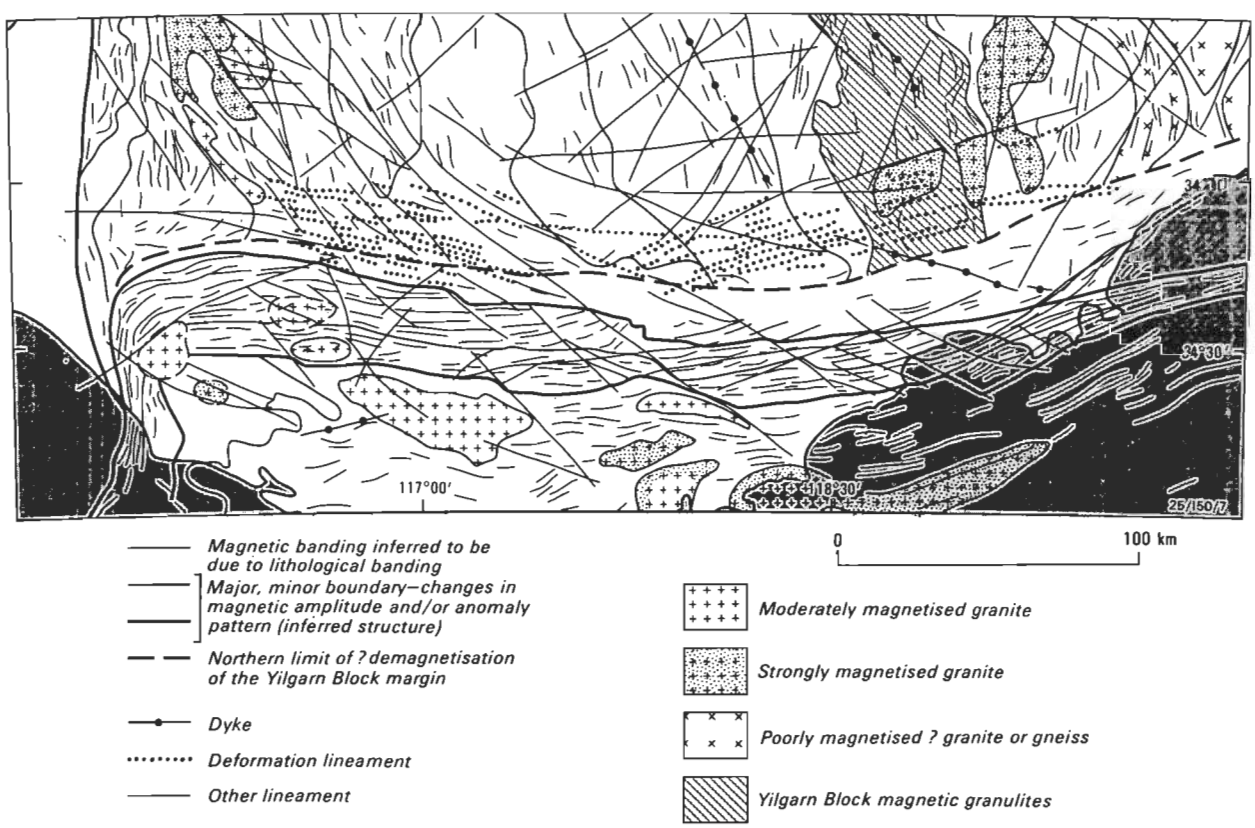

Figure 7. Detail of the aeromagnetic interpretation (Whitaker 1992) of the southern Yilgarn Craton and northern Albany Province. This highlights regions of deformed and demagnetised Yilgarn Craton; the transgressive northern boundary of the magnetic granulites of the Albany Province; brittle dislocation of the northern zone of the Albany Province by northwest trending faults; and folding of the northwestern Albany Province and southwestern Yilgarn Craton margins adjacent to the Perth Basin.

netisation in the northern zone is thought to map the distribution of intermediate pressure granulite. Rocks of the Yilgarn Craton to the north and the southern zone of the Albany Province are of lower metamorphic grade (Beeson et al. 1988). Taken together, the above features are compatible with the northern zone having been thrust from the mid to lower crust into higher crustal levels of lower metamorphic grade.

Sm–Nd (mantle differentiation) model ages of 3.1 to 2.7 Ga for samples from the northern zone (Fletcher et al. 1983) are considerably older than ages of 2.2 to 1.8 Ga from the southern zone. Fletcher et al. (1983) noted the similarity of the Archaean ages with those of the adjacent Yilgarn Craton, though the sample localities clearly fall in the Albany Province as defined from aeromagnetic data. These results have been largely confirmed by U–Pb ion–microprobe analyses (Black et al. 1992). Apparent contemporaneous ductile deformation of the southern zone is thought to preclude it from driving the thrusting of the northern zone. Perhaps the northern zone represents thrust Archaean basement to younger Proterozoic crust to the south.

Deformation of the southern margin of the Yilgarn Craton

The characteristics of magnetisation of the Yilgarn Craton change towards its southern boundary (Fig. 7). Over the interval from 50 to 20 km north of this boundary, the

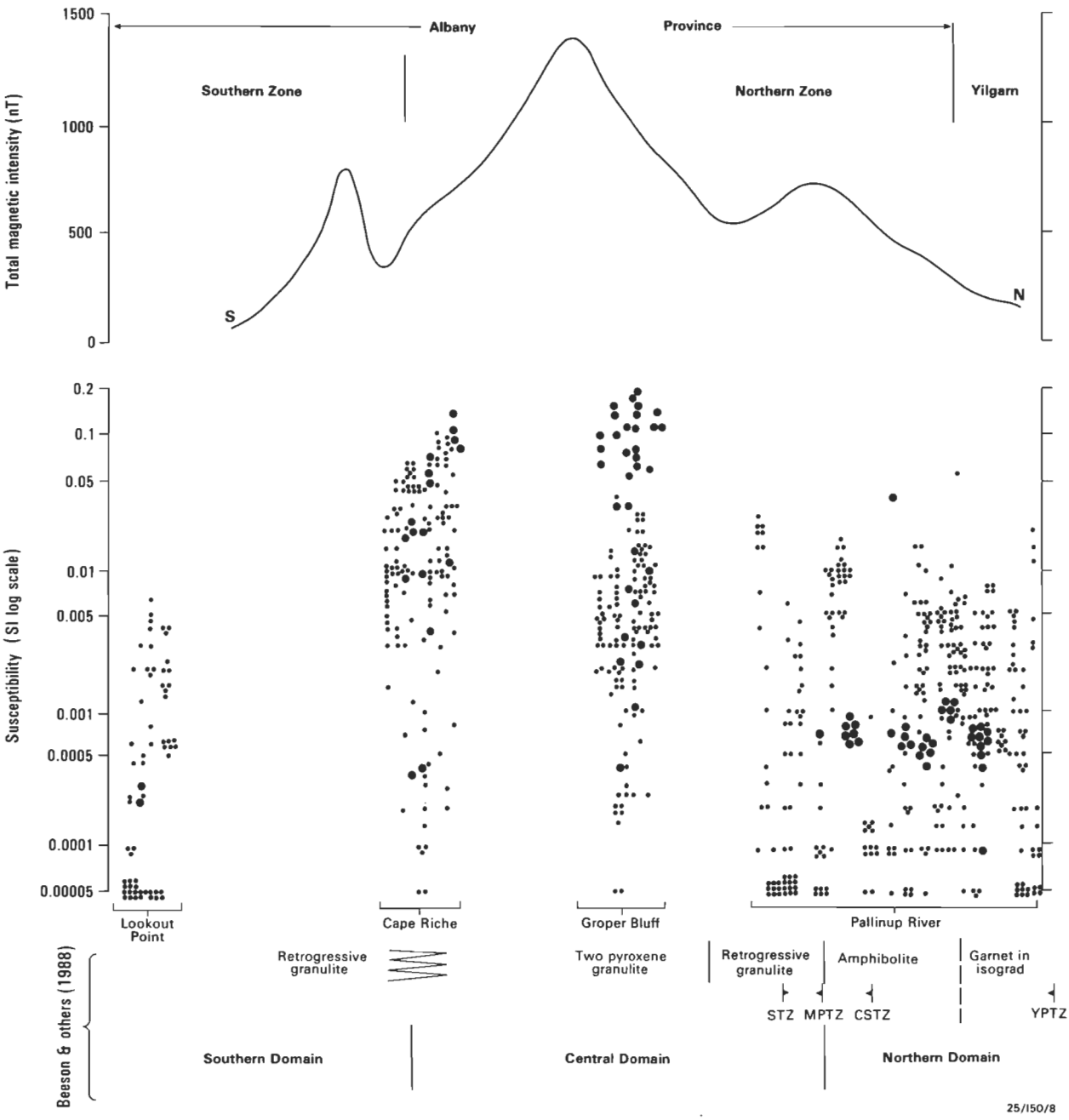

Figure 8. Section across the northern magnetic granulites of the Albany Province along 118°45′E, comparing an aeromagnetic profile (top), measured susceptibilities (centre, log SI scale, mafic compositions in large dots), and results of studies of metamorphism and structure by Beeson et al. (1988) (bottom). The section is located and labelled V in Figure 12.

Table 1. Average susceptibility (K_{av}), standard deviation (σ) and the number of samples (n) for felsic and mafic rocks from a traverse across the northern zone of the Albany Province, summarising the results plotted in Figure 8.

Southwestern Australia					*Norway*
Zone and metamorphic grade	*Rock type*	*n*	*K_{av} SI units*	*σ SI units*	*K SI units*
Yilgarn Craton amphibolite grade	Felsic	146	2.0×10^{-3}	2.7×10^{-3}	1.0×10^{-2}
	Mafic	5	6.7×10^{-4}	4.0×10^{-5}	
Northern zone Albany Province	Felsic	157	3.2×10^{-3}	2.0×10^{-3}	
garnet present, amphibolite grade	Mafic	24	7.4×10^{-4}	2.0×10^{-3}	
Northern zone Albany Province	Felsic	65	2.8×10^{-3}	6.0×10^{-3}	5.0×10^{-3}
retrograde granulite	Mafic	—	—	—	—
Northern zone Albany Province	Felsic	234	1.4×10^{-2}	1.8×10^{-2}	4.8×10^{-2}
2 pyroxene granulite	Mafic	52	6.0×10^{-2}	5.5×10^{-2}	6.7×10^{-2}
Southern zone Albany Province	Felsic	61	1.2×10^{-3}	1.5×10^{-3}	
amphibolite grade	Mafic	2	2.8×10^{-4}	3.0×10^{-5}	

Susceptibility for felsic gneiss of two-pyroxene granulite facies in the northern zone of the Albany Province is up to 10 times higher than for similar rocks at lower metamorphic grade to the north or south, while that of less abundant mafic composition is 10 to 100 times that of similar rocks at lower grade. The results are compared with those obtained by Schlinger (1985) for a deep crustal section in Norway.

north to north-northwest magnetic trends characteristic of the craton are increasingly overprinted by weak, sub-parallel sets of lineaments. The lineaments trend 100° in the west and 080° in the east. From 20 km north of the boundary to the boundary, lithological trends become rare and magnetisation decreases to low and is uniform. The decrease in magnetisation is thought to be largely due to loss of susceptibility (demagnetisation) associated with increasing southward structural deformation (Beeson et al. 1988) towards the southern boundary of the craton. Where lithological banding is inferred along the margin, it is grossly sub-parallel to the local boundary of the craton and sheared westward of correlatives farther north. The deformation is attributed to tectonic interaction between the Yilgarn Craton and the Albany Province; rocks from the margin of the craton record the approximate 1100 Ma (Black et al. 1992) tectonothermal event recorded throughout the Albany Province. Similar deformation and demagnetisation at the margin of crustal blocks has been described by Wellman (1992) for the southern margin of the Mount Isa and Arunta Blocks, and by Klasner & King (1986) for the southwest margin of the Superior Craton in North America.

The extensive deformation and demagnetisation of the southern margin of the Yilgarn Craton is evidence that the Albany Province was part of a rigid province or block during the Mid-Proterozoic and not merely a ductile zone of new crust generation. Characteristics of this style of tectonism differ from those observed for the interaction between the granite–gneiss (WGT; zones B and C, Fig. 5) and granite–greenstone terrane (SCP; zone A) within the Yilgarn Craton. At this boundary, tectonism produced a zone of similar strong foliation/deformation parallel to the boundary, but did not demagnetise either margin. The difference in deformation styles may be the consequence of fundamental differences in tectonism or due to the intracratonic boundary having been eroded to a deeper level (hence the more widespread granulite metamorphism), exposing rocks which were more ductile during tectonism.

In the east of the Albany Sheet area, the Albany Province trends offshore and truncates southwest-oriented lithological banding in the margin of the Yilgarn Craton (Zone F, Fig. 5). This area is partly covered by an aeromagnetic survey flown for ESSO (1972) and by BMR regional data. Interpretation of these data suggests that the crust in Zone F has been deformed by thrusting of Albany Province equivalents against a northeast–southwest craton boundary to the east of the sheet area. From these relationships, I infer that major thrusting events of the Albany Province occurred diachronously from east to west.

Perth Basin magnetic anomalies

The Perth Basin correlates with a region of few short-wavelength anomalies in the west of the sheet area (Figs 3 and 5). The transition from abundant short-wavelength anomalies over the Yilgarn Craton to largely long-wavelength anomalies associated with the basin is abrupt and coincides with the Darling Fault. The broad north–south-trending anomalies are attributed to basement underlying the basin. Shallowing of the basement to the south is indicated by a southward increase in amplitude and narrowing of the anomalies. Some short-wavelength anomalies are apparent and are attributed to Bunbury Basalt. The anomalies are dominantly reverse-polarised, narrow and meandering, indicative of lava flow in palaeochannels.

The northern zone of the Albany Province and the southwestern margin of the Yilgarn Craton are folded southward adjacent to the Darling Fault (Figs 3 and 5). Tectonism associated with the Proterozoic basement of the Perth Basin is a likely cause of this apparently ductile deformation; it differs from, and is inferred to overprint, the brittle deformation experienced by the northern zone during thrusting of the Albany Province about 1.1 Ga.

Gravity data and interpretation methods

The regional gravity data sets covering the Albany 1:1M sheet area are a road-based Perth Basin survey by WAPET in 1963, a BMR helicopter survey with an 11 km grid of stations covering the remainder of the land area (Fraser 1974), and shipborne BMR continental margin surveys with 50 km line spacing (Petkovic 1975). More detailed surveys with 1–4 km station spacing along roads include surveys of the Bridgetown 1:100 000 sheet area by the Geological Survey of Western Australia (Kevi 1988), and of the COLLIE, DUMBLEYUNG, PEMBERTON, and MT BARKER 1:250 000 Sheets areas by Otter N.L. in 1985.

The gravity interpretation is based on maps of Bouguer anomaly (Fig. 9) and residual Bouguer anomaly. The residual was generated by subtracting a regional surface with wavelengths of greater than 40 km from the Bouguer anomaly. The zero contour of the residual map coincides with the steepest Bouguer anomaly gradients and was largely used to map the boundaries between dense and relatively less-dense bodies. The observation spacing of the gravity anomalies (11 x 11 km) is much greater than that for magnetic anomalies (1.5 km x 60 m), so only long-wavelength gravity anomalies have been mapped, and their shape is poorly constrained. The gravity anomalies of Figure 9 will be referred to using the labels on the gravity interpretation (sources) map (Fig. 10). The gravity interpretation draws heavily on the coincidence of anomalies with geology.

Major features of the gravity map

The Yilgarn Craton is characterised by gravity anomalies that are diverse in shape and orientation, and by strong gravity gradients near its edges. Anomalies trend north–south over the Perth Basin, and east–west over the Albany Province.

Within the Albany 1:1M Sheet area, average Bouguer anomaly decreases by about 20 ($\mu m/sec^2/km$ in an east-northeast direction across the Yilgarn Craton (Fig. 9). There is no comparable free-air anomaly gradient (Wellman & Murray 1979), and so the Bouguer anomaly gradient must be due to the increase in mean elevation from the coast to 450 m in the east-northeast.

The Bouguer gravity high and gradient in the southwest of the Yilgarn Craton are attributed to the very much higher crustal density relative to crust to the west and south (figs 10 and 11 of Wellman 1978), slightly higher density relative to crust to the northeast (Drummond & Esa Mohamed 1986), and to the increase in the mean elevation to the east-northeast.

Yilgarn Craton gravity anomalies

The western boundary of the Yilgarn Craton coincides with the Darling Fault and a steep gravity gradient. The change in gravity from high over the craton to low over the Perth Basin is approximately 700 $\mu m/sec^2$, occurring over a distance of about 15 km. The gradient is inferred to define a steeply dipping boundary between dense upper crust of the Yilgarn Craton and less-dense sediments of

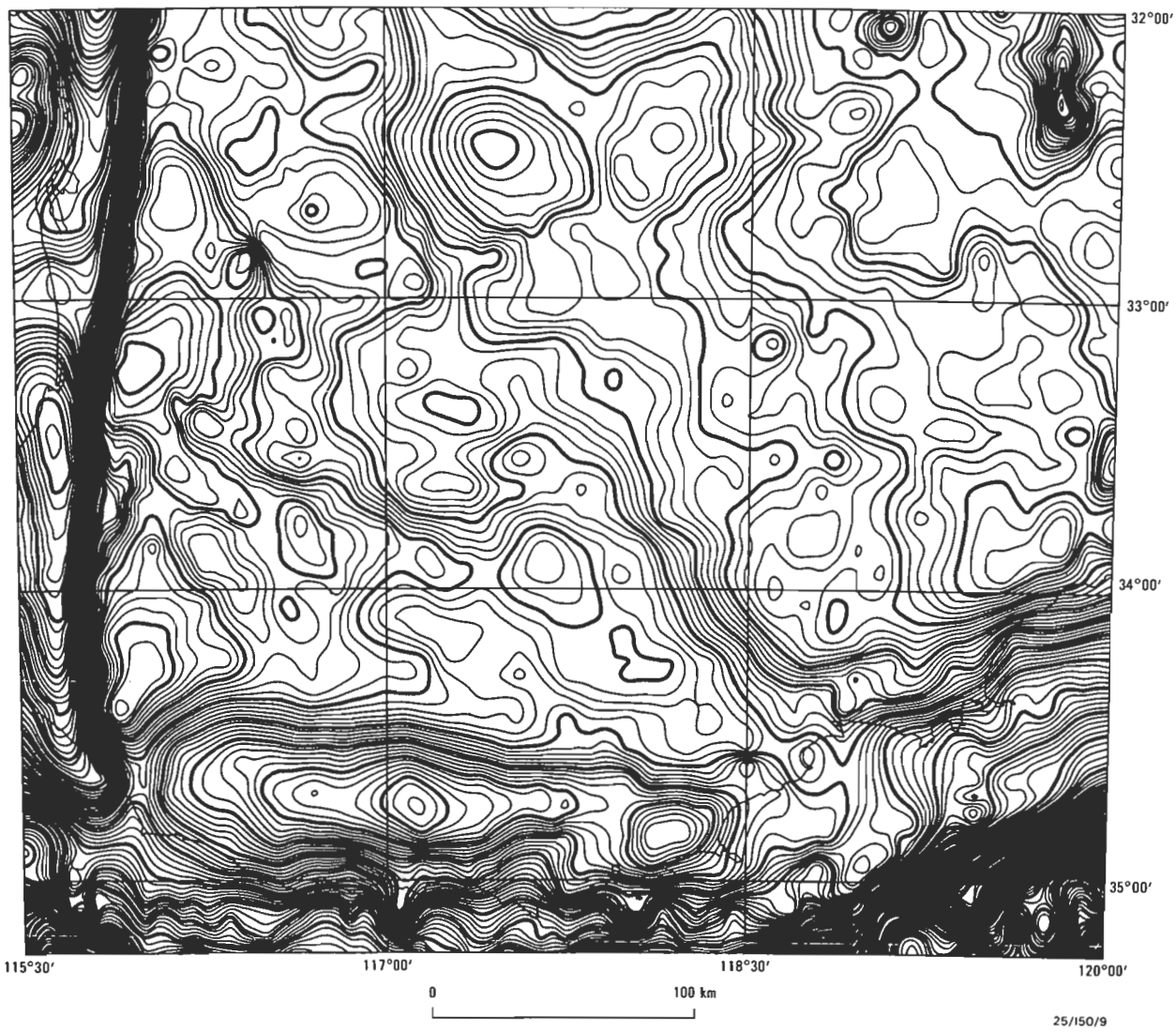

Figure 9. Bouguer gravity anomalies (contour interval 20 $\mu m/s^2$).

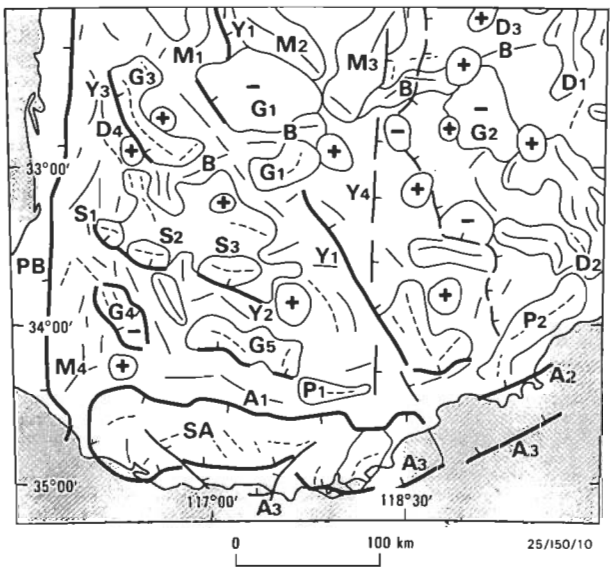

Figure 10. Gravity interpretation based on major gradients of the Bouguer anomaly and the zero line of the residual map. Major gradients are mapped by thick lines with ticks indicating down-slope direction (A1 to A3 & Y1 to Y3). Minor gradients are mapped by thin lines with ticks indicating down-slope direction. Axes of elongate gravity highs and lows are denoted by thin continuous and dashed lines, respectively. Relative gravity lows correlate with the Perth Basin (PB), southern Albany Province (SA), upper crust east of gradient Y_1, Proterozoic (P_1, P_2) and Permian sediments (S_1) overlying the Yilgarn Craton, and some granites (G_1 to G_5). Relative gravity highs are associated with the southwest Yilgarn Craton west of gradient Y_1, the northern magnetic granulites of the Albany Province, parts of the greenstone (D_1 to D_4) and metamorphic belts (M_1 to M_4), and the Binneringie Dyke Suite (B).

the Perth Basin.

Several gravity gradients with lower gravity values to either the east or northeast are located within the Yilgarn Craton (Y_{1-4}, Fig. 10). Of these, the north-northwest-trending gradient Y_1 (Fig. 10) has the greatest change in gravity (~300 μm/sec^2), and coincides with both the Southwest Seismic Zone and a change in upper-crustal seismic velocities (Drummond & Esa Mohamed 1986). Esa Mohamed (1985) attributed upper crustal velocities of approximately 6.3 km/sec south-southwest of the gravity gradient to lower crustal rocks at anomalously high levels in the crust, and upper-crustal velocities of about 6.1 km/sec east-northeast of the gradient to less-dense upper crustal rocks. This gravity gradient is wider (30–40 km) than that over the Darling Fault; the greater width may result from changes in density at a deep crustal level, a dipping boundary or a combination of both. Faults separating crust of average crustal density are considered the most likely cause of all the linear gravity gradients. An east-northeast alignment of residual gravity highs (B, Fig. 10) with a 20–40 μm/sec^2 amplitude comprise a second type of gravity lineament. The gravity high is attributed to dense mafic rocks of the Binneringie Dyke.

Granite is spatially associated with gravity lows G_1 to G_4 in Figure 10. The amplitude of residual lows due to granite in the Yilgarn Craton is greater in the west (80–120 μm/sec^2) than in the east (40–60 μm/sec^2). This difference is attributed to higher average crustal density in the west (as inferred from the seismic and gravity data), and consequently to higher-density contrast between granite and surrounding crust in the west.

Greenstone belts correlate with steep-sided residual gravity highs of 150–270 μm/sec^2 (D_{1-4}, Fig. 10). The poor relationship of anomaly outline to the shape of the belts as determined from magnetics and geology is undoubtedly the result of the broad gravity station spacing and the position of the stations relative to dense lithologies (BIF, ultramafic rocks and basalt). However, the long axes of anomalies are aligned with the elongation of corresponding belts.

Metamorphic belts correlate with residual gravity highs of 50–80 μm/sec^2; M_1 and M_2 with the Jimperding Metamorphic Belt and M_4 with the Balingup Metamorphic Belt. Gravity anomalies associated with metamorphic belts are of lower amplitude than those related to greenstone belts; this difference is attributed to a net lower density contrast of the metamorphic belts with the surrounding country rocks, reflecting a considerably lower abundance of dense lithologies, including basalt, dolerite and BIF. Gravity and magnetic anomalies associated with M_3 in Figure 12 are similar to those associated with the Jimperding Metamorphic Belt and are considered to delineate related crust. Zone B in the aeromagnetic interpretation (Fig. 5) is inferred to map a belt of highly magnetised granulites that encloses the Jimperding Metamorphic Belt. The belt traverses south-southeast, across the Yilgarn Craton. For much of this distance, it correlates approximately with a step in the east-northeast regional gravity gradient (Fig. 9). In detail, the centre of the broad gravity gradient defining the eastern side of the step is between 2 and 15 km east of the eastern edge of the belt as defined by the magnetic data. This offset perhaps results from an eastward dip of the belt, with the centre of the gravity gradient marking the position of the boundary at a deeper crustal level than that determined from the aeromagnetic data.

Proterozoic and Permian sediments overlying the Yilgarn Craton correlate with low-amplitude gravity lows. The residual lows are –20 μm/sec^2 over the Proterozoic Stirling Range beds (P1, Fig. 10), –80 μm/sec^2 over the Proterozoic Mount Barren Group (P2, Fig. 10), and –60 μm/sec^2 over the Permian Collie Basin (S1, Fig. 10). There are insufficient gravity and geological data to determine the cause of two adjacent, similar gravity lows to the east-southeast of Collie (S_2 and S_3, Fig. 10); Permian sediments or granite are considered the most likely causes.

Albany Province gravity anomalies

The Albany Province is dominated by strong east–west-trending gravity gradients. In the west of the Province, a major south-sloping gradient (A_1, Fig. 10) approximates the boundary determined from the aeromagnetic data between the northern and southern zones of the province. The gradient is used to infer that the net density of the upper crust of the southern zone is less than that of the northern zone of the province and the abutting Yilgarn Craton (Fig. 11). Farther east, a north-sloping gradient (A_2, Fig. 10) approximates the boundary between the northern zone of the province and the Yilgarn Craton. In this region, relatively low-density upper crustal rocks of the Yilgarn Craton are thicker than in the west (Esa Mohamed 1985) and are inferred from gravity data to be less dense than the rocks of the northern zone of the Albany Province. The location of the gravity gradients

A_1 & A_2 is controlled by both the surface distribution of the upper crustal density contrasts and position of the contrast with depth. Up to 30% high-density mafic granulite (2.92 t/m^3) within dominantly felsic granulite (2.64 t/m^3) of the upper crust of the northern zone is thought to make a significant contribution to the high density of the zone. A high-amplitude north-sloping gravity gradient, paralleling the southern coast (A_3, Fig. 10), is attributed to the change in crustal structure at the continental margin; this gradient complicates the gravity in the southeast where the Albany Province trends offshore.

Gamma-ray spectrometric data

Gamma-ray data are briefly discussed, as they were acquired by BMR in conjunction with aeromagnetic data for seven 1:250 000 sheets in the Albany 1:1M Sheet area. The survey specifications included 1500 m flight-line spacing and 60 m sampling interval. The detecting crystal volume was 16 litres for the most recent survey (COLLIE & western PEMBERTON), and approximately 5 litres for the other six sheets. Four channels of gamma-ray data were recorded and released as profile maps of potassium (K), uranium (U), thorium (Th), and total count (TC), and contours of TC. These maps were found to be very difficult to interpret. Pixel images of individual channels and a composite image of K (red), U (blue), and Th (green) were prepared for each 1:250 000 map sheet. The composite image proved to be the data format most appropriate for interpretation.

From a comparison of the images with the maps of geology and aeromagnetic and gravity data, it was concluded that the gamma-ray data largely outline features of the regolith on the Albany 1:1M Sheet. Several rivers in the west of the Yilgarn Craton are associated with high K count rates. Areas of subcropping granite and quartzo-feldspathic gneiss are associated with higher average count rates in all channels, contrasted with areas of regolith.

The main characteristics of gamma-ray data over outcropping basement are:

- over greenstone belts—very low count rates from all channels; and
- over granite—either high K count rates or high count rates in all channels.

At several places gross changes of count rate coincide with aeromagnetic lineaments. In some places, the change in radiation is correlated with changes in basement rock type; however, in other places the change in count rate probably relates to differential erosion of regolith across faults.

Mineralisation

Greenstone and metamorphic belts of the Yilgarn Craton host much of the mineralisation of the Albany 1:1M sheet area. Nickel and gold occur in greenstone in the east of the sheet at Forrestania (FO in Fig. 12) and gold at Boddington in the west (BO in Fig. 12; Symons et al. 1990). Known mineralisation is less abundant in metamorphic belts, but includes tin, tantalum, and lithium at Greenbushes (GB in Fig. 12; Hatcher & Clynick 1990), and sub-economic titanium–vanadium-bearing magnetite deposits (Baxter 1978). Significant mineralisation is not known from the Albany Province; however, the northern zone hosts the sub-economic Southdown magnetite deposit (SO in Fig. 12). Permian sediments host economic coal at Collie (SO in Fig. 12; Lowry 1976), bauxite is mined from regolith developed on the Yilgarn Craton adjacent to the Darling Fault (Sadleir & Gilkes 1976), and heavy-mineral sands are extracted from coastal strand lines overlying the Perth Basin (Baxter 1990; not plotted in Fig. 12). Of these deposits, only the Southdown

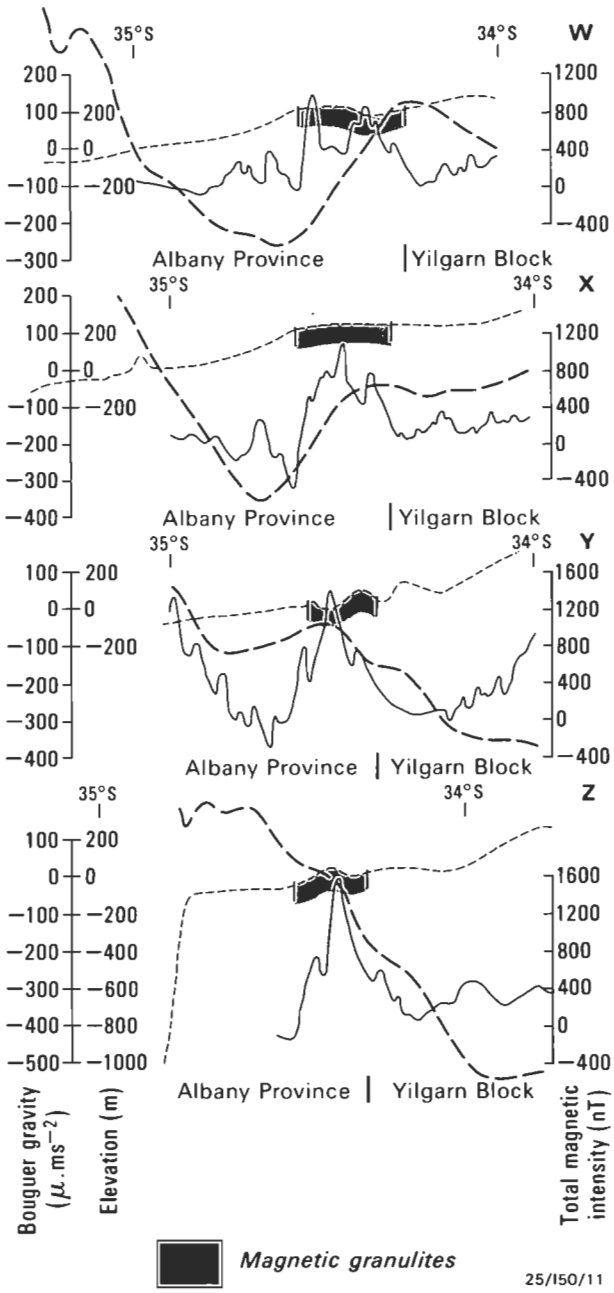

Figure 11. Profiles of Bouguer gravity (long dashed lines), aeromagnetics (thin continuous lines) and elevation (short dashed lines) across the southern Yilgarn Craton and Albany Province. The northern zone (magnetic granulites) of the Albany Province is labelled on the elevation profiles. Note the change in polarity of the gravity gradient from west to east, and its position relative to the northern zone (magnetic granulites) of the Albany Province. Location of the profiles is given in Figure 12 (W at 116°25′, X at 117°25′, Y at 118°45′, and Z at 119°30′).

magnetite deposit is directly located in the regional aeromagnetic data, although more detailed surveys should also locate both nickel and titanium–vanadium–magnetite deposits. None of the deposits is identifiable from interpretation of regional gravity and radiometric data.

The regional aeromagnetic and gravity surveys do, however, provide useful information on the distribution, extent and deformation of many of the hosts of mineralisation, particularly greenstone and metamorphic belts. Granite–greenstone terrane (Zone A, Fig. 12), as defined here, extends up to 100 km west of the approximate terrane boundary of Gee et al. (1986 and Fig. 10). Greenstone, inferred from the aeromagnetic data, is more extensive than indicated by the distribution of small outcrops on geological maps (e.g. Myers 1989) and is probably under-explored, particularly for gold. The position of the southern boundary of the Yilgarn Craton is not well constrained by geological mapping, owing to poor exposure and superimposed deformation. Interpretation of the aeromagnetic data provides an inferred position of the boundary and, thus, also a southern limit to the extent of greenstone. The Yilgarn Craton is cut by numerous lineaments attributed to faults and shears. Many of the lineaments dislocate greenstone and metamorphic belts, but may also have acted as conduits for mineralising fluids. Lineaments correlate with the margins of the down-faulted Collie Basin and may also have controlled emplacement of mineral-bearing intrusives (e.g. the Greenbushes Pegmatite).

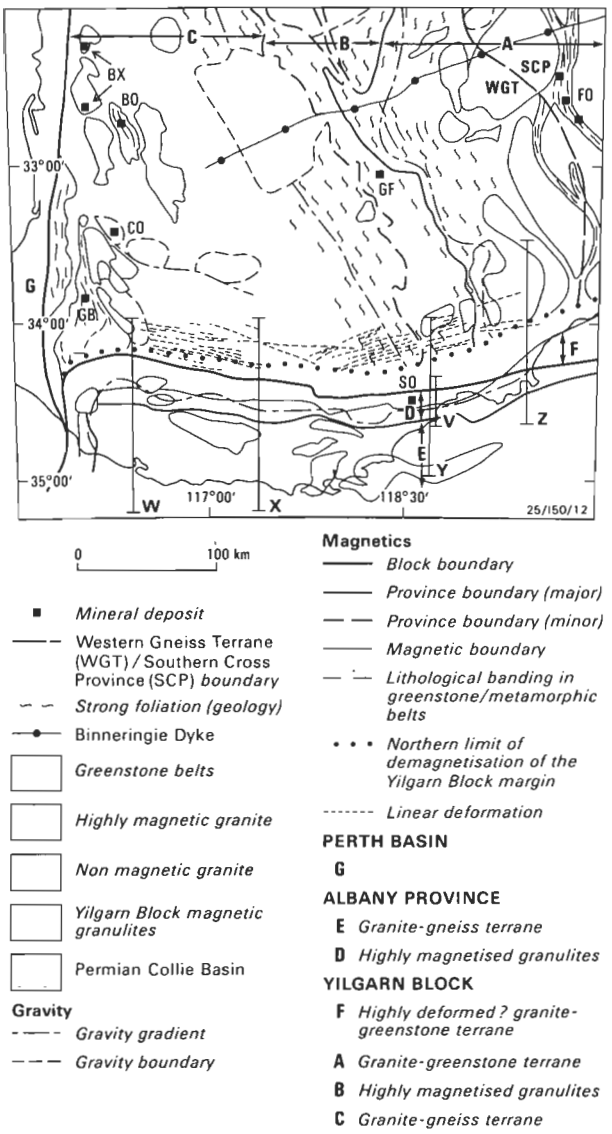

Figure 12. The model of the southwest Yilgarn Craton and Albany Province based on gravity, magnetics and geology (after Whitaker 1989). The significant mineral deposits (excluding mineral sands) are labelled BX (Darling Range, Al), BO (Boddington; Al, Au), CO (Collie; C), FO (Forrestania; Au, Ni), GB (Greenbushes; Sn, Ta, Li), GF (Griffins Find; Au), and SO (Southdown; Fe). The location of sections represented in Figures 8 (V) & 11 (W, X, Y, Z) are labelled.

Much of the Albany 1:1M Sheet is underlain by granite–gneiss terrane of relatively uniform composition, low variation in magnetisation and gravity, and relatively low prospectivity. In contrast, greenstone and metamorphic belts, and fault-bounded basins—which commonly host mineralisation—represent complex geological settings with diverse lithology. The extent of these entities and details of their internal structure and deformation have been delineated to various extent by the regional geophysical surveys. The integration of geology with the geophysical interpretation has provided a fuller understanding of the region than that provided by outcrop alone and, thus, a better framework in which to analyse the distribution of mineralisation.

Conclusions and summary

In the Albany 1:1M Sheet area, aeromagnetic and gravity data combined with surface geology provide complementary information on the nature of the basement. Of the regional geophysical data sets, the aeromagnetic data offer the most information on the Precambrian rocks of the sheet. These data outline major basement components, lithological banding, and superimposed deformation, including lineaments, as well as margin demagnetisation. Major gravity gradients coincide with many of the significant province boundaries interpreted from the aeromagnetic data. However, interpretation of the gravity data also defines a number of features not evident in the aeromagnetic data, such as a major change in crustal structure in the southwest Yilgarn Craton, several granites and the Permian Collie Basin. The radiometric data have not aided mapping of the Precambrian rocks of the sheet, but provide information on regolith, and, to some extent, the distribution of basement outcrop. Outcrop geology has proved invaluable in the interpretation of many of the geophysical anomalies and, conversely, the geophysical maps have helped to correlate between scattered basement outcrops.

The main findings are:

- The Yilgarn Craton of the Albany 1:1M Sheet area is composed of two structurally distinct zones. The eastern zone (Zone A) correlates with granite–greenstone terrane (Southern Cross Province) with broadly sinuous internal structure. The western boundary of granite–greenstone terrane is inferred to be 100 km west of that described by Gee et al. (1986). The western zone (Zones C) correlates with granite–gneiss terrane (Western Gneiss Terrane) of sparse, short, largely linear anomalies attributed to compositional banding, dominantly aligned north-northwest.

- A south-southeast-trending belt of highly magnetised granulites (Zone B) has similarity of internal structure

to granite–gneiss terrane immediately to the west (Zone C). The belt correlates with the Jimperding Metamorphic Belt in the north of the sheet and is inferred to map the continuation of this belt south-southeast to the deformed southern margin of the Yilgarn Craton. The eastern boundary of the belt marks both a change in inferred geology and structure and is considered a major intracratonic boundary.

- Comparison of seismic and gravity data over the Yilgarn Craton has assisted in the understanding of gravity patterns along the boundary between the craton and the Albany Province. Seismic results indicate that crust of the southwest Yilgarn Craton consists of a relatively thin upper crustal layer overlying an abnormal thickness of denser lower crustal rocks. The northern zone of the Albany Province is poorly resolved from this part of the Yilgarn Craton, and is also considered to be relatively dense. Crust of the southern Albany Province is believed to be less dense, and a major south-sloping gradient to lower gravity values approximates the boundary between the zones. Farther east, a north-sloping gradient to low-gravity values approximates the boundary between the northern zone of the Albany Province and thick, less-dense, upper crustal rocks of the Yilgarn Craton.

- The Albany Province is composed of two zones of different average magnetisation and internal structure. The northern zone is highly magnetised and relatively dense, and has a linear internal structure which is offset at regular intervals by dextral faults. The rocks of the zone are of granulite facies and are interpreted to be thrust mid to lower-crustal material. The southern zone is of lower average magnetisation and density with sinuous internal structure. Isotopic evidence (Black et al. 1992) suggests that the southern zone was formed during the early Proterozoic, whereas the northern zone contains at least some Archaean material. It is speculated that the northern zone is basement to the southern zone of the Albany Province.

- The southern margin of the Yilgarn Craton has been demagnetised up to 20 km north of the boundary. Abundant lineaments, oriented sub-parallel to the boundary, overprint lithological trends of the Craton for a further 30 km. These features are attributed to deformation associated with thrusting of the Albany Province. The extent of deformation and demagnetisation of the margin of the Yilgarn Craton is interpreted as evidence that the Albany Province behaved as a rigid block during thrusting in the Mid-Proterozoic.

- Granite, as mapped using the geophysical data sets, is readily classified on the basis of shape (angular to ovoid outline), average magnetisation, variation of magnetisation (uniform, polar, zoned), and, to a limited extent, by radioactivity levels.

- Low-amplitude, irregularly shaped magnetic lows are the most common lineament on the Albany 1:1M Sheet and are attributed to demagnetised fault and shear zones. Less common are lineaments composed of uniform section, normal and reverse-polarised anomalies, caused by dykes. However, many small dykes are not detected by the regional aeromagnetic surveys.

- Extensive areas of relatively homogeneous granite–gneiss terrane contain few mineral deposits and have low exploration potential. Greenstone and metamorphic belts, with greater diversity of rock type, permit better regional correlation and host significant mineral deposits. These belts can be delimited using regional aeromagnetic surveys. A detailed knowledge of regional boundaries, tectonic history, and the distribution of lithologies is vital to effective exploration. Interpretation of regional geophysical data, particularly in areas of extensive regolith and sparse outcrop, makes a significant contribution to that end.

- For regions of poor bedrock exposure, integration of magnetic, gravity, and geological mapping provides a fuller geological model than that provided by outcrop mapping alone. The model of the Albany 1:1M Sheet presented here aids understanding of metamorphism, deformation, geochronology, and distribution of mineralisation, placing them in a regional context.

Acknowledgments

The interpretations presented here were undertaken in an on-going joint project of 1:1M mapping of the Yilgarn Craton with the Geological Survey of Western Australia. Survey staff, including John Myers, Peter Dunn, Laslo Kevi (retired), and Greg Street (now of World Geoscience), are thanked for valuable contributions including discussion, maps and data. Lyal Harris, Claude Delor, and David Groves of the University of Western Australia, and Simon Wilde of Curtin University are acknowledged for their contribution through discussion. James Maxlow, formerly of Otter N.L., is acknowledged for both discussion and access to company gravity data. Peter Wellman of AGSO is thanked for interpreting the gravity data over the boundary between the Yilgarn Craton and Albany Province. The paper benefited from reviews by Ian Hone, Peter Williams, David Tucker, Bob Tingey and Peter Wellman. Programs used for manipulating the digital magnetic and gravity data were developed by Tony Luyendyk, Vadim Anfiloff and Alice Murray. The paper is published with the permission of the Executive Director, Australian Geological Survey Organisation, Canberra.

References

Arriens, P.A., 1971. The Archaean geochronology of Australia. *Geological Society of Australia, Special Publication*, 3, 11–23.

Baxter, J.L., 1978. Molybdenum, Tungsten, Vanadium and Chromium in Western Australia. *Geological Survey of Western Australia, Mineral Resources Bulletin* 11.

Baxter, J.L., 1990. Heavy mineral sand deposits of Western Australia. *In* Hughes, F.E. (editor). Geology of the mineral deposits of Australia and Papua New Guinea. *Australasian Institute of Mining and Metallurgy, Monograph* 14, 1587–1590.

Beeson, J., Delor, C.P. & Harris, L.B., 1988. A structural and metamorphic traverse across the Albany Mobile Belt, Western Australia. *Precambrian Research*, 40/41, 117–136.

Binns, R.A., Gunthorpe, R.J. & Groves, D.I. 1976. Metamorphic patterns and development of greenstone belts in the eastern Yilgarn Block, Western Australia. *In* Windley, B.F. (editor), *The Early History of the Earth*. Wiley, London, 303–313.

Black, L.P., Harris, L.B. & Delor, C.P., 1992. Reworking of Archaean and Early Proterozoic components during a progressive, Middle Proterozoic tectonothermal event in the Albany Mobile Belt, Western Australia, *Precambrian Research*, 59, 95–123.

Chin, R.J., 1986. Corrigin, Western Australia. *Geological*

Survey of Western Australia, 1:250 000 Geological Series Explanatory Notes.

Chin, R.J., Hickman, A.H. & Thom, R., 1984. Hyden, Western Australia. *Geological Survey of Western Australia 1:250 000 Geological Series Explanatory Notes.*

Chin, R.J. & Brakel A.T., 1986. Dumbleyung, Western Australia. *Geological Survey of Western Australia, 1:250 000 Geological Series Explanatory Notes.*

Drummond, B.J. & Esa Mohamed, R., 1986. Crustal structure in the south west seismic zone, Western Australia. *Geological Society of Australia, Abstracts*, 15, 59–60.

Esa Mohamed, R., 1985. A geophysical investigation of the southwest seismic zone, Western Australia. MSc Thesis, Western Australian Institute of Technology (unpublished).

ESSO Australia Limited, 1972. Bremer Basin aeromagnetic survey (WA–50–P & WA–51–P). *Geological Survey of Western Australian, Open File Report* S827.

Fletcher, I.R., Wilde, S.A., Libby, W.G. & Rosman, K.J.R., 1983. Sm–Nd model ages across the margins of the Archaean Yilgarn Block, Western Australia–II; southwest transect into the Albany–Fraser Province. *Journal of the Geological Society of Australia*, 30, 333–340.

Fountain, D.M. & Salisbury, M.H., 1981. Exposed cross-sections through the continental crust: implications for crustal structure, petrology and evolution. *Earth and Planetary Science Letters*, 56, 263–277.

Fraser, A.R., 1974. Reconnaissance helicopter gravity survey of the southwest of Western Australia, 1969. *Bureau of Mineral Resources, Australia, Record* 1974/26.

Gee, R.D., 1979. Structure and tectonic style of the West Australian Shield. *Tectonophysics*, 58, 327–369.

Gee, R.D., Myers, J.S. & Trendall, A.F., 1986. Relation between Archaean high-grade gneiss and granite–greenstone terrain in Western Australia. *Precambrian Research*, 33, 87–102.

Gee, R.D., Baxter, J.L., Wilde, S.A. & Williams, I.R., 1981. Crustal development in the Archaean Yilgarn Block, Western Australia. *Geological Society of Australia, Special Publication*, 7, 43–56.

Hatcher, M.I. & Clynick, G., 1990. Greenbushes tin–tantalum–lithium deposit. *In* Hughes, F.E. (editor). Geology of the mineral deposits of Australia and Papua New Guinea. *Australasian Institute of Mining and Metallurgy, Monograph* 14, 599–603.

Kevi, L., 1988. Bridgetown 1:100 000 Bouguer anomaly map. *Geological Survey of Western Australia, Record* 1988/2.

Klasner, J.S. & King, E.R., 1986. Precambrian basement geology of North and South Dakota. *Canadian Journal of Earth Sciences*, 23, 1083–1102.

Lowry, D.C., 1976. Tectonic History of the Collie Basin, Western Australia. *Journal of the Geological Society of Australia*, 23, 95–104.

McCall, G.J.H. & Peers, R., 1971. Geology of the Binneringie Dyke, Western Australia. *Sonderuk Geologische Rundschau*, 60, 1174–1263.

McCulloch, M.T., 1987. Sm–Nd isotopic constraints on the evolution of Precambrian crust in the Australian Continent. *American Geophysical Union, Geodynamic Series*, 17, 115–130.

Muhling, P.C. & Brakel, A.T., 1985. Mount Barker–Albany, Western Australia. *Geological Survey of Western Australia, 1:250 000 Geological Series Explanatory Notes.*

Myers, J.S., 1989. Albany 1:1M Sheet—Geology. Geological Survey of Western Australia, Perth.

Myers, J.S., 1990a. Pinjarra Orogen. *In* Geology and Mineral Resources of Western Australia. *Geological Survey of Western Australia Memoir* 3, 265–274.

Myers, J.S., 1990b. Mafic dyke swarms. *In* Geology and Mineral Resources of Western Australia. *Geological Survey of Western Australia, Memoir* 3, 126–127.

Myers, J.S., 1990c. Albany Fraser Orogen. *In* Geology and Mineral Resources of Western Australia. *Geological Survey of Western Australia, Memoir* 3, 225–264.

Nemchin, A.A., Pidgeon, R.T. & Wilde, S.A., in press. Timing of Late Archaean granulite facies metamorphism in the southwestern Yilgarn Craton of Western Australia: evidence from U–Pb ages of zircons from mafic granulites. *Precambrian Research.*

Nieuwland, D.A. & Compston, W., 1981. Crustal evolution of the Yilgarn Block near Perth, Western Australia. *Geological Society of Australia, Special Publication*, 7, 159–171.

Page, R.W., McCulloch, M.T. & Black, L.P., 1984. Isotopic record of major Precambrian events in Australia. *Proceedings of the 27th International Geological Congress*, 5, 25–72.

Petkovic, P., 1975. Geophysical results from the southwest margin. *Bureau of Mineral Resources, Australia, Record* 1975/180.

Pidgeon, R.T., 1990. Timing of plutonism in the Proterozoic Albany Mobile Belt, southwestern Australia. *Precambrian Research*, 47, 157–167.

Pidgeon, R.T. & Wilde, S.A., 1990. The distribution of 3.0 Ga and 2.7 Ga volcanic episodes in the Yilgarn Craton of Western Australia. *Precambrian Research*, 48, 309–325.

Rosman, K.J.R., Wilde, S.A., Libby, W.G. & De Laeter, J.R., 1980. Rb–Sr dating of granitic rocks in the Pemberton area. *Geological Survey of Western Australia, Annual Report*, 1980, 97–100.

Sadleir, S.B. & Gilkes, R.J., 1976. Development of bauxite in relation to parent material near Jarrahdale, Western Australia. *Journal of the Geological Society of Australia*, 23, 333–344.

Schlinger, C.M., 1985. Magnetisation of lower crust and interpretation of regional magnetic anomalies: Example from Lofoten and Vesteralen, Norway. *Journal of Geophysical Research*, 90, 11484–11504.

Symons, P.M., Anderson, G., Beard, T.J., Hamilton, L.M., Reynolds, G.D., Robinson, J.M., Staley, R.W. & Thompson, C.M., 1990. Boddington gold deposit. *In* Hughes, F.E. (editor), Geology of the mineral deposits of Australia and Papua New Guinea. *Australasian Institute of Mining and Metallurgy, Monograph* 14, 165–169.

Thom, R. & Chin, R.J., 1984. Bremer Bay, Western Australia. *Geological Survey of Western Australia, 1:250 000 Geological Series Explanatory Notes.*

Thom, R., Chin, R.J. & Hickman, A.H. 1984. Newdegate, Western Australia. *Geological Survey of Western Australia, 1:250 000 Geological Series Explanatory Notes.*

Tucker, D.H. & DAddario, G.W., 1986. Albany 1:1 000 000 map sheet, Magnetic Domains. Interpretation of aeromagnetic anomaly pixel map series. Bureau of Mineral Resources, Canberra.

Tucker, D.H., Anfiloff, V. & Bagliani, F., 1986. Albany (W.A.) Map Sheet; Total Magnetic Intensity, third generation compilation. 1:1 000 000 aeromagnetic anomaly pixel map series. Bureau of Mineral Resources, Canberra,

Turek, A. & Stephenson, N.C.N., 1966. The radiometric age of the Albany Granite and the Stirling Range Beds, southwest Australia. *Journal of the Geological Society*

of Australia, 13, 449–456.

Wellman, P., 1978. Gravity evidence for abrupt changes in mean crustal density at the junction of Australian crustal blocks. *BMR Journal of Australian Geology & Geophysics*, 3, 153–162.

Wellman, P., 1992. Structure of the Mount Isa region inferred from gravity and magnetic anomalies. *In* Stewart, A.J. & Blake, D.H. (editors). Detailed studies of the Mount Isa Inlier. *Australian Geological Survey Organisation, Bulletin*, 243, 15–27.

Wellman, P. & Murray, A.S., 1979. Free-air gravity anomalies (1:10 000 000 map). *BMR Earth Science Atlas of Australia*. Bureau of Mineral Resources, Canberra.

Whitaker, A.J. 1989. A geophysical model of the Precambrian of the Albany 1:1M sheet, Western Australia, and its relevance to economic geology. *Exploration Geophysics*, 20, 1/2, 195–199.

Whitaker, A.J., 1992. Albany magnetic and gravity interpretation (1:1 000 000 map), Bureau of Mineral Resources, Canberra.

Wilde, S.A. & Low, G.H., 1980. Pinjarra, Western Australia. *Geological Survey of Western Australia, 1:250 000 Geological Series Explanatory Notes.*

Wilde, S.A. & Walker, I.W., 1982. Collie, Western Australia. *Geological Survey of Western Australia, 1:250 000 Geological Series Explanatory Notes.*

Wilde, S.A. & Walker, I.W., 1984. Pemberton–Irwin Inlet, Western Australia. *Geological Survey of Western Australia, 1:250 000 Geological Series Explanatory Notes.*

Wilde, S.A. & Pidgeon, R.T., 1986. Geology and geochronology of the Saddleback Greenstone Belt in the Archaean Yilgarn Block, southwestern Australia. *Australian Journal of Earth Sciences*, 33, 491–501.

AGSO Journal of Australian Geology & Geophysics, 15 (3), 329–333 © Commonwealth of Australia 1994

Fluctuations in seismicity in the Dalton area, NSW, Australia, and their relevance to earthquake forecasting

Marion O. Michael-Leiba[1]

In the Dalton area, 60 km north of Canberra, Australia, earthquakes are strongly clustered in time, but the presence of multiple events with magnitudes around 2.8 is not a useful criterion for earthquake forecasting. If magnitude ML >2.7 events less than 14 months apart during the period 1960–1993 are grouped together, the magnitude ML(MAX) of the largest event of a group may be forecast from the relationship: ML(MAX) = 0.097 + 2.296 log t, where t months is the quiescent interval preceding the group in question and 2.8<ML(MAX)<4.2.

Introduction

The Dalton area, 60 km north of Canberra (Fig. 1), is one of several seismically active regions of eastern Australia. Several earthquakes have caused damage near the epicentre and been felt in Canberra. A magnitude ML 5.5 in 1949 also produced minor cracking in some Canberra buildings. The largest recorded earthquake had magnitude ML 5.6 and occurred in 1934 (McCue et al. 1989). It was the same size as the destructive December 1989 Newcastle earthquake. Michael-Leiba et al. (1988) discussed earthquake swarms as short-term precursors. The aim here is to investigate other fluctuations in seismicity and their usefulness for earthquake forecasting.

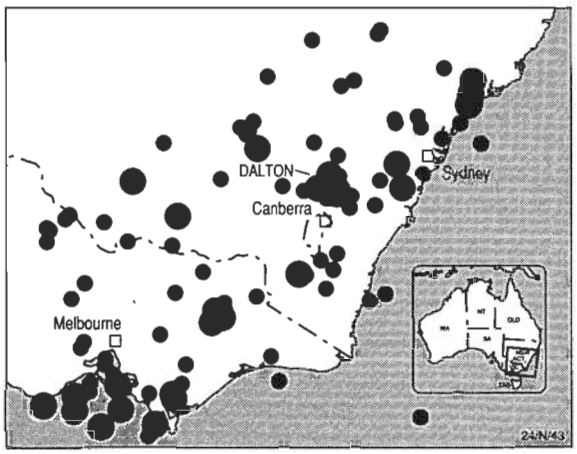

Figure 1. Locality map. Dalton is in the middle of the cluster of earthquakes indicated by the arrow. The black dots are epicentres of earthquakes with magnitudes ML 4.0 or greater.

Fluctuations in seismicity

The ten magnitude ML >3.9 events known to have occurred within 15 km of Dalton are shown in Table 1. When foreshocks and aftershocks within nine months of each other or of a main shock are removed, the number of events decreases to seven, three of which happened during the years 1949–1954. The seismicity during this short interval may have been anomalously high, but the data are too few to investigate statistically and may not be complete to magnitude ML 4.0 prior to 1960: much of the Australian National University (ANU) seismic net was established in 1958–59, and the seismograph coverage before then was very limited.

Table 1. Magnitude ML >3.9 earthquakes at distances of 15 km or less from the Dalton seismograph.

Date (UTC) Dy–Mo–Year	*Latitude °S*	*Longitude °E*	*Magnitude ML*
05–07–1888	34.8	149.1	5.3
18–11–1934	34.8	149.2	5.6
10–03–1949	34.74	149.2	5.5
07–09–1952	34.8	149.3	4.7
18–11–1952	34.8	149.3	4.4
19–11–1952	34.8	149.25	4.9
22–11–1952	34.8	149.3	4.6
09–06–1954	34.75	149.2	4.5
03–11–1971	34.777	149.166	4.0
09–08–1984	34.803	149.170	4.1

A seismograph was installed by ANU at Dalton in 1961, so events with magnitudes as small as ML 2.0 should be complete from 1962. They may well be complete from 1960, as there were ten ANU stations in New South Wales by then, but the accuracy of location would have been poorer than when the Dalton seismograph was in operation. Magnitude ML >2.7 earthquakes should be complete from 1960.

During the period 1960–1993, lower magnitude events are strongly clustered in time (Fig. 2). The events in Figure 2 are from the AGSO earthquake data-base: magnitudes have been converted for consistency with those determined using the attenuation in southeastern Australia derived by Michael-Leiba & Malafant (1992). For magnitude ML >2.5 earthquakes, this meant subtracting 0.2 from pre-1990 magnitudes. When foreshocks and aftershocks of magnitude ML >2.7 events within one month of each other or of a main shock are removed (as suggested by Michael-Leiba 1987 and followed by Gaull et al. 1990), the annual number of residual main shocks (Fig. 2, bottom histogram) fluctuates between zero and two—except for 1984, when there were five. As a magnitude ML 4.1 earthquake occurred in 1984, the elevated residual seismicity may be related to this. However, if the main shocks follow a Poisson distribution, then the five events in one year would be the result of the Poisson process. In this case, the time intervals between events would follow a negative exponential distribution (Lomnitz 1974). The Kolmogorov–Smirnov test (Siegel 1956) of goodness of fit to a negative exponential distribution with mean time interval 13.6 months is shown in Table 2. The greatest divergence, D, between the two distributions is 0.104. The critical value of D at the 0.05 level of significance is 0.24, so the null hypothesis of a negative exponential distribution cannot be rejected at the 0.05 level of significance. Consequently, there is insufficient

[1] Australian Geological Survey Organisation, GPO Box 378, Canberra ACT 2601.

evidence to regard the occurrence of five events in 1984 as other than the result of a Poisson process.

The presence of multiple events with magnitudes around 2.8 is not a useful criterion for earthquake forecasting in the Dalton area. The magnitude ML 4.0 earthquake in November 1971 had no ML >2.7 foreshocks in 1971, whereas the ML 4.1 event in August 1984 had three foreshocks in the preceding seven months. Also, seismicity was elevated in 1965, 1979 and 1987, with multiple events of magnitude around 2.8, without being precursory to ML >3.9 earthquakes.

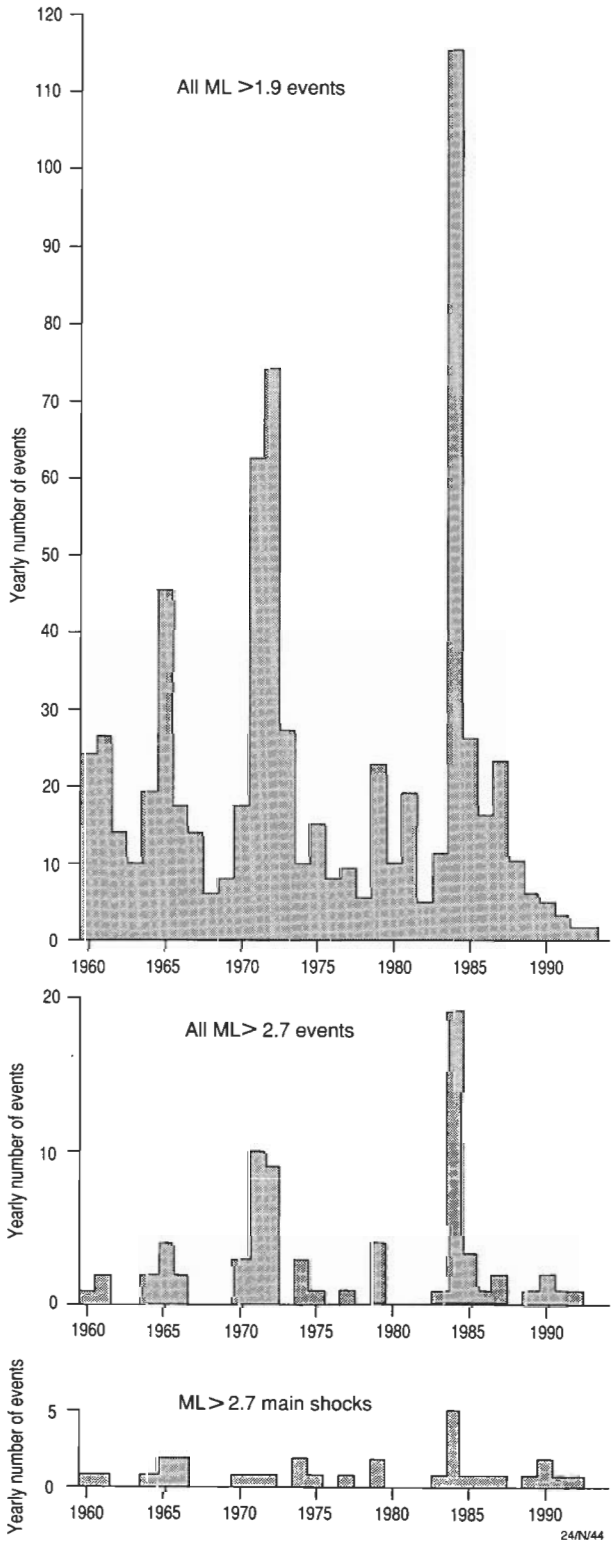

Figure 2. Yearly numbers of earthquakes at a distance of 15 km or less from the Dalton seismograph.

Table 2. Kolmogorov–Smirnov test on goodness of fit of time intervals between magnitude ML >2.7 main shocks at distances of 15 km or less from the Dalton seismograph (1960–1993) to a negative exponential distribution.

Interval (months)	*No. observations*	*Cumulative theoretical*	*Cumulative observed*	*D*
1	2	0.071	0.069	0.002
2	3	0.137	0.172	0.035
3	2	0.198	0.241	0.043
4	3	0.255	0.345	0.090
5	1	0.308	0.379	0.071
6	1	0.357	0.414	0.057
7	1	0.402	0.448	0.046
9	1	0.484	0.483	0.001
10	2	0.521	0.552	0.031
11	1	0.555	0.586	0.031
12	3	0.586	0.690	0.104
18	1	0.734	0.724	0.010
19	2	0.753	0.793	0.040
20	1	0.770	0.828	0.058
21	1	0.786	0.862	0.076
29	1	0.881	0.897	0.016
34	1	0.918	0.931	0.013
44	1	0.961	0.966	0.005
56	1	0.984	1.000	0.016

Forecasting from quiescent periods

Forecasting magnitude from quiescent interval

The magnitude ML 4.0 and 4.1 earthquakes in 1971 and 1984 were each preceded by a quiescent period of more than three years eight months with respect to magnitude ML >2.7 events, including foreshocks and aftershocks. During 1960–1993, there was no other three-year interval without an ML >2.7 event (Fig. 2). This suggests a relationship between the magnitude of an event and the length of the quiescent interval preceding it, possibly because of stress build-up during this period.

The quiescent periods before the 1971 and 1984 ML >3.9 events ended, respectively, 12 and 16 months before these earthquakes. During these 12 and 16 month periods leading up to the ML >3.9 events, the longest time between events of ML >2.7 was, respectively, 12 and 7 months. Also, 13.6 months is the mean interval between ML >2.7 main shocks; hence, I define a quiescent period as 14 months or more without an event exceeding magnitude ML 2.7. Then, magnitude ML >2.7 events (including foreshocks and aftershocks) less than 14 months apart constitute groups of one or more earthquakes, separated by the quiescent periods. There are ten such groups during the period 1960–1993 (Table 3). If ML(MAX) is the magnitude of the largest event in a group and t months is the time between the last event in the preceding group and the first event of the group in question, then the least squares line (Fig. 3) for nine pairs of observations (with ± indicating the standard errors

of the coefficients, calculated by small-sample statistics) is

$$ML(MAX) = (3.36 \pm 0.06) + (2.296 \pm 0.330)(\log t - 1.421)$$

or

$$ML(MAX) = 0.097 + 2.296 \log t \quad (1)$$

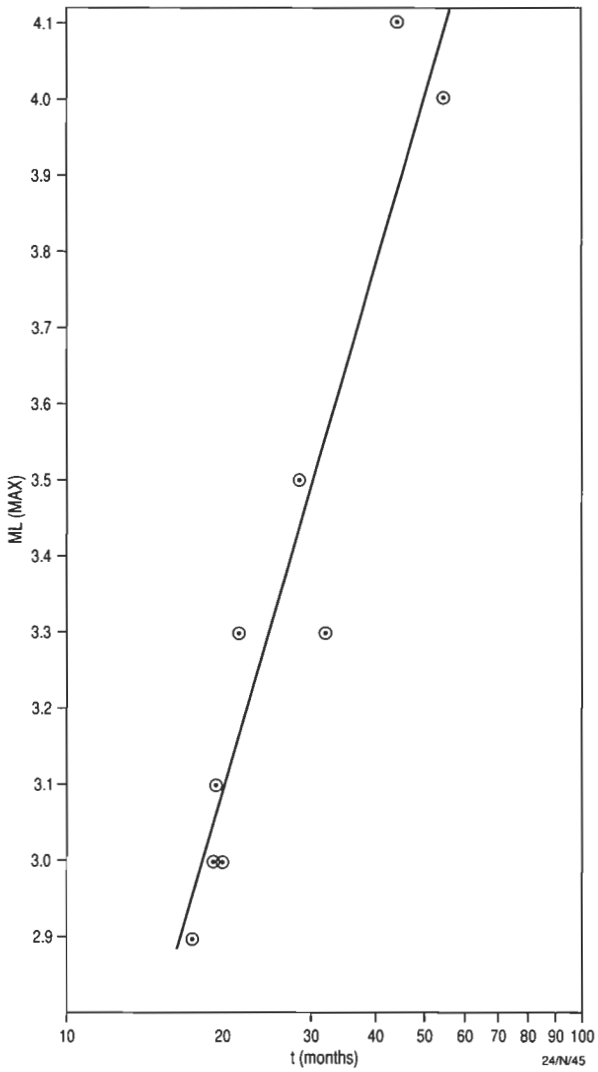

Figure 3. Relationship between magnitude of largest event in group ML(MAX), and length, t months, of quiescent period preceding it.

with a standard error of estimate of ML(MAX) of 0.15. The 95% confidence limits for the slope are 1.589<slope<3.003. Despite the small number of observations, the largest residual was only 0.25 ML (Table 3) and the magnitude range used to derive the relation was ML 2.9–4.1, so (1) may be useful for forecasting the magnitude of an impending event after a quiescent period (in terms of ML >2.7 events). However, it does not indicate if two or more events of equal maximum magnitude will occur in the group. This happened in two instances in Table 3. At the time of writing (2 June 1994), it is 23.0 months since the last ML >2.7 earthquake. If the next group of events were to start now, the 95% prediction interval for ML(MAX) from (1) would be 2.8<ML(MAX)<3.6.

Forecasting date of occurrence from ML(MAX)

If T months is the time interval measured from the start of the preceding quiescent period to the occurrence of the largest event of the group, then the date of this event may be estimated from the least squares relationship (Fig. 4)

$$\log T = (1.472 \pm 0.021) + (0.4295 \pm 0.0591)(ML(MAX) - 3.36)$$

or

$$\log T = 0.029 + 0.4295\ ML(MAX) \quad (2)$$

where ML(MAX) in (2) may be calculated from (1) provided that the largest event in the group is not the first. Three of the ten groups started with the largest earthquake and in this case (2) could not be used as a forecasting tool. The 95% confidence limits for the slope in (2) are 0.3028<slope<0.5562. For the nine pairs of observations (Table 4) used to derive equation (2), the standard error of estimate of the residuals was 5.2 months. Only two residuals exceeded this value, but the greatest was 11.4 months for the ML 4.0 event in 1971. The residual for the ML 4.1 earthquake in 1984 was only –0.8 months, but the 11.4 months residual for the 1971 event suggests that equation (2) may not be accurate enough to use as a short-term warning system for damaging earthquakes in the Dalton area.

Sensitivity of the ML(MAX) – log t relationship to changes in the minimum values of ML and t

Tests were conducted to ascertain how sensitive the relationship between ML(MAX) and the length, t, of the preceding quiescent period is to changes in the minimum

Table 3. Relationship between magnitude of largest event in group, ML(MAX), and length, t months, of quiescent period preceding it.

Date of Group	*t (months)*	*ML(MAX)*	*Least Squares ML*	*Residual*	*Comments*
14.08.1960–21.08.1961	—	2.8	—	—	3 events with ML2.8
18.04.1964–27.03.1966	31.9	3.3	3.55	–0.25	
21.10.1970–16.08.1972	54.8	4.0	4.09	–0.09	
22.03.1974–04.08.1975	19.2	3.0	3.04	–0.04	
05.04.1977	20.0	3.0	3.08	–0.08	
18.01.1979–12.07.1979	21.4	3.3	3.15	0.15	
24.03.1983–07.01.1986	44.4	4.1	3.88	0.22	
20.06.1987–26.06.1987	17.4	2.9	2.95	–0.05	
14.11.1989–15.04.1990	28.6	3.5	3.44	0.06	
24.11.1991–02.07.1992	19.3	3.1	3.05	0.05	2 events with ML3.1

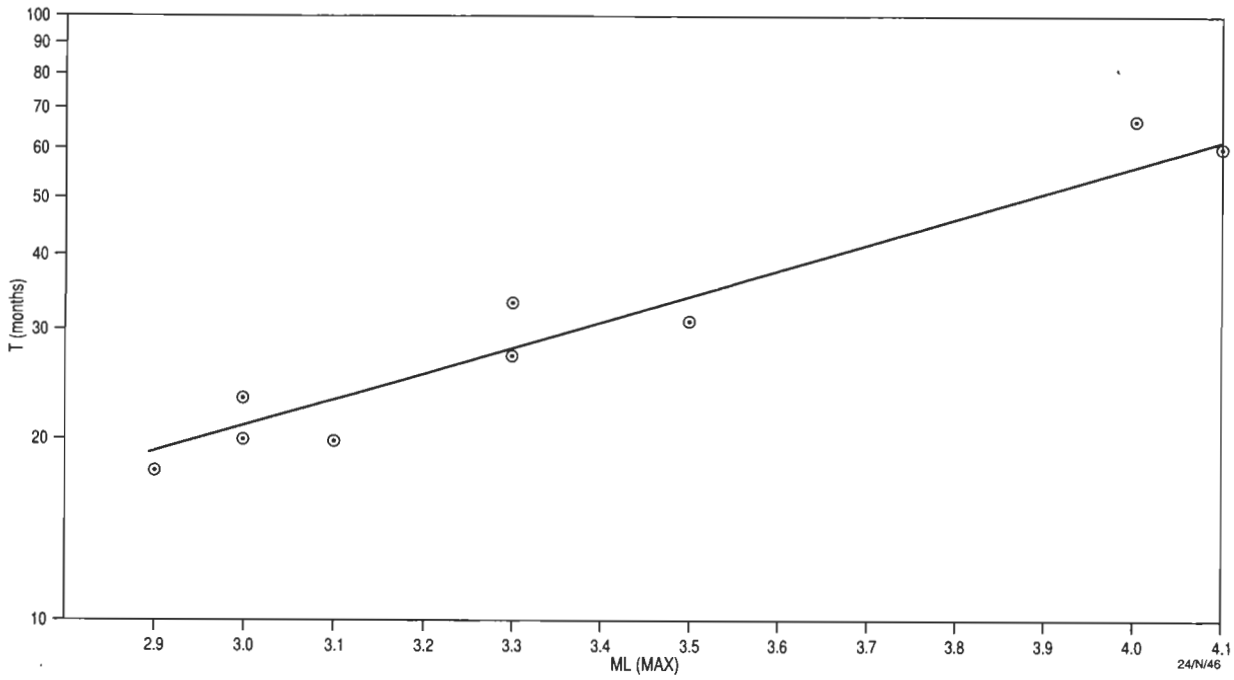

Figure 4. Relationship between time interval, T months, from start of preceding quiescent period to occurrence of largest event of group.

magnitude of the data set. The same 14 month minimum value of t was used.

In the Dalton area, epicentres tend to occur in two distinct zones, one to the north and the other to the south of the township, the southern zone being the more active (McCue et al. 1989). All the events delimiting groups and/or having the maximum magnitude in each group in Table 3 had their epicentres in the southern zone. For this reason, only events in this zone were considered in the sensitivity tests for magnitudes less than 2.8.

Table 4. Relationship between time interval, T months, from start of preceding quiescent period to occurrence of largest event of group. The groups are as in Table 3.

ML(MAX)	*Observed T*	*Estimated T*	*Residual (months)*
2.8	—	—	—
3.3	33.3	27.9	5.4
4.0	67.2	55.8	11.4
3.0	23.1	20.8	2.3
3.0	20.0	20.8	–0.8
3.3	27.2	27.9	–0.7
4.1	60.9	61.7	–0.8
2.9	17.6	18.8	–1.2
3.5	30.6	34.0	–3.4
3.1	19.3	22.9	–3.6

For ML 2.8 and above, the standard error of estimate of ML(MAX) by equation (1) is 0.15. For ML 2.7 and above, using a Microsoft EXCEL linear regression function, the relationship becomes

$$ML(MAX) = 2.14 \log t + 0.37 \quad (3)$$

with a standard error of estimate of ML(MAX) of 0.22 and a correlation coefficient of 0.88. For ML 3.0 and above, using the same package, the relationship is

$$ML(MAX) = 1.86 \log t + 0.54 \quad (4)$$

with a standard error of estimate of ML(MAX) of 0.27 and a correlation coefficient of 0.84. For ML 2.6 and above and ML 3.1 and above, there is no obvious relationship between ML(MAX) and t. Thus, a log-linear relationship holds for cut-off magnitudes in the range ML 2.7–3.0 when the minimum length of a quiescent period is defined as 14 months. For a quiescent period of 23 months, the values of ML(MAX) calculated from equations (3) and (4) are 3.3 and 3.1, respectively, which lie well within the 95% prediction interval, 2.8<ML(MAX)<3.6 of ML(MAX) from equation (1).

If the minimum length, t, of the quiescent period were taken to be less than 12 months, the ML 4.0 earthquake in 1971 would no longer appear to be related to the quiescent period of 54.8 months in Table 3. For minimum values of t in the range 13.0–17.0 months, the pattern of groups would be unchanged from that in Table 3. If the minimum t were chosen to be 24 months, the number of quiescent periods in Table 3 would decrease to four, insufficient data on which to base a useful regression.

Conclusions

The null hypothesis of a Poisson process cannot be rejected at the 0.05 level of significance for describing the occurrence of magnitude ML >2.7 main shocks in the Dalton area. Clustering occurs in the original data containing all ML >2.7 events, but does not appear to be useful for predicting ML >3.9 earthquakes. Quiescent periods may be helpful in forecasting earthquakes with magnitudes up to ML 4.1; however, there are no data at present to ascertain whether they may be useful for higher magnitude events.

The relationship between the magnitude of the largest event of a group of magnitude ML >2.7 earthquakes and the preceding quiescent period (with respect to ML >2.7 events) suggests that this magnitude is a function of stress build-up during the quiescent period. It may be a useful

magnitude forecasting tool, but the date of occurrence may not be able to be estimated with sufficient accuracy for short-term warnings of potentially damaging earthquakes.

Acknowledgments

Brian Gaull and I became aware of the quiet periods prior to the magnitude ML >3.9 earthquakes of 1971 and 1984 when working on another project in 1985. I am grateful to Stewart Dennis for performing the regressions for equations (3) and (4). I thank Phil McFadden for useful discussions on statistics and the nature of the earthquake process; Kevin McCue, David Denham, Brian Gaull, Gary Gibson, Phil McFadden and an anonymous referee for critically reading the manuscript and suggesting improvements; Jill Clarke and John Convine for drafting the figures; the staff of Research School of Earth Sciences, Australian National University, particularly Jan Weekes, for their data and cooperation; and the late Vicki Klein for many years of help and support with the Dalton earthquake-monitoring project.

References

Gaull, B.A., Michael-Leiba, M.O. & Rynn, J.M.W., 1990 Probabilistic earthquake risk maps of Australia. *Australian Journal of Earth Sciences*, 37, 169–187.

Lomnitz, C., 1974. *Global Tectonics and Earthquake Risk.* Elsevier, Amsterdam.

McCue, K., Kennett, B. L. N., Gaull, B. A., Michael-Leiba, M. O., Weekes, J. & Krayshek, C., 1989. A century of earthquakes in the Dalton–Gunning region of New South Wales. *BMR Journal of Australian Geology & Geophysics,* 11, 1–9.

Michael-Leiba, M.O., 1987. Temporal variation in seismicity of the Southwest Seismic Zone, Western Australia: implications for earthquake risk assessment. *BMR Journal of Australian Geology & Geophysics*, 10, 133–137.

Michael-Leiba, M., Klein, V., Weekes, J. & Krayshek, C., 1988. Earthquake swarms as short-term precursors in the Dalton–Gunning region, 34.70–34.86°S, 149.11–149.26°E, New South Wales, Australia. *Physics of the Earth and Planetary Interiors,* 53, 12–16.

Michael-Leiba, M. & Malafant, K., 1992. A new local magnitude scale for southeastern Australia. *BMR Journal of Australian Geology & Geophysics,* 13, 201–205.

Seigel, S., 1956. *Nonparametric Statistics for the Behavioral Sciences.* McGraw-Hill Kogakushu.

Editorial note: Some readers may wish to offer comments on both the observational and interpretive information in the above article.

The Editor would welcome discussions for publication in the *AGSO Journal of Australian Geology & Geophysics.*

AGSO Journal of Australian Geology & Geophysics, 15 (3), 335–345 © Commonwealth of Australia 1994

Landscape evolution and tectonics in southeastern Australia

C.D. Ollier[1] & C.F. Pain[2]

Rivers flowing north and west across southeastern Australia are older than the formation of the eastern continental margin and the Murray Basin. In the Jurassic and most of the Cretaceous, Australia was bound by land to the east (Pacifica), from which rivers carried sediment to the Eromanga–Surat Basin. The Otway–Gippsland Basin, bound to the north by the Victoria Divide, accumulated sediment from the early Cretaceous. At about 80 Ma, tectonic rifting along the line of the present continental shelf cut off the headwaters of Australian rivers then rising in Pacifica, beheading many rivers and reducing the sediment supply to the sedimentary basins. The input of coarse fluvial sediment to the Eromanga–Surat Basin ceased, but was maintained to the Otway–Gippsland Basin. In the Palaeocene, the Murray Basin started to sink, creating a divide between the Murray and Eromanga–Surat Basins and cutting off the southern sediment supply to the latter. Down-warping along the Tasman Sea margin formed the Great Divide between Tasman Sea drainage and the inland sedimentary basins. Rivers east of this divide were reversed, and a Great Escarpment was formed which retreated inland. Cainozoic volcanicity and Miocene faults with throws of hundreds of metres have further complicated the topography. The history derived from the study of river development and the evolution of major divides is paralleled by that of basin sedimentation. Basin down-warping formed the major divides, and led to the erosional development of the present landscape.

Introduction

The linked topics of highland uplift and river evolution in southeastern Australia have long been controversial. Some, such as Taylor (1911) and Ollier (1978), have proposed ancient movements and major changes in river pattern. Others have suggested that the parallelism between present rivers and valleys filled with Miocene basalt indicates little change in valley position since the Miocene. Bishop et al. (1985) wrote 'This part of eastern Australia has been cited repeatedly as providing excellent examples of drainage disruption primarily due to stream piracy (e.g. Taylor 1911; Ollier 1978), but all the evidence points to persistence of drainage.' and, in 1988, Bishop stated '... it is difficult to agree with Ollier's (1986, p. 113) recent claim that the general consensus is that significant warping and drainage disruption have occurred about the continental drainage divide ...'. Young (1989) and Nott (1992) reiterated this stance.

There are a number of studies pointing to a remarkable continuity of drainage during much of the Cainozoic (see Young 1978; Bishop 1988; Gale 1992; and references in these papers). These studies cannot be easily rejected, but it can be noted that they are mostly confined to small areas and their relevance to the broader picture is not demonstrated. At best, they indicate that drainage reorganisation is much older than was previously supposed.

One of the aims of the present paper is to show that the landscape history of southeastern Australia extends back well beyond the Miocene; another is to show that drainage disruption (not only by capture) is widespread, though often old. We believe that the origin of the Great Divide *was* associated with major drainage reorganisation, notwithstanding evidence of drainage stability since that time.

Following a brief statement of our interpretations of landscape evolution in southeastern Australia, we look at the sedimentary record of the flanking basins to provide evidence of variation in the location and extent of erosion in the highlands, and the timing of major changes in drainage direction. Then, we consider the origin and characteristics of the major drainage divides in southeastern Australia. The main rivers are discussed next, before consideration of tectonics and volcanism. Finally, the main points are integrated in a discussion.

[1] Centre for Resource and Environmental Studies, Australian National University, Canberra ACT 0200.

[2] Australian Geological Survey Organisation, G.P.O. Box 378, Canberra ACT 2601.

Outline of physiographic evolution

The story is complex, with geographical names that will be unfamiliar to many readers. Moreover, in many cases it is necessary to refute ideas currently held by other workers. For these reasons, we first present our interpretation of landscape evolution as a brief outline, without reference to sources.

Figure 1 shows the location of many of the geographical features mentioned in the text; others are found herein on other figures. Figure 2 shows the location of major sedimentary basins and divides in the study area.

In the Jurassic, Australia was still attached to other parts of Gondwana and land masses to the east (Pacifica). A watershed on the latter (the Tasman Divide—Fig. 2) was located perhaps two to three hundred kilometres east of and parallel to the present coast, and from it rivers carried sediment to the Eromanga–Surat Basin.

During the Cretaceous, an east–west-trending ridge, the Victoria Divide (Fig. 2), extended from the Tasman Divide through what are now the Victorian Highlands, separating the Eromanga–Surat Basin from the Otway, Torquay, and Gippsland Basins. Drainage carried sediment north from the Victoria Divide to the Eromanga–Surat Basin, and south to the Otway and Gippsland Basins.

About 80 Ma ago, the Tasman Sea opened by rifting followed by sea-floor spreading to form the modern continental edge of Australia and a new coastline. Much of the drainage from the old Tasman catchment was, therefore, cut off from the Eromanga–Surat, Otway, and Gippsland Basins with the formation of the Great Divide.

At the beginning of the Tertiary, the Murray Basin started to subside. The rivers flowing north from the Victoria Divide no longer reached the Eromanga–Surat Basin (which was thus deprived of coarse sediment from the south), but started to flow to the west, like the modern drainage of the Murray Basin. A new divide was formed between the Murray and Eromanga–Surat Basins, which is here called the Canobolas Divide. Traces of the ancient north-flowing rivers are still to be found crossing the Canobolas Divide (Fig. 2).

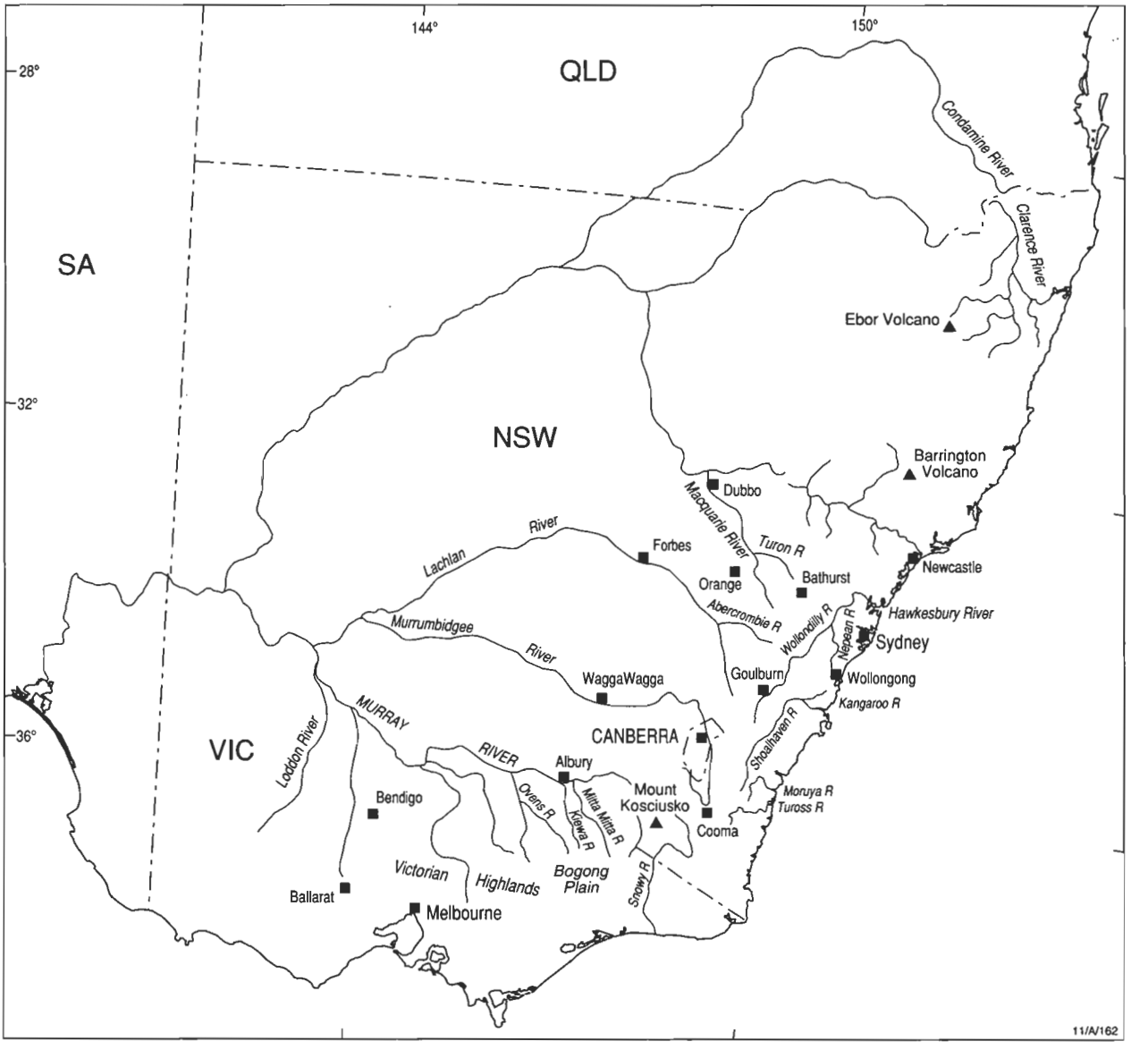

Figure 1. Main geographical features mentioned in the text.

The eastern edge of the Australian continent was downwarped to the new coast, some major rivers were reversed, and an early Great Divide was formed between the coast and the inland sedimentary basins. Even today, the Great Divide separates an area of simple dendritic drainage to the west from an area of more complex drainage to the east, although the divide itself has been shifted at times by volcanism, scarp retreat, and river reversal and capture. As new easterly drainage developed, valleys coalesced to form a Great Escarpment facing the Tasman Sea, separating a plateau from a highly eroded coastal belt. Cainozoic volcanism along much of the Great Divide, and Miocene faults with throws of hundreds of metres, particularly in the Snowy Mountains area, have further complicated the topography.

The palaeoplain

The oldest landforms in southeastern Australia are remnants of a palaeoplain that formed while Australia was still attached to other parts of Gondwana and land masses to the south and east. In the south a palaeoplain in what is now Victoria probably dates back to the Triassic (Hills 1975). In the east, the palaeoplain extended to a divide which was located perhaps two to three hundred kilometres east of and parallel to the present coast.

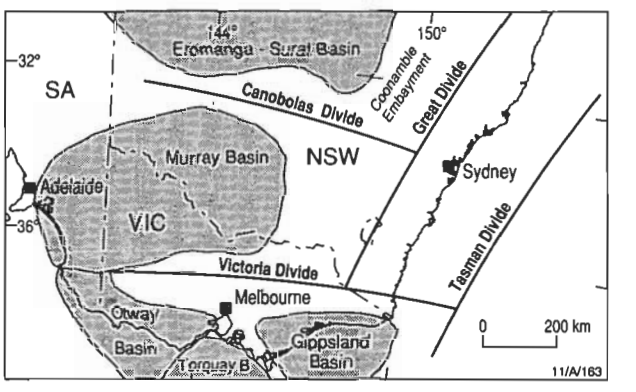

Figure 2. Diagramatic representation of the major basins, palaeo-divides and present divides in southeast Australia.

The palaeoplain probably had a relief similar to that found at present on its remnants. It has been considerably modified by tectonics and erosion, but, as will be shown, these modifications have not occurred everywhere and large remnants still exist in the present landscape. There is a large body of evidence (e.g. Ollier 1978; Young 1978; Bishop 1988) to show that these remnants have been little modified in the Cainozoic, and, by inference, that they have been little modified since before the break up of Gondwana.

The palaeoplain is an important feature of southeastern Australia, and it will be discussed below in a number of contexts.

The basins

The Eromanga–Surat Basin

The Eromanga–Surat Basin is filled with Jurassic and Cretaceous sediments. This paper is mainly concerned with the eastern Surat Basin, where sediments were mainly derived from the east and south, and the drainage which once reached its southern end (the Coonamble Embayment) (see Hawke & Cramsie 1984 and Wiltshire 1989 for more details of the depositionary sequences).

The Otway, Torquay, and Gippsland Basins

The Otway and Torquay Basins originated as a rift associated with opening of the Southern Ocean, while the Gippsland Basin formed as a result of incomplete rifting of an arm of the Tasman Sea some 15 Ma later. They existed through Cretaceous and Tertiary times. They derived some sediment from bounding hills to the north, but for much of their history they were mainly filled by volcanogenic sediment derived from the east. The Early Cretaceous fill is entirely terrestrial, but there is evidence of marine incursions in the younger strata.

On the continental margin, in both the Otway Basin and in the Strzelecki–Gippsland Basin, the same unconformity is found that separates the deformed volcanogenic Strezlecki Group from the overlying comparatively undeformed quartzose Latrobe Group (Veevers 1984, p. 176; Threlfall et al. 1976, p.46). The early basins were a rift, filled progressively from the eastern end over a period of 45 Ma by the products of intermediate volcanism (Veevers 1984, p. 137). On a more detailed scale, Hill et al. (in press) compared the onset of erosion of a granitic coastal area with local sedimentation. The onset of erosion in the mid-Cretaceous in the Wilsons Promontory area (the southernmost part of mainland Australia) is recorded in the sedimentary record in the adjacent Gippsland Basin, where the early Cretaceous Strezlecki Group contains, almost exclusively, volcaniclastics derived from a former volcanic chain to the east (Douglas 1988). The overlying late Cretaceous to Oligocene Latrobe Group sediments represent terrigenous material derived from the margins of the Gippsland Basin, such as Wilsons Promontory (Lowry & Longley 1991). The dominance of quartz and kaolin in these sediments (Hocking 1988) is the result of stripping of an extensively pre-weathered terrain. Sedimentation since the mid Cretaceous represents the progressive stripping of a deep weathering profile. Early stripping of saprolitic materials was followed by exposure and subsequent contributions from less-weathered zones in the profile.

The Murray Basin

The Murray Basin, which developed following the separation of Australia and Antarctica, is filled mainly with Tertiary sediments. Stephenson & Brown (1989) presented a summary of the development of the basin, including the Murray River. No Jurassic rocks are known beneath the Tertiary of the Murray Basin, but extensive Early Cretaceous sediments underlie western and northern areas of the basin, with upper surface elevations of around –200 to –600 m. These Cretaceous sediments are partly marine and can be correlated with those of the Eromanga Basin (Brown & Stephenson 1989). The Early Cretaceous sediments provide evidence of northerly and westerly drainage. They are volcanolithic in character and, as Stephenson & Brown (1989) noted, this is consistent with the idea that similar Cretaceous sediments in the Eromanga Basin were derived from the western part of the Otway Basin, presumably via the Murray Basin. A north–south bedrock rise separates the eastern and western parts of the Murray Basin, and marine beds are essentially confined to the western half (Brown & Stephenson 1989).

Stephenson & Brown (1989) noted that drainage into the Murray Basin from the north did not develop until at least the early Tertiary. From the Middle Eocene onwards, fluvial sedimentation of an early Murrumbidgee built a huge fan, marking the inception of sediment derived from the eastern highlands. In the Oligo-Miocene, a major marine incursion flooded the Murray Basin. In the Plio-Pleistocene, the eastern Murray Basin was filled with inland deltas (Shepparton–Cowra Formations), back-filling marginal valleys and burying Mio-Pliocene alluvium.

Offshore New South Wales

The present-day offshore area of New South Wales is receiving sediment, as it has since the initiation of the coast, and the sediments here should record events in the same way as those in the sedimentary basins on land. Ollier (1982a) proposed that this part of the coast originated as one side of a rift valley, with the rift now east of the continental shelf. The original rift valley sediments have drifted to the Lord Howe Rise (Jongsma & Mutter 1978) because of asymmetrical sea-floor spreading (Fig. 3), and the continental shelf is simple, sharp and close to the coast.

Erosion by the relatively short, steep rivers that flowed to the new coast rapidly modified the landscape. A Great Escarpment was formed, and in most places has retreated tens of kilometres inland (Ollier 1982a). Sediment accumulated in the off-shore zone as a large wedge (see Davies 1975 for a full discussion).

Assuming no loss or gain of material, the wedge of material eroded from the land should have a similar volume to the sedimentary wedge offshore (Fig. 4A). One place where it is possible to test this hypothesis is the area between Newcastle and Eden. This is a straight stretch of coastline where a series of offshore profiles has been determined (Davies 1975) that enables calculation of the volume of the offshore sedimentary wedge. The profiles indicate a clear basement to the sediments, which we assume to be the down-warped palaeoplain. The volume of eroded material was assumed to be roughly half a triangular prism of length 550 km, width 50 km (the rough distance between the Great Escarpment and the coast), and height 0.5 km (the average height of the

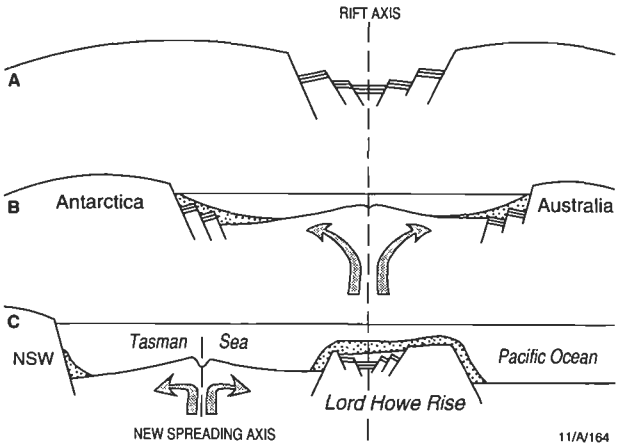

Figure 3. Sea-floor spreading (after Jongsma & Mutter 1978). A—The breakup of a continent to form a rift valley, which will be followed by sea-floor spreading. B—Symmetrical sea-floor spreading, as between Australia and Antarctica. C—Asymmetrical sea-floor spreading, as between Australia and the Lord Howe Rise.

escarpment). The eroded volume works out to be about 3400 km^3. The volume of offshore sediments (Fig. 4B), calculated using data from Davies (1975), is 3400 km^3. The coincidence suggests the model may be roughly correct and strengthens the link between studies of the erosional geomorphology of the highlands and sedimentation.

The divides

The Tasman Divide

Little is known of this divide, but Jones & Veevers (1983) speculated on its nature in plate tectonic terms. They stated that while the Tasman Divide existed, cratonic sedimentation in eastern Australia was dominantly by labile sediment from an andesitic orogen coincident with the then coast, but, south of Brisbane, oblique slip may be manifested in basaltic volcanism.

The Great Divide

The Great Divide lies roughly parallel to the coast of New South Wales, and separates the Murray Basin and Eromanga–Surat Basins from the Tasman Sea. Much of this divide is close to the eastern margin of a palaeoplain, sloping gently to the west and cut off abruptly on the eastern side by the Great Escarpment (Ollier 1982a). There are, however, many variations on this theme (Fig. 5), the significance of which will be clarified below.

In some places, the present Great Divide seems to follow an ancient line, possibly the original palaeodivide. For example, the divide between the Upper Shoalhaven and tributaries of the Murrumbidgee (between Canberra and the coast) is the low-relief Gourock Range. Here, streams on both sides of the Great Divide are not incised and have the same gradients, implying great age. In other places, headward erosion associated with rejuvenation on both sides of the divide has led to the formation of ridge-type divides. Elsewhere, erosion has isolated individual plateaus east of the Great Divide, such as the Barrington Tops Plateau (Pain 1983), and the Bulga and Comboyne Plateaus to the north of Barrington Tops (Pain & Ollier 1986).

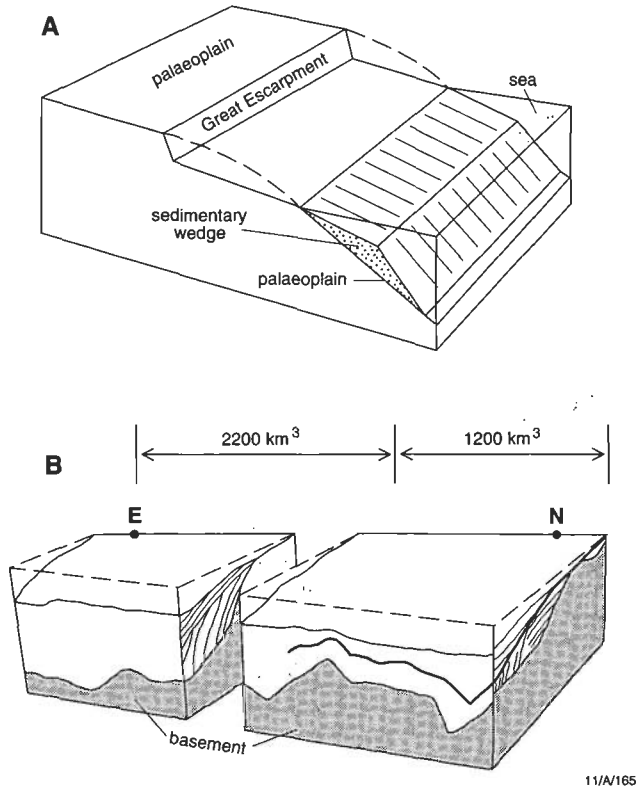

Figure 4. A—The east coast of New South Wales. The palaeoplain is down-warped to form the basement for marine sediments. Erosion of the land in front of the Great Escarpment provided the sediment for offshore depostion, so the volume of material eroded should roughly equal the volume deposited offshore. B—The offshore sediments between Eden (E) and Newcastle (N), with calculated volumes of sediment (Davies 1975). The larger volume to the south (left) results from erosion of a large area of weathered granite.

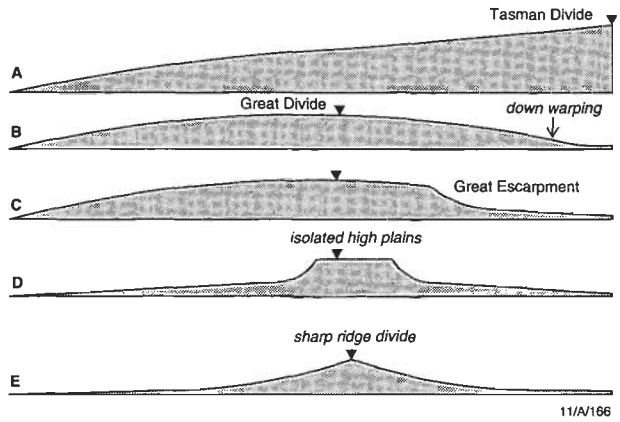

Figure 5. Evolution of the Great Divide of southeast Australia. A—Initial palaeoplain sloping down from the Tasman Divide. B—Down-warp of palaeoplain to coast, forming an initial divide. C—Formation and retreat of the Great Escarpment facing the coast. Much of the Great Divide is in this stage. D—Retreat of slopes from the coast and inland reduces the palaeoplain to isolated High Plains, common on the Victoria Divide. E—Continued retreat of the escarpment of the inland slopes consumes the High Plains and produces a sharp ridge divide, as along much of the Victoria Divide.

The height of the Great Divide is variable along its length, partly because of erosion, partly because of tectonics. From a low point at only 700 m near Goulburn, the divide rises north to about 1000 m, and to the south it rises more or less steadily to Cooma, and then to the exceptionally high section at Mount Kosciusko (2230 m).

Faulting has affected the divide in several places. Near Canberra, the Lake George Fault has direct topographic expression, giving rise to Lake George in a fault angle depression and an area of internal drainage. In the Kosciusko region major faulting of up to 1 km vertical movement has occurred, perhaps 20 Ma ago (Ollier & Wyborn 1989).

The Victoria Divide

In the Cretaceous, an east–west divide ran through Victoria, roughly coincident with the present divide, and from it a river system flowed north to the Eromanga–Surat Basin. The divide appears to have been originally fairly flat, and to have developed by warping of a palaeoplain, which probably dates back to the Triassic (Hills 1975).

Drainage south of the divide flowed into the Otway, Torquay, and Gippsland Basins, which were filled by sediment brought in mainly from the north. Valleys were cut into the palaeoplain and there was probably a stage of Great Escarpment formation as on the east coast, but this divide is older than the Great Divide and erosion has gone much further. Apart from the major plateau in the Kosciusko area, the palaeoplain is preserved as isolated smaller plateaus (locally called High Plains, such as Bogong Plain), and elsewhere the divide is a sharp ridge. Because the south-draining rivers in eastern Victoria were steeper and more erosive than the north-flowing ones, the divide has migrated north, and most of the Victorian High Plains are south of it. In this, they are similar to the Bulga and Comboyne Plateaus east of the Great Escarpment.

Although the east–west divide through Victoria appears to be a single entity, the part west of the longitude of Melbourne is in many ways distinct. From it, rivers drain north to the Murray Basin and south to the volcanic western plains, and the divide crosses subdued topography. Older volcanoes (up to 70 Ma old) erupted on or near the divide, as did many Miocene and younger volcanoes. Lava flows filled the old valleys and provide valuable information on age, gradient, and evolution. Much evidence of landscape evolution comes from 'deep leads', i.e. gold-bearing alluvium preserved beneath the lava flows. Certainly, the position of the divide has moved tens of kilometres north since 'deep lead' times (Ollier 1988, p. 146). It is possible that in the Cretaceous some of the major valleys flowed right across the Western Victoria Divide from a source much further south, but this remains unproven. Williams (1983) interpreted old gravels in the Bendigo area to be traces of huge Cretaceous rivers. Two major valleys are revealed by sub-Tertiary contours in the Murray Basin (Brown & Stephenson 1989). Thus, north–south drainage may have existed in the area during Cretaceous times.

The Canobolas Divide

Though not nearly so prominent topographically as the others, this divide is an important element of the present story. The divide (named after the Canobolas volcanic complex near Orange) leaves the Great Divide at 1300 m, descending across an undulating plateau to 900 m on the basalt east of Canobolas, a volcano that straddles and separates two different parts of the divide. The low divide to the west runs transverse to geological structures, and recent regolith mapping by AGSO (R. Chan personal communication 1994) has found evidence of former north—south valleys crossing it. The divide was in existence by at least the Middle Eocene (Stephenson & Brown 1989), and was formed by down-warping of the Murray Basin. The former north-flowing rivers were diverted to the west. The divide east of the Canobolas volcanic complex has no signs of old valleys crossing it, and therefore appears to be old and stable.

Lava flows from Canobolas Volcano flowed down valleys to the north, south and west, showing that the divide was established by 11.7 Ma (Wellman & McDougall 1974; Middlemost 1981). The present divide was, thus, in existence in the Middle Miocene and has suffered minimal erosion since then.

The volcano itself overlies alluvium probably laid down by north-flowing rivers that brought sediments across the area that is now the Murray Basin into the Eromanga Basin. The age of the alluvium on the divide could, therefore, be Cretaceous (see section above on The Basins).

West of Canobolas Volcano, the divide crosses granites and Silurian and Devonian sedimentary rocks. There are some prominent strike ridges, locally called "ranges", on Devonian quartzite, but a lot of the divide is flat. Late Mesozoic drainage crossed this divide from south to north, as indicated by the large volume of quartzose sediment in the Coonamble Embayment (the southern part of the Surat Basin) and by fluvial sediments of probable Cretaceous age, preserved at low points in the watershed.

The rivers

In this section, we will not describe all the drainage of southeastern Australia, much of which is very modern, but shall outline selected aspects that are relevant to the interpretation of the drainage evolution on the long time scale.

North-flowing rivers

A recent account of the Murrumbidgee River headwaters is by Ollier & Taylor (1988). Major drainage came from the south (Fig. 6) and is now truncated by the Great Escarpment, though a small section of the old drainage is preserved as Saucy Creek, and its tributary, Outskirts Creek, which follow an old valley-fill of Palaeocene sediments and basalt. A Palaeocene to Eocene volcanic shield centred on Brown Mountain, but with many points of eruption damming some north-flowing rivers and developing radial drainage locally. Drainage from the south found its way west around this Monaro Volcano and eventually into the Snowy River. Later, a huge fault (the Long Plain Fault) displaced the palaeoplain by up to a kilometre, leaving the 22 Ma Kiandra Flow hanging on the edge of the fault scarp (Fig. 6) and tilting the palaeoplain to the southeastern.

Rivers reversed by the tilting of the palaeoplain in turn met the Monaro Volcano and were diverted to either the Snowy River or the Murrumbidgee. Most of the Monaro Volcano has since been removed by erosion on the volcano itself and by the retreat of the Great Escarpment. This

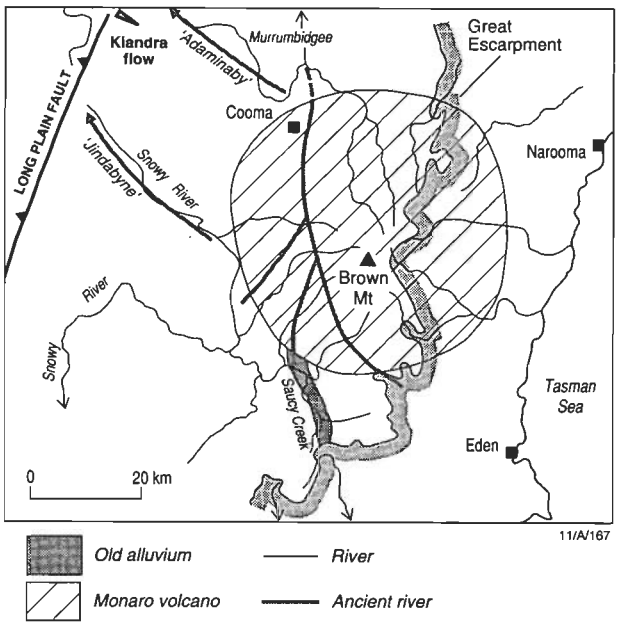

Figure 6. Diagram of the evolution of drainage near the Upper Murrumbidgee. Originally a river flowed north from Saucy Creek to join the north-flowing tract of the Murrumbidgee, and two other major rivers (the 'Jindabyne' and 'Adaminaby' Rivers). Eruption of a huge volcano centred on Brown Mountain initiated radial drainage on its surface and blocked Saucy Creek, which diverted into the Snowy River. Later faulting back-tilted the 'Jindabyne' and 'Adaminaby' Rivers, but the reversed rivers met the obstacle of the volcano and were diverted to become, respectively, the Upper Murrumbidgee and the Upper Snowy Rivers. Retreat of the Great Escarpment removed the headwaters of Saucy Creek and other southern rivers, and also removed much of the volcano (based on Ollier & Taylor 1988).

interpretation has been disputed by Taylor et al. (1989), who do not see the volcanics as a single volcano, and have suggested alternative reasons for the radial drainage. Brown et al. (1993) suggested that much of the Palaeocene pre-basalt drainage was southeast into the present Towamba River valley, and that Palaeocene and Eocene basalt dammed and diverted this already established southeasterly drainage.

Headwaters of the upper Murray (e.g. the Mitta Mitta River) rise on a plateau and drain north. The rivers encounter a series of faulted tilt blocks, through which they have cut deep gorges in antecedent courses. Fault displacements were in the range of 200 to 400 m.

North of the Western Victoria Divide, pre-Tertiary contours and isopachs on Palaeocene–Eocene Renmark Beds show two main rivers trending northwards into the Murray Basin (Macumber 1977), an eastern system, which continues the line of the present Loddon River, and a western system, which is a wholly buried valley. The Loddon River of today follows the course of Permian glacial deposits, confined to a palaeo-Loddon valley and overlain by Tertiary deep leads (Macumber 1977). Similarly, the Ovens Valley was a valley in Permian times, filled with glacial gravels. These gravels were stripped and replaced by Tertiary gravels, which were in turn stripped by the modern Ovens Valley erosion (Craig 1984).

Modified rivers of the east coast

Haworth & Ollier (1992) described and discussed the Clarence River, and showed that the barbed tributaries, the apparent continuation with the simple Condamine River west of the Great Divide, and the relationship to the formation of the Jurassic Clarence–Moreton Basin all suggest that this river was reversed in post-Cretaceous and probably pre-Miocene times.

Galloway (1967) presented a careful analysis of the Hunter River and showed that it was reversed. It already flowed in its present direction when the Goulburn lava flow was erupted in the Miocene, but the date of its origin has not yet been established.

The lower Shoalhaven is one of the most controversial areas of drainage in the country. Maps show barbed drainage, with the Kangaroo and other rivers joining the main stream at acute angles. The southern tributaries are very instructive, as this part of the Shoalhaven system is cut in deep gorges. The model is shown in Figure 7, and suggests down-warping of the palaeoplain to the east after the incision of the gorges across it.

Young & McDougall (1982) claimed that basalt near the coast must have been emplaced after the retreat of the Great Escarpment and the formation of the coastal plain. However, M.C. Brown (1983) pointed out that a monoclinal warp with a slope of only 2.5° would suffice to bring the palaeoplain to sea-level, complete with its cover of basalt. In fact, Young & McDougall (1982) noted a dip of about 2° for the base of the Wandrawandian Siltstone, although in their response to M.C. Brown they denied any large-scale post-basaltic warping (Young & McDougall 1983).

In our opinion, the controversy about tectonic lowering of the coastal lowlands in this area is much ado about very little. As noted above, very small amounts of warping are all that is needed. We are certainly not arguing for large-scale local post-basaltic warping, nor are we arguing for any faulting. Moreover, the evidence of silcretes, basalts and lateritic weathering quoted by Young and McDougall (1983) in support of no tectonic movement at all neglects the fact that no occurrence of these materials has been found near the base of the Great Escarpment. All are tens of kilometres to the east, which is in agreement with the present hypothesis that the palaeoplain, complete with its silcretes, basalts, and lateritic weathering profiles, was gently down-warped to the east. Moreover, this gentle down-warping would have been sufficient to cause major drainage disruptions and reversals.

Given the above arguments, it seems very likely that the lower Shoalhaven River is reversed. Where did it flow before reversal? Our suggestion is that it went to the upper Wollondilly and thence to the Lachlan (Fig. 8). Gentle down-warping (continuous with much more obvious monoclines further north) caused the reversal.

Some aspects of the Deua River are shown on Figure 9 and details are explained in the caption. This is one area where the Great Divide, the Great Escarpment, the coast, and the continental edge are all close together. It conforms to our hypothesis of early drainage being to the north and north–west, modified only after down warping, the formation of the new continental edge, and subsequent scarp retreat and river capture.

Although river capture is responsible for some of the complexities of the east coast rivers, more are tilt-induced

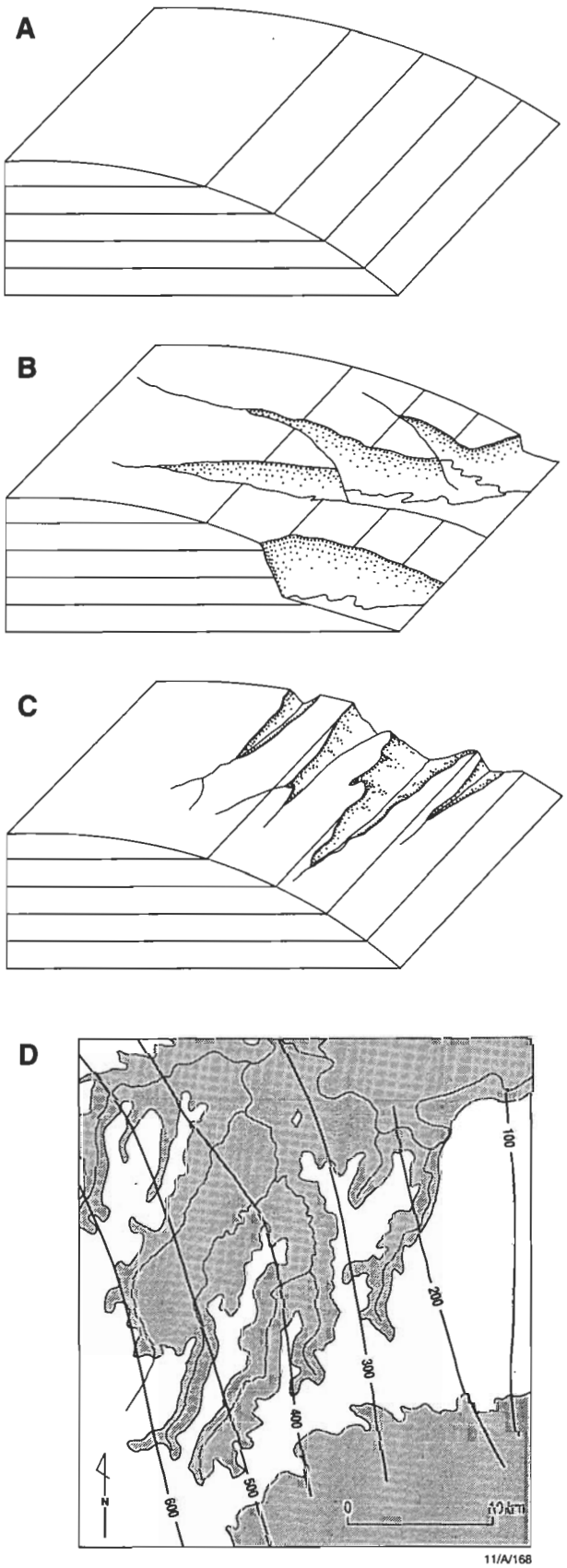

Figure 7. Generalised contours and the evolution of the Lower Shoalhaven. A—Contours on a down-warped surface. B—A down-warped surface dissected by valleys. Contours on the uneroded interfluves permit reconstruction of the old surface. This is the pattern expected if rivers were initiated on a simple down-warped surface. C—A representation of the down-warped surface in the Lower Shoalhaven area, with valleys almost parallel to the contours of the old surface. This pattern could occur only if the valleys were incised before the down-warp, i.e. they are antecedent. D—A map of the gorges and generalised contours in the Lower Shoalhaven area (after Ollier & Wyborn 1989). Note the similarity between this and C.

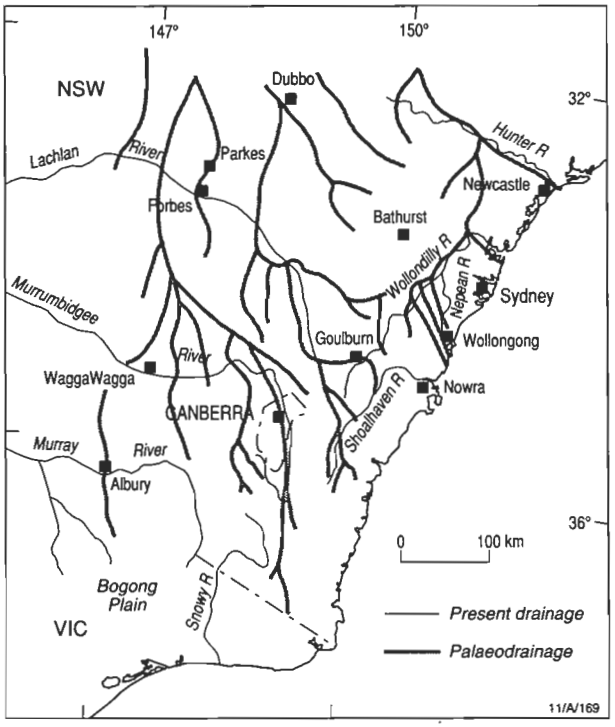

Figure 8. Approximate palaeodrainage and modern drainage in southeast Australia. The palaeodrainage is based on evidence of the kind presented in the text and figures of this paper. Of necessity, much of it is generalised.

reversals of rivers that followed their present course in the early Mesozoic, but in the opposite direction.

Summary of the Mesozoic drainage system

In the Mesozoic, the Kiewa and Mitta Mitta flowed north to join the Ovens and Goulburn in a north–west-flowing system. The upper Murray and Murrumbidgee united in a major system flowing north to the Coonamble Embayment in the Surat Basin (Fig. 2). The lower Shoalhaven went via the Lachlan to the Macquarie and, eventually, the Coonamble Embayment in the Surat Basin. The upper Shoalhaven, Deua, Moruya, and Tuross were tributary to this system, as was the system Wollondilly–Abercrombie–Coxs River–Macquarie–Turon. Two major rivers followed the Hawkesbury and Hunter valleys to the west, joined by the Nepean and Wollombi. This system drained the Permian and Triassic Sydney Basin, carrying large amounts of sand, which was deposited in the Surat Basin as the Pilliga Sandstone, a major Jurassic clastic fan deposit.

Tectonics, volcanoes and eustasy

Tectonics

Several major faults affect Gippsland and the Kosciusko area (Fig. 10). They have throws of several hundred metres, possibly reaching a kilometre, and are complicated; straight in plan even across country of high relief,

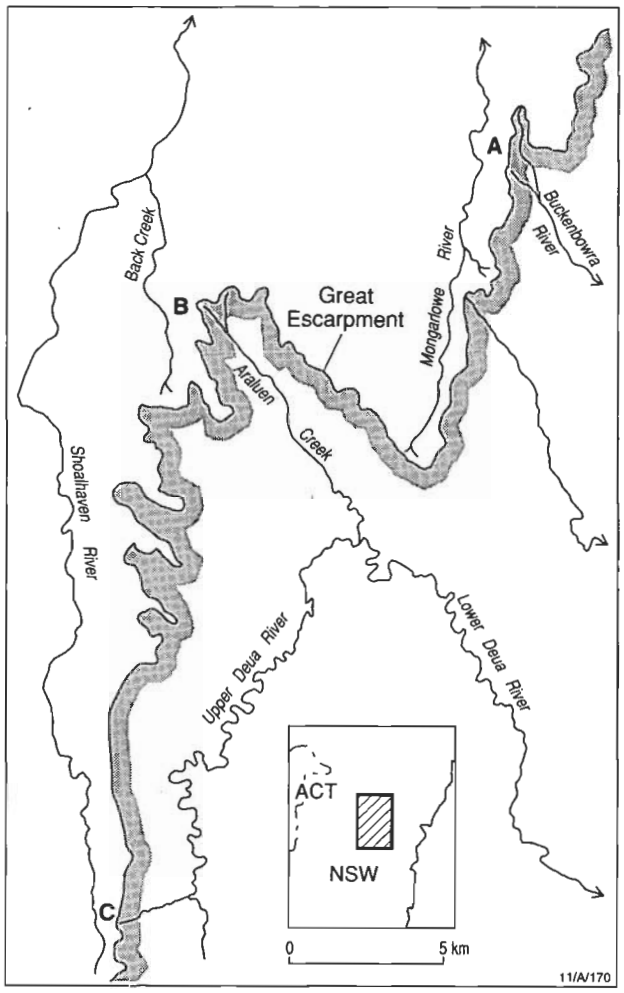

Figure 9. The Great Escarpment separating north-flowing rivers on the palaeoplain (left) from deranged drainage on the coastal side. Many rivers in the area show the marked bend exhibited by the Deua. Such bends could easily occur by river capture, as points A and B. After capture, the intervening narrow plateau remnant would be rapidly reduced. Possibly, the Upper Deua was once continuous with the Mongarlowe until captured by the Lower Deua. Another imminent capture is at point C.

in detail they show low-angle thrusts (Ollier & Wyborn 1989). Ollier & Wyborn suggested that these faults are basically normal faults that have undergone late thrusting at the base by spreading of the highlands. Tilt-block movement has caused river reversal (upper Snowy), superimposition (the Murray gorges, west of Mount Kosciusko), blockage (Lake George), and diversion (northern tributaries of Lake George). The major uplift of the Gippsland–Snowy Mountains block took place in Miocene times. Two uplift events in the western Murray Basin contributed to back-filling of the basin (Stephenson 1986). First, in the Late Miocene, tilting contributed to local erosion and infilling in the south of the basin and warping of the Parilla Sand. Second, reactivation of the Pinnaroo Block tilting in the Late Pliocene resulted in the formation of Lake Bungunnia.

Volcanoes

Volcanoes erupted throughout the Cainozoic, mainly along the major divides—Great Divide, Victoria Divide, and Canobolas Divide (Fig. 2). There was very little volcanic activity in the sedimentary basins except for the Late Tertiary and Quaternary activity of the western Victorian lava plains, where volcanics overlie a Tertiary syncline (Joyce 1975). Pre-basaltic river channels in western Victoria have longitudinal profiles that cross those of the present valleys, being steeper in the highlands and more gentle in the plains. This suggests uplift in the highlands and subsidence in the plains.

Volcanicity was widespread on the Great Divide and the eastern part of the Victoria Divide in Oligo-Miocene times, but was reduced or ceased in the Late Miocene. Major shield volcanoes on or near the Great Divide include the Ebor Volcano (Ollier 1982b), the Barrington Volcano (Pain 1983), and the Monaro Volcano (Ollier & Taylor 1988). The Canobolas Volcano (Middlemost 1981) erupted on the Canobolas Divide. These eruptions resulted in major drainage disruption and the formation and superimposition of radial drainage. Major volcanoes on the Great Divide caused further diversion of the drainage to the Hunter and Snowy Rivers in Palaeocene-Eocene times. Many smaller volcanoes produced lava flows, which provide useful data on the age and nature of landscape evolution.

Eustasy

Sedimentary cycles are found in all the basins and can be interpreted as eustatic cycles (C.M. Brown 1983; Brown & Stephenson 1989). In the Late Miocene, there was a major eustatic fall in sea-level, leading to major valley down-cutting, especially in Gippsland. The Murray Basin was flooded by a eustatic sea-level rise in the Early Pliocene. Appreciation of eustatic cycles is important, because sedimentary cycles can also be interpreted as reflections of tectonic movement in the highlands (Jones & Veevers 1983).

Discussion

River courses and tectonics

Large rivers can respond to tectonic uplift in two different ways (Ollier 1991). (1) If land is uplifted across the course of a large river, the river continues in its course by cutting an antecedent gorge. The rivers that cross the Himalayas from north to south are dramatic examples of this simple response to the relatively fast rates of river down-cutting versus slow rates of uplift. (2) Conversely, if a river is back-tilted, it cannot flow uphill and so is reversed, examples being provided by rivers flowing into Lake Victoria from the west (Ollier 1990a). On this basis, we can work out the sense of earth movements. Uplift and down-warping are not just relative—they are indicated absolutely by river behaviour.

In southeastern Australia, many river courses predate tectonic movement. From the two basic rules of river behaviour presented above, it is concluded that the Upper Murray cut antecedent gorges across uplifting fault blocks, whereas the coastal rivers were reversed by back-tilting with massive reorganisation of the drainage. Subsidence of the Murray Basin is indicated by incursions of marine sediments into an area that was formerly land. However, it was this subsidence, rather than the uplift of the Canobolas Divide, that diverted rivers from flowing north to the Eromanga Basin. The major divides were thus not formed by uplift, but by subsidence of their surroundings.

Uplift of the Eastern Highlands

There has been a great deal of speculation on this topic,

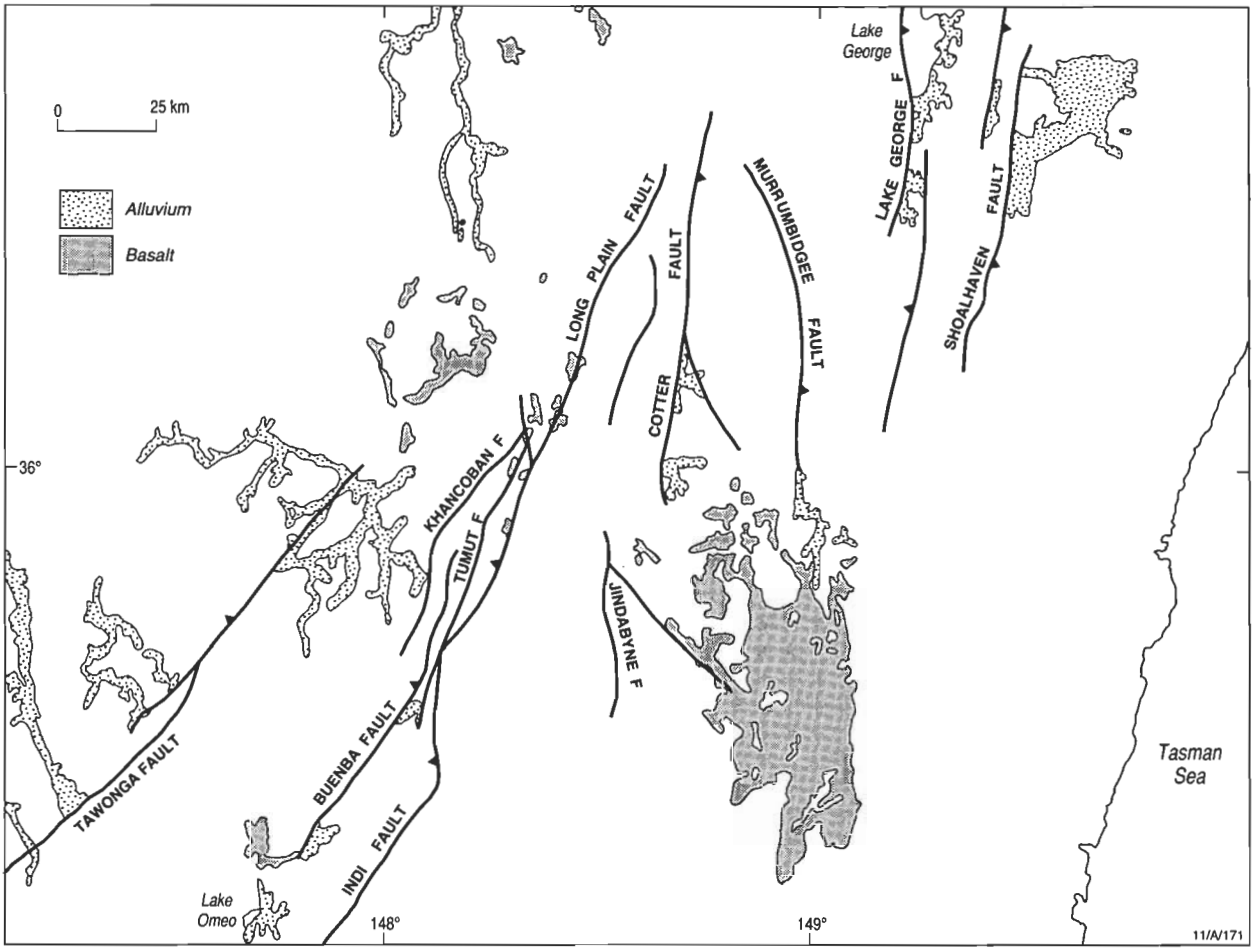

Figure 10. Major faults in southeast Australia (from Ollier & Wyborn 1989).

some specific to the region, and some in search of fundamental mechanisms. Only a few ideas can be discussed here.

Early writers believed uplift was largely associated with the '*Kosciusko Uplift*', a tectonic event at the very end of the Tertiary. The most recent exponent of this idea was probably Browne (1969), who wrote of 'Repeated differential uplift, chiefly in Late Pliocene and Early Pleistocene time (*Kosciusko Epoch*).' This idea was shown to be false by Ollier (1978), while the evidence we present here shows the presumed date of uplift to be quite wrong.

Smith (1982) and Karner & Weissel (1984) regarded the uplift as due to the passage of Australia over a hot spot (or hot line). However, given the different directions and ages of the divides, it seems impossible to design a suitable plan of hot lines that would be effective.

Lambeck & Stephenson (1986) suggested that residual stresses from a Palaeozoic orogeny were somehow revived in Cretaceous or Tertiary times to form the southeastern highlands. In fact, the fold axes of the Palaeozoic bedrock are essentially north–south, but the present divides all differ from that direction and from each other. The Miocene faults follow a different alignment again. Furthermore, there is no 'orogeny' that caused uplift, and some divides were formed by subsidence of neighbouring areas.

Jones & Veevers (1982) proposed a complex system of uplift and subsidence in the Eastern Highlands and adjacent basins, possibly better explained by eustasy, at least in the Murray Basin (C.M. Brown 1983). Their model shows the highlands in existence by the Cretaceous, which now seems correct for the Great Divide and the Victoria Divide.

Dumitru et al. (1991) studied fission-track data from southeastern Australia. They found a regular decrease in ages from 300–350 Ma a few hundred kilometres inland to 80–100 Ma along the coast, and interpreted this to be evidence of Late Cretaceous heating to temperatures ranging from less than 60°C in the interior to 120°C or more along the coast. They concluded that there had been 1.5–3 km of uplift and erosion along the east and south coastal regions, and that uplift and erosion were much less in areas 100 km inland.

This is inconsistent with the geomorphic evidence. Basalts show only a few hundred metres of erosion on most of the palaeoplain. Evidence presented by Young & McDougall (1992) suggested a maximum 325 m lowering of parts of the palaeoplain in southern New South Wales during the Cainozoic, and there is less than 1 km of erosion at the Great Escarpment. The young fission-track ages are all on the eroded side of the Great Escarpment, or where valleys have incised deeply into the palaeoplain. A thermal event might explain the fission-track data better than regional erosion, but it is hard to see a thermal

event taking the complex geographical pattern of the Great Escarpment. Perhaps the deep erosion is merely exposing a zone where depth-related temperature has caused apparently young fission-track ages.

Conclusions

In previous papers, we have been reluctant to provide a fundamental mechanism for uplift, not because we cannot offer one, but because there are too many; elsewhere Ollier (1990b) has listed twenty potential mechanisms. However, we suggest there has been too much emphasis on uplift and neglect of the equally important down-warping. There is considerable evidence to suggest that the highland axes have a very long life that began when they were part of a palaeoplain formed before Australia separated from the rest of Gondwanaland, and that the most important tectonic feature is the sagging of the basins that flank the divides. Down-warping of the basins formed the main divides, reversed rivers, and initiated erosion that led to formation of the Great Escarpment and other features, such as the Victorian high plains.

Uplift and down-warping are, of course, relative terms, but the evidence of major rivers, which can be interpreted despite eustatic changes, shows that subsidence has been a major tectonic factor. Instead of asking 'what caused uplift of the highlands?' we should ask 'what caused subsidence of the basins?'.

Acknowledgments

Bob Abell, Roslyn Chan, and Mike Craig commented on a draft of this paper.

References

Bishop, P., 1988. The eastern highlands of Australia. *Progress in Physical Geography*, 12, 159–182.

Bishop, P., Young, R.W. & McDougall, I., 1985. Stream profile change and longterm landscape evolution: early Miocene and modern rivers of the east Australian highland crest, central New South Wales, Australia. *Journal of Geology*, 93, 455–474.

Brown, C.M., 1983. Discussion: a Cainozoic history of Australia's Southeast Highlands. *Journal of the Geological Society of Australia*, 30, 483–486.

Brown, C.M. & Stephenson, A.E., 1989. Geology of the Murray Basin, southeastern Australia. *Bureau of Mineral Resources, Australia, Record* 1989/53.

Brown, M.C., 1983. Discussion: origin of coastal lowlands near Ulladulla, NSW. *Journal of the Geological Society of Australia*, 30, 247–248.

Brown, M.C., McQueen, K.G., Roach, I.C. & Taylor, G., 1993. Excursion guide to the Monaro volcanic province. *Australian Geological Survey Organisation, Record* 1993/61.

Browne, W.R., 1969. Geomorphology: general notes. *In* Packham, G.H. (editor), The Geology of New South Wales. *Journal of the Geological Society of Australia*, 16(1), 559–569.

Craig, M.A. 1984. The Permian geology, physiography and landscape evolution of northeastern Victoria. Unpublished MSc thesis, University of New England, Armidale.

Davies, P.J., 1975. Shallow seismic structure of the continental shelf, southeast Australia. *Journal of the Geological Society of Australia*, 22, 345–359.

Douglas, J.G., 1988. The Gippsland Basin. *In* Douglas, J.G. & Ferguson, J.A. (editors), *Geology of Victoria*. Geological Society of Australia, Victoria Division, 228–233.

Dumitru, T.A., Hill, K.C., Coyle, D.A., Duddy, I.R., Foster, D.A., Gleadow, A.J.W., Green, P.F., Kohn, B.P., Laslett, G.M. & O'Sullivan, A.J., 1991. Fission track thermochronology: application to continental rifting of south-eastern Australia. *APEA Journal*, 1991, 131–142.

Gale, S.J., 1992. Longterm landscape evolution in Australia. *Earth Surface Processes and Landforms*, 17, 323–343.

Galloway, R.W., 1967. Pre-basalt, sub-basalt, and post-basalt surfaces of the Hunter Valley, New South Wales. *In* Jennings, J.N. & Mabbutt, J.A. (editors), *Landform Studies from Australia and New Guinea*. ANU Press, Canberra, 293–314.

Hawke, J.M. & Cramsie, J.N., 1984. Contributions to the geology of the Great Australian Basin in New South Wales. *Geological Survey of New South Wales, Bulletin* 31.

Haworth, R.J. & Ollier, C.D., 1992. Continental rifting and drainage reversal: the Clarence Valley, New South Wales. *Earth Surface Processes and Landforms*, 17, 387–397.

Hill, S.M., Ollier, C.D. & Joyce, E.B., in press. Mesozoic deep weathering and erosion: an example from Wilsons Promontory, Australia. *Zeitschrift für Geomorphologie, N.F.*

Hills, E.S., 1975. *Physiography of Victoria*. Whitcombe and Tombs, Melbourne, 373 pp.

Hocking, J.B., 1988. Gippsland Basin. *In* Douglas, J.G. & Ferguson, J.A. (editors). *Geology of Victoria*. Geological Society of Australia, Victoria Division, 322–347.

Jones, J.G. & Veevers, J.J., 1982. A Cainozoic history of Australia's Southeast Highlands. *Journal of the Geological Society of Australia*, 29, 1–12.

Jones, J.G. & Veevers, J.J., 1983. Mesozoic origins and antecedents of Australia's Eastern Highlands. *Journal of the Geological Society of Australia*, 30, 305–322.

Jongsma, D & Mutter, J.C., 1978. Non-axial breaching of a rift valley: evidence from the Lord Howe Rise and the southeastern Australian margin. *Earth and Planetary Science Letters*, 39, 226–234.

Joyce, E.B., 1975. Quaternary volcanism and tectonics in southeastern Australia. *In* Suggate, R.P. & Cresswell, M.M.(editors), *Quaternary Studies*. Royal Society of New Zealand, Wellington, 169–176.

Karner, G.D. & Weissel, J.K., 1984. Thermally induced uplift and lithospheric flexural readjustment of the eastern Australian highlands. *Geological Society of Australia, Abstracts*, 12, 293–294.

Lambeck, K. & Stephenson, R., 1986. The post-Palaeozoic uplift history of southeastern Australia. *Australian Journal of Earth Sciences*, 33, 253–270.

Lowrey, D.C. & Longley, I.M., 1991. A new model for the mid-Cretaceous structural history of the northern Gippsland Basin. *APEA Journal*, 31, 143–153.

Macumber, P.G., 1977. Permian glacial deposits, tectonism, and the evolution of the Loddon Valley. *Mining and Geology Journal of Victoria*, 7, 34–36.

Middlemost, E.A.K., 1981. The Canobolas complex, N.S.W., an alkaline shield volcano. *Journal of the Geological Society of Australia*, 28, 33–49.

Nott, J.F. 1992. Long-term drainage evolution in the Shoalhaven catchment, southeast highlands, Australia. *Earth Surface Processes and Landforms*, 17, 361–374.

Ollier, C.D., 1978. Tectonics and geomorphology of the

Eastern Highlands. *In* Davies, J.L. & Williams, M.A.J. (editors), *Landform Evolution in Australasia*. ANU Press, Canberra, 5–47.

Ollier, C.D., 1982a. The Great Escarpment of Eastern Australia: tectonic and geomorphic significance. *Journal of the Geological Society of Australia*, 29, 13–23.

Ollier, C.D., 1982b. Geomorphology and tectonics of the Dorrigo Plateau, NSW. *Journal of the Geological Society of Australia*, 29, 431–435.

Ollier, C.D., 1986. Early Landform Evolution. *In* Jeans, D.N. (editor). *Australia: a Geography, Volume 1. The Natural Environment*. Sydney University Press, Sydney, 97–116.

Ollier, C.D., 1988. *Volcanoes*. Blackwell, Oxford.

Ollier, C.D., 1990a. Mountains. *In* Barto-Kyriakidis, A. (editor), *Critical Aspects of the Plate Tectonic Theory, Volume II Alternative Theories*. Theoprastus, Athens, 211–236.

Ollier, C.D., 1990b. Morphotectonics of the Lake Albert Rift Valley and its significance for continental margins. *Journal of Geodynamics*, 11, 343–355.

Ollier, C.D., 1991. A hypothesis about antecedent and reversed drainage. *Geografie Fisique Dinamique Quaternaire*, 14, 243–246.

Ollier, C.D. & Taylor, D., 1988. Major geomorphic features of the Kosciusko–Bega region. *BMR Journal of Australian Geology & Geophysics*, 10, 357–362.

Ollier, C.D. & Wyborn, D., 1989. Geology of Alpine Australia. *In* Good, R. (editor), *The Scientific Significance of the Australian Alps*. Australian Alps National Parks Liason Committee, Canberra, 35–53.

Pain, C.F., 1983. Geomorphology of the Barrington Tops area, New South Wales. *Journal of the Geological Society of Australia*, 30, 187–194.

Pain, C.F. & Ollier, C.D., 1986. The Comboyne and Bulga Plateaus and the evolution of the Great Escarpment in New South Wales. *Journal and Proceedings of the Royal Society of New South Wales*, 119, 123–130.

Smith, A.G., 1982. Late Cenozoic uplift of stable continents in a reference frame fixed to South America. *Nature*, 296, 400–404.

Stephenson, A.E., 1986. Lake Bungunnia—a Plio-Pleistocene megalake in southern Australia. *Palaeogeography, Palaeoclimatology, Palaeoecology*, 57, 137–156.

Stephenson, A.E. & Brown, C.M., 1989. The ancient Murray River system. *BMR Journal of Australian Geology & Geophysics*, 11, 387–395.

Taylor, T.G., 1911. Physiography of Eastern Australia. *Bureau of Meteorology, Australia, Bulletin*, 8 pp.

Taylor, G., McQueen, K.G. & Brown, M.C., 1989. Discussion: major geomorphic features of the Kosciusko–Bega region. *BMR Journal of Australian Geology & Geophysics*, 11, 123–125.

Threlfall, W.F., Brown, B.R. & Griffith, B.R., 1976. Gippsland Basin, offshore. *Australasian Institute of Mining and Metallurgy, Monograph*, 7(3), 41–67.

Veevers, J.J., 1984. *Phanerozoic Earth History of Australia*. Clarendon Press, Oxford.

Wellman, P. & McDougall, I., 1974. Cainozoic igneous activity in eastern Australia. *Tectonophysics*, 23, 49–65.

Williams, G.W., 1983. The Tertiary auriferous alluvial deposits of north central Victoria. *Bureau of Mineral Resources, Australia, Record* 1983/27, 137–143.

Wiltshire, M.J., 1989. Mesozoic stratigraphy and palaeogeography, eastern Australia. *In* O'Neil, B.J. (editor), *The Cooper and Eromanga Basins, Australia*. Proceedings of the Petroleum Exploration Society of Australia, Society of Petroleum Engineers and the Australian Society of Exploration Geophysicists, South Australian Branches, Adelaide, 279–291.

Young, R.W., 1978. The study of landform evolution in the Sydney Region: a review. *Australian Geographer*, 14, 71–93.

Young, R.W., 1989. Crustal constraints on the evolution of the continental divide of eastern Australia. *Geology*, 17, 528–530.

Young, R.W. & McDougall, I., 1982. Basalts and silcretes on the coast near Ulladulla, southern New South Wales. *Journal of the Geological Society of Australia*, 29, 425–430.

Young, R.W. & McDougall, I., 1983. Reply: origin of coastal lowlands near Ulladulla, N.S.W. *Journal of the Geological Society of Australia*, 30, 248–249.

Young, R.W. & McDougall, I., 1992. Long-term landscape evolution: Early Miocene and Modern Rivers in southern New South Wales, Australia. *Journal of Geology*, 101, 35–49.

AGSO Journal of Australian Geology & Geophysics, 15 (3), 347–357 © Commonwealth of Australia 1994

Marine benthic communities in the Early Carboniferous of New South Wales (Visean—*Delepinea aspinosa* Zone)

Ian H. Lavering[1]

The *Delepinea aspinosa* brachiopod Zone comprises two subzones: the *Inflatia elegans* and *Linoprotonia tenuirugosa* Subzones. Multivariate (cluster) analysis is used to identify benthic marine fossil communities (recurrent species associations) in samples collected from all known fossiliferous intervals of these subzones in the study area. The Euclidean distance coefficient, a weighted-pair grouping method, and a standardised data set are used to form dendrographic clusters inferred to represent recurrent species associations (communities). The results parallel those from faunas of the succeeding *Rhipidomella fortimuscula* Zone, i.e. several communities are evident and some species are numerically significant in more than one community. The communities of each subzone appear to intergrade rather than form rigid, depth-limited assemblages.

Faunas of the *I. elegans* Subzone cluster into four communities, including the *Unispirifer striatoconvolutus* community, present in substrates near or below wave-base on a marine shelf. The *I. elegans* community is closest in species composition to the *U. striatoconvolutus* community, but does not occupy the same geographic range; it may be a precursor community. Two other communities, the *Rhipidomella australis* and *Leptagonia analoga* communities, overlap in range with the first two communities and are inferred to have occurred in a mid-shelf setting.

Faunas of the subsequent faunal assemblage, the *Linoprotonia tenuirugosa* Subzone, are present on marine shelf substrates influenced by an actively prograding shoreline. The *Rhipidomella australis* community persisted into this subzone with a modified species composition. The *Rugosochonetes careyi* community is a new element.

Introduction

The Early Carboniferous brachiopod-dominated faunas of eastern Australia are present in a regionally extensive and complex stratigraphic framework (Figs 1 & 2) (Roberts 1975, 1981; Jones & Roberts 1976; Roberts & Engel 1980), which has been interpreted as a result of field studies by the New South Wales Geological Survey, various universities, and the Bureau of Mineral Resources (now Australian Geological Survey Organisation) (Roberts & Oversby 1974; Roberts & Engel 1987; Roberts et al. 1991, 1993). A detailed set of geological maps, stratigraphic reference sections, biostratigraphic zonations, and palaeogeographic reconstructions identify the stratigraphic range of fossiliferous intervals within the marine parts of the geological succession. Brachiopod-dominated faunas of these intervals have been grouped into unique assemblage zones, defined by either the presence of diagnostic species or overlapping species ranges (Roberts 1975; Jones & Roberts 1976; Roberts & Engel 1980, 1987; Roberts et al. 1976, 1991, 1993) (Figs 1–4).

The content and distribution of faunas in each zone have been the basis for regional correlations in Australia by Jones et al.(1973) and Jones & Roberts (1976). An important feature is the disappearance of large numbers of genera and species at the end of each zone (Roberts 1975, 1981; Roberts et al. 1976). Inferred causes of such faunal 'turnovers' are oscillations in sea-level, periodic influx of large volumes of volcanogenic sediment, and a gradually colder climate—all may contribute to the evident development of 'punctuated' brachiopod zonal assemblages (Roberts 1981).

According to Jenkins et al. (1993), conodont faunas of Eastern Australia, where they are preserved in the sequences discussed here, exhibit similar biostratigraphic divisions to those of the brachiopod zones (cf. Roberts et al. 1993). Early Carboniferous brachiopod-dominated assemblages of equivalent age in Western Australia are present in carbonate and quartz sandstone of the Carnarvon, Canning, and Bonaparte Basins (Runnegar & Campbell 1976; Lavering 1979, 1981). Contrasts in sediment type and palaeoclimate between the basins of eastern and western Australia are inferred to be the cause of differences between faunas of the two regions (Roberts 1985; Runnegar & Campbell 1976). One of the more pronounced changes in the faunal succession of eastern Australia took place at the end of the *Delepinea aspinosa* Zone, when the last of the warm-water cosmopolitan assemblages were followed by low-diversity, cold-water forms of the *Rhipidomella fortimuscula* Zone, in the Late Visean, and others in the Early Namurian (Roberts 1981).

In New South Wales, faunas of the *Delepinea aspinosa* Zone are best represented in reference sections containing (in part) the Woolooma and Flagstaff Formations (Roberts 1975). These sections, and others noted in adjacent parts of the Hunter region, were sampled and analysed as the basis for identifying component benthic communities (Lavering 1978, 1983). A study of faunas of the *Rhipidomella fortimuscula* Zone in these reference sections (Lavering 1993) concluded that depth-limited, or fixed-composition communities, similar to those noted in the Early Palaeozoic by Ziegler (1965) and Brett et al. (1993), were not evident. Instead, several species were numerically significant in more than one community of the *Rhipidomella fortimuscula* Zone.

This analysis of the preceding *Delepinea aspinosa* Zone outlines the distribution and abundance of species present. The *Delepinea aspinosa* Zone also provides a useful contrast with the succeeding *R fortimuscula* Zone faunas in that it contains two distinctive subzone assemblages, the *Inflatia elegans* and *Linoprotonia tenuirugosa* (previously *Gigantoproductus tenuirugosus*) Subzones, whereas the *Rhipidomella fortimuscula* Zone consists of a single biostratigraphic zonal assemblage. The results of the analysis indicate that the *Delepinea aspinosa* Zone was subject to complex and variable controls not related to either substrate type or water depth alone.

This study attempts to outline the nature of the community groups present and the individual patterns of species distributions and abundance. The extent of effects of either the time-averaged bias resulting from the fossilisation, or the intergrading nature of the original living species assemblages, cannot be assessed in detail, although mechanical

[1] Exploration & Production Impacts Section, Petroleum Resources Branch, Bureau of Resource Sciences, PO Box E11 Queen Victorian Terrace, Parkes, ACT 2600.

reworking of the preserved remains is not widespread. Additional work is required to undertake such assessment. The aim here is to measure the abundances of fossilised remains rather than parent biological populations.

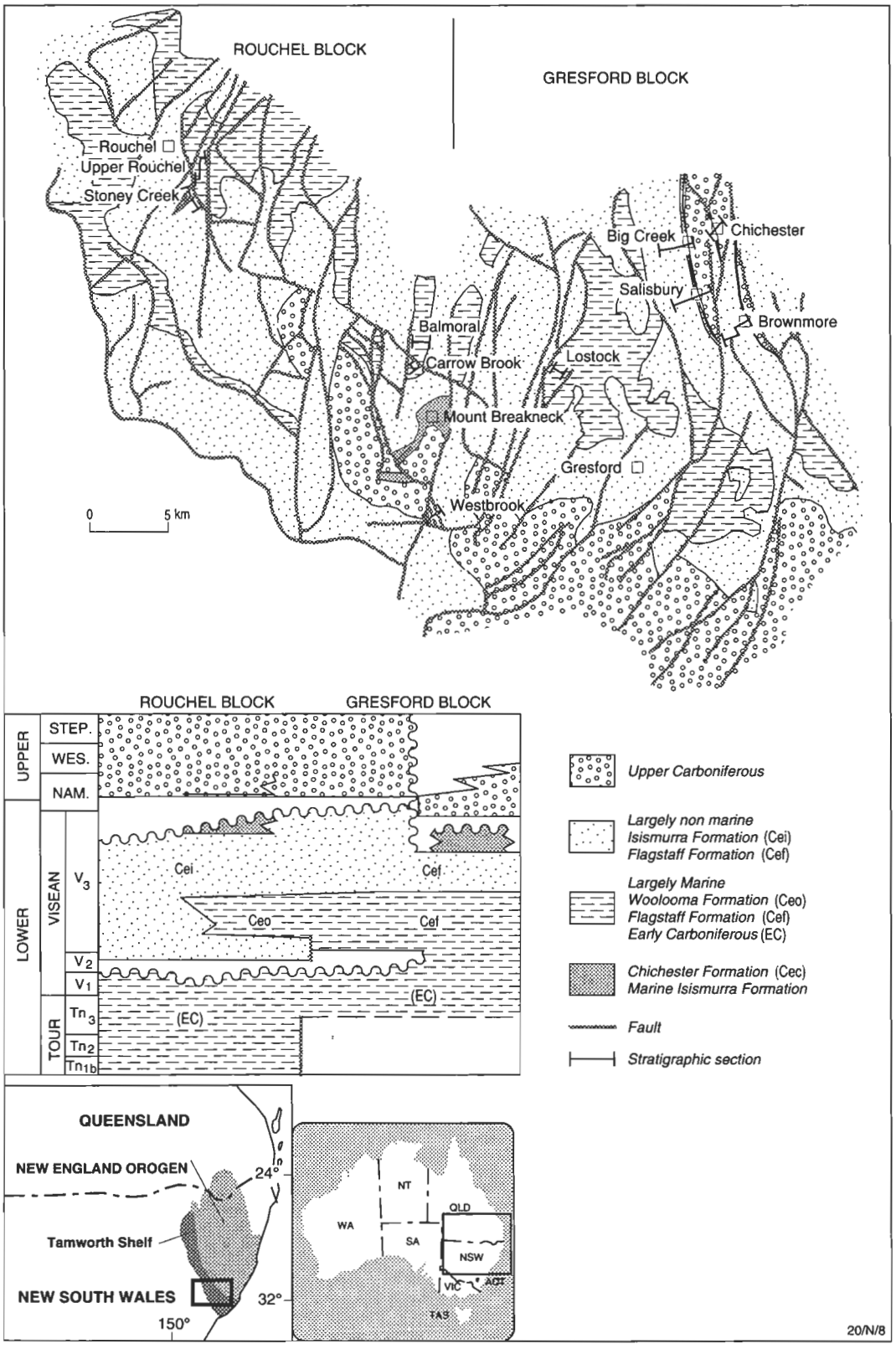

Figure 1. Location and regional geology of the Carboniferous sequence in the Hunter region (after Roberts et al. 1991) and, particularly, the Visean sequences in the Hunter region. The Flagstaff Formation(Cef) is mainly marine siltstone and sandstone. Largely marine units include the Dangarfield, Waverley, Ararat, Bingleburra, and Woolooma Formations (Ceo). The Isismurra/Flagstaff Formations are mostly non-marine, except for the Isismurra near Mount Breakneck and the lower part of the Flagstaff which are marine. The Upper Carboniferous comprises mainly non-marine Mt Johnstone Formation, Paterson Volcanics and Seaham Formation. Schematic stratigraphy after Roberts & Engel (1987) and Roberts et al. (1991).

Regional stratigraphy

Faunas of the *Delepinea aspinosa* Zone comprise one of eight brachiopod assemblage zones in the Early Carboniferous of eastern Australia. They are preserved in sediments of the Woolooma and Flagstaff Formations in the Rouchel and Gresford districts of the Hunter Region, at the Rouchel, Westbrook, Lostock, Salisbury, and Chichester locations shown in Figure 1 (Roberts & Oversby 1974; Lavering 1974, 1978; Roberts et al. 1991, 1993).

The stratigraphic and sedimentological results of Lindley (1981, 1984) Roberts & Engel (1987) and Roberts et al. (1991, 1993) show structural control of sedimentation patterns, particularly within the Flagstaff Formation, and some control over the nature of the sequences deposited. Major fault-bounded terrains ('blocks') have been defined in the Carboniferous (late Visean) sequence by Roberts & Engel (1987); each has its own unique structural style and stratigraphy. Marine sequences with faunas of the *Delepinea aspinosa* Zone are present in two of these blocks—the Rouchel and Gresford Blocks (Figs 1–4).

Differences in stratigraphic succession in these and other blocks have been identified as being due to movement along the major bounding faults during periods of active sedimentation (Roberts & Engel 1987) with major active volcanic and related non-marine sediment sources. Fossiliferous marine units and non-marine sequences are evident in several major stratigraphic sections identified in the Hunter region as a result of detailed mapping work (Lavering 1978; Roberts et al. 1991).

The Woolooma Formation is confined to the Rouchel Block, which is the western limit of marine shelf sedimentation in the time interval represented by faunas of the *Delepinea aspinosa* Zone. The Gresford Block has a thicker marine sequence of equivalent age, i.e. the Flagstaff Formation, and laterally equivalent non-marine units, noted by Lindley (1984), described by Hamilton et al. (1974) and sampled, in part, for conodont faunas by Jenkins et al. (1993). The faunas of the *Delepinea aspinosa* Zone examined in this study are from marine shelf sediments of the Woolooma and Flagstaff Formations in both the Rouchel and Gresford Blocks (Roberts & Engel 1987) (Figs 1–5).

As noted above, the *Delepinea aspinosa* brachiopod zone comprises two subzones, the *Inflatia elegans* Subzone and the *Linoprotonia* (previously *Gigantoproductus*) *tenuirugosa* Subzone. Faunas of the former subzone are present in the Woolooma Formation and lower part of the Flagstaff Formation, and faunas of the latter subzone are present in the Flagstaff Formation. Some of the more subtle structural controls of sedimentation in these and other formations of the Early Carboniferous sequence have become evident recently as result of new dating of volcanic units. These results have revised the age of some sequences and clarified that of others (Roberts & Engel 1987; Roberts et al. 1991, 1993). As a consequence, the timing of major volcanic activity has been clarified, and fault-related patterns of sedimentation identified with more precision (Roberts et al. 1993).

Stratigraphy and palaeogeography

Roberts et al. (1991) outlined how marine sediments of the upper part of the Woolooma Formation were formed

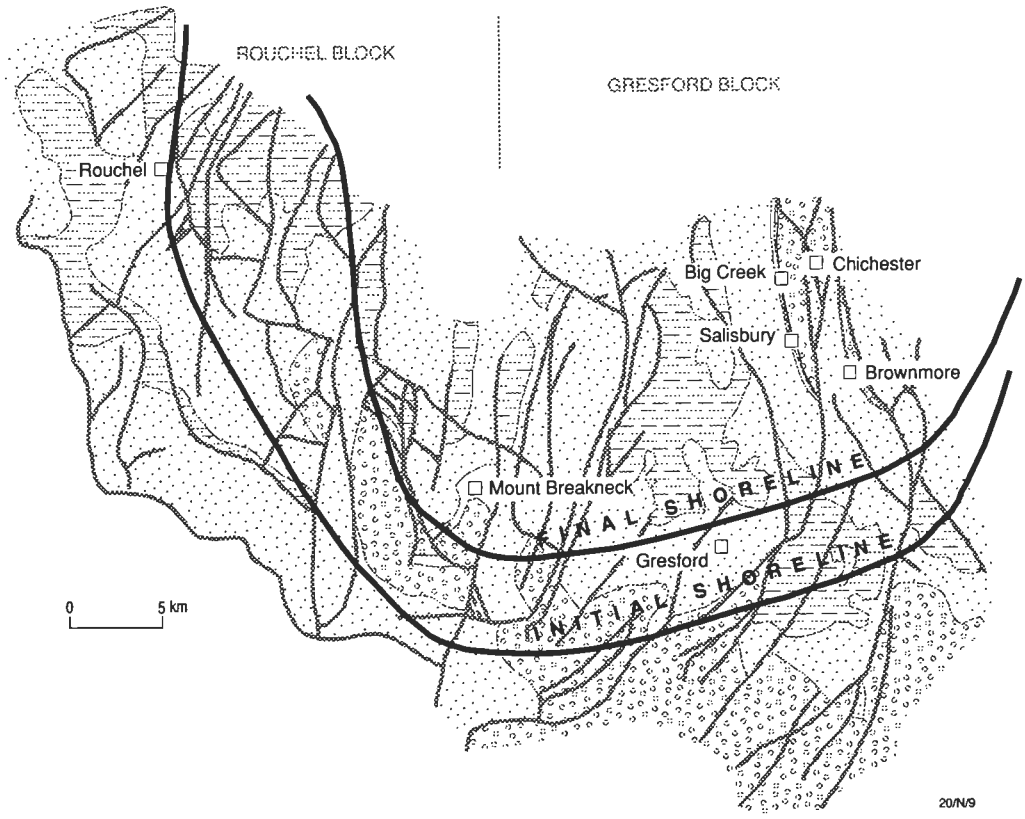

Figure 2. Palaeogeographic setting of the Hunter region for the time interval represented by faunas of the *Inflatia elegans* Subzone. Shoreline shifts during the time interval and considerable thickening of the sequence are evident away from the shoreline (after Roberts et al. 1991).

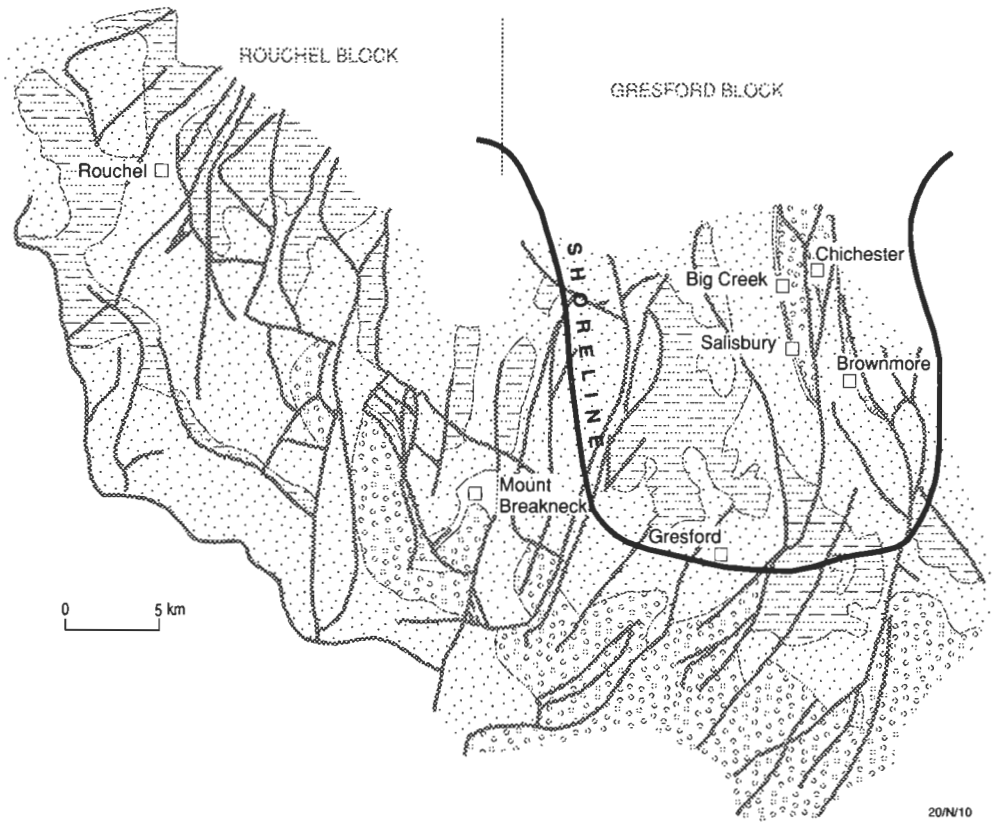

Figure 3. Palaeogeographic setting of the Hunter region for the time interval represented by faunas of the *Linoprotonia* (previously *Gigantoproductus*) *tenuirugosa* Subzone (after Roberts et al. 1991).

following an early to middle Visean marine transgression which inundated part of the Rouchel Block (Fig. 2). The western limit of this transgression was marked by deposition of shallow-marine siltstone, sandstone, and minor limestone west of the Stoney Creek section, and clouds of airborne volcanic material, which settled onto the marine shelf and on land.

Along the eastern edge of the Rouchel Block deeper-water areas of the Woolooma Formation received turbidite fan and minor storm-generated debris flows. Included in material deposited by such debris flows are brachiopod and gastropod shells in the Balmoral section of Lavering (1974; Roberts et al. 1991).

Woolooma Formation sediments containing faunas of the *Inflatia elegans* Subzone are present in sections at Stoney Creek and Upper Rouchel (Roberts & Oversby 1974; Roberts et al. 1991) and in the Carrow Brook region (Roberts 1975; Lavering 1978). Near the end of the time represented by the *Inflatia elegans* Subzone, renewed influx of volcanogenic sediments resulted in infilling of the marine shelf and a vertical transition to non-marine sandstone, siltstone, and conglomeratic sandstone of the Isismurra Formation. No faunas of the *Linoprotonia tenuirugosa* Subzone are present in sequences of the Rouchel Block, or the western part of the Gresford Block.

Sedimentation in the Flagstaff Formation was continuously marine in the northeastern part of the Gresford Block, although the southwestern part received laterally equivalent non-marine sediments. According to Lindley (1984), the lowermost marine parts of the Flagstaff Formation, the Allyn River Member and the Underbank Mudstone Member, comprise, respectively, turbidite fan and marine shelf sequences. Of these, only the marine shelf sequence (Underbank Mudstone Member) contains faunas of the *Inflatia elegans* Subzone, although sparse fragments of brachiopods are present in distal turbidites of the Allyn River Member in the eastern part of the Gresford Block (Lindley 1984). Similarly, with the fossiliferous material in the Woolooma Formation, shelf sequences contain much of the preserved faunas, whereas turbidite and storm-generated debris flow sequences contain relatively sparse and poorly preserved shelly material.

The Brownmore Sandstone Member, Bangrove Limestone Member and Lostock Sandstone Member of the Flagstaff Formation only contain faunas of the *Linoprotonia tenuirugosa* Subzone (Roberts 1975; Lindley 1984). These units constitute the marine tongue of an alluvial fan–delta system, which also deposited the non-marine portion of the Flagstaff Formation in the western part of the Gresford Block (Figs 3 & 4).

The Brownmore Sandstone Member comprises massive and parallel-bedded lithic sandstone, friable mudstone, and some fossiliferous horizons (Lindley 1984). The overlying Bandon Grove Limestone is a biogenic limestone composed of crinoid fragments, solitary corals, and brachiopods, but grading laterally into cross-bedded calcareous sandstone. The sequence was deposited during a period of low clastic influx onto the marine shelf. The fan–delta system, which deposited much of the upper part of the Flagstaff Formation, stopped prograding because of reduced sediment supply. Consequently, much of the

at least 500 times the size of the largest species being examined. The bulk-sampling approach used in this analysis satisfies this last criterion; the largest species present, *Linoprotonia tenuirugosa*, is less than 1/500 the volume of the containers used to collect each sample (Lavering 1993).

Time-averaging and *post mortem* disturbance have been identified as factors likely to impact upon fossilised faunas and provide a biased sample of the original living populations (Walker & Bambach 1971, 1974; Kidwell & Bosence 1991). Fossil horizons may represent the collective remains of several generations, and, hence, any analysis of recurrent associations between species is time-averaged. Flessa et al. (1993) have made quantitative estimates of time-averaging and stratigraphic disorder in recent shallow-marine (intertidal) habitats. They concluded that stratigraphic disorder in the preservation of shelly intertidal remains is a product of time-averaging, as well as physical and biological mixing. Tidal deposits they examined contained shells spanning 3500 years age in a single horizon. Such results do not allow for resolution of short-term phenomena. They suggest that no detailed reconstruction of environments is possible without demonstrating a close age of preserved material. Sampling a thin unit or single bedding plane is insufficient (Flessa et al. 1993). Results will tend to be affected by time-averaging or reworking.

Results

There was no evidence of major *post mortem* transportation or selective preservation of hard-shelled species in the samples examined. However, although direct age-dating of the sampled material is not available, it is likely that the recurrent species associations identified are time-averaged to some degree and represent the preserved remains of more than several overlapping generations. An outcome of such time-averaging is that original (biological) species assemblages (communities) are also masked by shifts in the geographic distribution of species over time. A series of intergrading, rather than geographically isolated, community groups would thus be preserved.

In the localities examined, many delicate details of shell morphology are preserved, such as spines of brachiopods, and few bivalve shells are disarticulated. Soft-bodied bottom-feeding organisms could not be identified apart from their feeding and dwelling traces. Despite the potential impact of time-averaging, lack of preservation of soft-bodied organisms, and disturbance by *post mortem* transportation, preserved marine invertebrate fossil faunas are primary indicators of palaeoenvironments (Johnson 1964; MacDonald 1969a, b, 1975; Petersen 1972, 1975; Tipper 1976a, b; Warme 1969, 1971; Warme et al. 1976).

The specimens collected and examined were, in many instances, preserved with relatively minor damage to shell ornament and close to their inferred living orientation. Some slight disturbance to shell orientation was evident, but indications of transport or reworking were not widespread. Fossil horizons with evidence of considerable transport were not included in the community analysis; they are limited to the easternmost parts of the Rouchel

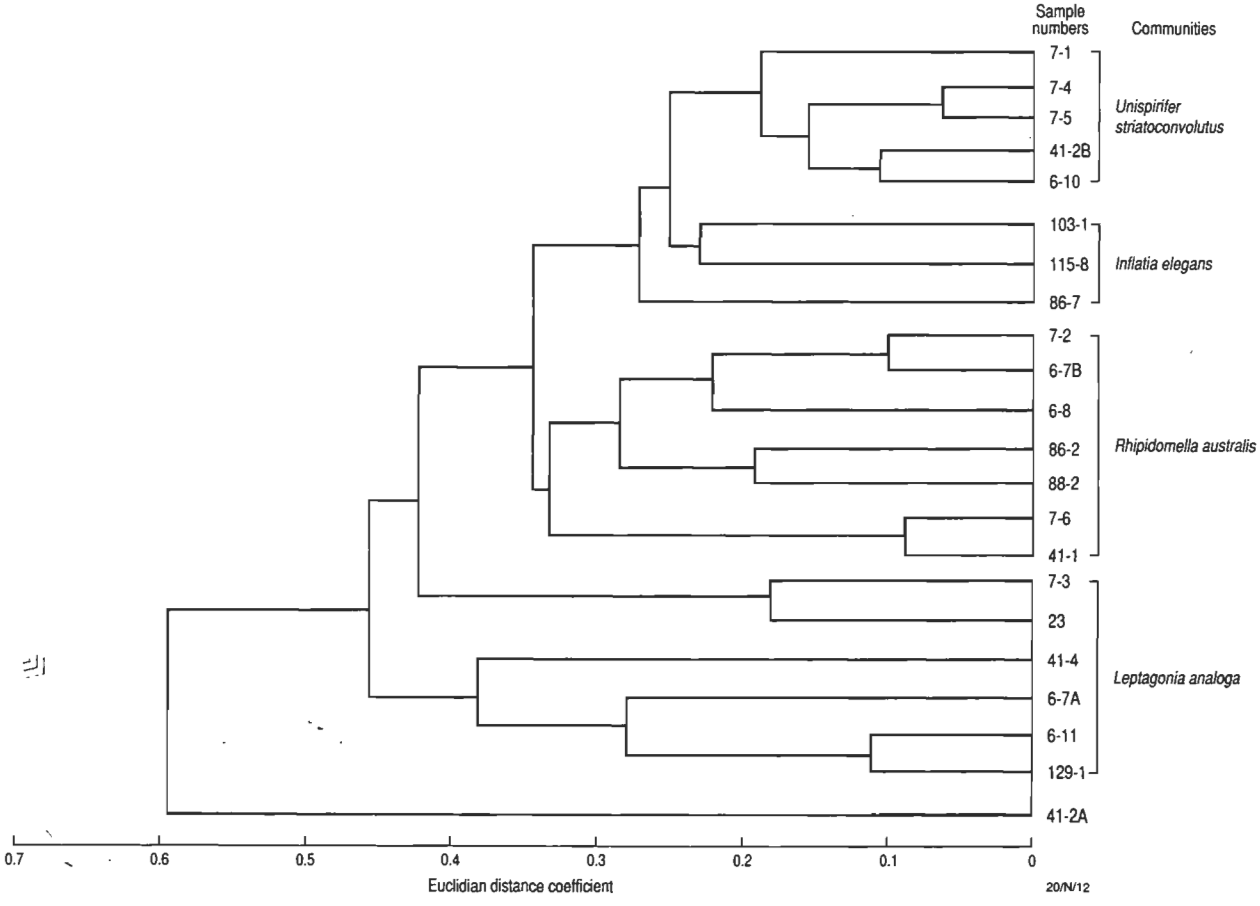

Figure 5. Multivariate cluster analysis of the *Inflatia elegans* Subzone faunas using the standardised weighted pair group method of Davis (1973).

marine extension of the alluvial fan–delta formed a shelf on which carbonate was deposited. Lindley (1984) inferred that the Mount Rivers Ignimbrite Member and Bandon Grove Limestone Member are time equivalents, because they occur at similar stratigraphic levels.

The Lostock Sandstone Member comprises sandstone and mudstone, passing vertically into medium and coarse-grained sandstone and conglomerate. The sequence is apparently marine (Lindley 1984), consisting of delta-front to offshore sediments, overlain by a shelf carbonate unit, the Verulam Oolite Member, and an ash-fall tuff . The latter rock unit is apparently a lateral equivalent of the Martins Creek Ignimbrite Member, present throughout the non-marine sequence as a distinctive stratigraphic marker. It extends from central parts of the Gresford Block, where it forms the uppermost part of the Wallaringa Formation, across the Rouchel Block as a major component of the Isismurra Formation (Lavering 1974; Roberts & Oversby 1974).

Within this somewhat complex stratigraphic and palaeogeographic framework the *Delepinea aspinosa* Zone faunal communities have been analysed to determine the nature of recurrent species associations (communities) within each subzone,

Reference sections

To identify benthic community types of the *Delepinea aspinosa* Zone preserved within the marine Woolooma and Flagstaff Formations, material was collected from thirty-eight fossiliferous horizons (Fig. 4) in nine stratigraphic sections (Roberts 1975; Lavering 1974; Etheridge 1975; Roberts et al. 1991). Fossiliferous horizons in the Woolooma Formation at Stoney Creek (six), Upper Rouchel (four), Carrow Brook (two), and Westbrook (six), and the Flagstaff Formation at Lostock (six), Brownmore (eight), Salisbury (two), Big Creek (two), and Chichester (two) were sampled and the species identified and counted. Samples were collected by removing fossiliferous layers from exposed bedding planes. Approximately 25 kg was collected at each site. Samples were disaggregated, so that most if not all fossiliferous remains could be identified. The material is lodged in the Department of Applied Geology, University of New South Wales (Lavering 1978). The letters A, B and C refer to horizons at the same location, sampled in ascending order.

Ager (1963) noted that as more of a representative fossil sample is examined, the number of species counted will approach an asymptotic limit, which is the actual number of species preserved. Hence, a certain sample size is required to obtain a representative collection; this depends both on the density of specimens and diversity (total number of species preserved). Chang (1967) and Dennison & Hay (1967) sampled a specific area of substrate to obtain a minimum representative sample. An alternative, and more practical approach, outlined by Tipper (1976a, b), suggests that a volume of material is required

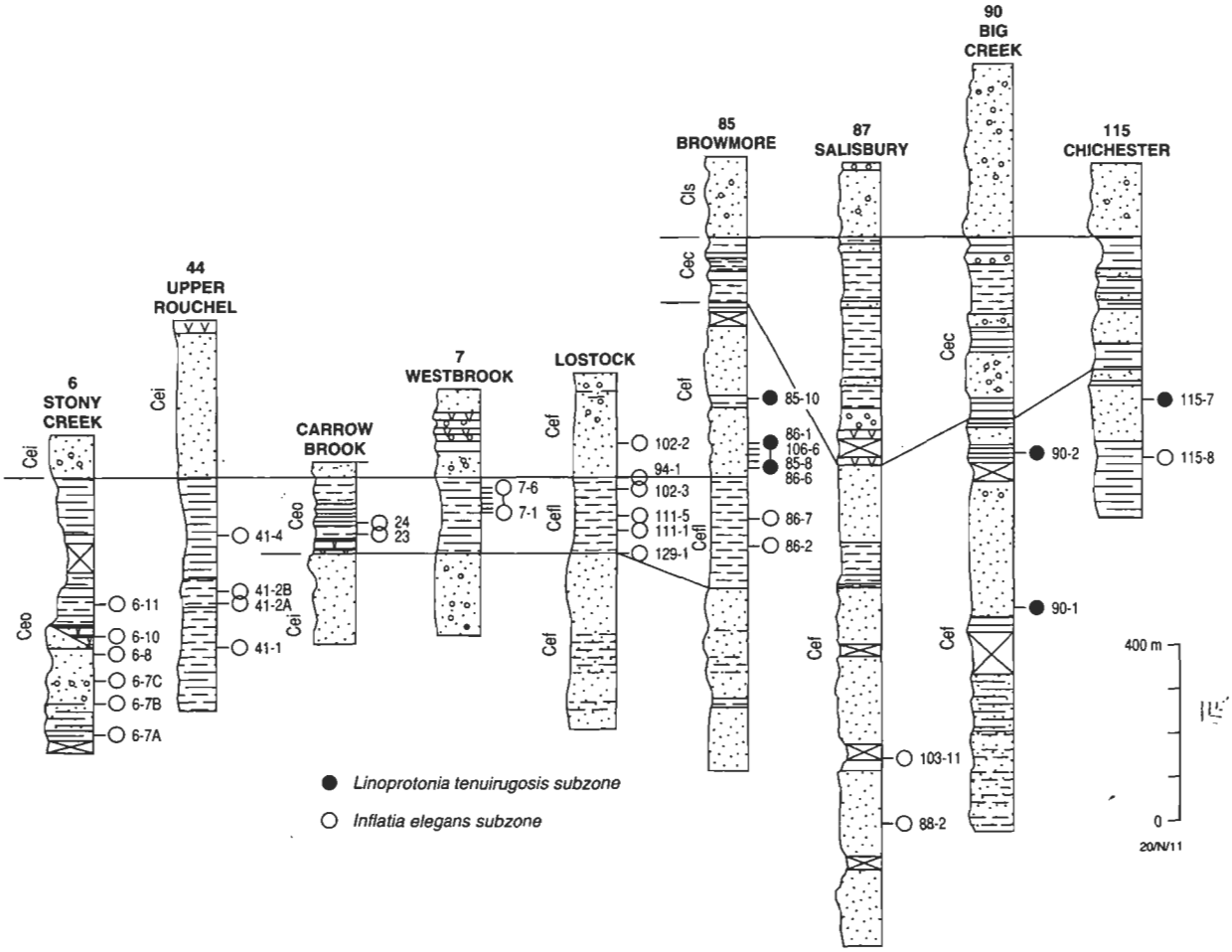

Figure 4. Stratigraphic sections of the Woolooma and Flagstaff Formations in the Hunter region which contain faunas of the *Delepinea aspinosa* Zone (*Inflatia elegans* and *Linoprotonia tenuirugosa* Subzones).

and Gresford Blocks—in the Woolooma Formation (Carrow Brook section, Fig. 4) and parts of the Brownmore Sandstone Member of the Flagstaff Formation (Lindley 1984). Samples from these horizons comprised fragments of gastropod and larger brachiopod specimens in a coarse-grained sandstone, also containing small rip-up shale clasts.

The samples analysed have a high proportion of brachiopods (90% of specimens counted), many preserved in their inferred living orientation or in orientations indicating only slight disturbance. Other forms include bivalve, gastropod, coral, bryozoan, trilobite, echinoid, and crinoid material. The brachiopods are largely spiriferid and strophomenid forms (productid and chonetid), with terebratulid, orthid, and rhychonellid forms represented by only one or two species. Other analytical results, such as the number of species per sample and other compositional information derived from the study, are listed by Lavering (1978).

The abundance of each species was used as a basis for clustering samples from the two faunal assemblages into groups with similar faunal content. As the species are present in more than one cluster of samples, it is possible that the communities are intergrading and reflect the time-averaging effect typical of marine shelf faunas (Flessa et al. 1993). Multivariate (cluster) analysis of the *Delepinea aspinosa* Zone (*Inflatia elegans* and *Linoprotonia tenuirugosa* Subzones) shows the following results.

Multivariate (cluster) analysis

A multivariate (cluster) analysis computer program was used to determine the underlying pattern of recurrent species associations. The method is based on a program by Davis (1973) which standardises data and groups samples into clusters using the Euclidean distance coefficient. This statistic measures the similarity of samples, based on the presence and abundance of species. The smaller the Euclidean distance coefficient between samples, the greater the degree of similarity. The most similar samples are clustered initially and additional clusters are formed thereafter until all samples are aggregated into a dendrograph (Figs 5 & 6), using a weighted pair grouping outlined by Davis (1973). Additional information on the program for this analysis was outlined by Thompson (1978), who used it to determine the numerical similarity of a number of Australian Carboniferous brachiopod forms.

The thirty-eight samples in the *Inflatia elegans* Subzone generate four unique clusters; one sample remains unclustered (Fig. 5). The first cluster in the dendrograph contains five samples (7–1, 7–4, 7–5, 41–2B & 6–10), those clustering at 0.1–0.2 indicating a high level of similarity. The second cluster has three samples and clusters onto the first between 0.25 and 0.28. The third and largest cluster of seven samples has high to moderate similarity. The fourth cluster of five samples has moderate to poor similarity (0.45–0.85). The three samples in the *Linoprotonia tenuirugosa* Subzone generate one unique cluster; one sample remains unclustered (Fig. 6).

The common species in samples of the first cluster in the *Inflatia elegans* Subzone are *Unispirifer striatoconvolutus, Orthotetes australis, Rhipidomella australis,* and *Productina striata.* One difference between the samples in each cluster is the relative abundance of each of these common species. The clusters (communities) appear to represent abstractions from a continuum of overlapping species populations—each species is not necessarily limited to a single cluster, but can be present as a significant component of more than one. These communities are a marked contrast to the Early Palaeozoic communities outlined by Ziegler (1965) and Brett et al. (1993), which are a series of depth-limited, species assemblages. In those assemblages, few species are present in more than one depth-limited community (Anderson 1971; Brett et al. 1993).

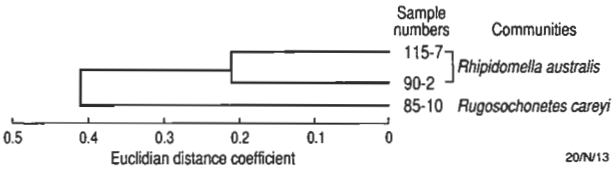

Figure 6. Multivariate cluster analysis of the *Linoprotonia tenuirugosa* Subzone faunas using the standardised weighted pair group method of Davis (1973).

The contrast with the expected depth-limited zonation of species highlights one of the significant results identified by this study—the apparently intergrading nature of the communities identified by clustering. The interpretation placed on these results is that the Early Carboniferous benthic species populations overlap and do not appear to have coincident geographic or depth-limited boundaries.

The results of the present cluster analysis contrast with those of Keen (1977), who employed a similar method. In his study, the composition of each identified cluster group was unique and very little, if any, overlap between species was evident. In the present study of the *Delepinea aspinosa* Zone faunas, however, the combined effects of both gradational species overlap and the time-averaged preservation of species populations from more than a single generation result in a pattern dominated by the effects of overlapping species ranges and hence, intergrading and overlapping communities. The four communities outlined with these patterns are described below.

Inflatia elegans Subzone communities

Unispirifer striatoconvolutus community

The four samples in the first cluster (*Unispirifer striatoconvolutus* community, Fig. 5) contain a total of 310 specimens of 30 species or taxa. The community was preserved in silt, mud and calcareous sand substrates near, or below wave-base in a marine shelf sequence of the Woolooma Formation at Stoney Creek, Upper Rouchel and Westbrook (Fig. 4). It is dominated by the numerically abundant *U. striatoconvolutus* (40% of all specimens), with an elongate shell, well suited to conditions of limited physical disturbance at or near wave-base (Lavering 1983). The other major species present are all different shell types: *Orthotetes australis* (strophomenid), *Rhipidomella australis* (orthid), and *Productina striata* (productid).

Table 1. ***Unispirifer striatoconvolutus*** **community (total of 30 species and 310 specimens counted).**

Rank	*Species*	*Specimens*
1	*Unispirifer striatoconvolutus*	66
2	*Orthotetes australis*	56
3	*Rhipidomella australis*	38
4	*Productina striata*	33
5	*Inflatia elegans*	18
6	*Balanoconcha elliptica*	10
7	*Brachythyris elliptica*	8
8	*Pernopecten travellynensis*	6
9	*Scoloconcha geniculata*	6
10	*Schizophoria verulamensis*	6
11	*Schuchertella* sp. *C*	6
12	*Pleuropugnoides* sp. *B*	3
13	*Nuculana etheridgei*	3
14	*Dielasma picketti*	3
15	*Brachythyris* sp.	3
16	*Bellerophon* sp.	2
17	*Rugosochonetes caryei*	2
18	*Mourlonia* sp.	2
19	*Peruvispira kuttungensis*	2
20	*Echinoconchus gradatus*	2
21	*Waagenoconcha delicatula*	2
22	*Marginatia patersonensis*	1
23	*Productina* sp.	1
24	*Cleiothyridina australis*	1
25	*Athyris* sp.	1
26	*Kitakamithyris uniplicata*	1
27	*Leptagonia analoga*	1
28	*Delepinea aspinosa*	1
29	*Loxonema lamellosa*	1
30	Rugose coral	1

Inflatia elegans community

The three samples of this community (cluster 2, Fig. 5) contain 23 species, represented by 147 individuals. The community is present in siltstone and mudstone of the Underbank Mudstone Member of the Flagstaff Formation. This part of the sequence was deposited below wave-base in the marine shelf sequence of the Underbank Mudstone Member at Salisbury, Brownmore, and Chichester (Fig. 4). The *Inflatia elegans* community has fewer species than the *U. striatoconvolutus* community and is present in different stratigraphic sequences; yet in the clustering results (Fig. 5) the two communities are the most similar of those sampled from the *I. elegans* Subzone. Five of the six most numerous species present in the *U. striatoconvolutus* community are also present, but not as abundant, in the *Inflatia elegans* community. One possible explanation is that the similarity between the two communities is that the *I. elegans* community was a precursor to the *U. striatoconvolutus* assemblage.

Table 2. ***Inflatia elegans*** **community (total of 23 species and 147 specimens counted).**

Rank	*Species*	*Specimens*
1	*Inflatia elegans*	32
2	*Schuchertella concentrica*	16
3	*Rugosochonetes careyi*	15
4	*Spirifer osbornei*	10
5	*Kitakamithyris triseptata*	9
6	*Didontopteria* sp.	8
7	*Kitakamithyris uniplicata*	8
8	*Marginicintus reticulatus*	6
9	*Schizophoria verulamensis*	6
10	*Athyris wiragullensis*	5
11	*Leptagonia analoga*	5
12	*Nuculana etheridgei*	5
13	*Delepinea aspinosa*	4
14	*Spathella* sp.	4
15	*Sanguinolites sp.*	3
16	*Echinoconchus gradatus*	2
17	*Bellerophon* sp.	2
18	*Orthotetes australis*	2
19	*Syringothyris* sp. *A*	1
20	*Pleuropugnoides sp. B*	1
21	*Brachythyris* sp.	1
22	*Rhipidomella australis*	1
23	*Dielasma picketti*	1

Rhipidomella australis community

The *Rhipidomella australis* community is geographically widespread, being present in the Woolooma Formation in reference sections at Stoney Creek, Upper Rouchel, and Westbrook (Fig. 4). It is also present in the Underbank Mudstone Member of the Flagstaff Formation at Salisbury and Brownmore. The community has 36 species represented by 300 specimens. Species with the largest population sizes are orthid, strophomenid and flat-lying chonetid forms. *Rhipidomella australis* and *Schizophoria verulamensis,* the two most numerous species present, are both orthids and evidently well suited to inhabiting marine shelf substrates from inshore areas below wave-base to areas well away from the shoreline. This community overlapped the range of the more diverse *Leptagonia analoga* community, restricted to a narrow part of the marine shelf.

Table 3. ***Rhipidomella australis*** **community (total of 36 species and 300 specimens counted).**

Rank	*Species*	*Specimens*
1	*Rhipidomella australis*	79
2	*Schizophoria verulamensis*	44
3	*Delepinea aspinosa*	21
4	*Balanoconcha elliptica*	17
5	*Unispirifer striatoconvolutus*	13
6	*Loxonema lamellosa*	12
7	*Leptagonia analoga*	11
8	*Orthotetes australis*	11
9	*Mourlonia* sp.	8
10	*Pleuropugnoides* sp. *B*	8
11	*Marginatia patersonensis*	8
12	*Marginicintus reticulatus*	8
13	*Inflatia elegans*	6
14	*Schuchertella* sp. *C*	6
15	*Kitakamithyris uniplicata*	6
16	*Schuchertella concentrica*	4
17	*Voiseyella anterosa*	4
18	*?Pecten* sp.	4
19	*Kitakamithyris* sp.	4
20	*Athyris wiragullensis*	3
21	*Waagenoconcha delicatula*	3
22	*Brachythyris* sp.	2
23	*Cleiothyridina segmentata*	2
24	*Spirifer osbornei*	2
25	*Streptorhynchus spinigera*	1
26	*Pernopecten trevallynensis*	1
27	*Fluctuaria campbelli*	1
28	*Dielasma picketti*	1
29	*Nuculana etheridgei*	1

30	*Productina striata*	1
31	*Bellerophon* sp.	1
32	*Syringothyris* sp.	1
33	*Kitakamithyris trispetata*	1
34	*Stegacanthia abbotti*	1
35	*Asyrinxia lata*	1
36	*Rugosochonetes caryei*	1

Leptagonia analoga community

This community comprises the fourth cluster in Figure 5 and is the most diverse community, even though it is present in a narrow range of the marine shelf formed during the time interval of the *I. elegans* Subzone. Forty species, represented by 456 specimens, are present in the community, all preserved in siltstone and mudstone of the Woolooma Formation at Stoney Creek, Upper Rouchel, Carrow Brook, and Westbrook, as well as a single collection from the Flagstaff Formation at Hilldale. The community overlaps with part of the range of the more widespread, but less diverse, *Rhipidomella australis* community (Fig. 5).

Table 4. *Leptagonia analoga* community (total of 40 species and 456 specimens counted).

Rank	*Species*	*Specimens*
1	*Spirifer osbornei*	48
2	*Leptagonia analoga*	44
3	*Unispirifer striatoconvolutus*	40
4	*Kitakamithyris sp.*	28
5	*Rhipidomella australis*	25
6	*Brachythyris* sp.	23
7	*Schuchertella* sp. *C*	21
8	*Eomarginifera tenuimontis*	21
9	*Marginicintus reticulatus*	20
10	*Inflatia elegans*	19
11	*Schizophoria verulamensis*	16
12	*Asyrinxia lata*	15
13	*Fluctuaria campbelli*	14
14	*Rugosochonetes careyi*	14
15	*Asyrinxia wiragullensis*	9
16	*Nuculana etheridgei*	9
17	*Orthotetes australis*	9
18	*Balanoconcha elliptica*	8
19	*Cleiothyridina australis*	7
20	*Waagenoconcha delicatula*	6
21	*Dielasma picketti*	6
22	*Delepinea aspinosa*	6
23	*Pleuropugnoides* sp. *B*	6
24	*Stegacanthia abbotti*	6
25	*Marginatia patersonensis*	5
26	*Mourlonia* sp.	4
27	*Streptorhynchus spinigera*	4
28	*Palaeoneilo* sp.	4
29	*Sanguinolites* sp.	3
30	*Crurithyris* sp.	3
31	Rhynchonellid	3
32	*Loxonema lamellosa*	2
33	*Kitakamithyris uniplicata*	1
34	*Kitakamithyris triseptata*	1
35	*Peruvispira kuttungensis*	1
36	*Pecten* sp.	1
37	*Punctospirifer amblys*	1
38	*Echinoconchus gradatus*	1
39	*Bellerophon* sp.	1
40	*Strapollus davidi*	1

Only three samples from this subzone are present in the sequence shown in Figure 6, in the Brownmore Sandstone Member of the Flagstaff Formation. The levels of similarity between the three samples are comparable to that exhibited by the *I. elegans* Subzone communities in Figure 5. Two samples in the *Linoprotonia tenuirugosa* Subzone (115-7 and 90-2), clustering at a similarity level of 0.22, contain the surviving elements of the *Rhipidomella australis* community, which was the most widespread association in the preceding subzone. The other sample (85-10) is the only representative of a new community, the *Rugsochonetes careyi* community, which was located closer to the shoreline and has a different species composition (Table 6).

Table 5. *Rhipidomella australis* community (total of 18 species and 180 specimens counted).

Rank	*Species*	*Specimens*
1	*Rhipidomella australis*	86
2	*Rugosochonetes careyi*	13
3	*Cleiothyridina* sp.	10
4	*Delthyris papilionensis*	10
5	*Orthotetes australis*	9
6	*Punctospirifer* sp.	9
7	*Eomarginifera megalotis*	8
8	*Asyrinxia lata*	6
9	*Pleuropugnoides sp. B*	5
10	*Unispirifer striatoconvolutus*	5
11	*Voiseyella* sp.	4
12	*Coledium laevis*	3
13	*Scoloconcha geniculata*	2
14	*Fluctuaria campbelli*	2
15	*Dielasma picketti*	2
16	*Kitakamithyris triseptata*	2
17	*Crurithyris* sp.	1
18	*Stegacanthia abbotti*	1

Table 6. *Rugosochonetes caryei* community (total of 14 species and 56 specimens counted).

Rank	*Species*	*Specimens*
1	*Rugosochonetes careyi*	12
2	*Unispirifer striatoconvolutus*	12
3	*Spirifer osbornei*	8
4	*Marginicintus reticulatus*	7
5	*Leiochonetes salisburyensis*	3
6	*Krotovia procidua*	3
7	*Scoloconcha geniculata*	3
8	*Fluctuaria campbelli*	2
9	*Kitakamithyris triseptata*	2
10	*Spathella* sp.	1
11	*Pleuropugnoides* sp. B	1
12	*Stegacanthia abbotti*	1
13	*Nuculana etheridgei*	1
14	*Brachythyris elliptica*	1

Discussion

The analysis and clustering of samples from the *Delepinea aspinosa* Zone (Woolooma and Flagstaff Formations) indicate that the communities are likely to reflect both time-averaged and gradational, not fixed, associations inhabiting a specific depth zone (Petersen community concept—Petersen 1913). As such, the communities accord with the concept of Whittaker (1967, 1970) and

Gauch (1986), who suggested that, depending on underlying environmental gradient trends, communities are likely to reflect abstractions from a continuum of intergrading species assemblages, rather than distinct entities of fixed composition (Shi 1993). The clustered groups of the *Delepinea aspinosa* Zone contain several common species populations; it is inferred this reflects the distribution of the original living population and the time-averaging that occurs in preservation of such fossilised remains.

The four benthic marine fossil communities recognised in faunas of the *Delepinea aspinosa* Zone are considered to be representative, if slightly time-averaged, collections of living invertebrates (largely brachiopods), because of their wide geographic occurrence and repeated representation in several geographic locations and stratigraphic sequences.

The underlying aim of this study has been to identify the structure of species associations and provide more detailed information on the species distribution and abundances which underlie changes in this part of the fossil record. The original work in collecting, analysing, and counting species data was discussed in detail by Lavering (1978) and summarised for the succeeding *R. fortimuscula* Zone by Lavering (1993). For faunas of both the *R. fortimuscula* and *D. aspinosa* Zone, the relationships between the pattern of species distribution, community groups, and environmental factors which control them are complex. They can only be referred to in general terms, because of the broad and complex nature of the sedimentary sequence in which they are preserved. Some of the geological complexities, such as structural control of sedimentation, have only become evident recently (Roberts et al. 1991, 1993) well after the data used for this study were collected.

Conclusions

Sampling and cluster analysis of faunas of the late Visean (Early Carboniferous) *Delepinea aspinosa* Zone in the Hunter region of New South Wales indicate that a series of gradational benthic communities is present. The occurrence of a few widespread species as dominant forms in more than one community and the absence of specific habitat or depth-related assemblages indicate that the communities intergrade and are abstractions from a continuum formed by overlap of species populations.

Multivariate cluster analysis (Fig. 5) identifies a total of four marine communities in the *I. elegans* Subzone, all of which appear to intergrade. The *Unispirifer striatoconvolutus* community was present in silt, mud and calcareous sand palaeosubstrates near or below wave-base of a marine shelf area. The *Inflatia elegans* community inhabited quiet-water shelf conditions below wave-base and away from the shoreline. The *Rhipidomella australis* and *Leptagonia analoga* communities are present throughout the shelf sequence, but differ in diversity and composition.

The *Linoprotonia tenuirugosa* Subzone contains persisting elements from the *Rhipidomella australis* community, the most widespread association in the earlier subzone, and the *Rugosochonetes careyi* community, which was located closer to the marine shoreline; it was a new community without analogue in the previous subzone.

Marine benthic communities of the *Delepinea aspinosa* Zone provide an illustration of the cumulative effects of gradational faunal boundaries and the inherent (areal) patchiness of species populations. Major periodic fluctuations in environmental parameters are likely to be reflected in the fossil record where the populations of more than a single generation are preserved.

Acknowledgments

John Roberts (UNSW) provided information on recent developments in correlation, age dating, and structural evolution. Alan Williams and Russ Temple of the Bureau of Resource Sciences (BRS) provided input on both the scientific and editorial aspects. Publication is with the permission of the Director of the Petroleum Resources Branch of BRS. John Talent (Macquarie University), Neil Archbold (Deakin University), and Bob Nicoll (AGSO) greatly improved the form of the manuscript. John Convine (CSU, AGSO) drafted the text figures.

References

Ager D.V., 1963. *Principles of palaeoecology*. McGraw-Hill, New York, 317 pp.

Anderson, E.J., 1971. Environmental models for Palaeozoic communities. *Lethaia,* 4, 287–302.

Brett, C.E., Boucot, A.J. & Jones, B., 1993. Absolute depths of Silurian benthic assemblages. *Lethaia,* 26, 25–40.

Chang, Y., 1967. Accuracy of fossil percentage estimation. *Journal of Paleontology,* 41, 500–502.

Davis, J.C., 1973. *Statistics and data analysis in geology*. John Wiley & Sons, New York, 550 pp.

Dennison, J.M. & Hay, W.W., 1967. Estimating the needed sampling area for subaquatic geological studies. *Journal of Paleontology,* 41, 706–708.

Ekdale, A.A., 1974. Recent marine molluscs from northeastern Quintana Roo, Mexico. *In* Wiedie, A.E. (editor). Field Seminar on water and carbonate rocks of the Yucatan Peninsula, Mexico, *Geological Society of America Guidebook* No. 2, 199–218.

Etheridge, L.K., 1975. Geology of the Westbrook district of New South Wales. B.Sc.(Hons) thesis, Department of Applied Geology, University of New South Wales, (unpublished).

Flessa, K.W., Cutler, A.H. & Meldahl, K. H., 1993. Time and taphonomy: quantitative estimates of time-averaging and stratigraphic disorder in a shallow marine habitat. *Paleobiology,* 19(2), 266–286.

Gauch, H.G., 1986. *Multivariate analysis in community ecology*. Cambridge University Press, Cambridge, 298 pp.

Hamilton, G., Hall, G.C. and Roberts, J., 1974. The Carboniferous non-marine stratigraphy of the Paterson-Gresford district, New South Wales. *Journal and Proceedings of the Royal Society of New South Wales,* 107, 76–86.

Jenkins, T.B.H., Crane, D.T. & Mory, A.J., 1993. Conodont biostratigraphy of the Visean Series in eastern Australia. *Alcheringa*, 17, 211–283.

Johnson, R.G., 1964. The community approach to palaeoecology. *In* Imbrie, J. & Newell, N.D. (editors). *Approaches to palaeoecology*. John Wiley & Sons, New York, pp. 107–134.

Jones, P.J., Campbell, K.S.W. & Roberts, J., 1973. Correlation chart for the Carboniferous System of Australia. *Bureau of Mineral Resources, Australia, Bulletin* 156A.

Jones, P.J. & Roberts, J., 1976. Some aspects of Carbon-

iferous biostratigraphy in eastern Australia: a review. *BMR Journal of Australian Geology & Geophysics,* 2, 177–208.

Keen, M.C., 1977. Ostracod assemblages and the depositional environments of the Headon, Osborne and Benbridge Beds (Upper Eocene) of the Hampshire Basin. *Palaeontology,* 20, 405–446.

Kidwell, S.K. & Bosence, D.J. 1991. Taphonomy and time-averaging of marine shelly faunas. *In* Allison, P.A., & Briggs, D.E.G. (editors). *Taphonomy. Releasing the data locked in the fossil record.* Plenum, New York. pp. 115–209.

Lavering, I.H., 1974. Geology of the Carrow Brook district of New South Wales. B.Sc.(Hons) thesis, Department of Applied Geology, University of New South Wales (unpublished).

Lavering, I.H., 1978. A palaeoenvironmental analysis of some Early Carboniferous sediments and benthic marine invertebrate faunas from the Southern New England Belt of New South Wales. Ph.D. thesis, University of New South Wales (unpublished).

Lavering, I.H., 1979. Palaeogeographic and palaeoecological significance of *Rhipidomella michelini* in the Carboniferous of the Carnarvon Basin. *Geological Survey of Western Australia Annual Report 1978,* 89–91.

Lavering, I.H., 1981. Carboniferous macroinvertebrate biostratigraphy and palaeoenvironments of the Carnarvon Basin: a review of data and interpretations. 5th Australian Geological Convention, Perth, *Geological Society of Australia, Abstracts,* 3, 65.

Lavering, I.H., 1983. Diversity, structure and composition of some Early Carboniferous benthic marine faunas in the Southern Tamworth Shelf. In *17th Symposium on Advances in the Study of the Sydney Basin,* University of Newcastle, pp. 65–66.

Lavering, I.H., 1993. Gradational benthic marine communities of the *Rhipidomella fortimuscula* Zone (late Visean), New South Wales. *AGSO Journal of Australian Geology & Geophysics,* 14(4), 361–370.

Lindley, I.D., 1984. Stratigraphic revision of the Early Carboniferous Flagstaff Formation, southern New England Belt, N.S.W. *Royal Society of New South Wales, Journal and Proceedings,* 117, 7–14.

MacDonald, K.B., 1969a. Quantitative studies of salt marsh mollusc faunas from the North American Pacific Coast. *Ecological Monographs,* 39, 33–60.

MacDonald, K.B., 1969b. Molluscan faunas of the Pacific coast salt marshes and tidal creeks. *Veliger,* 11, 399–405.

MacDonald, K.B., 1975. Quantitative community analysis: recurrent group and cluster techniques applied to the Sonyea Group, New York. *Journal of Geology.* 82, 473–499.

Petersen, C.G.L., 1913. Valuation of the sea. II. The animal communities of the sea bottom and their importance for marine zoogeography. *Report of the Danish Biological Station,* 21, 1–44.

Petersen, C.H., 1972. Species diversity, disturbance and time in the bivalve communities of some coastal lagoons. Ph.D dissertation, University of California, Santa Barbara. (unpublished).

Petersen, C.H., 1975. Stability of species and of communities for the benthos of two lagoons. *Ecology,* 56, 958–965.

Reineck, H.E. & Singh, I.B., 1973. *Depositional sedimentary environments.* Springer-Verlag, Berlin.

Roberts, J., 1975. Early Carboniferous brachiopod zones of eastern Australia. *Journal of the Geological Society of Australia,* 22, 1–32.

Roberts, J., 1981. Control mechanisms of Carboniferous brachiopod zones in eastern Australia. *Lethaia,* 14, 123–134.

Roberts, J. 1985. Carboniferous faunas of the Tasman Belt, Eastern Australia. Third Circum-Pacific Terrane Conference, Sydney, *Geological Society of Australia, Abstracts,* 14, 196–201.

Roberts, J. & Oversby, B., 1974. Geology of the Rouchel district of New South Wales. *Bureau of Mineral Resources, Australia, Bulletin,* 147.

Roberts, J. & Engel, B.A., 1980. Carboniferous palaeogeography of the Yarrol and New England Orogens, eastern Australia. *Journal of the Geological Society of Australia,* 27, 167–186.

Roberts, J. & Engel, B.A., 1987. Depositional and tectonic history of the southern New England Orogen. *Australian Journal of Earth Sciences,* 34, 1–20.

Roberts, J., Hunt, J.W. & Thompson, D.M., 1976. Late Carboniferous marine invertebrate zones of eastern Australia. *Alcheringa,* 1, 197–225.

Roberts, J., Engel, B. & Chapman, J., 1991. Geology of the Camberwell, Dungog and Bulahdelah 1:100 000 Sheets 9133, 9233, 9333. New South Wales Geological Survey, Department of Mineral Resources. Sydney.

Roberts, J., Jones, P.J. & Jenkins, T.B.H., 1993. Revised correlations for Carboniferous marine invertebrate zones of eastern Australia. *Alcheringa,* 17, 353–376.

Runnegar, B. & Campbell, K.S.W., 1976. Late Palaeozoic faunas of Australia. *Earth-Science Reviews,* 12, 235–257.

Shi, G.R., 1993. Multivariate data analysis in palaeoecology and palaeobiogeography—a review. *Palaeogeography, Palaeoclimatology, Palaeoecology,* 105, 199–234.

Thompson, D.M., 1978. A numerical taxonomic study of Late Carboniferous Spiriferida from eastern Australia. *Alcheringa,* 2, 225–230.

Tipper, J.C., 1976a. A method for the quantitative estimation of the faunal content of well-cemented fossiliferous rocks. *Journal of Paleontology,* 50, 175–179.

Tipper, J.C., 1976b. A method and Fortran program for quantitative sampling in paleontology. *Computers & Geosciences,* 1, 195–201.

Warme, J.E., 1969. Live and dead molluscs in a coastal lagoon. *Journal of Paleontology,* 43, 141–150.

Warme, J.E., 1971. Palaeoecological aspects of a coastal lagoon. *University of California Publications in Geological Science,* 87, 1–131.

Warme, J.E., Ekdale, A.A., Ekdale, S.F. & Petersen, C.H., 1976. Raw material for the fossil record. *In* Scott, R.W. & West, R.R. (editors), *Structure and classification of palaeocommunities.* Dowen, Hutchison & Ross, London. pp. 143–170.

Walker, K.R. & Bambach, R.K., 1971. The significance of fossil assemblages from fine-grained sediments: time-averaged fossil communities. *Geological Society of America. Abstracts with Programs,* 3, 783–784.

Walker, K.R. & Bambach, R.K., 1974. Analysis of communities. *In* Ziegler, A. M. (editors). *Principles of benthic community analysis. Compendium of the Sedimentological Laboratory,* University of Miami, 4, 8.1–8.20.

Whittaker, R.H., 1967. Gradient analysis of vegetation. *Biological Review,* 42, 207–264.

Whittaker, R.H., 1970. *Communities and ecosystems.* Macmillan, New York, 158 pp.

Ziegler, A.M., 1965. Silurian marine communities and their environmental significance. Nature, 270, 270–272.

AGSO Journal of Australian Geology & Geophysics, 15 (3), 359–365 © Commonwealth of Australia 1994

First record of shared species of Late Permian small foraminiferids in Australia and Russia: time correlations and plate reconstructions

V. Palmieri[1], C.B. Foster[2], & E.V. Bondareva[3]

At least 12 species of small calcareous foraminiferids known from early Late Permian assemblages from Arctic Russia and adjacent areas also occur in assemblages from the eastern Australian Ingelara Formation of the Bowen Basin (Queensland). A key species is *Pseudonodosaria borealis* (Gerke 1952), newly recognised in Australia. The shared species allow direct correlation with Late Permian Russian assemblages of Kazanian age. This is the first microfaunal evidence of correlative strata in Gondwana; previous chronologic ties in this region have relied on rare and geographically scattered records of ammonoids from both eastern and western Australia. Other shared foraminiferids from the Ingelara Formation include taxa described in 1914 by Tscherdynzev [*Nodosaria krotovi*, *N. noinskii* and *N. netchajevi*, *Lenticulina (Astacolus) rotaliaeformis*]; and by Gerke in 1952 and 1961 [*Frondicularia inflata*, *F. bella*, *F. prima*, *F. tijanica*, *F. dilemma*, *Tristix permiana*, *Nodosaria cuspidulata*]. A brief synonymy shows that almost all of these Russian taxa may have been recognised previously in Australian assemblages, but under different names. *Pseudonodosaria serocoldensis* (Crespin 1945) is considered an ancestor of *P. borealis* and its appearance in older assemblages in both Spitsbergen (Kungurian) and Australia (Bowen Basin, late Artinskian) suggests that similar evolutionary developments of the faunas occurred throughout a continuous seaway that connected these areas since the early Permian. Migration of these benthic forms is presumed to have occurred via deep ocean currents and suggests that either Arctic Russia (Nordvik Basin, Siberia: parts of Novaya Zemlya) and Spitsbergen were in closer proximity to Australia than is generally accepted in modern plate reconstructions for the Late Permian or, most likely, that new oceanic dispersal patterns are required to explain their distribution.

Introduction

The Permian System was defined by Sir Roderick Impey Murchison in 1841 from rock sections from the Russian Platform and the adjacent Ural Mountains. Correlation with the marine sequences which characterise the earliest Permian through to the lowermost stage of the Late Permian (Kazanian), has been achieved using many faunal groups, including ammonoids, corals, brachiopods, bivalves, conodonts, fusulinid foraminiferids and other small foraminiferids. Historically, primacy for correlation outside Russia has been accorded to the ammonoids, but their record is often scattered and, for reasons of size, they are less useful in subsurface drillhole studies. The last three mentioned groups are microfossils, and are widely used in subsurface studies, but they too have limitations imposed by palaeoclimate and environmental conditions. For example, fusulinids and conodonts are restricted to relatively warm waters.

Reef limestones with diverse faunas of the earliest Permian, vast accumulations of salt of the late Early Permian, and the predominantly red-bed, non-marine rocks of the uppermost Permian (Tatarian) indicate that the climate during this Period, in the type areas of the Russian Platform, ranged from warm to hot (see Ignatev 1976, Molin et al., 1986, Chuvashov 1993). This climatic regime contrasts strongly to that of the Gondwanan countries, which display evidence of widespread glaciation during the earliest Permian, with a gradual amelioration of conditions, and culminating in red-bed deposition towards the close of the Permian. Because of the cold water conditions, no fusuline faunas are known from Australia, and conodonts, belonging to the same broad-ranging Early Permian zone, have been found at only two localities in Western Australia (see Skwarko 1993). Other faunal elements, notably brachiopods, bivalves, and corals were similarly affected by water temperatures, and therefore have provided only tenuous links with Russian marine faunas.

Correlation between the Former Soviet Union and Australia

Ammonoids from scattered Australian localities, mostly in Western Australia, provide the few good correlations with the Early Permian Sakmarian to Kungurian Stages of Russia (see Glenister et al. 1993 for summary). A recently discovered brachiopod fauna in Western Australia, may correlate with the Russian Ufimian, but the evidence is equivocal, and the age determination is by default, namely that the fauna appears younger than Kungurian but older than Kazanian (Archbold 1994). Other suggested megafaunal correlations between the Russian type Permian and Australian sequences are less secure, relying on superposition, suggested faunal similitude at either generic or species level, and faunal ties through Pakistan and boreal parts of the Former Soviet Union (FSU). Dickins (1989) has discussed the probable age (Kazanian) of the uppermost faunas of eastern Australia, and an excellent summary of Permian faunas from Western Australia is provided by Archbold et al. (1993).

The non-marine intervals of the Permian of the Russian Platform are correlated variously within Russia and the FSU by either plant microfossils (spores, pollen, algal cysts), or plant megafossils, or non-marine ostracods, bivalve faunas, and land tetrapods (e.g. Varyukhina et al. 1981; Meyen 1982; Molin et al. 1986; Gorskii & Kalmkova 1986; Lozovskiy 1992). With the exception of spores and pollen from Australia, which have some shared species, the other groups have not been studied sufficiently to be useful for intercontinental correlation. Spore pollen species and genera are currently being reviewed and their usefulness is being assessed (e.g. Foster & Gomankov 1994). Currently, there are two schools of thought: either shared miospore species do exist, reflecting some common ancestry and a basis for correlation; or the apparently similar morphotypes result from homeoplasy (parallel evolution), that is without any close common ancestry (see Gomankov 1992).

[1] Formerly of the Geological Survey Division, Department of Minerals and Energy, GPO Box 194, Brisbane, Australia, 4001

[2] Australian Geological Survey Organisation, GPO Box 378, Canberra, Australia, 2601

[3] Department of Stratigraphy, VNII Okeangeologya, Moyka 120, St Petersburg, Russia

Sample location

Figure 1 shows the location GSQ Springsure 18, a fully cored stratigraphic bore in the Bowen Basin, drilled by the Geological Survey of Queensland. A complete description of the stratigraphy, and accompanying electric log suites, is given by Balfe (1982). The interval which concerns our study is within the silty mudstone/silty sandstones and tuffs (479–483 m) assigned to the Ingelara Formation, which, *in toto*, spans 367–507 m. In this study we are not concerned with the lithologic nomenclature of the studied section. It is well described and characterised by electric logs. However, we are aware that a correlative section in another bore, AFO Arcturus 1 (see Fig. 1), also considered to be Ingelara Formation by Balfe (1982), has been correlated previously with a younger lithologic unit (Peawaddy Formation) by Mollan et al. (1969).

As well as the foraminiferids reported here, a poorly preserved marine fauna occurs over the 140 m interval. It contains mostly indeterminate shelly fragments, hyoliths, indeterminate conulariids; the few identifiable forms include bivalves (*Glyptoleda* sp.), gastropods (*Platyteichum* sp.), and brachiopods (*Tomiopsis ingelarensis*; Parfrey pers comm. 1993). The forms are consistent with fauna recovered from the Ingelara Formation at other localities. Plant microfossils have been recovered from samples at 480.18, 484.12, 498.78, and 499.32 m, and all assemblages contain the Upper Stage 5 palynological zone index spore *Dulhuntyispora parvithola* (Balme & Hennelly) Potonié 1960 (see Draper et al. 1990).

Foraminiferal studies

Crespin (1945, 1947, 1958) was the first to report on foraminiferids from Queensland. Her pioneering work has been superseded by a comprehensive study of both surface samples and borehole material (Palmieri 1994). Preliminary results of this study and a new zonation scheme were published by Palmieri (1983). In the 1983 study, small non-fusuline calcareous foraminiferids from Queensland were compared with faunas from Novaya Zemlya, Arctic Russia (see Kalashnikov et al. 1981). Our subsequent joint research of Russian and Australian collections, including variable pressure scanning electron microscopy of Gerke's (1952) foraminiferal holotypes from Arctic Russia (Nordvik Basin), confirmed the presence in the Australian section of *Pseudonodosaria borealis* (Gerke), and at least 11 other species. Our comparative studies, including thin sections of the test wall, confirmed the identity of the Australian specimens assigned to *P. borealis* (cf. Figs 2, 3, 4). Table 1 lists all key species and, where applicable, shows their probable synonymy with Australian taxa. Further taxonomic work is in progress by Palmieri. A partial synonymy list for *P. borealis* is given in Appendix 1. We focussed on *P. borealis* because this species (Figs 2, 3, 4) is a characteristic element of Kazanian assemblages from Arctic Russia and the Russian Platform (Gerke 1952, 1961; Zolotova et al. *in* Gorskii & Kalmkova 1986; Gorskii & Guseva 1990; V. Igonin written comm. 1993). *P. borealis* first appears, as rare single examples, in the immediately underlying late Early Permian (Gerke 1961, p. 37). But it is its abundance and co-occurrence with taxa such as *Nodosaria krotovi*, *N.*

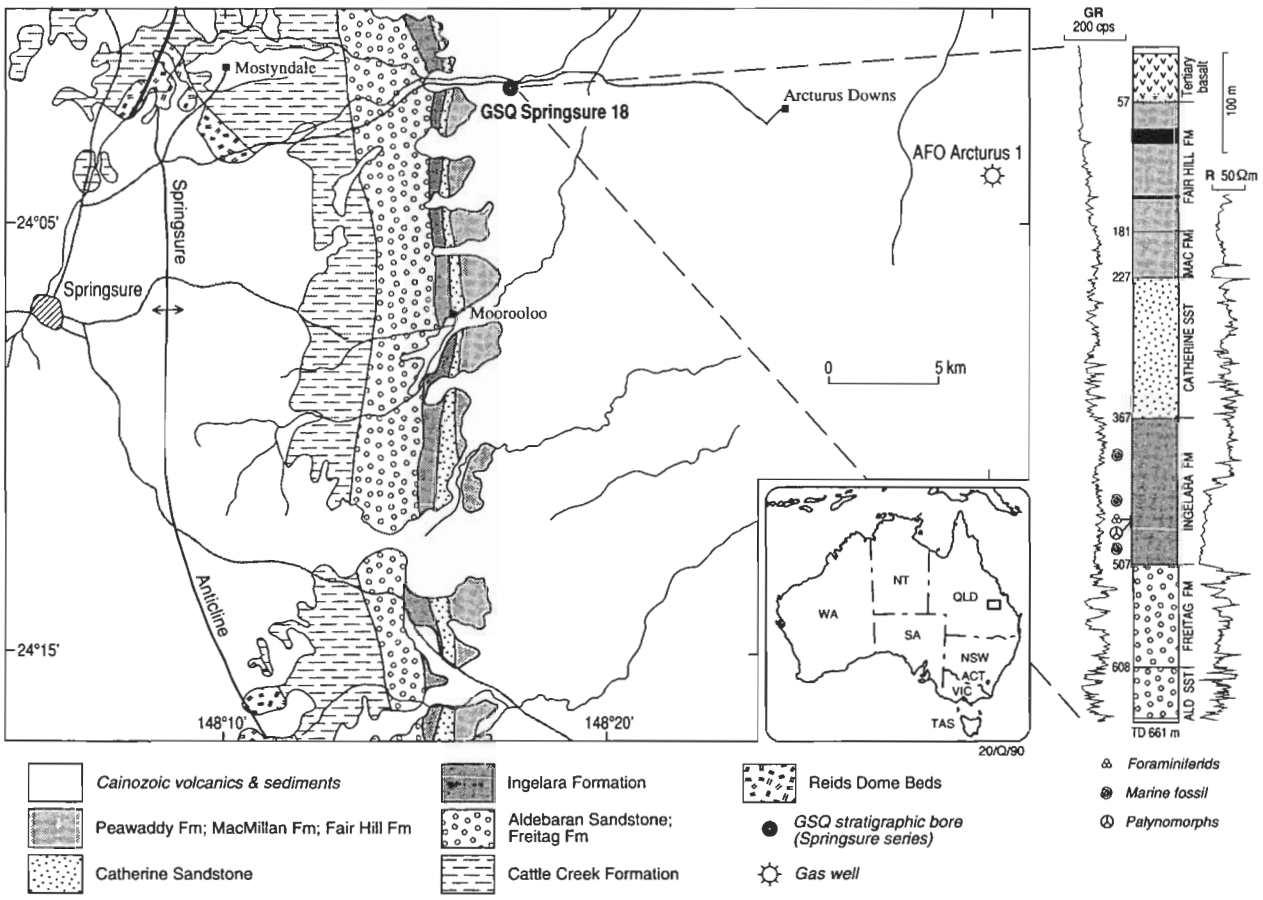

Figure 1. Surface geology and well section and electric log suites from GSQ Springsure 18, Bowen Basin, Queensland.

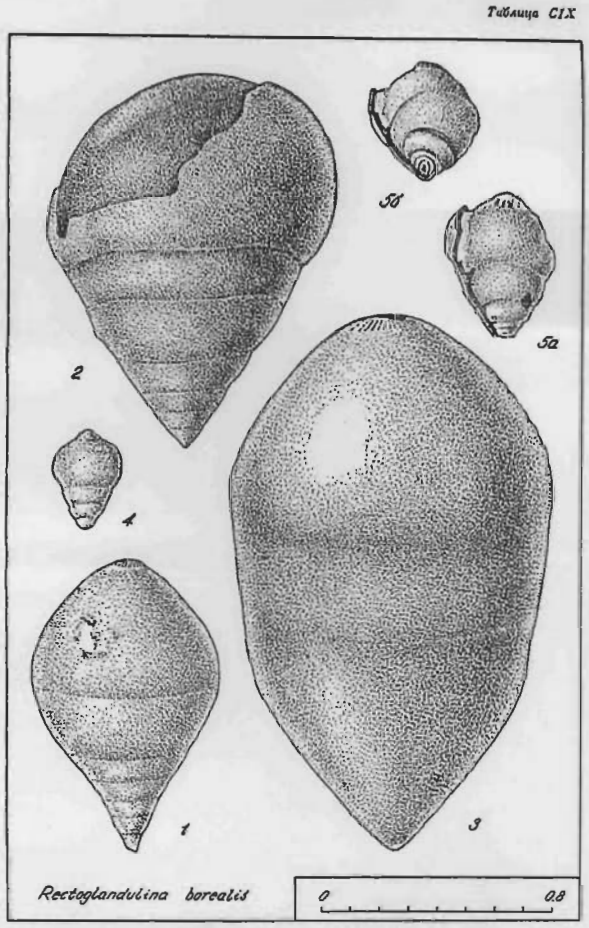

Figure 2. ***Pseudonodosaria borealis*** **(Gerke 1952) from Russia. Plate CIX reproduced from Gerke (1961). 1–4: type material from the Upper Permian 'Horizon of diverse foraminifera'. 1. Holotype (see Fig. 4K and Appendix). 2, 3, 4. Paratypes from the Nordvik Basin, borehole R 2, from 1664 and 1672 m. 5. Example from the Lower Permian 'Horizon of smooth foraminiferids', Nordvik Basin, borehole R 2 at 1843 m.**

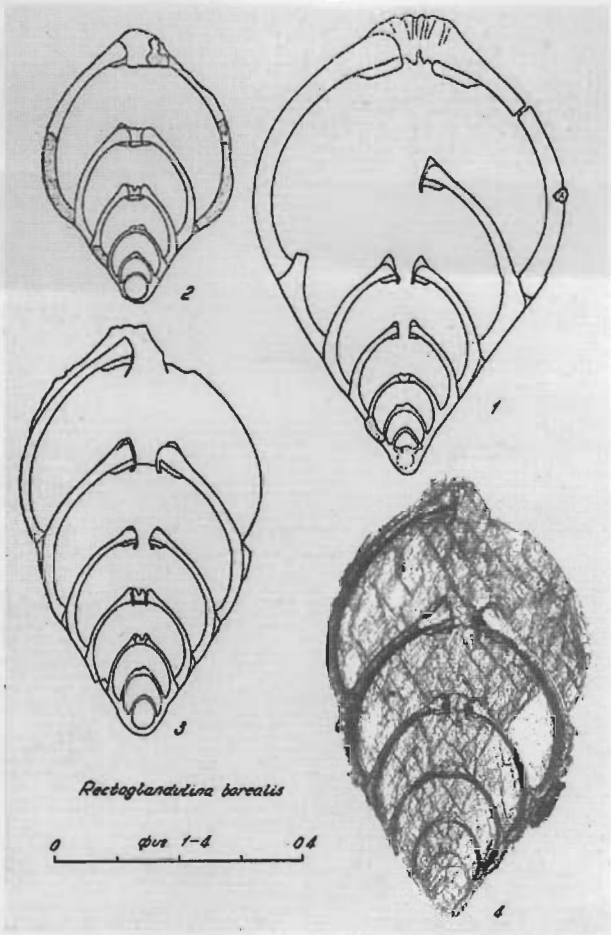

Figure 3. ***Pseudonodosaria borealis*** **(Gerke 1952) from Russia. Line drawings reproduced from Gerke (1961, Pl. CXI), photomicrograph *4* is the same specimen drawn as *3*. Nordvik Basin, Upper Permian, 'Horizon of diverse foraminifera'. Borehole K 255, at 674, 673, and 659 m, respectively.**

noinskii, and *Frondicularia bella* (see Table 1) that are diagnostic of the Kazanian assemblages referred to above. In the Russian Arctic sections, *P. borealis* occurs as a common element in Gerkes (1961) 'Horizon of diverse foraminifera', which includes taxonomically diverse assemblages (85 species, of which only 15 are agglutinated forms) comprising mostly 'frondiculariids, together with large nodosariids and pseudonodosariids' (including rectoglanduliniids of Gerke). The Horizon marks a widespread, relatively deep water, marine transgressive event. In Queensland, *P. borealis* also occurs very commonly and its abundance characterised the informal *P. minuta* zone of Palmieri (*in* Draper et al. 1990; see Appendix). This informal zone also marks a widespread transgressive event in the Bowen Basin. Elsewhere in Australia, *P. borealis*, as *P. serocoldensis* (see Appendix and below), has been figured from subsurface samples of the Lightjack Member of the Liveringa Formation in the Canning Basin, Western Australia (Crespin 1958). Curiously, only one other species, an arenaceous foraminiferid (*Ammodiscus erugatus* Crespin 1958), was reported from the same subsurface Lightjack Member sample. No other Australian occurrences of *P. borealis* are as yet known.

Recognition of *P. borealis*, and associated Russian taxa (Table 1), provides unequivocal evidence for the first Late Permian (Kazanian) correlation based on small foraminiferids between Russia and Australia. As noted above, earlier claims that the Kazanian could be recognised from Australian marine megafaunal assemblages were based only on comparisons of perhaps one or two species and arguments of superposition. These arguments were not entirely convincing and did not involve an assemblage of species, as reported here (see Runnegar 1969; Waterhouse 1976, Dickins 1989, Dickins et al. 1989 for reviews).

Like the apparently shared plant microfossils referred to above, it might be argued that the common occurrence of these foraminiferids in Australia and FSU simply reflects the bipolar distribution of cool waters at that time (Fig. 5). Such an argument cannot be sustained, however, because of the number of shared species involved and, more importantly, the presence of an ancestral form of *P. borealis* in both the Australian and Arctic assemblages, *P. serocoldensis* (Crespin). In Australia, the ancestral form first occurs with the ammonoid *Neocrimites* sp. in both the basal Byro Group of the Carnarvon Basin, Western Australia and in the upper Cattle Creek Formation, Queensland, and on this megafaunal evidence both are considered to be of late Artinskian, Baigendzhinian age (see Dear 1972; Glenister et al. 1993). In Spitsbergen, Sosipatrova (1967) figured specimens of *P. serocoldensis* from the Kungurian part of the Kapp Starostin Formation

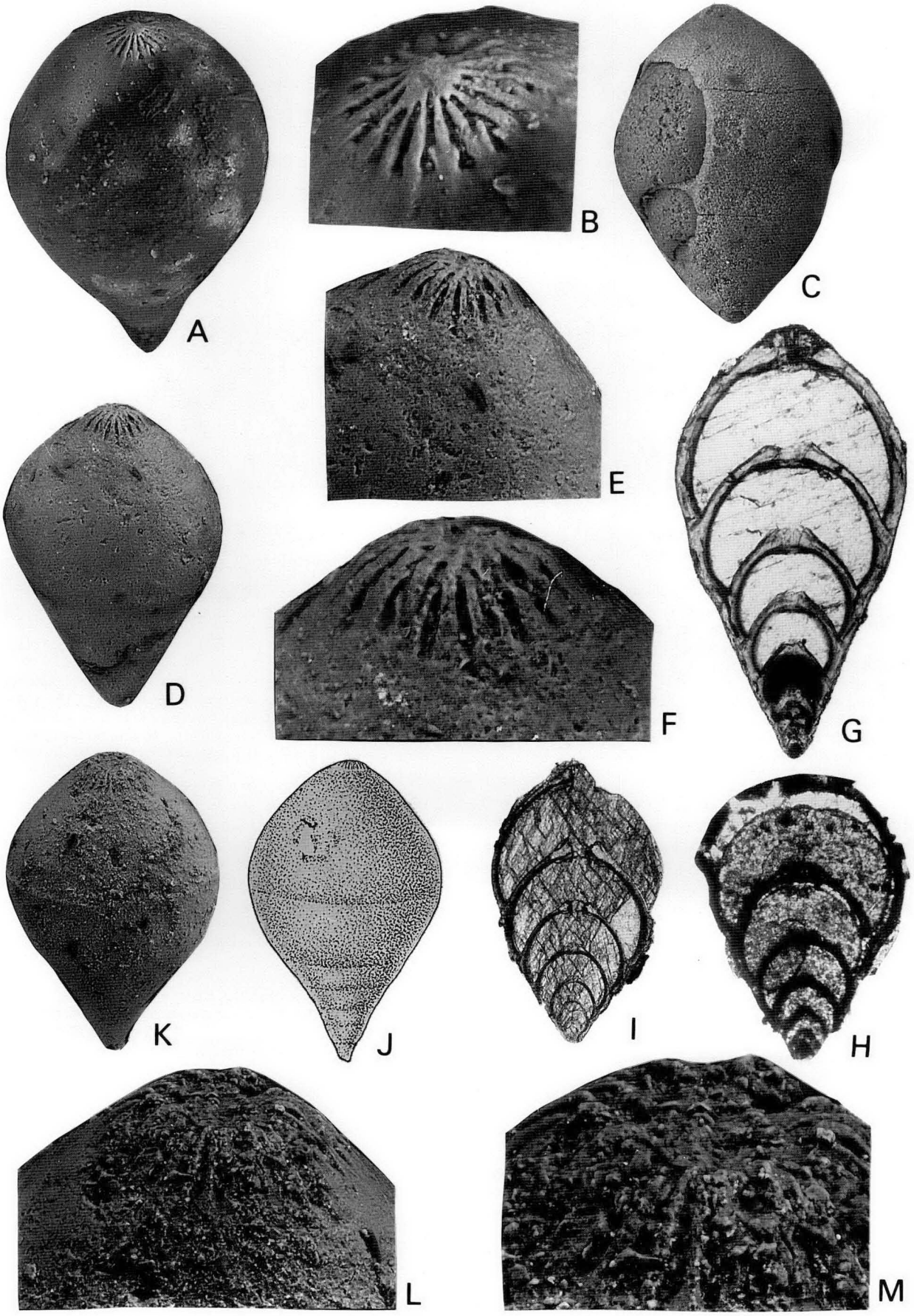
A
B
C
D
E
F
G
K
J
I
H
L
M

Figure 5. Geographic distribution of *Pseudonodosaria borealis* in Australia and Arctic Russia. (Reconstruction after Scotese 1990).

Table 1. List of foraminiferida recorded from the Ingelara Formation in GSQ Springsure 18, core 479–483. Names in *bold face italic* are accepted as valid. Probable synonyms are shown in non-bold italic font.

Australian named taxa	*Russian named taxa*
Howchinella aulax (Crespin 1958)	***Frondicularia inflata*** Gerke 1952
Howchinella costata Palmieri 1994	
Howchinella hillae (Crespin 1958)	
Howchinella impolita (Crespin 1958)	
Howchinella incisa Palmieri 1994	***Frondicularia bella*** Gerke 1952
Howchinella parri (Crespin 1958)	
Howchinella striatosulcata (Crespin 1958)	
Howchinella woodwardii (Howchin 1894 pars)	***Frondicularia prima*** Gerke 1962
Icthyolaria crassatina Palmieri 1994	
Icthyolaria limpida (Crespin 1958)	***Frondicularia dilemma*** Gerke 1952
Icthyolaria sutilis (Crespin 1958)	*Frondicularia tijanica* Gerke 1962
Nodosaria draperi Palmieri 1994	
N. ex gr. *N. raggatti* (Crespin 1958)	***Nodosaria krotovi*** Tscherdynzev 1914
N. ex gr. *N. raggatti* (Crespin 1958)	***N. noinskii*** Tscherdynzev 1914
N. ex gr. *N. raggatti* (Crespin 1958)	***N. netchajevi*** Tscherdynzev 1914
	N. cuspidatula Gerke 1950
Pseudonodosaria minuta (non. nud. Palmieri *in* Draper et al. 1990)	***Pseudonodosaria borealis*** (Gerke 1952)
Pseudonodosaria serocoldensis (Crespin 1945)	
Eocristellaria initialis (Crespin 1958)	***Lenticulina (Astacolus) rotaliaformis*** (Tscherdynzev 1914)
Pseudotristix sp. 2 (Palmieri 1994)	***Tristix permiana*** (Gerke 1952)

Figure 4. *Pseudonodosaria borealis* (Gerke 1952) from Queensland and Russia. A–H: all Queensland specimens, from GSQ Springsure 18, core, 483 m. A. x 150. B. Detail of aperture of specimen A (x 500). C. x 200. D. x150. E, F. Apertural views of specimen G (x 300 and x 600, respectively). G. Thin section (x 56). H. Thin section (x 70); note that aperture of final chamber is broken away. I–M: type material from the Nordvik Basin, illustrated by Gerke (1961). I. Photomicrograph of thin section from Nordvik Basin (see Fig. 3 for details) (x 87). K, J. Holotype N 230/104 (see Appendix for details). Both at the same scale (x 55); this is the first SEM photomicrograph of the holotype. L, M. Details of aperture of holotype, (x 300 and x 600, respectively).

(see also Mangerud & Konieczny 1993 for review). The assemblage data, occurrences of *P. serocoldensis* and its successor, *P. borealis*, are strong evidence of faunal similitude and, therefore, seaway communication between Australia and the Arctic basins of Russia and Spitsbergen. Moreover, in discussing the Early Permian foraminiferal assemblages from the Nordvik Basin, Russia, Gerke (1961, p. 29, translation) noted 'In Australia very similar, and probably the same species (as in the Nordvik Basin), can be found, in significant numbers, in Permian sediments which according to Crespin (1958) are correlatives of the Artinskian Stage [*Hyperamminoides elegans* (Cushman et Waters)] and to the Artinskian Stage Crespin also assigns forms which are very similar with ours (e.g.) *H. proteus*, *H. hadzeli* (Crespin), *H. acicula* (Parr), *Hyperammina coleyi* Parr, *H. fletcheri* Crespin, *H. fusta* Crespin, and others. Some of these forms in Australia are also characteristic (of assemblages) from analogues of the Kungurian Stage.' Gerkes findings, together with those presented here, demonstrate that seaways between Australia and Russia existed during the Early through Late (Kazanian) Permian.

Current Permian reconstructions show these areas to be almost at opposite poles, separated by a warm to hot equatorial belt (Fig. 5). Migration of benthic foraminiferids is possible by means of cold water currents, even at abyssal depths, as these forms require no light, but obviously require a dispersal mechanism; none of those currently proposed move currents from pole to pole. From our evidence, another configuration of the Permian land masses seems probable, or at least different oceanic circulation patterns must be proposed.

Conclusions

Detailed study of Permian small foraminiferid faunas has shown that at least 12 species are shared between Russia and Australia. In particular, they indicate a correlation with the type Kazanian of the Russian Platform. This is the first such evidence for correlation between Gondwanan Permian and a Russian type section based on marine microfaunas. The occurrences of an ancestral form of the key species, *Pseudonodosaria borealis* (Gerke), at Gondwanan and Eurasian localities, as well as the shared species reported here, is strong evidence that the present faunas are contemporary and do not result from parallel evolution. This evidence demands either reassessment of the position of continental land masses during the Permian or new oceanic dispersal patterns to explain their present distribution.

Acknowledgments

This paper results from a joint work program made possible with grants to Foster and Bondareva through the Australia–Russia Bilateral Science and Technology Program of the Department of Industry, Technology and Regional Development. It forms part of an assessment of Gondwanan and Russian Permian microfaunas and palynofloras being coordinated by Foster. We thank Dr Victor Igonin of Kazan University, Tatarstan, for his comments regarding the age range of *P. borealis* and the age of the present assemblage. Dr Sue Parfrey, Department of Minerals and Energy, Queensland, kindly provided information about the macrofauna from GSQ Springsure 18. Dr David Haig of the Department of Geology, University of Western Australia, generously provided access for Bondareva to Permian collections and facilities at the University. Dr Sally Stowe of the Electron Microscope Unit in the Research School of Biological Sciences, Australian National University, is thanked for kindly allowing us use of the variable pressure SEM for this study. Dr I. Premoli Silva (Università degli studi di Milano) and Dr Gregory P. Wahlman (Amoco Production Company, Houston) are thanked for their critical reviews of the manuscript.

References

Archbold, N.W., 1994. Ufimian (mid-Permian) brachiopods from the Perth Basin, Western Australia. Abstracts & Programme, Australasian Palaeontological Convention—94. Macquarie University Centre for Ecostratigraphy and Palaeobiology (MUCEP), School of Earth Sciences, Sydney, NSW, p. 18.

Archbold, N.W., Dickins, J.M. & Thomas, G.A., 1993. Correlation and age of the Permian marine faunas in Western Australia. *Geological Survey of Western Australia, Bulletin*, 136, 11–18(text), 20–28(references).

Balfe, P.E., 1982. Permian stratigraphy of the Springsure–Arcturus Downs area. *Queensland Government Mining Journal*, 83, 133–159.

Chuvashov, B.I. (editor-in-chief), 1993. Permian System: guides to geological excursions in the Uralian type localities. *Occasional Publications ESRI (Earth Sciences and Resources Institute, University of South Carolina), New Series*, 10, 303 pp.

Crespin, I., 1945. Some Permian foraminifera from eastern Australia. *Proceedings of the Royal Society of Queensland*, 56, 23–30.

Crespin, I., 1947. Foraminifera in the Permian rocks of Australia. *Bureau of Mineral Resources, Australia, Bulletin*, 15.

Crespin, I., 1958. Permian foraminifera of Australia. *Bureau of Mineral Resources, Australia, Bulletin*, 48, 207 pp.

Dickins, J.M., 1989. Youngest Permian marine macrofossil fauna from the Bowen and Sydney Basins, eastern Australia. *BMR Journal of Australian Geology & Geophysics*, 11, 63–79.

Dickins, J.M., Archbold N.W., Thomas G.A. & Campbell H.J., 1989. Mid-Permian correlation. *XIe Congrès International de Stratigraphie et de Géologie du Carbonifère, Beijing 1987, Compte Rendu*, 2, 185–198.

Dear, J.F., 1972. Preliminary biostratigraphic subdivision of the Permian brachiopod faunas in the northern Bowen Basin and their distribution throughout the basin. *Geological Survey of Queensland, Report* 49, 19 pp.

Draper, J.J., Palmieri, V., Price, P.L., Briggs, D.J.C. & Parfrey, S.M., 1990. A biostratigraphic framework for the Bowen Basin. *In* Beeston, J.W. (compiler), Proceedings of Bowen Basin Symposium 1990. Geological Society of Australia (Queensland Division), Brisbane, 26–35.

Foster, C.B. & Gomankov, A.V., 1994. A new structure in pollen assigned to *Striatopodocarpites* Sedova 1956 and *Protohaploxypinus* Samoilovich emend. Morbey 1975, from the Late Permian (Tatarian) of the Russian Platform. *AGSO Journal of Australian Geology & Geophysics*, 15, 235–238.

Gerke, A.A., 1952. *Microfauna of Permian rocks of the Nordvik region and its stratigraphical significance.* Leningrad (in Russian).

Gerke, A.A., 1961, Foraminifera of the Permian, Triassic and Liassic deposits of the oil regions of north and central Siberia. *Trudy Nauchno-issledovatalskogo In-*

stituta Geologii Arktiki, 120, 519 pp. (in Russian).

Glenister, B.F., Rogers, F.S. & Skwarko, S.K., 1993. Ammonoids. *Geological Survey of Western Australia, Bulletin*, 136, 54–63.

Gomankov, A.V., 1992, The interregional correlation of the Tatarian and the problem of the Permian upper boundary. *International Geological Review*, 34, 1015–1020.

Gorskii V.P. & Guseva, E.A. (editors), 1990. The decision of the stratigraphical committee on the Middle and Upper Paleozoic of the Russian Platform. VSEGEI, Leningrad, 35 charts (in Russian).

Gorskii V.P. & Kalmkova, M.A. (editors), 1986. Atlas of characteristic complexes of Permian fauna and flora of the Ural and Russian Platform. *Trudy New Series, VSEGEI*, 331, 328 pp. (in Russian).

Ignatev, V.I., 1976. *The formation of the Volga–Ural Anticlise in the Permian Period.* Kazan State University, 256 pp. (in Russian).

Kalashnikov, N.B., Molin, V.A., Fefilova, L.A. & others (editors), 1981. *Permian deposits of Novaya Zemlya.* Nedra, Leningrad, 152 pp.(in Russian).

Lozovskiy, V.R., 1992. The Permian–Triassic boundary in continental series of Laurasia and its correlation with the marine scale. *International Geology Review*, 34, 1008–1014.

Mangerud, G. & Konieczny, R.M., 1993. Palynology of the Permian succession of Spitsbergen, Svarlbard. *Polar Research*, 12, 65–93.

Miklukho-Maclay, K.V., 1964, *Kazanian Lagenida from Russian Platform.* Leningrad (in Russian).

Miklukho-Maclay, K.V., 1965. *Some details about the foraminifera from the Kazanian Basin.* Leningrad (in Russian).

Molin, V.A., Budanov, G.F., Koloda, N.A. & Plotinikov, M.A., 1986. *Permian red-coloured formations of the northern Russian Platform.* 'Nauka', Leningrad, 112 pp. (in Russian).

Mollan, R.G., Dickins, J.M., Exon, N.F. & Kirkegaard, A.G., 1969. Geology of the Springsure 1:250 000 Sheet area, Queensland. *Bureau of Mineral Resources, Australia, Report* 123, 119 pp.

Molostovskiy, E.A., 1992. Paleomagnetic stratigraphy of the Permian System. *International Geological Review*, 34, 1001–1007.

Palmieri , V., 1983. Biostratigraphic appraisal of Permian foraminifera from the Denison Trough–Bowen Basin (central Queensland). In *Permian Geology of Queensland.* Geological Society of Australia, Queensland Division, 139–154.

Palmieri, V., 1994. Permian foraminifera from the Bowen Basin. *Queensland Geology*, 6, 1–126.

Runnegar, B.N., 1969. The Permian faunal succession in eastern Australia. *Geological Society of Australia, Special Publication,* 2, 73–98.

Scotese, C.R., 1990. Atlas of Phanerozoic plate tectonic reconstructions. International Lithosphere Program (IUGG-IUGS) Paleomap Project. Paleomap Project Technical Report No. 10-90-1 (published in conjunction with the GSA Short Course on Phanerozoic Plate Tectonic Reconstructions).

Skwarko, S.W., 1993. Conodonts. *Geological Survey of Western Australia, Bulletin*, 136, p. 72.

Sosipatrova, G.P., 1967. *The Paleozoic foraminifera of Spitsbergen.* Leningrad (in Russian).

Sosipatrova, G.P., 1981. *In* Kalashnikov & others, *Permian deposits of Novaya Zemlya.* Leningrad, Nedra (in Russian).

Tscherdynzev V., 1914. *Foraminifera from the Permian deposits of the east part of Russia.* Kazan (in Russian).

Waterhouse, J.B., 1976, World correlations for Permian marine faunas. *University of Queensland Papers, Department of Geology*, 7, 232 pp.

Zoltova, V.P., Miklukho-Maclay, K.V & Uharskaya, L.B., 1986. Small foraminiferids. *In* Gorskii V.P. & Kalmykova, M.A. (editors), Atlas of characteristic complexes of Permian fauna and flora of the Ural and Russian Platform. *Trudy New Series, VSEGEI*, 331, 10–11, pls 20–24 (in Russian).

Appendix: Selected synonymy for *Pseudonodosaria borealis* (Gerke 1952)

Order FORAMINIFERIDA Eichwald 1830

Suborder Lagenina Delage & Herouard 1896

Superfamily Nodosariacea Ehrenberg 1838

Family Nodosariidae Ehrenberg 1838

Genus *Pseudonodosaria* Boomgaart 1949

Pseudonodosaria borealis (Gerke 1952)

1952 *Pseudoglandulina borealis* Gerke, pp. 144–146, plate XVI, figs 4–7; plate XXV, figs 1–3. **Holotype refigured here in Fig. 2 and Fig. 4.**

1958 *Rectoglandulina serocoldensis* (Crespin 1945)—Crespin, p. 107, pl. 27, fig. 9 (*non* pl. 27, figs 6, 7, 8, 10, which includes the holotype of *R. serocoldensis* (Crespin 1945).

1961 *Rectoglandulina borealis* (Gerke) in Gerke: plate CIX, fig. 1–5; plate CXI, figs 1–3 (no description). **Plate CIX reproduced here as Fig. 2.**

1990 *Pseudonodosaria minuta* (*non. nud.*)—Palmieri (*in* Draper et al. 1990), no description.

1993 *Pseudonodosaria serocoldensis* (Crespin 1945)—*in* Skwarko, pl. 7, fig. 23 (no description; same as pl. 27, fig. 9 of Crespin 1958).

1994 *Pseudonodosaria serocoldensis* (Crespin 1945)—*in* Palmieri, pars, p. 48, pl. 28, figs 1–2. **fig. 1 reproduced here as Fig. 4G.**

Holotype: N 230/104 from Ilya Cape, Nordvik Basin, Upper Permian (Kazanian) 'Horizon of diverse foraminifera', borehole R2, depth 1664 m. Specimens are currently housed in the collections of VNIIOkeangeologya, St Petersburg (**refigured here as Fig. 4K**).

AGSO Journal of Australian Geology & Geophysics, 15 (3), 367–379 © Commonwealth of Australia 1994

Seximembrate apparatus structure of the Late Cambrian coniform conodont *Teridontus nakamurai* from the Chatsworth Limestone, Georgina Basin, Queensland

Robert S. Nicoll[1]

The multielement structure of the Late Cambrian euconodont *Teridontus nakamurai* (Nogami, 1967) is shown to be a seximembrate apparatus consisting of Sa, Sc, Sb, Sd, Pb and Pa elements. No M element has been identified and none is expected in this type of conodont. All elements are coniform with a hyaline base and albid tissue in the cusp extending from the apex of the basal cavity to near the cusp tip. The cusp tip is usually hyaline. The albid tissue is dense and the juncture of hyaline and albid tissues at the basal cavity apex is usually abrupt and planar, rather than tapered as found in most coniform element species. Albid tissue fills the entire diameter of the cusp, and there is no outer layer of hyaline tissue. The S elements have a relatively long base and are differentiated by their cross-sectional shape. The P elements have a short base and different cross-sectional shapes. The surface of all elements is covered with a very fine striate ornament, but the elements lack other surface structures, such as keels, carinae, costae and grooves.

Introduction

Cambrian coniform euconodonts have frequently been regarded as single element apparatuses. This has been seen in the literature in statements like 'one-element apparatus ... symmetrical simple cone, usually erect to reclined ... cross section circular to slightly oval' (Miller, 1980, p.33) or 'unimembrate apparatus of erect or somewhat reclined coniform elements of circular or slightly elliptical cross section' (Sweet, 1988, p. 52), both referring to *Teridontus*. However, closer examination of abundant specimens of coniform-coniform conodont species usually demonstrates that a number of discrete element morphologies can be consistently segregated, and thus a multielement apparatus may be recognised. Further, there is a consistent morphologic pattern that can be observed in diverse genera, and this pattern is amenable to application of the M–S–P element designation scheme of Sweet (1988).

Numerous papers have dealt with the recognition of coniform apparatuses, including Lindström (1971), Viira (1974), Dzik (1976), and Fåhraeus & Hunter (1985). Cross-section of the base and distribution of costae and other surface morphologic features have been used to define these coniform apparatuses. However, few workers have recognised the full range of elements in any of the coniform–coniform apparatuses, nor have they suggested a fully systematic approach, such as that used here, for definition of the apparatus components.

Teridontus nakamurai (Nogami, 1967) is one of the early euconodont coniform species with well-developed albid tissue (white matter) in the cusp. Elements of this species can be segregated into six discrete morphologic types and can thus be defined as a seximembrate apparatus. The elements can be assigned to the element types Sa, Sc, Sb, Sd, Pb and Pa.

Nogami (1967) described four new species of Cambrian conodonts from China. His material came from a 2.5 kg sample of the Yanzhou (Yencho) Member of the Fengshan Formation, collected near Huolianzhai, Benxi City, Liaoning Province, northeast China (An, 1982). The new species were *Acodus cambricus, Hertzina? tricarinata, Oneotodus nakamurai* and *O. terashimai*. The other elements of the fauna were referred to species previously described by Müller (1959, 1964). Only one species named in this fauna, *Oneotodus nakamurai*, now assigned to *Teridontus* (Miller, 1980), has an essentially solid cusp with dense albid tissue filling the entire cusp diameter.

In most Late Cambrian conodont faunas of the *Eoconodontus* Zone (Miller, 1988), the majority of the taxa consist of species with deeply excavated basal cavities, and there are few species with a relatively long and solid cusp. Thus, despite the diversity of the Yanzhou fauna and similar faunas from other localities, the unique morphologic feature of the albid tissue distribution in elements of *Teridontus nakamurai* makes it an ideal candidate for study of early euconodont coniform apparatus structure. Establishment of the apparatus structure of *Teridontus nakamurai* required a sample with abundant (500+) elements of good preservation with a low colour alteration index (CAI) value.

A sample, collected in 1993, of the Late Cambrian Chatsworth Limestone (Fig. 1) in the Burke River Structural Belt of the Georgina Basin (see locality information) contains a somewhat similar fauna (Table 1) to that described by Nogami (1967). The recovery of over 1000 *Teridontus nakamurai* elements now allows a complete analysis of this apparatus. A spot sample (JHS 89/001) collected at a road-metal quarry in 1989 had yielded a small conodont fauna, including 15 *T. nakamurai* elements. In 1990, a short measured section was collected from the locality (Fig. 2), but none of the samples produced an abundant fauna.

Re-collecting in 1993 produced an abundant conodont fauna in a single sample (GB93-004/C), which also contained an abundant trilobite fauna. The trilobite fauna includes the species *Rhaptagnostus clarki maximus* (Shergold, 1975), *Rhaptagnostus papilio* (Shergold, 1972), *Lophosaukia torquata* Shergold, 1972, and *Palacorona torosa* Shergold, 1975 (Shergold, pers. comm. 1994).This trilobite fauna has been previously identified from the lower part of the exposed middle portion of the Chatsworth Limestone in the Black Mountain section (Shergold, 1975; Shergold & Nicoll, 1992). The exposure in the quarry and around Dribbling Bore apparently represents a slightly deeper water facies of the Chatsworth Limestone than that exposed at Black Mountain, and the quarry exposure is laterally equivalent to the Gola Beds (Druce & Jones, 1971). Samples from the locality contain a moderately diverse conodont fauna containing at least 10 multielement species (Table 1).

[1] Australian Geological Survey Organisation, GPO Box 378, Canberra ACT 2601.

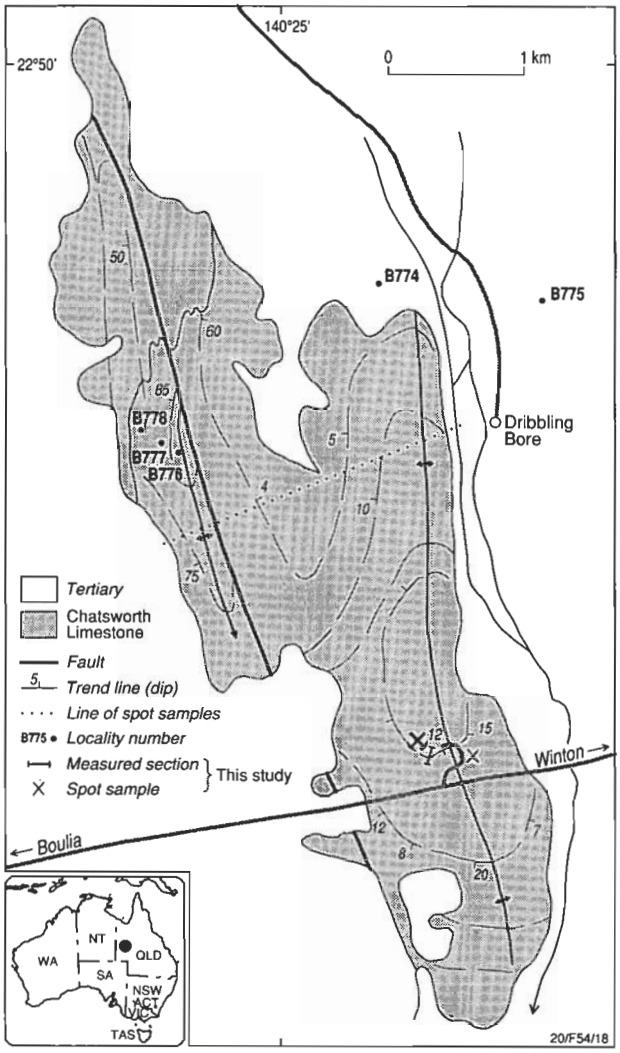

Figure 1. Location of quarry, measured section GB90-004, and spot sample traverse GB93-004. The B samples and line of spot samples are from the Druce & Jones (1971) study. Samples from the present study are indicated by the measured section line and X symbols.

Based on the trilobite faunas, this interval of the Chatsworth Limestone is assigned to the *Rhaptagnostus clarki maximus/R. papilio* Zone. Using the zonation established in the Black Mountain section (Shergold & Nicoll, 1992), this should equate with the *Teridontus nakamurai* Zone, but the conodont fauna from this sample places it slightly younger, in the *Hispidodontus resimus* Zone (Shergold & Nicoll, 1992), based on the presence of *Eoconodontus notchpeakensis, Proconodontus muelleri, P. serratus* and *Teridontus nakamurai*. This fauna equates with the *Eoconodontus notchpeakensis* Subzone of the *Eoconodontus* Zone of Miller (1988).

Apparatus elements of *Teridontus nakamurai*

The full complement of apparatus elements of *Teridontus nakamurai* was established after detailed examination of the abundant specimens in sample GB93-004/C. The sample contains only two coniform species with a long solid cusp, and only one, *T. nakamurai*, has the cusp formed by dense albid tissue and an abrupt and planar,

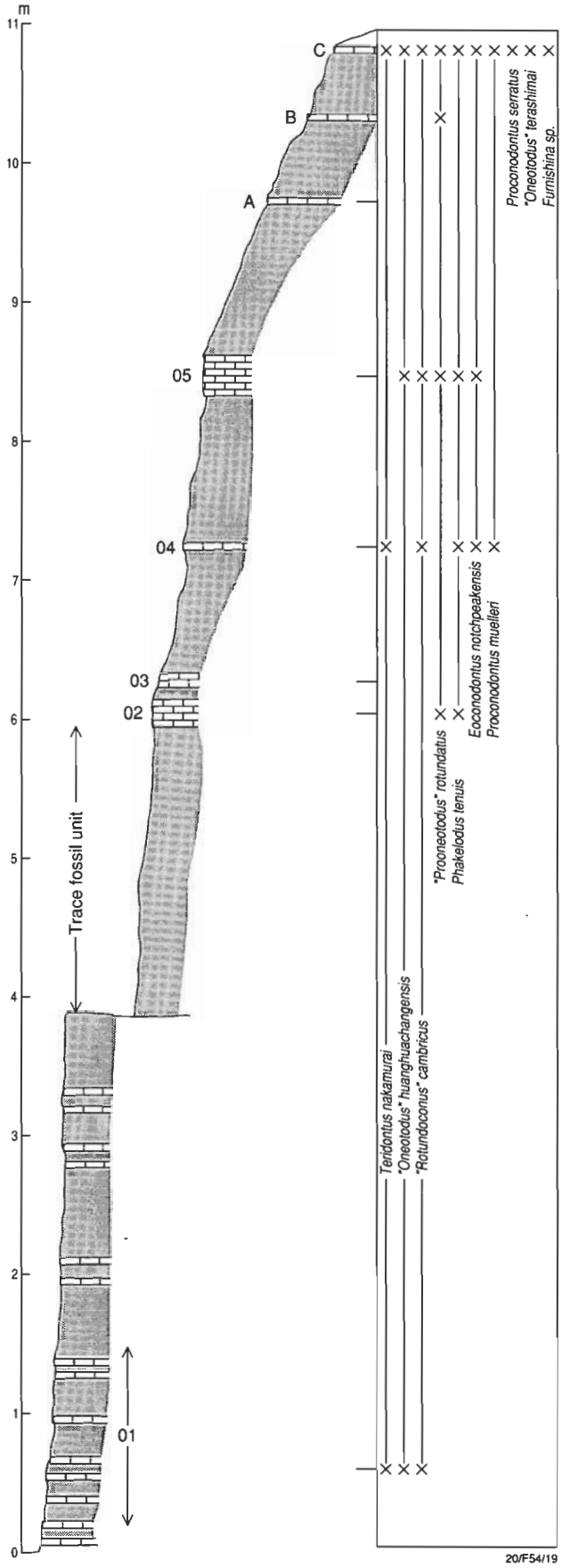

Figure 2. Measured section of Chatsworth Limestone in south wall of quarry and approximate position of traverse samples.

hyaline to albid tissue transition in the cusp. Two major groupings of *T. nakamurai* elements were identified; those with a relatively short base, the P elements, and those with a relatively long base, the S elements (Fig. 3). Within each of these groups a further subdivision was made, based on the morphology of the base of the element.

The S elements are segregated into four morphologic groups based on the cross-section of the basal margin of the element. The Sa element position is assigned to the element with a symmetrical basal section (Fig. 4). Those elements with a strong laterally compressed and slightly asymmetric base are assigned to the Sc position (Figs. 5 & 6). Elements with a laterally compressed and oval base are assigned to the Sb position (Figs. 7 & 8). Elements with an irregular subcircular base, flattened on one side, are assigned to the Sd position (Figs. 9 & 10).

Similarly, those elements with a short base have either a laterally compressed (oval) basal outline, the Pb element (Figs. 11 & 12), or an obliquely compressed basal outline, the Pa element (Figs. 13 & 14).

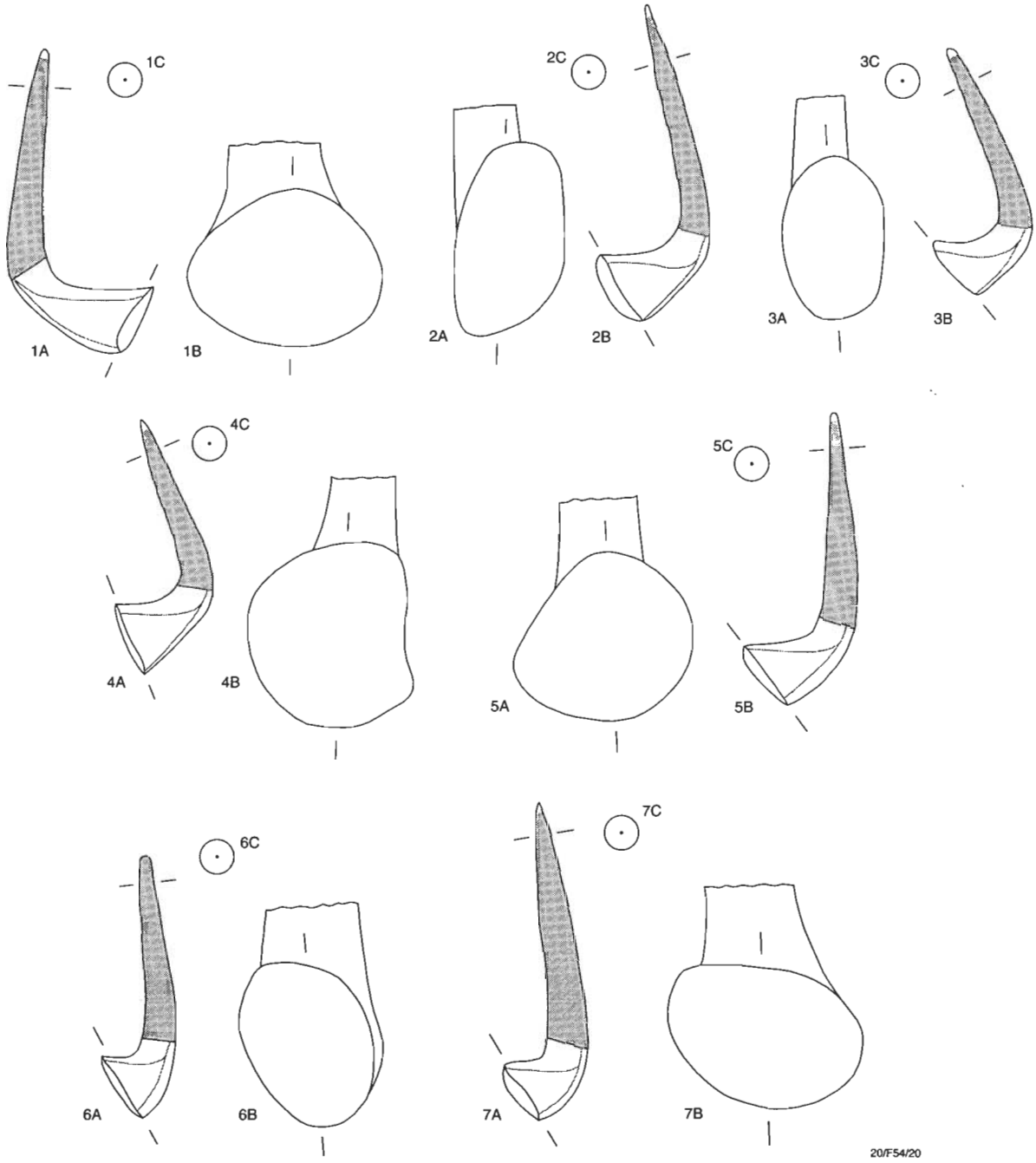

Figure 3. Outline of *Teridontus nakamurai* elements, showing: a lateral view (A, x55), the cross-section of the basal margin (B, x135) as viewed from the posterior, the cross-section of the upper part of the cusp (C, x135), the outline shape of the basal cavity (dotted line), and the distribution of albid tissue (shaded pattern); 1—Sa element (CPC33175) right lateral view; 2—right Sc element (CPC33179) inner lateral view; 3—right Sb element (CPC33183) inner lateral view; 4—left Sd element (CPC 33185) inner lateral view; 5—right Sd element (CPC33187) inner lateral view; 6—right Pb element (CPC33191) inner lateral view; 7—right Pa element (CPC33194) inner lateral view.

Table 1. Distribution of conodonts in samples from the measured section samples GB90-004 / 1–5, traverse samples GB93-004 / A–C and spot sample JHS 89/001.

JHS 89/			
/001	130 elements	3 kg	
	"Rotundoconus" cambricus (Nogami, 1967)		12
	"Prooneotodus" rotundatus (Druce & Jones, 1971)		20
	Eoconodontus notchpeakensis (Miller, 1969)		13
	Furnishina sp.		2
	"Oneotodus" huanghuachangensis Ni, 1981		20
	"Oneotodus" terashimai Nogami, 1967		1
	Proconodontus muelleri Miller, 1969		7
	Phakelodus tenuis (Muller, 1959)		28
	Teridontus nakamurai (Nogami, 1967)		17
GB90-004/			
/01	9 elements	3 kg	
	"Oneotodus " huanghuachangensis		2
	"Rotundoconus" cambricus (Nogami, 1967)		1
	Teridontus nakamurai		4
/02	5 elements	3 kg	
	"Prooneotodus" rotundatus (Druce & Jones, 1971)		2
	Phakelodus tenuis (Muller, 1959)		1
/03	0 elements	3 kg	
/04	120 elements	3 kg	
	Eoconodontus notchpeakensis (Miller, 1969)		19
	"Oneotodus" huanghuachangensis Ni, 1981		2
	Proconodontus muelleri Miller, 1969		6
	Phakelodus tenuis (Muller, 1959)		68
	Teridontus nakamurai (Nogami, 1967)		1
/05	16 elements	3 kg	
	"Rotundoconus" cambricus (Nogami, 1967)		3
	"Prooneotodus" rotundatus (Druce & Jones, 1971)		1
	Eoconodontus notchpeakensis (Miller, 1969)		8
	Phakelodus tenuis (Muller, 1959)		3
	Teridontus nakamurai (Nogami, 1967)		1
GB93-004/			
/A	0 elements	2 kg	
/B	2 elements	2 kg	
	"Prooneotodus" rotundatus (Druce & Jones, 1971)		2
/C	1527 elements	5 kg	
	"Prooneotodus" rotundatus (Druce & Jones, 1971)		110
	"Rotundoconus" cambricus (Nogami, 1967)		50
	Eoconodontus notchpeakensis (Miller, 1969)		75
	Furnishina sp.		2
	"Oneotodus" huanghuachangensis Ni, 1981		23
	"Oneotodus" terashimai Nogami, 1967		2
	Proconodontus muelleri Miller, 1969		
	Proconodontus serratus Miller, 1969		
	Phakelodus tenuis (Muller, 1959)		50
	Teridontus nakamurai (Nogami, 1967)		1066

This subdivision of coniform element morphologies in *Teridontus* mirrors that in other Late Cambrian and Early Ordovician coniform genera, such as *Drepanoistodus* and *Drepanodus*. In all these seximembrate forms, a 4–2 pattern (S–P) can be recognised, with morphologic differentiation within each group established on base morphology and cross-section of the basal margin of the element. No M element is present in these genera; the "oistodontiform" element is interpreted as a Pa element and not an M element on the basis of its symmetry. Both Pa and Pb elements are related by similar morphology of the base of the element.

In his original description of *Oneotodus nakamurai*, Nogami (1967) illustrated five elements, each with a different cross-sectional shape. Four of these elements (Nogami, 1967, pl. 1, figs. 9, 11–13) are here retained in *T. nakamurai*, and one (pl. 1, fig. 10) is assigned to *'Oneotodus' huanghuachangensis* Ni (1981). The holotype (Nogami, 1967, pl. 1, fig. 9, text-fig. 3A) is here identified as an Sd element. Nogami (1967) demonstrated the apparent slight twist of the Sd element and showed the subround basal section, features observed in the Sd elements from this study.

The Pa element was illustrated by Nogami (1967, pl. 1, fig. 13, text-fig. 3C) and is the only element of the apparatus to have a notably oblique, rather than lateral, compression of the basal cross-section. The Sa element (Nogami, 1967, pl. 1, fig. 12, text-fig. 3B) is symmetrical with a dorso-ventral compression of the basal cross-section. The Sc element (Nogami, 1967, pl. 1, fig. 11, text-fig. 3D) has a strong lateral compression of the basal cross-section.

Although Nogami (1967, p. 216) did not discuss in detail the different element types present in his material, he stated in his diagnosis that the 'cross section [is] strongly differentiated'. This remark, prior to the general recognition of multielement assemblages, indicates that he considered a number of morphologically distinct elements were probably present within *Oneotodus nakamurai*.

Nowlan (1985) in his description of *Teridontus gracillimus* noted a variable length of the base and roundness of the cross-section and suggested that a similar variation in elements could be found in *T. nakamurai*.

Coniform apparatus structure and suprageneric classification

Early suggestions that the number of element types in the conodont apparatus might be highly variable (Barnes et al., 1979) have given way to a general recognition that most ramiform–ramiform and ramiform–pectiniform apparatuses are septimembrate. Coniform apparatuses have generally been thought to range from unimembrate to quinquimembrate in structure (Sweet, 1988). However, studies of Late Cambrian and Early Ordovician coniform taxa are now recognising that many of them consist of seximembrate apparatuses with a coniform–coniform (S–P) structure, lacking an element in the M position. Other coniform–coniform apparatuses are septimembrate and contain an M element pair.

The recognition by Clark (1981) and Sweet (1988) of orders and families in conodont classification, however complicated by a lack of knowledge of the full apparatus composition of many species and genera, has been based on the premise that all euconodonts represented essentially one type of conodont animal. However, there is now reason to think that this premise may be incorrect. This study, along with examination of other Late Cambrian and Early Ordovician conodont faunas, indicates that there may be a primary subdivision of euconodonts into two major groupings. The first group consists of exclusively seximembrate coniform–coniform apparatuses with only S and P elements present (Sa, Sc, Sb, Sd–Pb, Pa). This group roughly corresponds to the Order Protopanderodontida as defined by Sweet (1988).

The second group consists of septimembrate apparatuses (M, Sa, Sc, Sb, Sd–Pb, Pa) composed of coniform,

ramiform and pectiniform elements. This numerically larger group contains most of the remaining orders and families recognised by Sweet (1988).

Morphologic features indicate that both of these groups are contained within the category of 'conodonts', whatever taxonomic level they may be. The importance of recognising this subdivision of conodont types lies in the control that this will have on understanding the evolutionary relationships of the various generic lineages and not on the inclusion of a genus within the taxonomic group 'conodont'.

Conclusion

The Late Cambrian seximembrate euconodont *Teridontus nakamurai* has well-defined albid tissue and shows the establishment of a complex apparatus structure of coniform euconodonts early in the history of the group. The apparatus, divisible in a 4–2 pattern of S–P elements, typifies the basic structural morphologic pattern of many Late Cambrian and Early Ordovician conodonts with only coniform elements. The four S elements are differentiated on cross-section morphology of the element base. The two P elements, distinctively separated from the S elements by the shorter length of their base, are also distinguished from each other by the cross-section of the element base. There is no identifiable element in the M position.

The division of euconodonts into two fundamental categories is here recognised. The first category includes those predominantly coniform–coniform apparatuses with a seximembrate composition of S and P elements, but lacking an M element. The second, and more numerous category includes, the coniform/ramiform/pectiniform apparatuses with a septimembrate (or octimembrate) apparatus that includes a pair of M elements.

Systematic palaeontology

Genus ***Teridontus*** Miller, 1980

Type species. *Oneotodus nakamurai* Nogami, 1967

Emended diagnosis. Seximembrate apparatus of coniform elements with a hyaline base and a cusp that contains albid tissue from the apex of the basal cavity to near the cusp tip. The albid tissue is dense and the juncture of hyaline and albid tissues at the basal cavity apex is abrupt and planar, rather than tapered as in most coniform species. The S elements have a relatively long base and the P elements, a short base. The cross-section of the cusp is round to subround. Element types Sa, Sc, Sb, Sd, Pb and Pa are differentiated. The S and P elements are subdivided on the cross-section of the basal margin. There is no M element. Surfaces of the elements are striate.

Remarks. The emended diagnosis of *Teridontus* given by Ji & Barnes (1994) is rejected as not applicable to the type species of the genus. The lateral compression of the cusp of some elements, the presence of lateral grooves, costae and keels, and the suberect morphology of the Sa element are not found in elements of *Teridontus nakamurai*. Further investigation of Late Cambrian and Early Ordovician species of *Teridontus* and related genera is needed to adequately define the latitude of morphologic variability that should be contained in this genus.

The distribution of albid tissue and surface sculpture in *Teridontus* are here regarded as the key morphologic features for recognition of this genus. Miller (1980) identified the 'cusp composed almost entirely of white matter', the microstriae and the ovate cross-section as the principal characteristics of the genus. This study confirms Miller's observations and rejects suggestions by Landing (1983) that these features are not of distinguishing taxonomic significance. Close observation of the albid to hyaline tissue transition of *Teridontus* and its descendant *Hirsutodontus* (Miller, 1969) indicates that both can be distinguished by the dense albid tissue in the cusp that has an abrupt planar transition to hyaline tissue at the apex of the basal cavity. *Teridontus* lacks the nodes or spines found on the cusp of the various species of *Hirsutodontus*. Neither *Teridontus* or *Hirsutodontus* appear to be closely related to the genus *Clavohamulus* Furnish (1938) because the nature of the albid tissue is different. In *Clavohamulus*, the albid tissue is divided into a bundle of closely appressed fibres (Druce, 1978, fig. 5w, x), but in *Teridontus* and *Hirsutodontus* the cusp is solid.

Teridontus nakamurai (Nogami, 1967)

Figs. 3–15

Material studied. 1066 elements of *T. nakamurai* were recovered from the 5 kg sample, GB93-004/C. Not all the S elements were sorted to the individual element type or to left/right position. Distribution of elements: Sa, 53; Sc, 100 (45L, 55R); Sb, 65 (32L, 33R); Sd, 71 (36L, 35R); undifferentiated Sc/Sb/Sd elements, 505; Pb, 143 (30L, 24R, 89 undifferentiated L/R); Pa, 129 (58L, 71R).

Synonymy.

1967 *Oneotodus nakamurai* Nogami, (part), pp. 216–217, pl. 1, figs 9, 11–13, text-figs 3A–D only; not pl. 1, fig. 10, text-fig. 3E = *'Oneotodus' huanghuachangensis* Ni.

v. 1971 *Oneotodus nakamurai* Nogami; Druce & Jones, pp. 82–83, pl. 10, figs 1–8, text-figs 26i, j.

1980 *Teridontus nakamurai* (Nogami) Miller, pp. 34–35, pl. 2, figs 15–16, text-figs 3A, B.

v. 1971 not *Oneotodus nakamurai* Nogami; Jones, p. 58, pl. 4, figs 1–4 = *Teridontus datsonensis* (Druce & Jones).

1994 not *Teridontus nakamurai* (Nogami) Ji & Barnes, pp. 64–65, pl. 24, figs 1–9, text-fig. 37C.

Emended diagnosis. Seximembrate coniform apparatus with dense albid tissue in the cusp, usually with an abrupt transverse and planar transition to a hyaline base at the cusp apex. Elements usually have a hyaline cusp tip. Numerous very fine linear to anastomosing striae, on a rounded cusp, extend nearly to the basal margin. Base of P elements relatively short; base of S elements relatively long.

Description. The six element types in the apparatus all have a hyaline base and a dense albid cusp. In all elements, the cusp is round in cross-section, but the cross-section of the base is highly variable between element types. The elements lack keels or carinae, but the surface is covered with very fine linear striae that are discontinuous and anastomosing. The striae extend to near the basal margin,

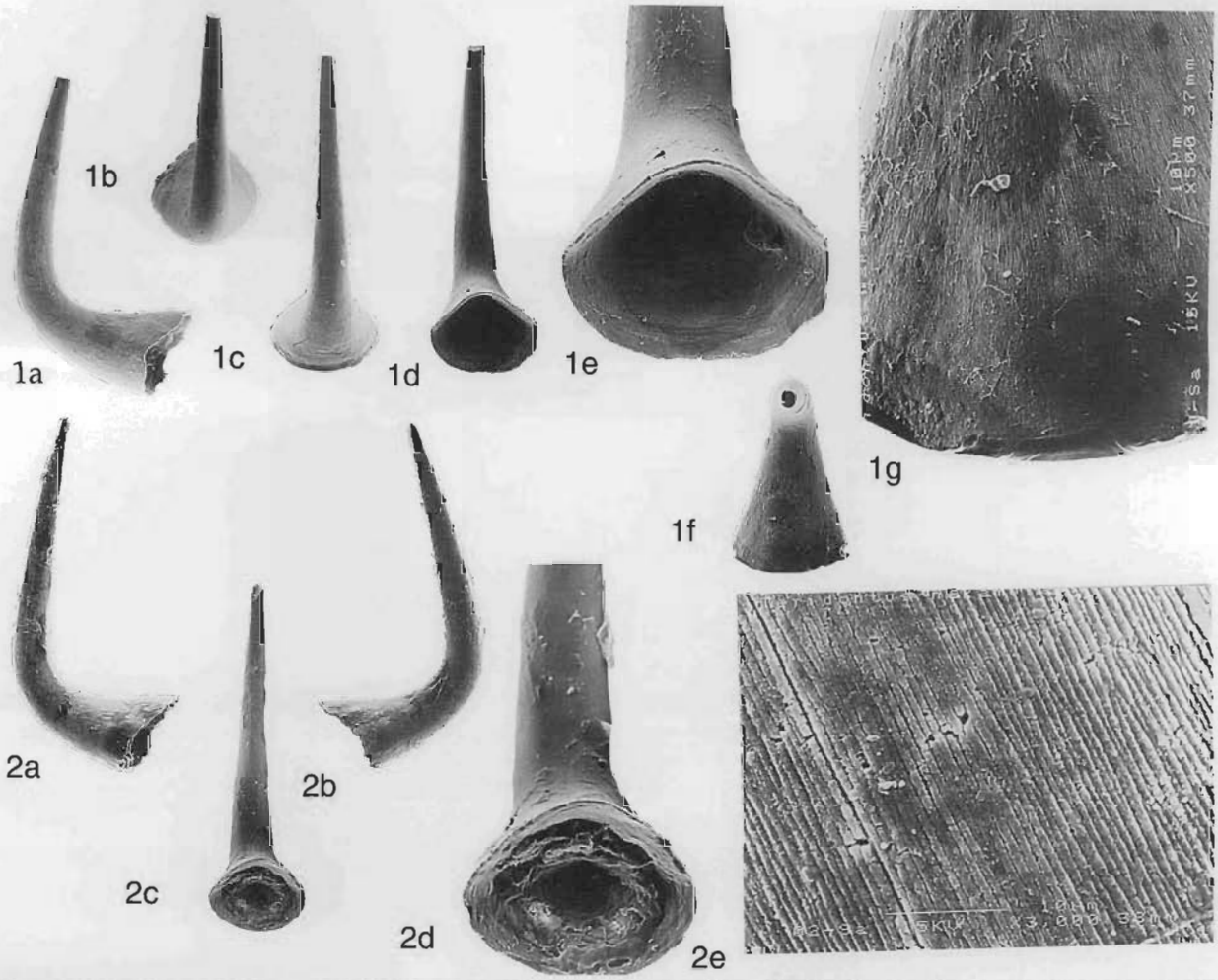

Figure 4. *Teridontus nakamurai* **Sa elements. All elements from sample GB93-004/C; all x55 except as noted. 1—Sa element (CPC33175): 1a, right lateral view; 1b, oblique anterior view; 1c, anterior view; 1d, posterior view; 1e, posterior view (x135); 1f, oral view; 1g, oral view (x300), showing smooth strip lacking striae parallel to the basal margin. 2—Sa element (CPC33176): 2a, right lateral view; 2b, left lateral view; 2c, posterior view; 2d, posterior view (x135); 2e, striae (x1000).**

but a narrow band adjacent to the basal margin is smooth. The angle between the posterior margin of the cusp and the upper margin of the base is essentially a right angle in all elements. The upper part of the cusp may be slightly recurved. The S elements have a long base, about twice the length of the base of the P elements. The individual S and P element types are distinguished on the cross-section of the basal part of the element.

The basal cavity (Fig. 3) extends as a gently tapering cone to near the anterior margin of the base, where it is bent upward as a narrowing tube to terminate at the base of the albid tissue. At the apex of the basal cavity the hyaline tissue of the base is abruptly replaced by albid tissue across the entire width of the cusp. The juncture of tissue types forms a planar disc across the cusp. Examination of broken elements failed to differentiate a hyaline outer layer on the cusp.

The Sa element (Fig. 4) is the only symmetrical element of the apparatus and has a base that is slightly longer than that of the rest of the S elements. The ovate base is dorsoventrally compressed (Figs. 4.1e, 4.2d) and the basal margin is more evenly rounded anteriorly than posteriorly.

The Sc, Sb and Sd elements are differentiated only by the cross-section of the basal part of the element. Mirror image pairs are found in each element type. The Sc elements (Figs. 5, 6) have an irregular laterally compressed base with subparallel sides, which narrow toward a rounded anterobasal corner (Figs 5.1a, 5.2f, 6.1d, 6.2g). If left and right elements are placed with inner lateral surfaces together, the posterior-basal corners are further from the axial plane of the element pair than are the anterobasal corners.

The Sb elements (Figs. 7, 8) have a nearly symmetrical ovate basal cross-section that is laterally compressed. In section view (Figs 7.2b, 8.1d), the base is egg-shaped, narrowing slightly toward the anterobasal corner. The element is asymmetrical, because the cusp, like the Sc and Sd elements, is deflected slightly away from the axial plane of the base.

The Sd elements (Figs 9, 10) have the largest basal cross-section of the S elements. It is rounded on the outer margin of the base (Figs 9.1d, 9.2f, 10.1c, 10.2d), but the inner margin it is flattened or slightly depressed. This outline and the position of the cusp gives the element a slightly twisted appearance.

The Pb and Pa elements have cusps that are identical to those found in the S elements, but the bases differ. Both

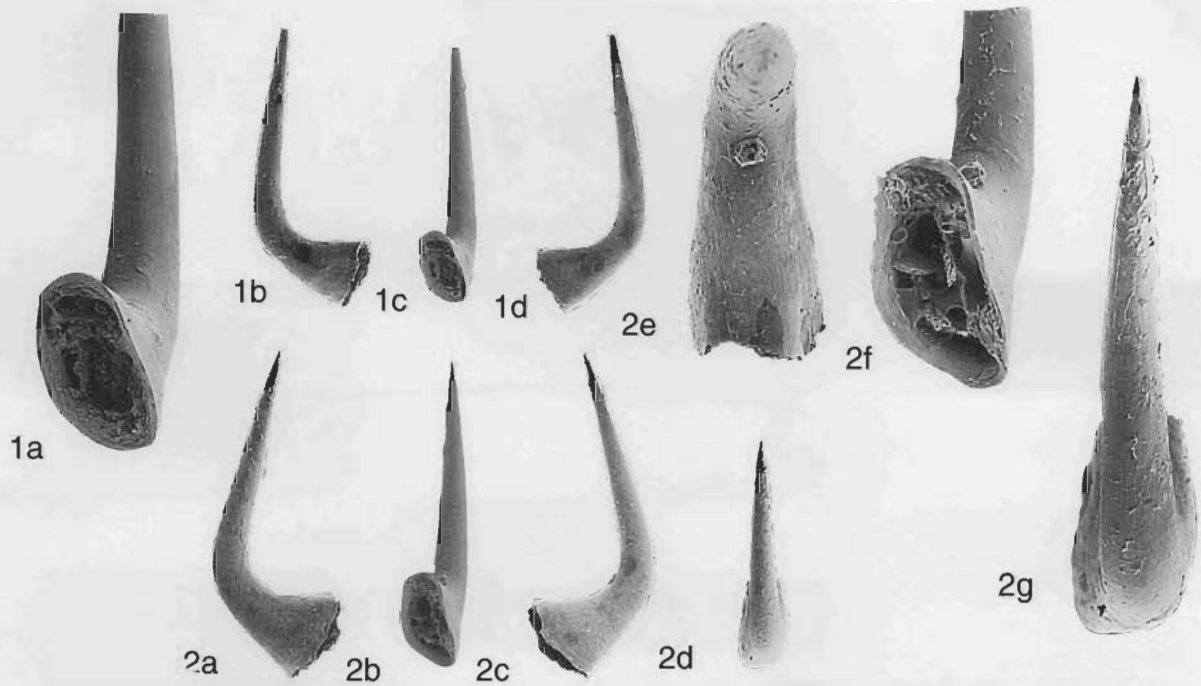

Figure 5. *Teridontus nakamurai* **Sc elements. All elements from sample GB93-004/C. All x55 except as noted. 1—Sc element (CPC33177) left element: 1a, posterior view (x135), showing shape of basal cross-section; 1b, outer lateral view; 1c, posterior view; 1d, inner lateral view. 2—Sc element (CPC33178) left element: 2a, outer lateral view; 2b, posterior view; 2c, inner lateral view; 2d, anterior view; 2e, oral view (x135); 2f, posterior view (x135), showing shape of basal cross-section; 2g, anterior view (x135).**

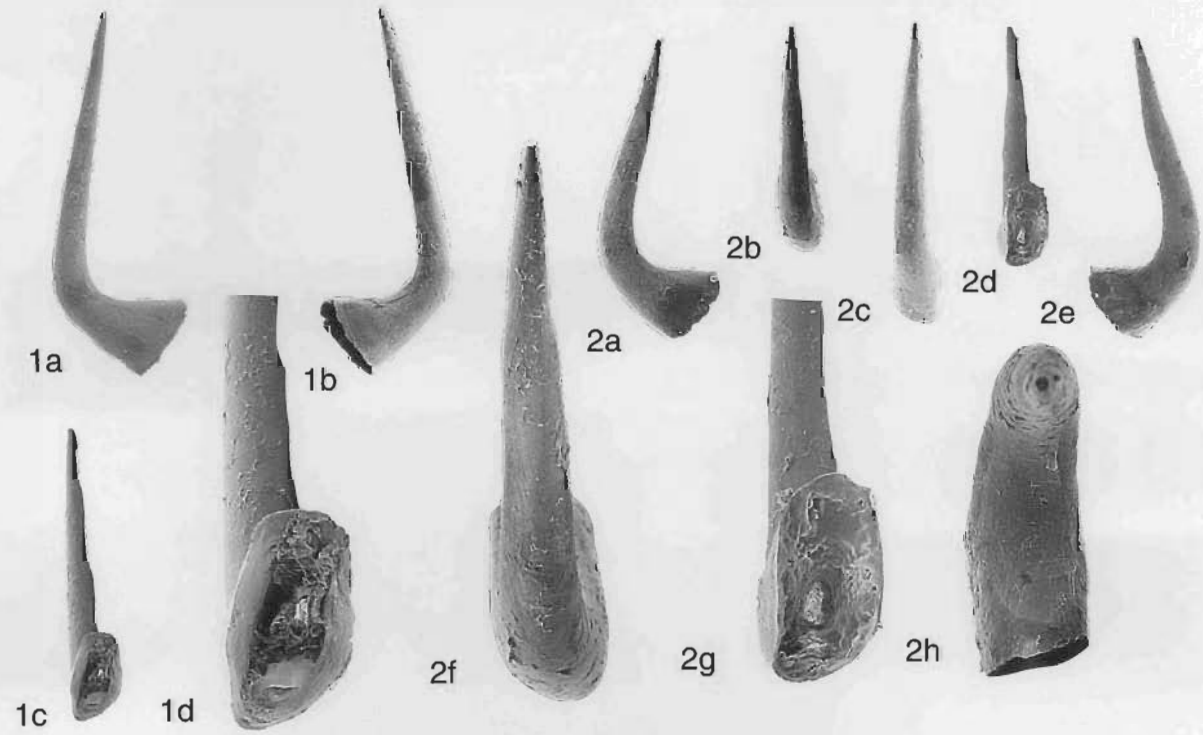

Figure 6. *Teridontus nakamurai* **Sc elements. All elements from sample GB93-004/C. All x55 except as noted. 1—Sc element (CPC33179) right element: 1a, inner lateral view; 1b, outer lateral view; 1c, posterior view; 1d, posterior view (x135), showing shape of basal cross-section. 2—Sc element (CPC33180) right element: 2a, inner lateral view; 2b, anterior view; 2c, oblique anterior view; 2d, posterior view; 2e, outer lateral view; 2f, anterior view (x135); 2g, posterior view (x135), showing outline of basal cross-section; 2h, oral view (x135).**

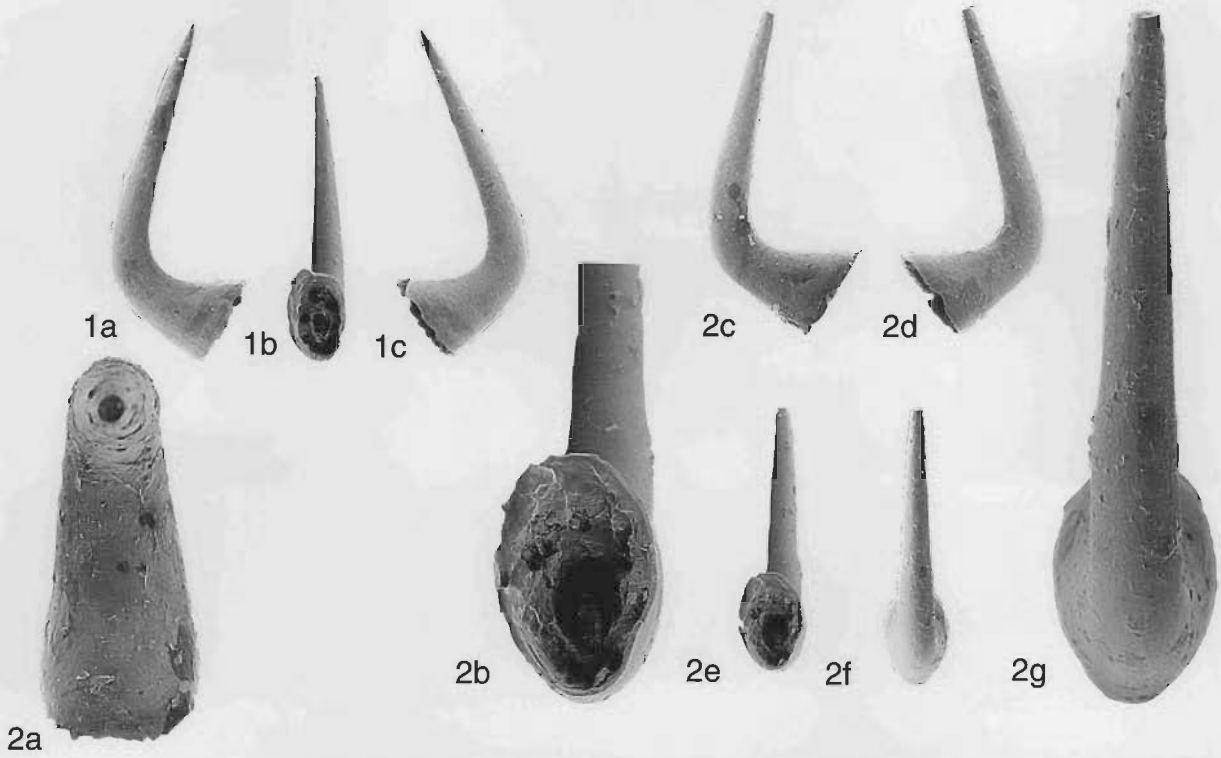

Figure 7. *Teridontus nakamurai* **Sb elements. All elements from sample GB93-004/C. All x55 except as noted. 1—Sb element (CPC33181) left element: 1a, outer lateral view; 1b, posterior view; 1c, inner lateral view. 2—Sb element (CPC33182) left element: 2a, oral view (x135); 2b, posterior view (x135), showing outline of basal cross-section; 2c, outer lateral view; 2d, inner lateral view; 2e, posterior view; 2f, anterior view; 2g, anterior view (x135).**

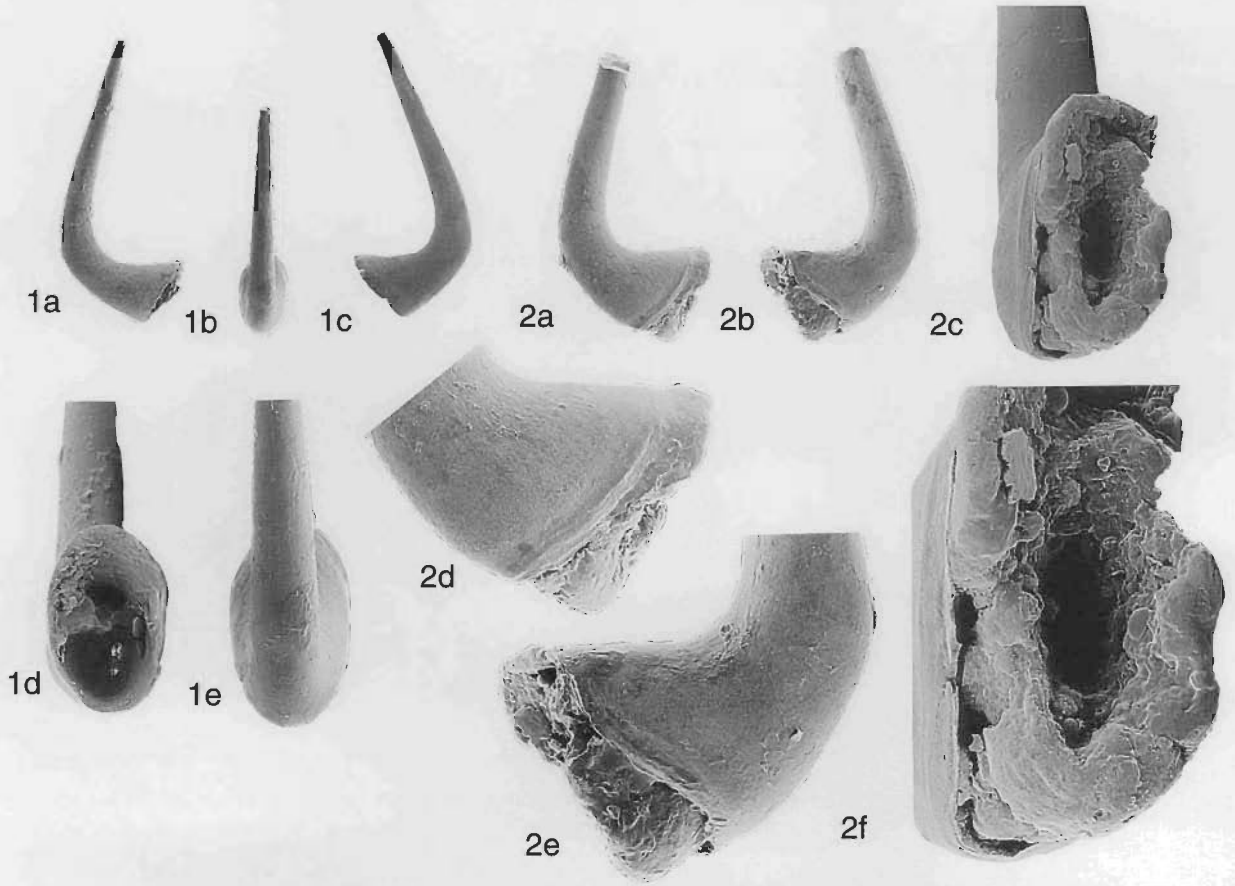

Figure 8. *Teridontus nakamurai* **Sb elements. All elements from sample GB93-004/C. All x55 except as noted. 1—Sb element (CPC33183) right element: 1a, inner lateral view; 1b, outer lateral view; 1c, anterior view; 1d, posterior view (x135), showing outline of basal cross-section; 1e, anterior view (x135). 2—Sb element (CPC33184) right element: 2a, inner lateral view; 2b, outer lateral view; 2c, posterior view (x135), showing attachment cone; 2d, inner lateral view (x135), showing attachment cone; 2e, outer lateral view (x135), showing attachment cone; 2f, attachment cone (x260).**

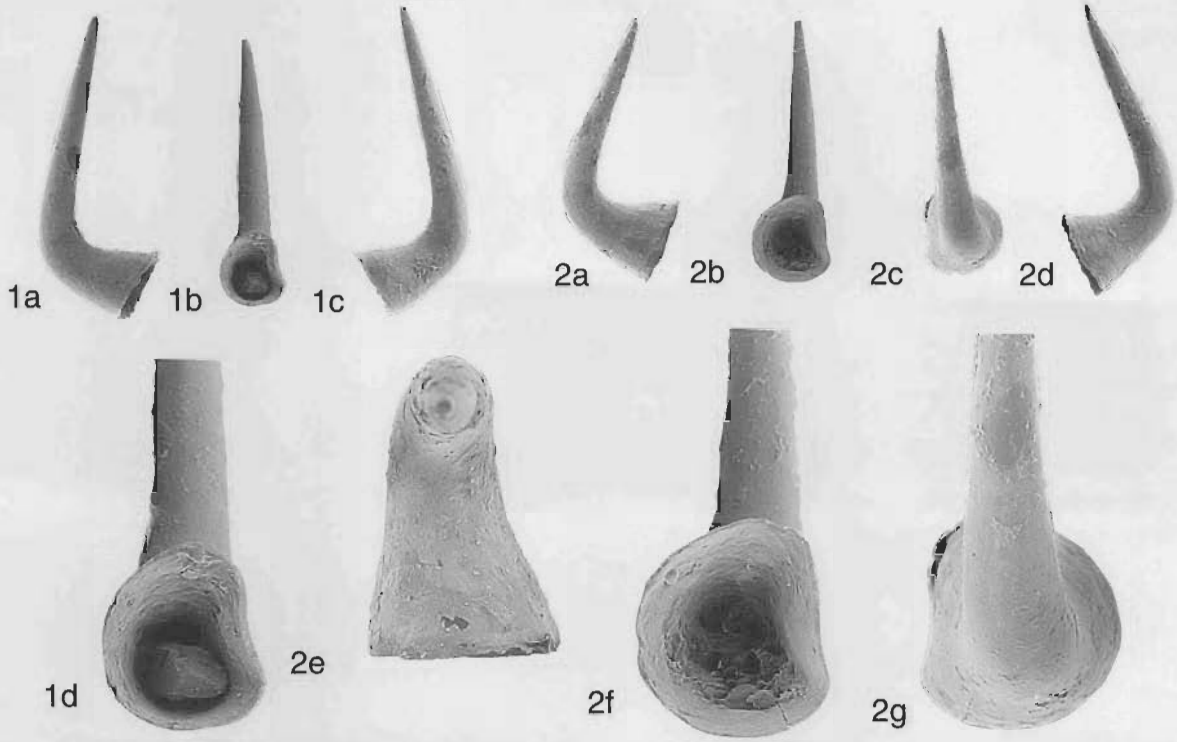

Figure 9. *Teridontus nakamurai* **Sd elements. All elements from sample GB93-004/C. All x55 except as noted. 1—Sd element (CPC33185) left element: 1a, outer lateral view; 1b, posterior view; 1c, inner lateral view; 1d, posterior view (x135), showing outline of basal cross-section. 2—Sd element (CPC33186) left element: 2a, outer lateral view; 2b, posterior view; 2c, anterior view; 2d, inner lateral view; 2e, oral view (x135); 2f, posterior view (x135), showing outline of basal cross-section; 2g, anterior view (x135), showing outline of basal cross-section.**

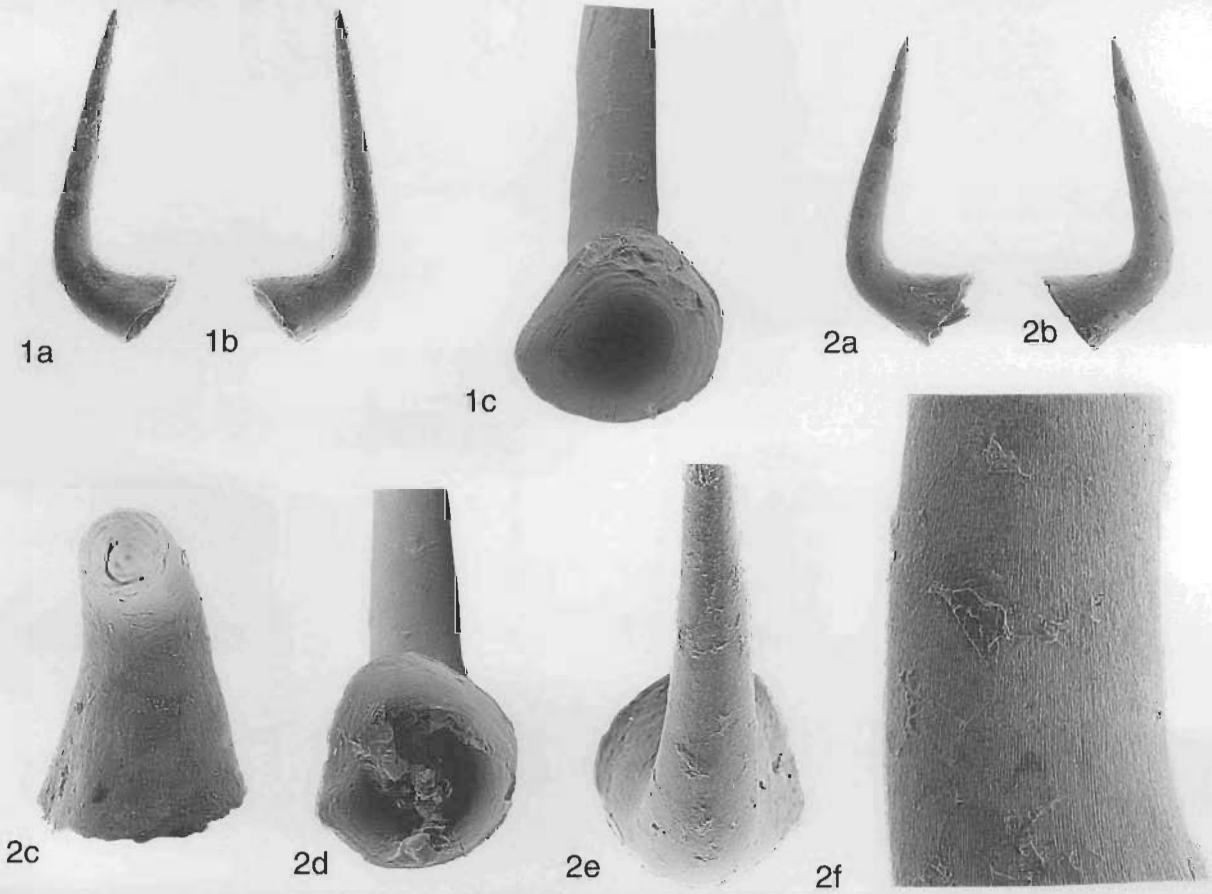

Figure 10. *Teridontus nakamurai* **Sd elements. All elements from sample GB93-004/C. All x55 except as noted. 1—Sd element (CPC33187) right element: 1a, inner lateral view; 1b, outer lateral view; 1c, posterior view (x135), showing outline of basal cross-section. 2—Sd element (CPC33188) right element: 2a, inner lateral view; 2b, outer lateral view; 2c, oral view (x135); 2d, posterior view (x135), showing outline of basal cross-section; 2e, anterior view (x135), showing outline of basal cross-section; 2f, striae on lateral margin of cusp (x430).**

P elements have a short base, about half the length of that of the Sa element. The Pb elements (Figs 11, 12, 15) have the base laterally compressed (Figs 15.1, 15.2) and the Pa element has the base obliquely compressed (Figs 15.3–6, 13.2d, 14.2h). The Pb element basal cross-section is an irregular oval, widest near the posterior margin (Figs 15.1, 15.2). The left and right elements have slightly different cross-sections. The right element (Fig. 12) is more rounded, the left element (Fig. 11) has the base margin slightly indented on the inner side, where it would sit adjacent to the right element in a reconstructed apparatus orientation (Fig. 15.1/2).

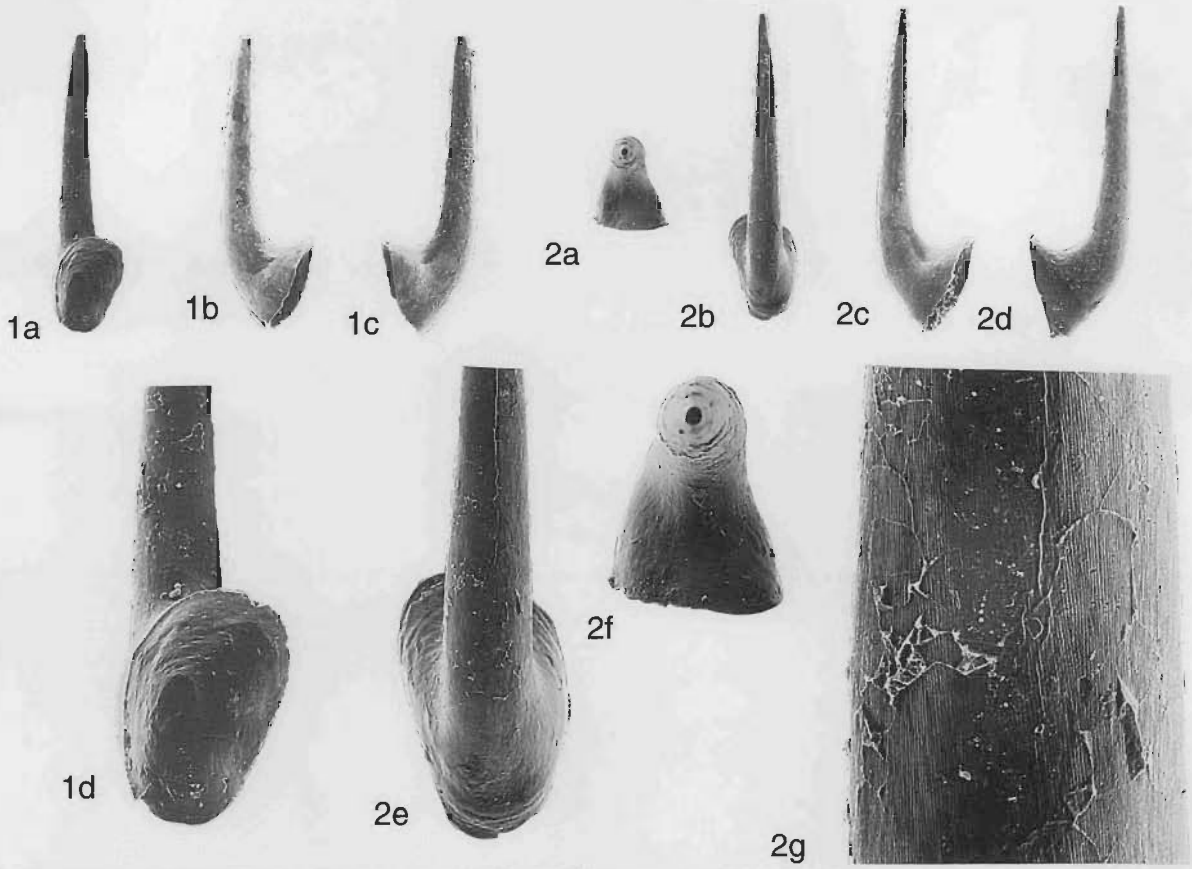

Figure 11. *Teridontus nakamurai* **Pb elements. All elements from sample GB93-004/C. All x55 except as noted. 1—Pb element (CPC33189) left element: 1a, posterior view; 1b, outer lateral view; 1c, inner lateral view; 1d, posterior view (x135), showing outline of basal cross-section. 2—Pb element (CPC33190) left element: 2a, oral view; 2b, anterior view 2c, outer lateral view; 2d, inner lateral view; 2e, anterior view (x135), showing outline of basal cross-section; 2f, oral view (x135); 2g, striae on cusp (x540).**

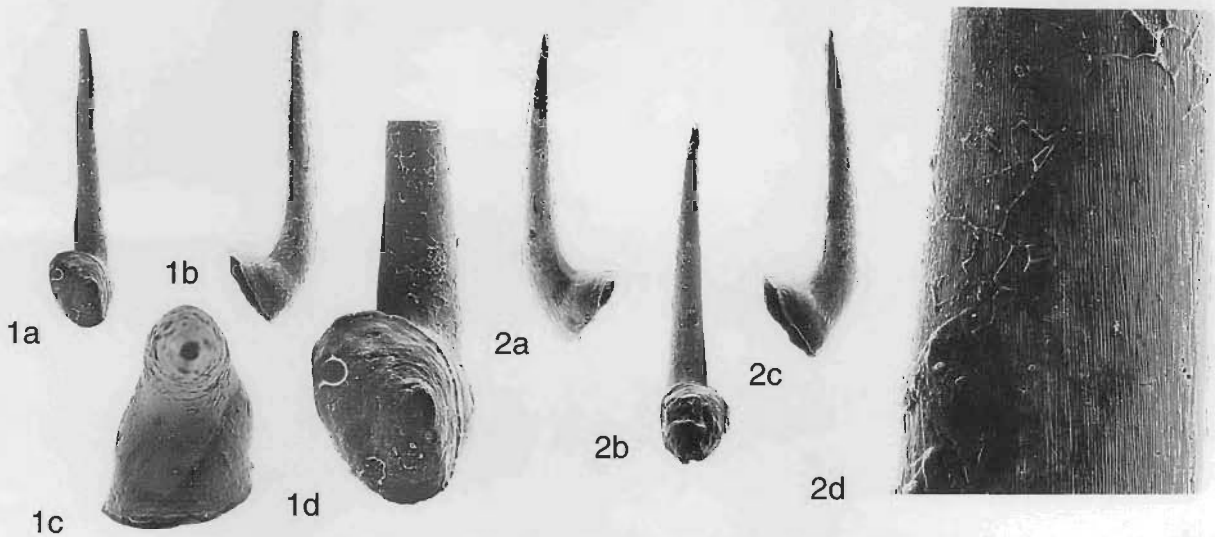

Figure 12. *Teridontus nakamurai* **Pb elements. All elements from sample GB93-004/C. All x55 except as noted. 1—Pb element (CPC33191) right element: 1a, posterior view; 1b, outer lateral view; 1c, oral view (x135); 1d, posterior view (x135), showing outline of basal cavity cross-section. 2—Pb element (CPC33192) right element: 2a, inner lateral view; 2b, outer lateral view; 2c, posterior view; 2d, striae on cusp (x520).**

The Pa elements (Figs 13, 14, 15) have a basal cross section that is compressed obliquely to the axis of the cusp, that is with the long axis of the base roughly at a right angle to the core axis of the cusp. The margin adjacent to the cusp is flattened and the opposite side is rounded. In a reconstructed element pair (Figs 15.3-6), the cusps are directed away from the axial plane of the apparatus, matching the orientation of the Pb elements.

Remarks. The reconstructed apparatus composition of *Teridontus nakamurai*, composed of six element types and lacking an M element pair, is typical of many Late Cambrian and Early Ordovician coniform conodont apparatuses.

Ji & Barnes (1994) have presented an emended diagnosis of *Teridontus nakamurai*, in which they recognise four element morphologies: c, b, a and e. The e element has a laterally compressed cusp and no such element has been found in this study. The c element illustrated by Ji & Barnes (1994, pl. 24, fig. 5) is not illustrated in lateral view, but appears to be more erect than the Sa elements associated with *T. nakamurai* by this study. For these reasons, the material illustrated by Ji & Barnes (1994) as *T. nakamurai* is here excluded from that species and their emended diagnosis of the species is thus invalid. It is also observed that the material studied by Ji & Barnes (1994) is significantly younger than the material studied by Nogami (1967) or that used in this study.

Teridontus datsonensis is distinguished from *T. nakamurai* by the presence of furrows on one or both sides of the elements. *T. nakamurai* is distinguished from *T. gracillimus* by its larger size and proportionally longer base of the P elements. Referring to the type specimens of *T. gracillimus* illustrated by Nowlan (1985, Figs. 8.2, 8.3), the paratype (8.2) is considered to be a P element and the holotype (8.3) is considered to be an S element, probably an Sa element.

Locality information

All samples used in this study were obtained from a road-metal quarry on the north side of the Boulia–Winton Highway, 54.5 km east of Boulia. The quarry lies near the southern end of the Dribbling Bore locality of Druce & Jones (1971, fig. 6). The exposure continues the line of anticlinal structures that include Black Mountain (Unbunmaroo), Mt Ninmaroo and Mt Datson. All these localities expose the Late Cambrian Chatsworth Limestone.

Samples from the quarry section have been collected on three different trips to the locality. The first collection by John H. Shergold and John R. Laurie in 1989 was a single grab sample (JHS 89/001) from a limestone bed near the top of the exposed section. In 1990, a short section was measured in the quarry wall and five samples (GB90-004/1-5) representative of the section were collected. None of these samples (Table 1) contained abundant elements of *Teridontus nakamurai*. In 1993 an additional three samples (GB93-004/A-C) were collected about 100 m east of the line of section and stratigraphically above the top sample of the section. These latest samples are only located approximately in the section (Fig. 2).

Acknowledgments

I thank Ray Ethington (University of Missouri–Columbia), Sandy McCracken (Geological Survey of Canada) and Jim Miller (Southwest Missouri State University) for their constructive suggestions on the manuscript. John Laurie reviewed an early version of the text. SEM photography and printing by R.W. Brown, AGSO.

References

An, Tai-xiang, 1982. Study on the Cambrian conodonts from North and Northeast China. *Science Reports of the Institute of Geoscience, University of Tsukuba, section B= Geological Sciences*, 3, 113–159.

Barnes, C.R., Kennedy, D.J., McCracken, A.D., Nowlan, G.S. & Tarrant, G.A., 1979. The structure and evolution of Ordovician conodont apparatuses. *Lethaia*, 12, 125–151.

Clark, D.L, 1981. Classification. *In* Clark, D.L. (editor), *Treatise on Invertebrate Palaeontology—Part W, Miscellanea, Supplement 2, Conodonta*, W102–W103.

Druce, E.C., 1978. A key North American conodont found in the Georgina Basin. *BMR Journal of Australian Geology & Geophysics*, 3, 351–355.

Druce, E.C. & Jones, P.J., 1971. Cambro-Ordovician conodonts from the Burke River Structural Belt, Queensland. *Bureau of Mineral Resources, Australia, Bulletin*, 110, 1–159.

Dzik, J., 1976. Remarks on the evolution of Ordovician conodonts. *ACTA Palaeontologica Polonica*, 21, 395–455.

Fåhraeus, L.E. & Hunter, D.R., 1985. The curvature-transition series: integral part of some simple-cone conodont apparatuses (Panderodontacea, Distacodontacea, Conodontata). *ACTA Palaeontologica Polonica*, 30, 177–189.

Furnish, W.M., 1938. Conodonts from the Prairie du Chien (Lower Ordovician) Beds of the upper Mississippi Valley. *Journal of Palaeontology,* 12, 318–340.

Ji Zailiang & Barnes, C. R., 1994. Lower Ordovician conodonts of the St. George Group, Port au Port Peninsula, western Newfoundland, Canada. *Palaeontographica Canadiana* 11, 1–149.

Jones, P.J., 1971. Lower Ordovician Conodonts from the Bonaparte Gulf Basin and the Daly River Basin, Northwestern Australia. *Bureau of Mineral Resources, Australia, Bulletin,* 117, 1–80.

Landing, E., 1983. Highgate Gorge: Upper Cambrian and Lower Ordovician continental slope deposition and biostratigraphy, northwestern Vermont. *Journal of Paleontology*, 57, 1149–1187.

Lindström, M., 1971. Lower Ordovician conodonts of Europe. *Geological Society of America, Memoir* 127, 21–61.

Miller, J.F., 1969. Conodont fauna of the Notch Peak Limestone (Cambro-Ordovician), House Range, Utah. *Journal of Paleontology*, 43(2), 413–439, pls. 63–66.

Miller, J. F., 1980. Taxonomic revisions of some Upper Cambrian and Lower Ordovician conodonts with comments on their evolution. *University of Kansas Paleontological Contributions*, 99, 1–44.

Miller, J.F., 1988. Conodonts as biostratigraphic tools for redefinition and correlation of the Cambrian–Ordovician Boundary. *Geological Magazine*, 125, 349–362.

Müller, K.J., 1959. Kambrische Conodonten. *Zeitschrift der Deutschen Geologischen Gesellschaft*, 111, 434–485.

Müller, K.J., 1964. Conodonten aus dem unteren Ordovizium von Südkorea. *Neues Jahrbuch für Geologie und Paläontologie, Abhandlung*, 119, 93–102.

Ni Shi-zhao, 1981. Discussion on some problems of

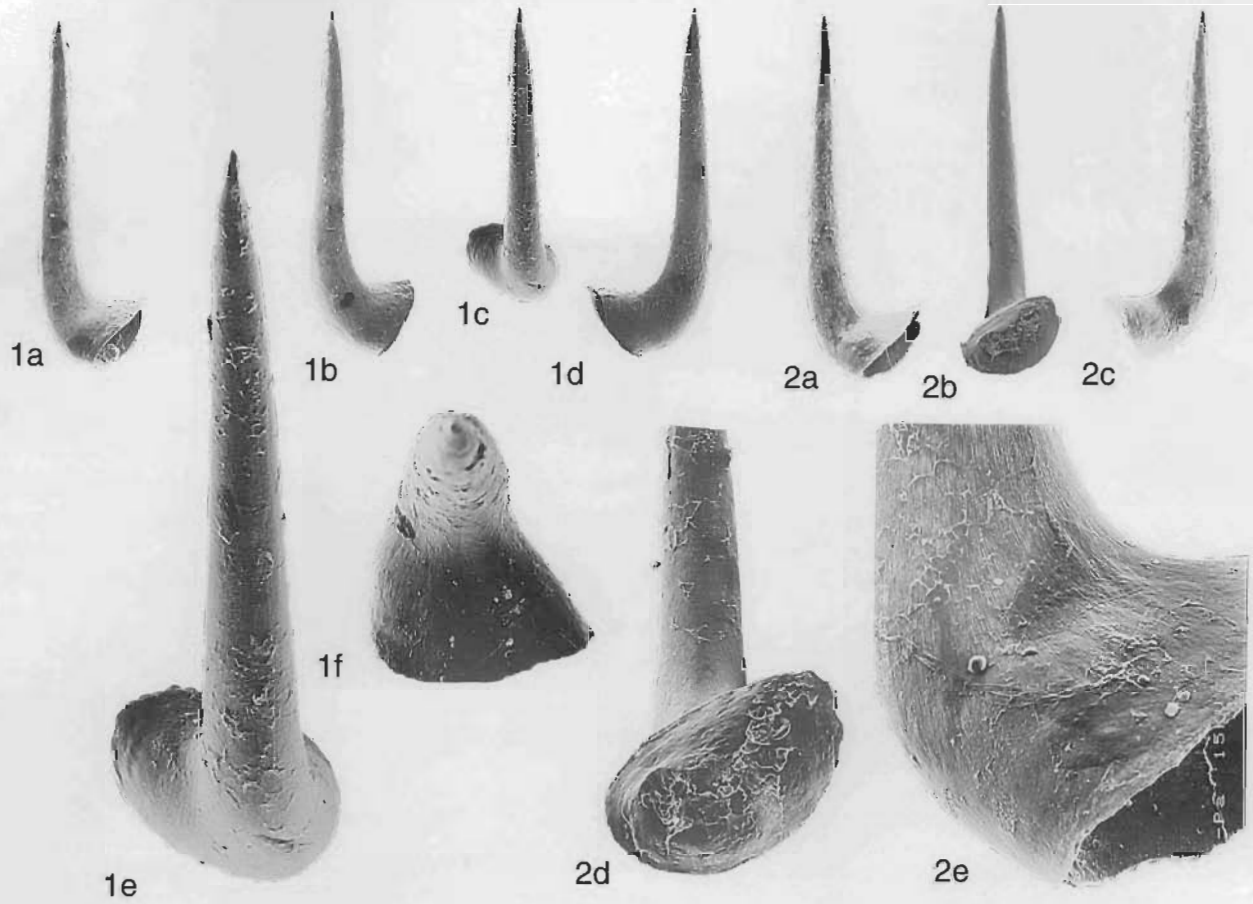

Figure 13. Caption on opposite page.

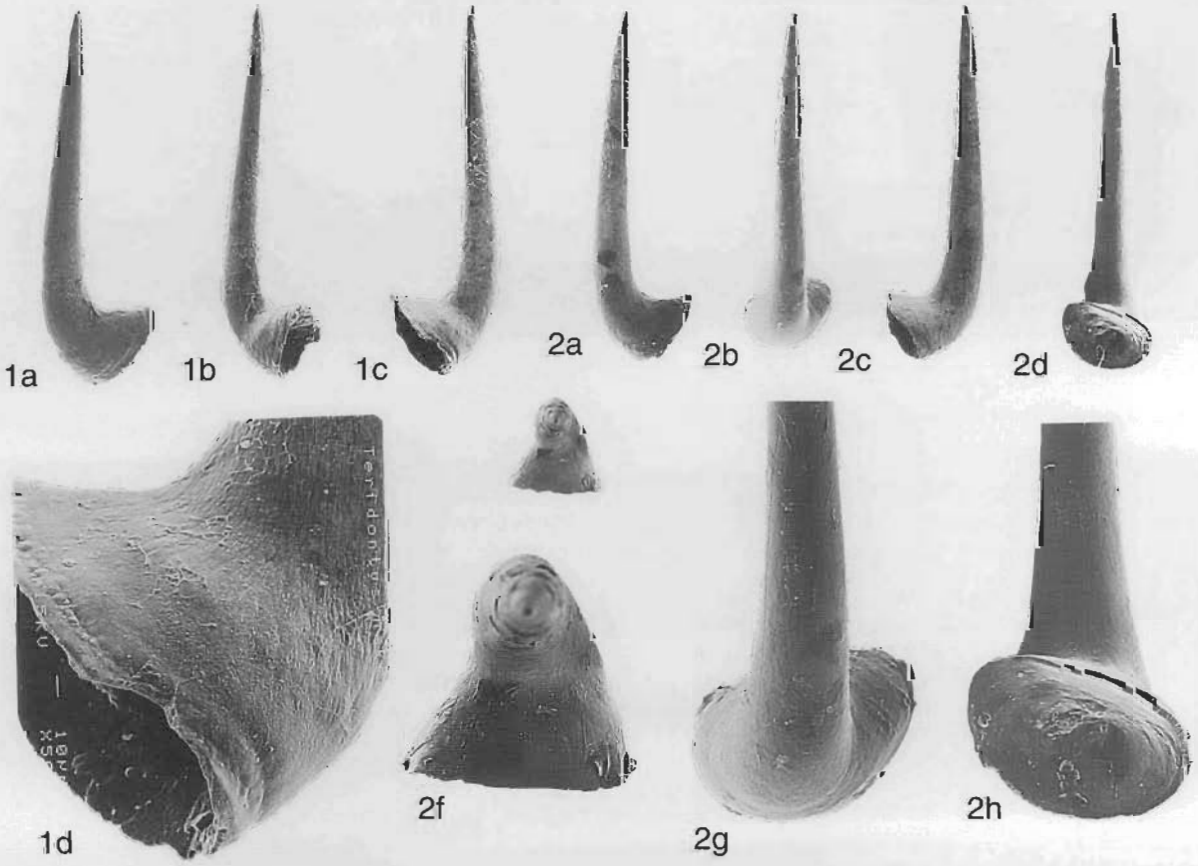

Figure 14. Caption on opposite page.

Figure 13. *Teridontus nakamurai* **Pa elements, left elements. All elements from sample GB93-004/C. All x55 except as noted. 1—Pa element (CPC33195): 1a, oblique outer lateral view; 1b, outer lateral view; 1c, anterior view; 1d, inner lateral view; 1e, anterior view (x135); 1f, oral view (x135). 2—Pa element (CPC33196): 2a, outer lateral view; 2b, posterior view; 2c, inner lateral view; 2d, posterior view (x135); 2e, oblique outer lateral view (x250), showing loss of striae near basal margin.**

Figure 14. *Teridontus nakamurai* **Pa elements, right elements. All elements from sample GB93-004/C. All x55 except as noted. 1—Pa element (CPC33193): 1a, inner lateral view; 1b, oblique inner lateral view; 1c, outer lateral view; 1d, inner basal margin (x270), showing band that lacks striae parallel to basal margin. 2—Pa element (CPC33194): 2a, inner lateral view; 2b, anterior view; 2c, outer lateral view; 2d, posterior view; 2e, oral view; 2f, oral view (x135); 2g, anterior view (x135); 2h, posterior view (x135).**

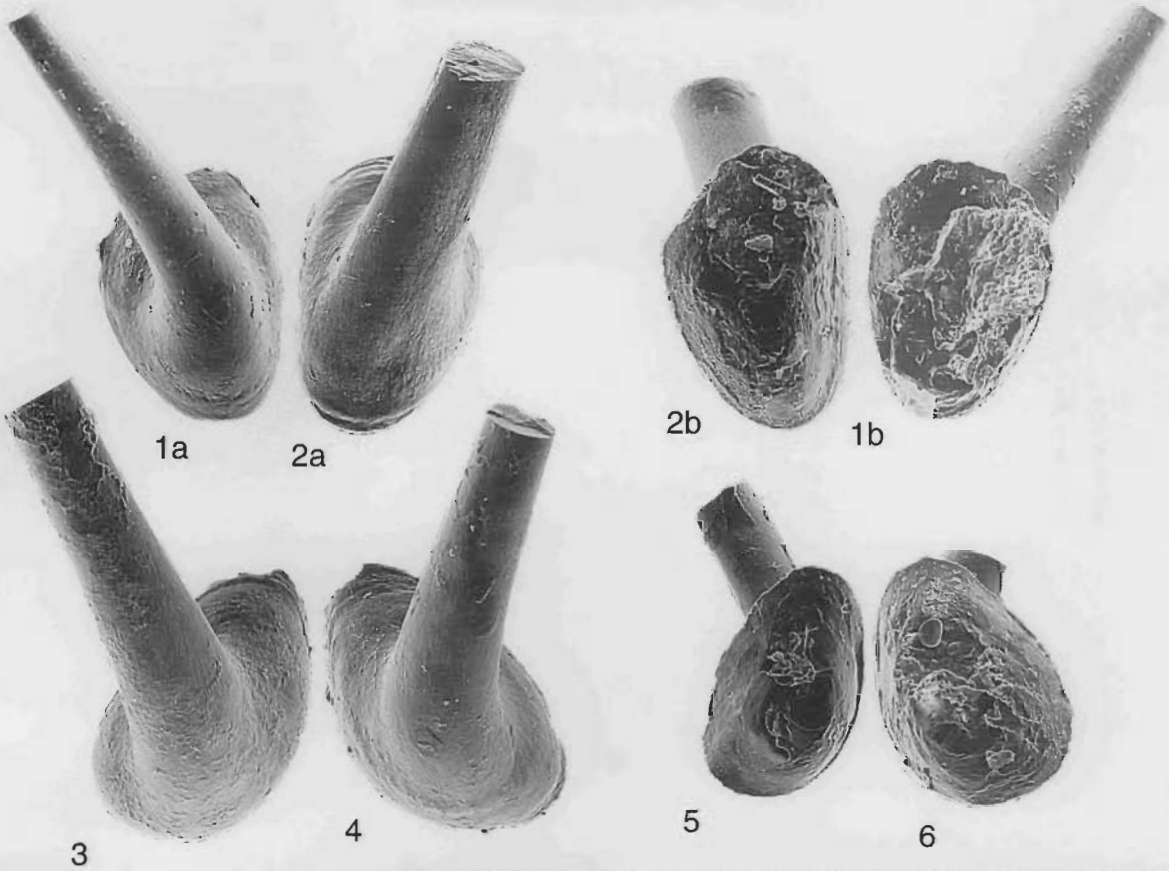

Figure 15. *Teridontus nakamurai* **Pb and Pa elements. Paired elements, viewed from the anterior and posterior to demonstrate the reconstructed position of the elements in life orientation in the conodont animal. Note the slight asymmetry of the element pair, especially in the Pb element, with a flattening of the inner lateral basal margin of the left element that accommodates the more rounded right element basal margin. All elements from sample GB93-004/C. All x135. 1—Pb element (CPC33197) right element: 1a, oral view; 1b, basal view. 2—Pb element (CPC33198) left element: 2a, oral view; 2b, basal view. 3—Pa element (CPC33199) right element, oral view. 4—Pa element (CPC33200) left element, oral view. 5—Pa element (CPC33201) left element, basal view. 6—Pa element (CPC33202) right element, basal view.**

Ordovician stratigraphy by means of conodonts in eastern part of Yangtze Gorges Region. *Selected papers on the 1st Convention of Micropaleontological Society of China*, Science Press, Beijing, 127–133.

Nogami, Y., 1967. Kambrische conodonten von China, Teil. 2 Conodonten aus den hoch oberkambrischen Yencho-Schichten. *Memoirs of the College of Science, University of Kyoto, Series B, 33(4) Geology and Mineralogy*, 211–218, 1 pl.

Nowlan, G.S., 1985. Late Cambrian and Early Ordovician conodonts from the Franklinian Miogeosyncline, Canadian Arctic Islands. *Journal of Paleontology*, 59, 96–122.

Shergold, J.H., 1975. Late Cambrian and Early Ordovician trilobites from the Burke River Structural Belt, western Queensland. *Bureau of Mineral Resources of Australia, Bulletin* 153 (2 vols), 251 pp., 58 pls.

Shergold, J.H. & Nicoll, R.S., 1992. Revised Cambrian–Ordovician boundary biostratigraphy, Black Mountain, western Queensland. *In* Webby, B.D. & Laurie, J.R. (editors.) *Global Perspectives on Ordovician Geology*. Balkema, Rotterdam, 81–92.

Sweet, W.C., 1988. *The Conodonta: morphology, taxonomy, paleocology, and evolutionary history of a long-extinct animal phylum*. Oxford University Press, Oxford, 212 pp.

Viira, V., 1974. Ordovician conodonts of the east Baltic. *Eesti NSV Teaduste Akadeemia Geoloogia Instituut, Tallin*, 142 pp.

AGSO Journal of Australian Geology & Geophysics, 15 (3), 381–394 © Commonwealth of Australia 1994

Physical and petrological characteristics of basaltic eruption sites in the Monaro Volcanic Province, southeastern New South Wales, Australia

I.C. Roach[1], K.G. McQueen[1] & M.C. Brown[1]

The Monaro Volcanic Province in southeastern New South Wales is an Early to Middle Tertiary intraplate volcanic province of lava field style, similar to the Newer Volcanic Province of southwestern Victoria. The lava pile is dominated by nepheline basanite, alkali olivine basalt and transitional basalt with minor olivine tholeiite and nepheline hawaiite. Olivine nephelinite lavas occur near the top of the lava pile. The lavas are interbedded with Tertiary sediments and hyaloclastites, some of which have formed in lakes, probably developed by lava damming the pre-basaltic drainage. Thick weathering profiles, in some cases bauxitic, are developed on many of the flows in the lava pile, suggesting long breaks between eruptions at particular sites. This is consistent with sporadic eruptions from widely scattered vents.

Most known eruption sites in the province are represented by volcanic plugs of aphanitic to coarse-grained nepheline basanite, olivine nephelinite, nepheline hawaiite and alkali olivine basalt. Fractionated varieties of these rocks also occur together with minor feldspar-rich and titanian augite-rich cumulates. The predominant plug type is aphanitic to fine-grained nepheline basanite, containing mantle xenoliths and/or kaersutite amphibole.

Basement fractures have had a major influence on the position of volcanic centres. Plugs are concentrated along two northwest-trending linear zones: the Bemboka Zone in the north; and the Berridale–Towamba Zone in the south. The Berridale Fault–Towamba Lineament is a major crustal feature of the region. Other basement structures, including north-northeast-trending faults, appear to have controlled some eruption centres away from the two major zones.

Introduction

The Monaro Volcanic Province is a Tertiary intraplate mafic lava field in the southern highlands of New South Wales (Fig. 1). It covers an area of 4200 km^2 and originally contained at least 630 km^3 of mafic lavas and minor pyroclastic rocks. Palynological dates from pollen and plant remains in sediments immediately below and intercalated with the lavas and K–Ar radiometric dates of eruptive rocks indicate an age of 57.5–34.0 Ma for the main part of the province(Taylor et al. 1990; Wellman & McDougall 1974, corrected to revised decay constants).

More than 65 volcanic plugs (definite and probable) have been discovered during recent studies of the lava field by staff and students of the University of Canberra and geologists from the New South Wales Geological Survey (Pratt et al. 1993). Before the work by the University of Canberra and the Geological Survey, only two possible eruption points had been identified (Lambert & White 1965; Wellman & McDougall 1974). No detailed descriptions of the volcanic plug rocks have been published.

In this paper we describe the nature and distribution of these recently discovered eruption sites in the Monaro Volcanic Province. We also discuss their petrological features, relationships with the lavas of the province and implications for eruption style, and also the association of eruption centres with basement structures. Detailed information on the major and trace element geochemistry of the intrusive and extrusive rocks of the province and implications for magma source will be published separately

Previous studies

Basalts in the Monaro Volcanic Province were first described by Clarke (1860), although Browne (1914) was the first to attempt a serious description of two major eruptive rock types. The mineralogy and geochemistry of a number of the lava flows were described in a pioneering paper by Kesson (1973). Taylor et al. (1985) described the pre-basaltic topography of the Northern Monaro and suggested possible locations of volcanic plugs. Ollier & D. Taylor (1988) described aspects of the geomorphology of the Kosciusko–Bega region and attributed basaltic volcanism in the area to a circular shield volcano (the Monaro Volcano) centred on Brown Mountain. The notion of a single central volcano was refuted by Taylor et al. (1989), who introduced the term Monaro Lava Field as a more apt description of the province. Clark (1987) described the geochemistry of basalts on the Bombala 1:100 000 sheet and Brown et al. (1988) gave a brief description of additional lava flows, volcanic plugs and pyroclastic rocks from the same area, including some further geochemical data. Roach (1991) combined data from previous studies with new analyses to describe the petrology and geochemistry of 28 volcanic plugs. Edgecombe (1992) reassessed the available geochemistry and analysed a number of mantle xenoliths to briefly describe the thermobarometric conditions of the upper mantle during the time of eruption. Most recently, Pratt et al. (1993) published a general description of the province. An overview of intraplate volcanism in eastern Australia, with a brief description of the Monaro Volcanic Province by Knutson & Brown (1989), is included in Johnson (1989).

Regional and tectonic setting

The Monaro Volcanic Province lies on a basement of Palaeozoic rocks of the southern Lachlan Fold Belt, in the Tasman Orogenic Zone of eastern Australia. These rocks comprise tightly folded Ordovician and Silurian sedimentary and metasedimentary rocks, Siluro-Devonian granitoids and felsic volcanoclastics. Gently folded Late Devonian felsic volcanic and sedimentary rocks also crop out in the northern part of the province (Crook et al. 1973; Powell 1983; Williams et al. 1975).

The region has two small low-pressure type metamorphic complexes—the Cooma Metamorphic Complex (Hopwood 1976; Munksgaard 1988) and the Cambalong Complex (McQueen et al. 1986). Basement rocks south of Cooma are intruded by the Jurassic Myalla Road Syenite (Barnes & Herzberger 1975).

Basalts and volcanoclastic rocks of the province are underlain by Early Tertiary alluvial and lacustrine deposits containing fossilised tree trunks, leaves, pollens and lignite (Taylor et al. 1990). Early Tertiary alluvial gravels and sands contain angular to rounded fragments of

[1] Centre for Australian Regolith Studies, University of Canberra, P.O. Box 1, Belconnen, ACT, 2616, Australia

Ordovician and Silurian metasedimentary rocks, Silurian volcanoclastic rocks, Late Silurian to Early Devonian granitoids, and Devonian clastic rocks from the local area. Lacustrine deposits consist of laminated brown to white clays and silts, dark organic-rich muds, lignites, and coals with minor interbedded fluvial and lake shoreline sands and gravels (Brown et al. 1993). Gravel deposits have survived undisturbed on hilltops throughout the province, but some were reworked during the period of volcanism into deposits containing basalt cobbles in palaeochannels within the lava pile. Quartz sand and gravel silcrete, containing pre-basaltic sediments and fossils, line some of the pre-basaltic surfaces.

The basement of the Monaro Volcanic Province is cut by a series of faults striking north–south, east–west, northeast–southwest and northwest–southeast. Some of the larger north–south-striking faults can be traced over a large distance of the Lachlan Fold Belt, from Victoria to central New South Wales. Many of these are thought to have been initiated very soon after granitoid intrusion into the local area, as they affect the granitoids and are paralleled by aplite dykes, particularly in the Jindabyne region (White et al. 1975). North–south-trending faults in the basement are responsible for the horst and graben landscapes which dominate parts of southeastern New South Wales, and helped shape the lava pile. A prominent

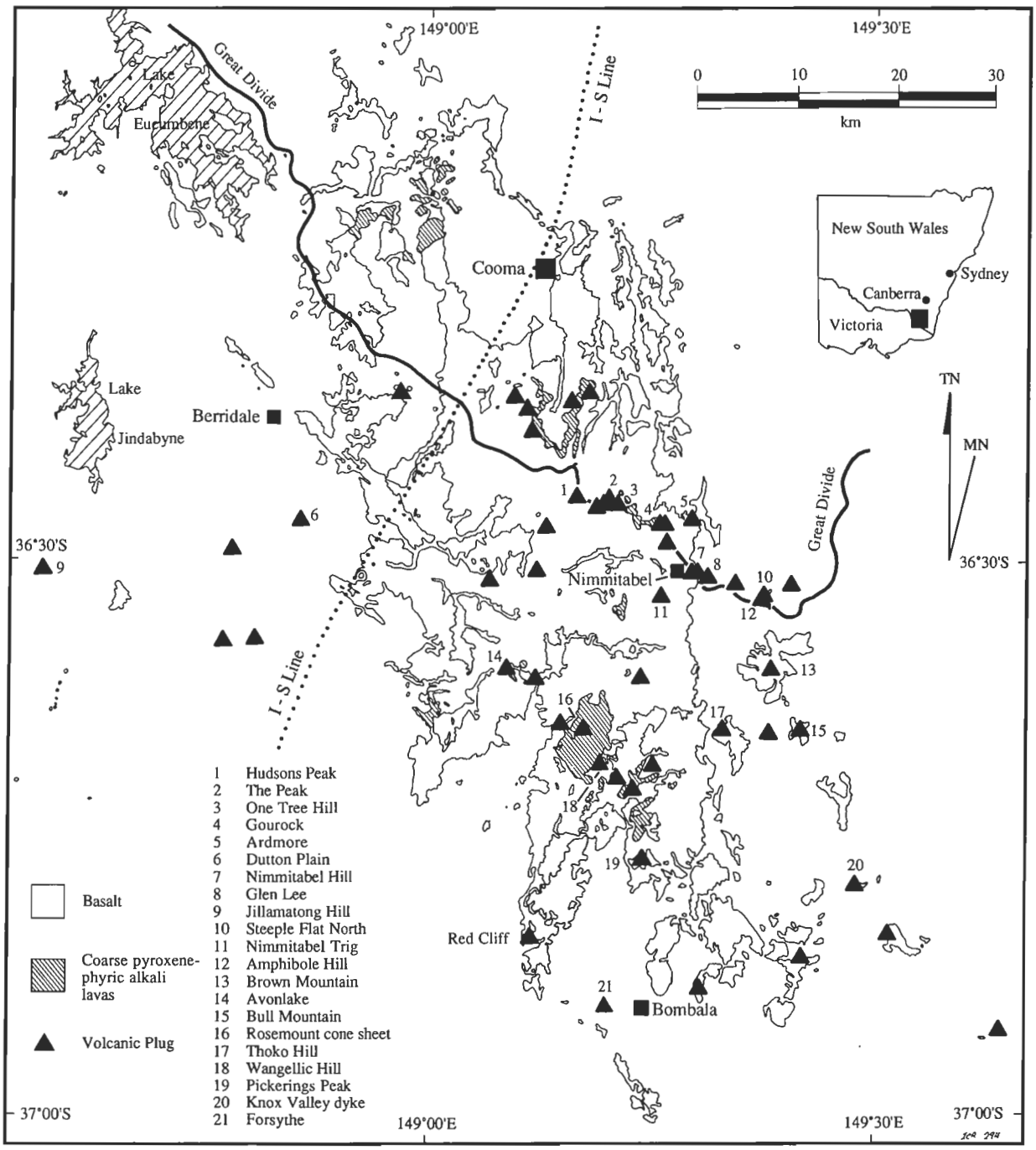

Figure 1. Locality map, showing the outcrop of basalt and distribution of volcanic plugs in the Monaro Volcanic Province, and outcrops of coarse pyroxene-phyric alkali lavas (including the mapping of K.R. Sharp in the northwest). Location of the I–S Line is adapted from Powell (1983) after Price & Taylor (1977). The basalt outline is adapted from 1:100 000 geological sheet compilations.

fault scarp on a horst to the eastern side of the province partly prevented the lava pile from encroaching further eastwards (Brown et al. 1993). The Berridale Fault, a major northwest–southeast-striking structure (Fig. 2), appears to terminate in the Jindabyne Thrust Fault on its western side (White et al. 1975). The Berridale Fault possibly continues southeast as the Towamba Lineament, slightly offset by movement on north–south structures now covered by the lava pile. Another northwest-trending feature, the Bemboka Lineament, is defined by the straight course of the Bemboka River and an established fault on the northwest side of the province (Fig. 2). These oblique faults appear to have exerted some structural control over the geomorphology of the province and have been active over a long time, as indicated by early strike-slip movements affecting Siluro-Devonian granitoid intrusions and post-basalt vertical movements, which have warped and tilted the lava pile. Some faults in the region are still active, as indicated by continued seismic activity in the Snowy Mountains region (Lambert & White 1965; White et al. 1975).

Criteria for recognising volcanic plugs

The Monaro Volcanic Province is highly eroded and dissected by rivers and creeks, and primary volcanic structures, such as cinder cones or maars, are generally not preserved. In the absence of primary volcanic structures, a number of criteria based on other characteristics have been established to recognise volcanic plugs within the province. Based on observations in the Monaro and other eastern Australian volcanic provinces, they include:

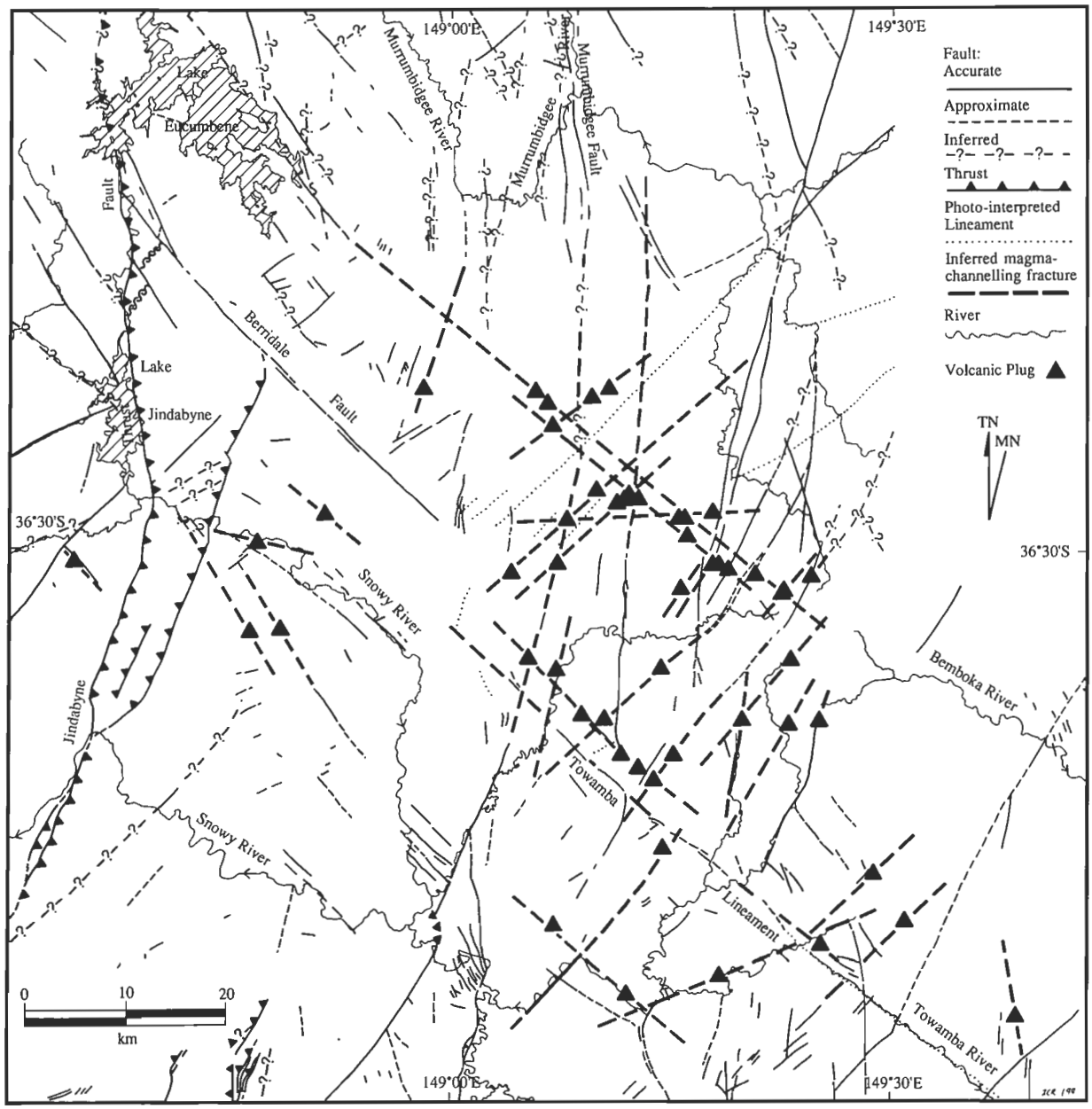

Figure 2. The location of lineaments and volcanic plugs in the Monaro Volcanic Province. The Bemboka Zone is defined by the large collection of plugs in the north (stippled), in line with the eastern arm of Lake Eucumbene and the Bemboka River. The Berridale–Towamba Zone is defined by the linear collection of plugs in the south (stippled), between the Berridale Fault and the Towamba Lineament. Known faults and major rivers are taken from 1:100 000 geological sheet compilations. Lineaments are drawn from a 1:100 000 edge-enhanced Landsat 4 image of the Monaro Volcanic Province.

1. Jointing: some volcanic plugs display sub-vertical and/or sub-horizontal jointing, which may be radial, concentric or polygonal (columnar; Fig. 3A–D). Sub-vertical and sub-horizontal radial and concentric joints are commonly observed in medium to coarse-grained volcanic plugs within the province (Fig. 3A, C–D). Shallowly plunging to sub-vertical polygonal joints are observed in most of the aphanitic and fine-grained plugs and dykes (Fig. 3B).

2. Flow alignment: phenocrysts and elongate xenoliths and xenocrysts in most plug rocks are sub-vertically to vertically aligned. Steeply dipping flow banding is also seen in aphanitic and fine-grained plug rocks.

3. Xenoliths and xenocrysts: aphanitic and fine-grained plugs contain large numbers of mantle and crustal xenoliths and xenocrysts (Fig. 3E). Lava flows in the province are usually devoid of xenoliths.

4. Petrographic differences: plug rocks may be recognised where they are petrographically different from surrounding lava flows at the same elevation. A mafic rock outcrop standing alone on basement rocks may be considered a plug if it meets other criteria.

5. Weathering: plug rocks weather at different rates to surrounding lava flows and basement rocks, resulting in differences in topographic expression. Plug rocks are always less weathered than the surrounding lavas.

6. Topographic expression and shape: plugs vary in size and shape, depending on their relative age, their petrography, and whether they intrude basement rock or previously extruded basalt flows (Fig. 4). Plugs range from 10 m to over 200 m across and some stand over 100 m above the surrounding terrain. Others have very subdued topographic expression. Normally, plugs appear as conical or round-topped hills, but they may have no significant topographic expression, especially where they intrude basement rocks away from the main body of lava flows. They are mostly circular to elliptical in plan, although some are irregular pipe-shaped bodies. Dykes normally have moderate topographic relief and elogated outcrop patterns.

7. Volcanic structures: coarse pyroclastic debris generally indicates the presence of a volcanic vent or plug nearby.

8. Crystal settling: some large vents contained lava lakes. One of these is a compositionally zoned body with concentration of more dense pyroxene crystals towards the base. Compositionally zoned bodies may be considered volcanic plugs if they meet other criteria.

9. Megascopic features: plugs are commonly positioned over fractures and lineaments in the basement rocks which manifest as small faults or monoclines within the overlying basalts, visble on airphotos and satellite images of the province.

Rock types and field relationships

The Monaro Volcanic Province is characterised by a series of broad volcanic plains separated by terraced flat-topped hills, composed of multiple lava flows, and round-topped hills on the larger volcanic plugs (Fig. 4). The volcanic pile consists dominantly of nepheline basanites, alkali olivine basalts and transitional basalts with minor olivine tholeiites (Fig. 5). Minor olivine nephelinites occur in the upper part of the sequence. The lava pile is up to 400 m thick and is now deeply dissected. An estimated 100–200 m of material has been removed from the top of the lava pile in some areas (Roach 1991). Many lava flows have well-developed interflow weathering profiles, some topped by bauxite horizons up to 3.5 m thick (Taylor et al. 1990; Brown et al. 1992). Some bauxitic layers contain quartz-rich sediments and plant fossils, indicating reworking.

Included in the volcanic pile are a series of thickly bedded, coarse pyroxene-phyric, medium-grained alkali lavas (Figs 1, 3F) (Brown et al. 1992; Pratt et al. 1993). Pratt et al. (1993) named two of these lavas flows north of Hudsons Peak the Bondo Dolerite Member, after a local sheep station (Fig. 1). Mapping by Edgecombe (1992) recognised at least four individual flows of similar composition near the base of the lava pile around the Wangellic Hill area, and a large outcrop has been recognised in the northwest of the province during recent mapping by K.R. Sharp (unpublished) and the authors (Fig. 1). Similar rocks have been described from the Southern Highlands Province of New South Wales by Wass (1973), who interpreted them as a late-stage crystal-rich differentiate erupted close to vents.

Volcanic plugs and dykes intrude at all levels in the lava pile. Small to medium size (10–50 m across) plugs can be found exposed in river and creek valleys and on the sides or tops of small terraced hills (Fig. 4F), whereas large plugs tend to form stand-alone hills, either peaked or round-topped, depending on their composition (Fig. 4A–D). Dykes are commonly over 10 m wide and 40–50 m long and stand out above the surrounding lavas (e.g. Amphibole Hill, Knox Valley; Fig. 1). An olivine nephelinite cone sheet, 1 km across, rich with mantle xenoliths, has also been recognised at Rosemount (Edgecombe 1992; Fig. 1). Aphanitic plugs in the Palaeozoic basement tend to erode quicker than the basement rocks and form low outcrops of 10 m or more across with little or no topographic relief, making them very difficult to locate. Wide medium to coarse-grained plugs are relatively resistant to weathering and either form conical peaks standing high above the surrounding basalt plains (e.g. Hudsons Peak; Figs 1, 4A) or slightly elevated flat-topped hills (e.g. Bull Mountain; Fig. 1).

The majority of volcanic plugs are aphanitic nepheline basanites which normally contain large numbers of mantle and crustal xenoliths and xenocrysts (e.g. Jillamatong Hill, Rosemount cone sheet, Wangellic Hill, Dutton Plain, Forsythe) and/or kaersutite amphibole (e.g. Amphibole Hill, Glen Lee) in contrast to the surrounding lavas. These may have a strongly pitted 'swiss cheese' appearance (Fig. 3E) from the weathering out of mantle xenoliths and/or amphibole (e.g. Wangellic Hill, Gourock, Dutton Plain; Fig. 1). Rare mantle xenolith-bearing flows have been recognised at Wangellic Hill (Edgecombe 1992), but the xenolith concentration is much lower than in the nearby plug rocks, and the xenoliths are usually smaller and much more weathered. Medium and coarse-grained plug rocks lack mantle xenoliths and xenocrysts.

Possible lava lakes have been identified at Bull Mountain (Stockton 1988) and Thoko Hill (Brown et al. 1993),

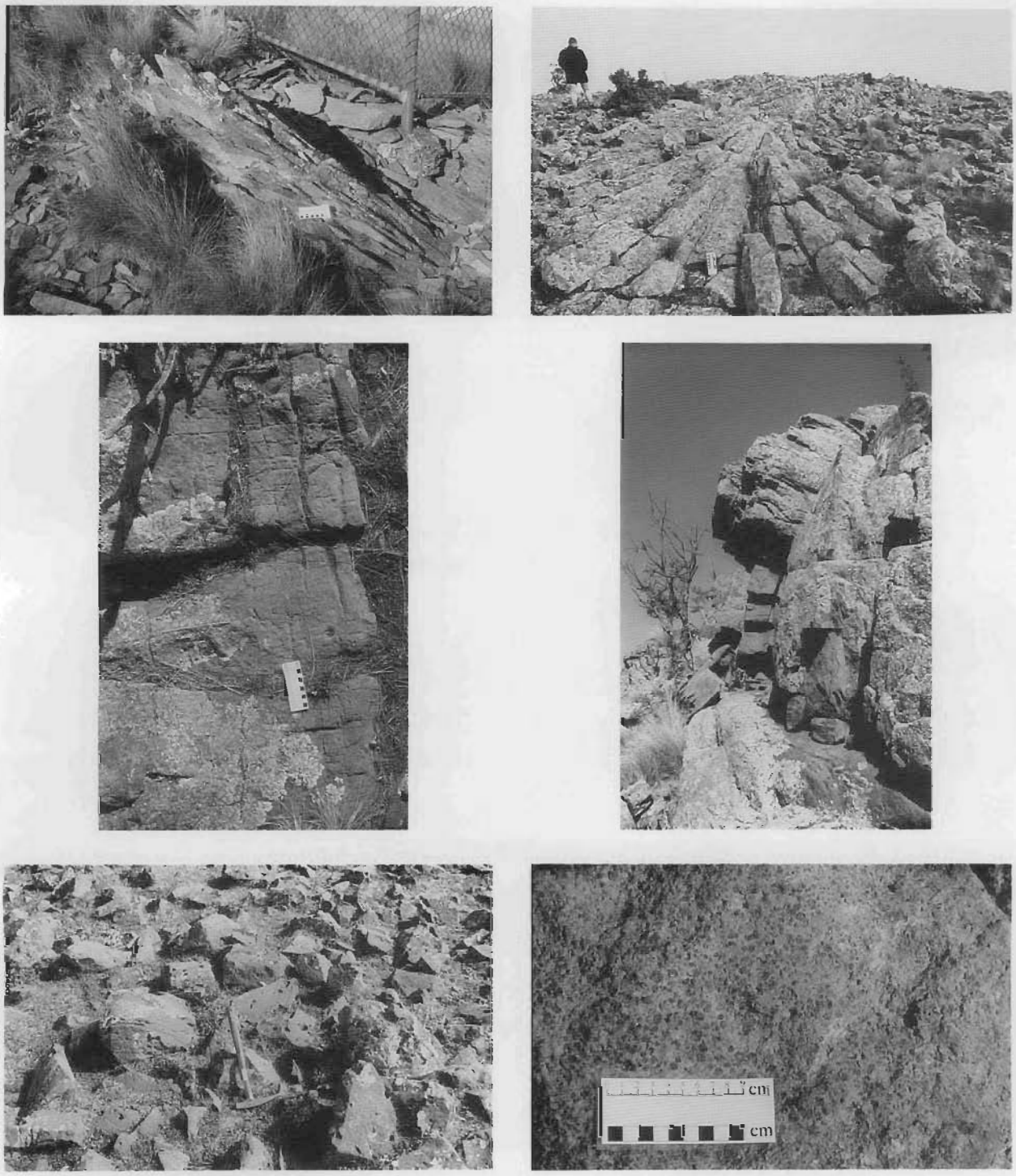

Figure 3. Intrusive and extrusive rocks of the Monaro Volcanic Province.

A. (top left) Finely jointed medium-grained fractionated nepheline basanite on Hudsons Peak. Closely spaced intersecting joints give the outcrop a bladed appearance, not found in any of the other volcanic plugs. Joints dip towards the centre of the plug, to the right in this picture. **B**. (top right) Entablature in a mantle xenolith-bearing aphanitic olivine nephelinite plug The Peak, approx. 3 km ESE of Hudsons Peak. Columns range up to 40 cm wide and over 1 m long; mantle xenoliths range up to 10 cm across. **C**. (centre left) Overhead view of closely spaced radial, concentric and conical joints in medium-grained nepheline hawaiite in the Avonlake East plug. The centre of the plug is to the left of the photograph. Conical joints are near-horizontal in this part of the outcrop. **D**. (centre right) Side view of the Avonlake East plug, showing radial, concentric, and conical joints. Concentric joints curve over, following the isothermal surface of the plug, and conical joints become subvertical near the top of the plug. A 5 cm diameter, 50 cm long tube vesicle is present underneath the prominent overhang in the upper middle of the picture. Fig. 3C is of a small horizontal platform just beneath the bottom of this picture. **E**. (bottom left)'Swiss cheese' rock from the top of the Wangellic Hill plug. This outcrop comprises mantle xenolith-bearing blocky aphanitic olivine nephelinite and is typical of the aphanitic and fine-grained plug rocks of the Monaro Volcanic Province. Prominent flow-banding can be seen in some of the blocks. Holes in the rock are weathering pits after mantle xenoliths. **F**. (bottom right) Coarse pyroxene-phyric alkali lava from one of two flows near the base of Wangellic Hill, one of six known volcanic plugs on the Berridale–Towamba Zone. Pieces of this flow, or that immediately underlying it, are present as xenoliths in the Wangellic Hill plug (Fig. 3E), the top of which is approximately 80 m vertically above this outcrop. Similar rocks cropping out north of Hudsons Peak were named Bondo Dolerite Member by Pratt et al. 1993.

both southeast of Nimmitabel (Fig. 1). Both features are near-circular tabular bodies rising above the surrounding basement rocks. Bull Mountain is 850 m across, about 60 m thick, and composed of medium to coarse-grained titanian augite-cumulate nepheline basanite. Thoko Hill is about 1800 m across, about 65 m thick, and composed of fine to medium-grained alkali olivine basalt. Thoko Hill lavas overlie weathered coarse pyroclastics at its

Figure 4. Volcanic plugs and terraced lavas of the Monaro Volcanic Province.
A. (top left) Hudsons Peak, medium-grained fractionated olivine nephelinite; a prominent landmark on the Monaro Plains at 1231 m ASL. Hudsons Peak lies in the approximate centre of the Bemboka Zone and is accompanied by two smaller plugs of similar composition, one 2.2 km ESE and the other 3.6 km E. View looking NW. **B.** (top right) The Brothers volcanic plugs viewed from the NW. North (left), Middle and South Brother (right) are all composed of mantle xenolith-bearing aphanitic olivine nephelinite and are at the northwestern end of the Bemboka Zone. The terrace at the base of North Brother consists of coarse pyroxene-phyric alkali lava (Fig. 3F). North Brother rises approximately 200 m above the level of the road in the photo. The Brothers are the most prominent landmarks of the northern Monaro Plains. **C.** (centre left) One Tree Hill (left) and an unnamed plug about 4 km E of Hudsons Peak, viewed from the NNE. One Tree Hill consists of mantle xenolith-bearing aphanitic olivine nephelinite and rises about 90 m above the plain in the foreground. The smaller plug is about 3 m high, of similar composition to Hudsons Peak, and appears to be a subsidiary eruption site. **D.** (centre right) Bungee Peak, an aphanitic olivine nephelinite plug, 6 km NW of Wangellic Hill on the Berridale–Towamba Zone. The plug is partly eroded by Bungee Peak Creek, running from right to left in front of the talus slope on the plug. Basalt columns up to 2 m long and 60 cm wide are found on the talus slope; the plug rises about 80 m from the creek bed. View looking NE from the Jincumbilly Road. **E.** (bottom left) Gently east-dipping lava flows in a small butte in the Maclaughlin River valley, about 4 km south of the Avonlake plugs. The lava flows have relatively fresh bases grading up into highly weathered tops, some bauxitised. View looking S. **F.** (bottom right) The twin Avonlake plugs, at the northeastern end of the Berridale–Towamba Zone, consist of medium-grained nepheline hawaiite. The eastern plug (left) is the larger of the two and shows complex radial, concentric, and conical jointing (Fig. 3C, D). Terraced hillslopes in the background comprise alkali olivine basalt flows. View looking SE.

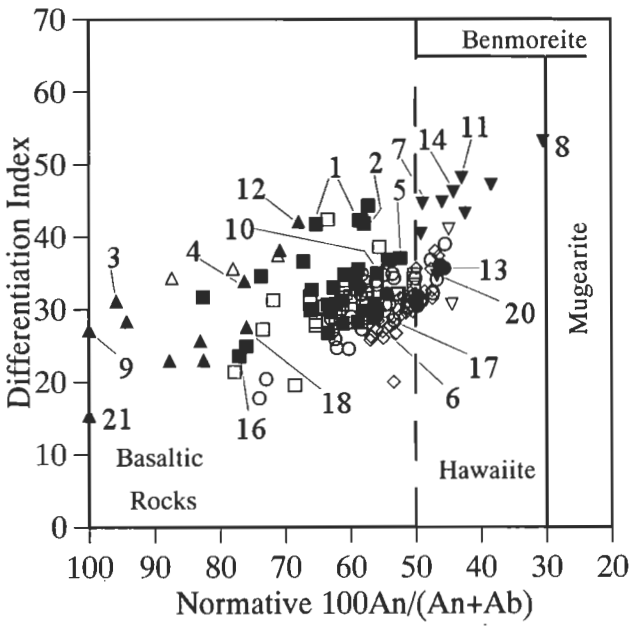

Figure 5. Normative albite versus Differentiation Index classification for 165 volcanic rocks from the Monaro Volcanic Province, following the scheme of Johnson & Duggan (1989). Numbered symbols refer to localities in Figure 1. CIPW norms were calculated by recalculating Fe^{3+}/Fe^{2+} = 0.2 and by normalising major oxides (without LOI) to 100% loss free. Differentiation Index is calculated by DI = Q+Or+Ab+Ne+Lc+Ks. Data include those of Kesson (1973) and the authors.

southern margin. Lava lakes have possibly filled maars formed by phreato-magmatic eruptions. Remnants of a maar have been located at Red Cliff northwest of Bombala (Fig. 1). The maar wall consists of eroded base-surge tuff deposits of alkali olivine basaltic composition, lying very close to the base of the lava pile and near to an alluvium-filled depression, 700 m across (Brown et al. 1993).

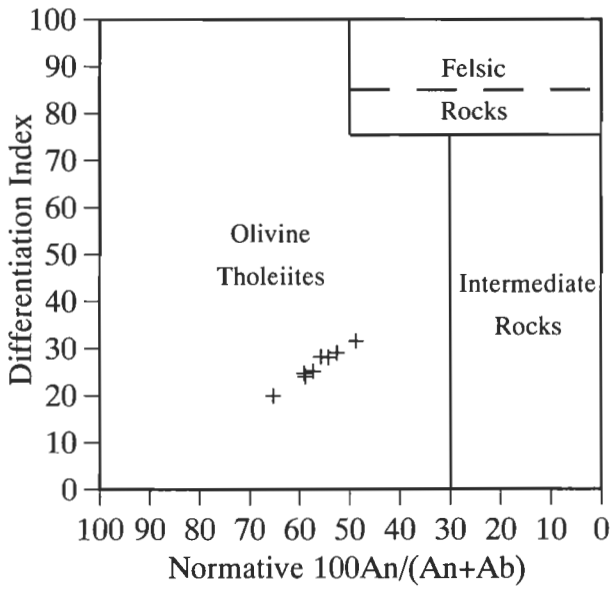

Distribution and structural control of eruption sites

Lineaments in the Monaro Volcanic Province can be traced from basement faults through the lava pile as monoclines or small offsets on some lava flows and bauxite horizons, and as drainage lines on airphotos and satellite images. Some lineaments run parallel to a number of major faults in the basement surrounding the province (Fig. 2). The dominant series of faults in the basement strike north–south (e.g. the Murrumbidgee Fault) and northwest–southeast (e.g. the Berridale Fault—Lambert & White 1965; and the Towamba and Bemboka lineaments). These structures are complemented by a series of northeast–southwest-striking faults and a recently recognised series of east–west-striking structures which are concentrated in the centre of the province (Roach 1991).

Most volcanic plugs are distributed along two northwest–southeast-trending zones parallel to the Bemboka Lineament and the Berridale Fault–Towamba Lineament (Fig. 2). About half of all known plugs in the north of the province fall in a narrow zone, which we have called the Bemboka Zone, running from the south of Cooma to east of Nimmitabel, parallel to the Bemboka Lineament. A smaller concentration of plugs fall in a zone, which we have called the Berridale–Towamba Zone, running from Avonlake to Inverlochie in the central south of the province, parallel to the Berridale Fault–Towamba Lineament. Volcanic plugs outside these two zones are distributed on dominant northeast–southwest structures and subordinate northwest–southeast, north–south and east–west-striking lineaments, generally between the two major zones and in the west and southeast of the province.

The Bemboka Zone coincides with the Great Divide (Fig. 1) for about 40 km. It has a high proportion of nephelinitic and basanitic plugs, and the greatest topographic relief and highest elevation of the Monaro Volcanic Province. The Berridale–Towamba Zone is about 20 km long, and outcrops of coarse titanian augite-phyric alkali lavas are more common adjacent to the two major zones of volcanism. Plugs also appear to be concentrated to the east of the I–S Line, believed to be a major subcrustal terrane boundary (Chappell et al. 1988).

Petrography

Volcanic rocks in the Monaro Volcanic Province have been classified using the scheme of Johnson & Duggan (1989), supplemented by petrographic and geochemical criteria after Best (1982).

Four major rock types have been identified in the volcanic plugs of the Monaro Volcanic Province—nepheline basanite (29 plugs), olivine nephelinite (11 plugs), nepheline hawaiite (9 plugs) and alkali olivine basalt (6 plugs). These rock types occur both as aphanitic to fine-grained and medium to coarse-grained forms, including fractionated feldspar-rich rocks and titanian augite-rich cumulates. Alkali olivine basalt, olivine nephelinite and nepheline basanite are normally distinguished in thin section by the presence or absence of nepheline and plagioclase, the variety of plagioclase and the varieties of phenocryst phases. True nepheline hawaiites are recognised by the presence of more evolved varieties of feldspar, including sanidine, anorthoclase and andesine/oligoclase, and minor pyroxene, opaques and olivine. Major-element mineral compositions, obtained by electron-microprobe analysis, and textural characteristics were used to distinguish melt-derived and mantle xenolith-derived phases in the rocks.

Aphanitic olivine nephelinites contain subhedral to euhedral skeletal and glomerophyric olivine phenocrysts, anhedral mantle-derived olivine xenocrysts, colourless mantle-derived clinopyroxene with purplish titanian augite overgrowths, partially to fully corroded orthopyroxene xenocrysts and rare purplish titanian augite phenocrysts. The groundmass comprises purplish prismatic titanian augite, acicular apatite, blebby to euhedral opaques (mostly titanian magnetite with ilmenite and ulvöspinel exsolutions), euhedral nepheline and/or analcime, microscopic red-brown mica flakes, 0–< 5% modal bytownite feldspar microlites, brown glass and occasional radiating acicular zeolite (thompsonite or natrolite). Clear low-relief haloes are common around microscopic crystals of olivine or titanian augite in these rocks. Electron-microprobe analysis reveals these haloes to be sanidine. Amphibole (kaersutite) is common in the more alkali-rich plugs as rounded fragments, subhedral prisms or cleavage fragments, some over 4 cm across (e.g. Amphibole Hill, Nimmitabel Hill, The Peak; Fig. 1). Amphibole grains show a range of reaction states from entirely unaltered to grains with reaction rims of feldspar, clinopyroxene and rhönite. Pleonaste spinel is a common megacryst phase in a number of plugs. Other megacrysts include titanian magnetite with ilmenite exsolution lamellae, found in two olivine nephelinite plugs at Gourock, and red-brown mica observed in the Glen Lee and Nimmitabel Trig plugs (Fig. 1).

Aphanitic nepheline basanites contain skeletal and glomerophyric melt-derived olivine phenocrysts, anhedral mantle-derived olivine xenocrysts, clear mantle-derived clinopyroxene xenocrysts with purplish titanian augite overgrowths, partially to fully corroded orthopyroxene xenocrysts, purplish titanian augite phenocrysts and glomerocrysts and > 5% modal bytownite/labradorite feldspar in the groundmass. Other minerals in the groundmass include nepheline, analcime, apatite, opaques, red-brown mica, brown glass and occasionally radiating zeolite (thompsonite or natrolite).

Aphanitic alkali olivine basalt contains skeletal and glomerophyric melt-derived olivine phenocrysts, anhedral mantle-derived olivine xenocrysts, single and glomerophyric titanian augite phenocrysts and bytownite/labradorite feldspar phenocrysts, some occurring as radiating clusters of lath-like phenocrysts and needles. The ground mass consists of prismatic titanian augite, acicular apatite, microlites and subhedral blebs of opaque oxides (mostly titanian magnetite), bytownite feldspar microlites, rare red-brown mica, brown glass and some radiating zeolite (thompsonite or natrolite).

Most fine to medium-grained plug rocks are mineralogically similar to aphanitic counterparts. However, coarse-grained fractionated plugs or titanian augite cumulate-rich plugs have a wide range of feldspars and/or large distinctly zoned titanian augite phenocrysts with hourglass zoning, akin to those described by Wass (1973) in rocks from the Southern Highlands Volcanic Province of New South Wales. Fractionated plugs are normally medium to coarse-grained, feldspar-rich (up to about 70% of the mode) and contain feldspar phenocrysts with bytownite cores and andesine rims and interstitial anorthoclase and sanidine. Olivine and titanian augite are scarce in these rocks and olivine is relatively iron-rich (Fo_{40-60}). Feldspar-rich fractionated plugs include the twin Avonlake plugs (nepheline hawaiite; Figs. 3C–D, 4F), Ardmore (fractionated nepheline basanite) and Steeple Flat North (fractionated nepheline basanite; Fig. 1).

Rocks in the Bull Mountain lava lake grade from titanian augite-rich cumulate basanite at the base to a more feldspar-rich variety at the top (Fig. 1). These rocks contain large (up to 1 cm) single and glomerophyric titanian augite phenocrysts, frequently with rims of pale-green aegirine-augite, and feldspar phenocrysts with labradorite cores grading to oligoclase rims. Olivine (Fo_{45-66}), anorthoclase, sanidine and opaques occur in the interstices. Large titanian augite phenocrysts commonly enclose feldspar microlites, which show lath orientation parallel to growth faces. The composition of included feldspars changes from labradorite near the cores of large titanian augite phenocrysts to oligoclase near the rims.

Thick flows of coarse titanian augite-phyric, medium-grained alkali lavas are concentrated in four areas within the province (Figs 1, 3F). These lavas typically have titanian augite-rich bases which grade into feldspar-rich tops and appear to grade laterally into feldspar-rich fine- to medium-grained alkali basalts. In many cases the upper parts of the flows are extremely weathered or have been removed by erosion (Brown et al. 1992; Edgecombe 1992). Titanian augite phenocrysts (up to 2 cm) appear similar to those at Bull Mountain and also similar to those described by Wass (1973) in that they display hourglass zoning. However, they are mostly glomerophyric with olivine and feldspar inclusions in the outer rims. Occasional poorly preserved olivine (Fo_{59-60}) phenocrysts are also noted. The groundmass comprises sanidine and labradorite–bytownite feldspar crystals.

Major element geochemistry

The range of volcanic rocks known in the Monaro Volcanic Province has been broadened from the preliminary study of Kesson (1973) by extending petrographical and geochemical studies to the volcanic plugs. Brown et al. (1988) and Roach (1991) analysed volcanic plugs and discovered several kaersutite-bearing nephelinitic and

Table 1. Major element analyses and CIPW norms of representative plug rocks and lavas from the Monaro Volcanic Province.

	R47	*R46*	*R3*	*R109*	*R42*	*R56*	*R8*	*BO20*	*R146*	*BO9*	*R145*	*R149*
SiO_2	47.00	47.80	47.40	42.10	46.60	43.60	45.90	42.30	45.30	45.60	44.40	47.20
TiO_2	2.03	1.84	1.96	2.20	2.86	2.95	2.03	2.07	2.03	1.85	1.67	1.73
Al_2O_3	14.89	14.26	16.95	13.42	15.82	14.38	16.93	12.70	14.08	11.50	13.56	14.38
Fe_2O_3	1.79	1.69	1.72	1.83	1.80	1.75	1.53	1.85	1.91	1.75	1.99	1.88
FeO	8.94	8.44	8.58	9.14	9.00	8.75	7.66	9.26	9.57	8.77	9.96	9.14
MnO	0.16	0.16	0.18	0.19	0.18	0.16	0.17	0.16	0.17	0.14	0.16	0.16
MgO	7.73	9.01	5.37	12.01	3.96	9.15	5.80	12.60	10.20	11.60	11.62	9.85
CaO	10.38	9.32	10.24	10.69	8.18	7.87	9.79	10.40	10.85	13.40	9.20	8.29
Na_2O	2.64	3.28	3.79	2.38	3.89	5.19	4.45	3.70	2.32	2.20	1.71	2.56
K_2O	1.73	1.54	1.46	1.49	2.67	2.70	2.50	1.32	1.12	0.86	0.74	1.23
P_2O_5	0.69	0.72	0.76	1.04	0.84	1.49	1.28	1.10	0.45	0.38	0.40	0.51
H_2O+	0.89	1.35	1.30		3.90	1.58	1.44	1.40	1.01	1.00	2.94	1.60
H_2O-	0.74	0.32	0.33		0.80	0.44	0.23	0.20	0.80	0.30	1.35	1.07
CO_2	0.10	0.31	0.06		0.03	0.08	0.21	0.10	0.06	0.20	0.07	0.07
LOI	0.96	1.98	1.69	3.38	4.73	2.10	1.88	1.70	1.00	1.50	3.46	1.96
Rest		0.00	0.00		0.00	0.00	0.00	0.70		0.51		
Total	**100.43**	99.95	**99.95**	99.44	**100.21**	99.96	99.86	99.55	100.61	99.84	102.61	101.19
mg-ratio	59.11	64.08	51.03	69.09	43.02	63.61	55.84	69.59	64.07	68.84	66.80	64.62
Or	10.46	9.30	8.78	9.17	16.56	16.32	15.10	8.03	6.77	5.19	4.61	7.53
Ab	20.29	23.94	23.04	6.65	23.65	8.50	13.72	4.61	15.39	8.89	15.26	22.45
An	24.22	20.08	25.39	22.42	18.71	8.16	19.26	14.57	25.28	19.39	28.64	25.00
Ne	1.39	2.40	5.20	7.75	5.90	19.73	13.41	14.96	2.54	5.49	0.00	0.00
Mt	2.59	2.45	2.49	2.65	2.61	2.54	2.22	2.69	2.77	2.54	2.89	2.65
Il	3.94	3.57	3.79	4.35	5.70	5.73	3.94	4.05	3.94	3.59	3.35	3.41
Ap	1.63	1.70	1.79	2.51	2.04	3.53	3.03	2.62	1.07	0.90	0.98	1.22
Di	19.42	18.11	17.51	20.67	15.00	17.60	17.82	25.04	21.69	37.05	13.54	11.47
Hy	0.00	0.00	0.00	0.00	0.00	0.00	0.00	0.00	0.00	0.00	11.66	9.92
Ol	16.05	18.45	12.01	23.82	9.83	17.89	11.49	23.44	20.55	16.95	19.08	16.34
D.I.	32.14	35.64	37.03	23.57	46.11	44.55	42.23	27.60	24.70	19.58	19.88	29.98
N.P.	54.42	45.62	52.42	77.12	44.17	48.96	58.39	75.96	62.16	68.56	65.23	52.69

CIPW norms are calculated using the method of Johnson & Duggan (1989) with $Fe^{3+}/Fe^{2+} = 0.2$. The mg-ratio is calculated using 100Mg/(Mg+ΣFe) after setting the major oxides (without LOI) to 100% loss free and recalculating the Fe-ratio. The Differentiation Index (D.I.) is calculated by Q+Or+Ab+Ne+Lc+Ks. The Normative Plagioclase (N.P.) is calculated by 100An/(An+Ab). Primary rocks in the Monaro Volcanic Province are considered as those with mg >67 and Ni and Cr >200 ppm. Refer to Figure 1 for plug locations. R47: Fractionated alkali dolerite from the lava lake at Thoko Hill. R46: Near-primary alkali olivine basalt from the Brown Mountain plug. R3: Fractionated nepheline basanite from the Ardmore plug. R109: Primary nepheline basanite from the Rosemount cone sheet. R42: Relatively highly fractionated nepheline hawaiite from the twin Avonlake plugs. R56: Kaersutite-rich nepheline hawaiite from Nimmitabel Hill. R8: Fractionated olivine nephelinite from Hudsons Peak. BO20: Primary olivine nephelinite from Bungee Peak (6 km NW of Wangellic Hill). R146: Coarse pyroxene-phyric alkali lava (part of the Bondo Dolerite) from the base of The Brothers (Fig. 4B; 8 km NNE of Hudsons Peak). BO9: Coarse pyroxene-phyric alkali lava from Mount Cooper, 3.5 km ENE of Wangellic Hill. R145: Olivine tholeiite lava from near the eastern base of The Brothers. R149: Transitional basalt lava from near the eastern base of the Brothers.

basanitic plugs and feldspar-rich nepheline hawaiite plugs. The main geochemical characteristics of the province are summarised below and representative analyses are provided in Table 1.

All the volcanic rocks have a low SiO_2 content, ranging from 40.2 to 48.5 wt % (Fig. 6). The SiO_2 content is not normally distributed, and there are three modes on the SiO_2 histogram at approximately 40.25, 44.25 and 46.7 wt % SiO_2 (Fig. 7). Total alkalis vary between 2.5 wt % (olivine tholeiite) and 9.1 wt % (kaersutite-rich nepheline hawaiite) and Na_2O is always more abundant than K_2O (Fig. 6). Some analyses are contaminated with amphibole, resulting in some kaersutite-rich nephelinitic and basanitic plug rocks plotting in the nepheline hawaiite field rather than the nepheline basanite field in Figure 5. These rocks (e.g. Nimmitabel Hill, Glen Lee, Nimmitabel Trig and Amphibole Hill; Figs 1, 6) contain up to 20% modal kaersutite, but are obviously basanitic to nephelinitic by their mineralogy. Most analyses show a high mg-ratio (Fig. 8), although those with mg > 70 are moderately to highly contaminated with mantle material. The more fractionated feldspar-rich rocks (e.g. Avonlake, Bull Mountain) lie between mg 62 and mg 44, but some of the kaersutite-rich plugs (e.g. Glen Lee, Nimmitabel Trig) also appear fractionated, probably because of the additional iron and calcium provided by abundant kaersutite.

Rocks with < 45 wt % SiO_2 are all olivine- and nepheline-normative (Fig. 9). Rocks with > 45 wt % SiO_2 are mostly olivine- and hypersthene-normative. All of the volcanic plugs and other intrusives analysed are nepheline-normative (Fig. 9). Many of the flows are also nepheline-normative, but none are as undersaturated as the alkali-rich plugs. While the majority of flows are nepheline normative (71), a large minority are hypersthene-normative and are transitional (31) or tholeiitic (8).

All of the rocks contain modal olivine, titanian augite, opaque oxides and apatite and nearly all contain plagio-

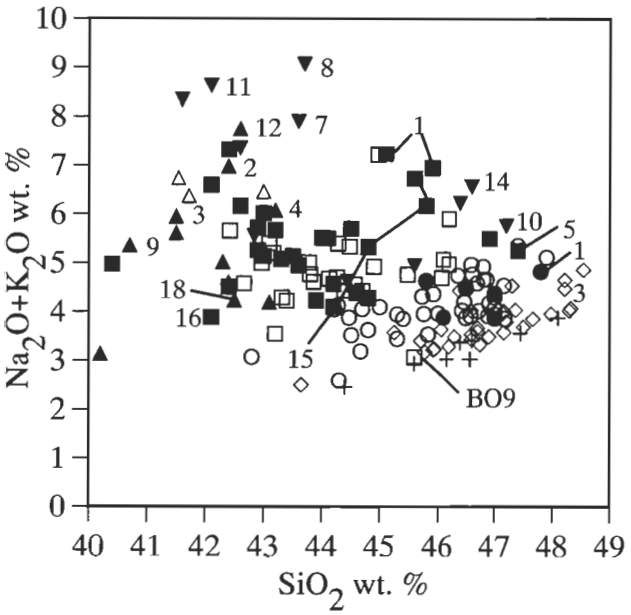

Figure 6. Total alkali–silica diagram for 165 basaltic rocks from the Monaro Volcanic Province (symbols as in Fig. 5). Numbered symbols refer to localities in Figure 1. Data include those of Kesson (1973) and the authors. Joined symbols represent four analyses from different levels of the Bull Mountain lava lake (location 15). Sample BO9 is of coarse pyroxene-phyric alkali lava near Wangellic Hill (Fig. 3F).

clase. Total normative mafic mineral content is mostly 45%. Normative albite is normally > 50, except in a few of the more fractionated rocks.

The compositions of rocks from the lava flows and plugs show some overlap in chemical abundances, but have some significant differences, which are well illustrated on the total alkali–silica diagram (Fig. 6) and normative plots (Fig. 9). All the known plug rocks are nepheline-normative, suggesting that the feeders for the hypersthene-normative lavas have not yet been located or sampled because they are either covered by later flows or are relatively inconspicuous. The latter is likely because nepheline-normative feeders have been recognised by their strong contrast in composition to surrounding hypersthene-normative lavas. Lavas and pyroclastics corresponding to the nepheline-normative plugs were probably deposited at the top of the volcanic pile, and may have been largely removed by subsequent erosion.

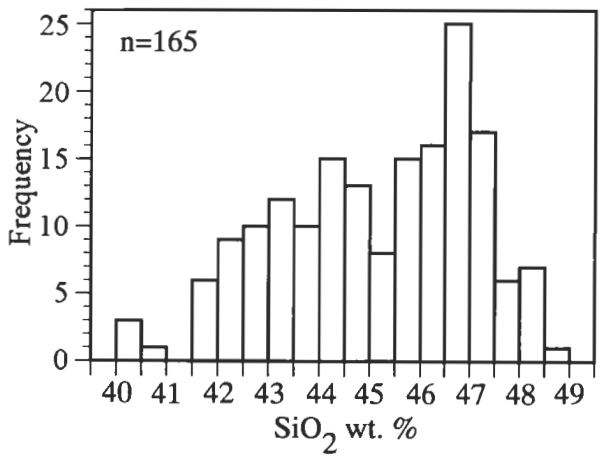

Figure 7. SiO_2 histogram of 165 basaltic rocks from the Monaro Volcanic Province. Data include those of Kesson (1973) and the authors.

Xenoliths and xenocrysts

Most aphanitic and fine-grained plugs in the province contain crustal and mantle xenoliths and xenocrysts. Olivine nephelinite and low-silica nepheline hawaiite plug rocks tend to contain mantle and crustal xenoliths, together with amphibole and red-brown mica megacrysts, in varying proportions. Nepheline basanite and alkali olivine basalt plugs tend to contain mantle and crustal xenoliths only.

Mantle xenoliths are generally coarse-grained, equant, granular members of the Cr-diopside suite (O'Reilly & Griffin 1988), containing olivine, orthopyroxene, clinopyroxene (apple-green Cr-diopside) and Cr-spinel. They range in size from small ragged fragments (< 5 mm) to large angular and sub-rounded nodules over 10 cm across in some plugs (e.g. Amphibole Hill, The Peak; Fig. 1). The majority of mantle xenoliths are spinel lherzolites and harzburgites. Wehrlites, pyroxenites and dunites form only a small portion of the assemblage (Roach 1991; Edgecombe 1992).

Titanian pargasite amphibole is found in textural equilibrium with the other phases in spinel lherzolite xenoliths from the Glen Lee, Amphibole Hill and Wangellic Hill plugs (Roach 1991). Phlogopite was noted in a vein in one spinel lherzolite xenolith (Edgecombe 1992) and a thin vein of clinopyroxenite in another (Roach 1991) from the Amphibole Hill plug. Strong foliation or other tectonic fabrics are generally not noted in the mantle xenoliths; however, a foliated wehrlite band was noted in one lherzolite xenolith from the Rosemount cone sheet (Edgecombe 1992; Fig. 1). Most olivine grains in mantle xenoliths possess variable extinction perpendicular to

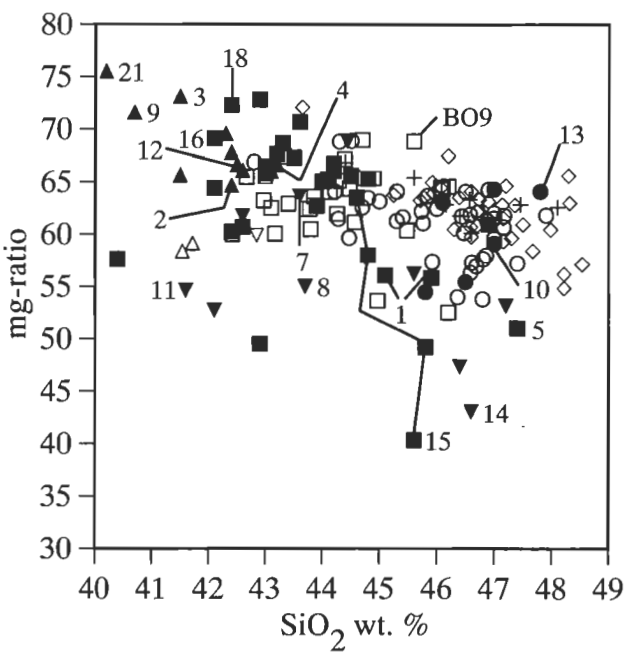

Figure 8. SiO_2 versus mg-ratio for 165 basaltic rocks from the Monaro Volcanic Province. Data include those of Kesson (1973) and the authors (symbols as in Fig. 5). Numbered symbols refer to localities in Fig. 1. The mg-ratio is calculated as $100Mg/(Mg+\Sigma Fe)$ using $Fe^{3+}/Fe^{2+} = 0.2$.

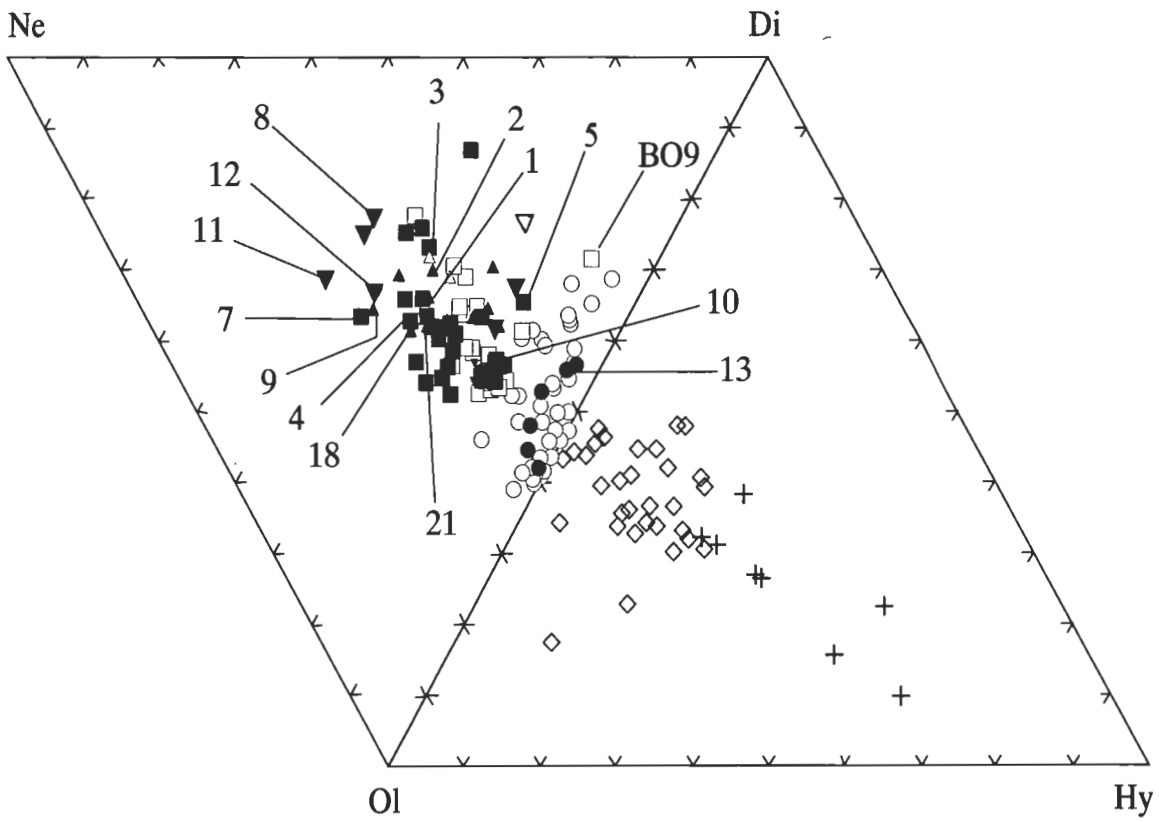

Figure 9. Normative compositions in the field Ne–Ol–Di–Hy for 165 basaltic rocks from the Monaro Volcanic Province (symbols as in Fig. 5). CIPW norms were calculated by normalising major oxides (without LOI) to 100% loss free and recalculating Fe^{3+}/Fe^{2+} = 0.2. Sample BO9 is of the coarse pyroxene-phyric alkali lava near Wangellic Hill (Fig. 3F). Data include those of Kesson (1973) and the authors.

fractures within individual grains, suggesting limited deformation (Roach 1991; Edgecombe 1992).

Mantle xenocrysts are anhedral and consist of olivine, Cr-spinel, orthopyroxene and clinopyroxene derived from disaggregated mantle xenoliths. In thin-section, the olivine xenocrysts usually have variable extinction and ragged edges and, in some cases, have a reaction rim of microscopic opaques. Orthopyroxene xenocrysts are surrounded by reaction coronas of microscopic clinopyroxene and opaques where they have reacted with the melt. Clinopyroxene xenocrysts are clear or greenish in colour and may exhibit euhedral overgrowths of purplish titanian augite which has crystallised from the melt around the central xenocryst as a coloured corona, usually in optical continuity with the core. Cr-spinel xenocrysts are red-brown in colour, although rare grey-coloured Fe-spinel is noted from the One Tree Hill plug (Fig. 1).

Crustal xenoliths include equant, coarse-grained two-pyroxene plagioclase granulite and metasediments (quartzite, feldspathic quartzite), while the crustal xenocrysts include single quartz grains and compositionally zoned feldspars. The feldspars are the only foreign phase preserved in the more coarse-grained plug rocks of the province. All the crustal xenoliths and xenocrysts, except for the granulites, are surrounded by a thick reaction corona of titanian augite and glass.

Discussion

Fractures in the Palaeozoic basement have had a major influence in controlling the location of eruption sites within the Monaro Volcanic Province. All known plugs lie on one or more known faults or lineaments which can be traced through the covering lavas to major fractures in the basement outside the province (Fig. 2). Fractures which appear to have had most control on the location of volcanic plugs are large northwest–southeast-striking fractures and lineaments and a conjugate set of subsidiary northeast–southwest-striking fractures.

Eruption sites are concentrated in two broad, linear zones: the Bemboka Zone, between Cooma and Nimmitabel, and the Berridale–Towamba Zone, located above the Berridale–Towamba Lineament (Fig. 2). The Berridale–Towamba Lineament is a major crustal structure with a long history of movement. Many of the volcanic plugs in the zones are aligned on northwest–southeast trends parallel to major basement fractures, although a minority also appear to be more directly controlled by shorter conjugate northeast–southwest-trending fractures. Extension of the crust normal to the structures or, possibly, transtensional movement along the structures in the Early Tertiary would have provided a suitable conduit for basaltic magmas rising from the upper mantle.

The concentration of eruption sites on the Bemboka Zone and the Berridale–Towamba Zone is consistent with the palaeo-stress field in southeastern Australia and opening along existing northwest–southeast-trending structures and, to a lesser extent, their northeast–southwest-trending conjugates during the time of active volcanism. In-situ compressive stress measurements from boreholes by Denham (1988) indicate a present northwest–southeast compression in southeastern Australia, similar to the

theoretical stress field of Cloetingh & Wortel (1985). Pilger (1982) mapped the orientations of mafic dykes and aligned volcanic centres throughout eastern Australia and concluded that the stress field in southeastern Australia was tensional in a northeast–southwest direction for a time during the Tertiary. Duncan & McDougall (1989) suggested that a period of crustal tension, or at least relaxation, occurred from about 80 Ma to about 35 Ma, coinciding with a period of slow plate motion on the Indo-Australian plate and the opening of the Tasman Sea, thus promoting intraplate lava field volcanism in eastern Australia.

A large number of basanitic and nephelinitic plugs are concentrated along the Bemboka Zone, which has the highest elevation in the Monaro Volcanic Province and coincides with the position of the current Great Divide (Fig. 1). The Bemboka Zone also has the greatest topographic relief of the province and, therefore, is regarded by us as the site of the most sustained or most recent volcanism. The trend of this zone, which is parallel to the Berridale–Towamba Lineament and in line with a mapped basement fault and the Bemboka Lineament, suggests that it is also developed along a major crustal structure with a similar tectonic history. These crustal structures probably represented a window to the lower crust and upper mantle which moved across sites of magma generation during movement of the Australian plate in the Early to Middle Tertiary. This mechanism could explain the overall spatial concentration of sporadic basaltic volcanism in this area to form the Monaro Volcanic Province. Radiometric age determinations for volcanic plugs are limited and at this stage it is not possible to assess the detailed timing of volcanism along the two zones. K–Ar ages for two plugs on the Bemboka Zone—Hudsons Peak, 39.5 ± 1.0 and 37.2 ± 1.0 Ma (Wellman & McDougall 1974) and Amphibole Hill, 47.7 ± 0.3 Ma (Taylor et al. 1990)—indicate volcanism at least between 47 and 37 Ma. No K–Ar ages are available for plugs on the Berridale–Towamba Zone, although a sample of the coarse pyroxene-phyric alkali lava from near the base of the lava pile close to this zone yielded a K–Ar age of 51.0 ± 0.3 Ma (Taylor et al. 1990).

Outcrops of the coarse pyroxene-phyric alkali lavas are concentrated around the Bemboka Zone and the Berridale–Towamba Zone (Fig. 1). These lavas are pyroxene-rich, moderately fractionated alkali basalts and basanites, which probably represent crystal-rich cumulates erupted from crustal magma chambers or reservoirs located in or near the two major zones of volcanism. The depth of these reservoirs is not known, but the fractional crystallisation of the large pyroxenes in the lavas appears to have occurred at low pressure, as interpreted by Wass (1973) for similar rocks from the Southern Highlands Province of New South Wales. Outcrops of these lavas appear to occur at various levels of the lava pile, so the lithostratigraphic name Bondo Dolerite Member (Pratt et al. 1993) should not be used to describe all these rocks.

A series of east–west-striking lineaments (Roach 1991) have been observed within the immediate vicinity of the lava pile. Because these are centred on the main part of the province and do not penetrate far into the Palaeozoic basement away from the lava pile, they are believed to be the direct result of volcanism and could represent fractures which accommodated stress caused by magmatic underplating and doming of the crust (Roach 1991).

Volcanism in the province commenced from widely spaced centres with some suggestion of a period of phreato-magmatic activity in the water-saturated low-lying areas and the formation of alkali basaltic cinder cones in higher, drier parts. Evidence of possible phreato-magmatic volcanism exists as an eroded base-surge deposit in the walls of Cambalong Creek near Red Cliff (Fig. 1). Evidence of possible cinder cone volcanism also exists as deposits of pyroclastic material at the southern base of Thoko Hill. Other deposits have possibly been covered by later lavas or rapidly eroded on exposure.

Fluid, lava-field style volcanism appears to have been the dominant style of activity, filling well established stream valleys in the basement (cf. Taylor et al. 1990). Eruptions appear to have been sporadic and from numerous vents. Lavas were dominantly alkali olivine basalt and transitional basalt with minor olivine tholeiite in the early development of the volcanic pile, but nepheline basanite and olivine nephelinite lavas became more abundant as volcanism progressed. The most likely reason for the change in silica saturation with time is that the heat source driving volcanism in the province gradually waned, producing a smaller percentage partial melt and more undersaturated magmas (Frey et al. 1977) until volcanism ceased in the Middle Tertiary.

Lava flows became interbedded with lacustrine and river sediments, including fluvial and lacustrine gravel, sand, silt and clay, and hyaloclastite deposits where lavas flowed into lakes or rivers (Taylor et al. 1990; Brown et al. 1992, 1993). Fossilised wood and low-grade coals are also interbedded with lava flows (Taylor et al. 1990). The presence of these materials suggests that some pre-basaltic river systems were dammed during the period of volcanism and there were long pauses between subsequent lava flows—the latter being inferred from the thickly bedded interflow sediments in some areas.

Periods of significant volcanic quiescence are also indicated by the presence of cool-climate bauxite horizons within the volcanics (Taylor et al. 1990; Brown et al. 1992). Wellman & McDougall (1974) suggested that breaks in volcanic activity may have been as long as 3 Ma and that volcanism occurred in three distinct periods: at 53 Ma, 49–45 Ma and 39–36 Ma. However, the Bega (BMR) No. 7 drill hole indicates the existence of no less than seven individual weathering profiles within lava flows near Myalla Lake (Brown et al. 1992). This evidence suggests that volcanism was either sporadic or occurred at widely spaced centres, thus giving the appearance of periods of inactivity.

The majority of volcanic plugs discovered are basanitic and only eleven nephelinitic, nine hawaiitic and six alkali basaltic plugs have been recognised. This situation may be due to burial of the earlier alkali basaltic, transitional and tholeiitic eruption sites. These plugs may also be under-represented because they are more difficult to detect, owing to their petrographic and geomorphic similarity to the surrounding lavas. Alternatively, earlier eruption sites may have become conduits for later, more undersaturated magmas, destroying the evidence of the former eruptions.

The new evidence for numerous eruption sites concentrated along two linear zones controlled by major basement structures, together with geochemical evidence indicating that the volcanic rocks in the province are relatively

unfractionated (Kesson 1973; Roach 1991) and the large age range of the province, clearly indicates that the volcanic pile was not erupted from a central volcano. Eastern Australian central volcanoes contain a range of primary to highly fractionated intrusive and volcanic rocks and normally exhibit large-scale structures such as collapsed calderas, ring dykes, concentric dykes and sills (Cas 1989). None of the highly fractionated rocks associated with eastern Australian central volcanoes are found within the Monaro Volcanic Province, nor are there any remnants of the typical large-scale structures. Central volcanoes also typically show gravity and magnetic anomalies associated with a central intrusive complex (Wellman 1989). Taylor et al. (1989) noted that such anomalies are lacking in the Monaro Volcanic Province.

Conclusions

We have introduced a method for recognising eruption sites in the eroded terrain of the Monaro Volcanic Province. Not all sites are as immediately recognisable as some of the larger plugs in the province, but with careful study we hope to recognise more plugs in areas which appear to have extensive basalt cover, but no eruption sources. The location of eruption sites was largely controlled by major fractures within the Palaeozoic basement resulting in two northwest–southeast-trending concentrations of plugs on the Bemboka Zone and Berridale–Towamba Zone and others dispersed widely over the length and breadth of the province. Reactivation or tensional opening along these pre-existing fractures in response to northeast–southwest tensional stress appears to be the most likely method for magma emplacement. All evidence indicates that volcanism was of a lava-field style and was not related to a central volcanic complex. The resultant lava pile was irregular and partly bounded by basement escarpments, rather than being circular (cf. Ollier & D. Taylor 1988). Volcanism is now recognised to have been very sporadic in nature, rather than occurring in three distinct pulses as Wellman & McDougall (1974) suggested. Although long pauses are indicated by deep weathering profiles and bauxites within the lava pile, volcanism probably occurred in other areas of the province while local cessations endured.

Acknowledgments

The authors thank the Haylock Family of Yandra Station via Nimmitabel, NSW, for accommodation in the field. We also thank P.C. Lewis, G.W. Pratt and the New South Wales Geological Survey for providing information and funds for some of the geochemical analyses. K.R. Sharp of Cooma, New South Wales, provided mapping data for the coarse pyroxene-phyric lavas in the northwest of the province. D.J. Ellis (Department of Geology, ANU) and W.F. McDonough and R.L. Rudnick (Research School of Earth Sciences, ANU) provided advice and constructive criticism to I.C.R. N. Ware (Research School of Earth Sciences, ANU) helped with the electron-microprobe analyses. P. Millsteed and G. Fisher (University of Canberra) provided technical support. P. Ogilvie (University of Canberra) photographed the maps and processed the prints in this paper. The Department of Geology, ANU, provided rock-crushing facilities. This research was supported by a University of Canberra Research grant. The authors thank M.B. Duggan, R.W. Johnson, A. Robertson, R.W. Schön, M.J. Sheared and F.L. Sutherland for their comments on an early version of the manuscript. I.C.R. thanks Leanne Langton for her continuing support of his studies.

References

Barnes, R.G. & Herzberger, G.A. 1975. *Bega 1:250 000 Metallogenic Map.* Geological Survey of New South Wales, Sydney.

Best, M.G. 1982. *Igneous and Metamorphic Petrology.* W.H. Freeman and Co., New York.

Brown, M.C., Clarke, I., McQueen, K.G. & Taylor, G. 1988. Early Tertiary volcanism in the Southern Monaro Region, New South Wales. *Geological Society of Australia, Ninth Australian Geological Convention, Abstracts*, 21.

Brown, M.C., McQueen, K.G. & Taylor, G. 1992. A core through the Monaro basalt: Bega (BMR) No. 7. *Australian Journal of Earth Sciences*, 39, 555–559.

Brown, M.C., McQueen, K.G., Roach, I.C. & Taylor, G. 1993. Monaro Volcanic Province. IAVCEI Canberra 1993 excursion guide. *Australian Geological Survey Organisation, Record* 1993/61.

Browne, W.R. 1914. The geology of the Cooma district, NSW, Part I. *Journal of the Royal Society of New South Wales*, 48, 172–222

Cas, R.A.F. 1989. Lava forming eruptions and flow features. *In* Johnson, R.W. (editor), *Intraplate Volcanism in eastern Australia and New Zealand.* Cambridge University Press, Melbourne, 57–68.

Chappell, B.W., White, A.J.R. & Hine, R. 1988. Granite provinces and basement terranes in the Lachlan Fold Belt, southeastern Australia. *Australian Journal of Earth Sciences*, 35, 505–521.

Clark, I. 1987. Compositional variation in the Monaro Basalt on the Bombala 1:100,000 scale sheet. Canberra College of Advanced Education research paper (unpublished).

Clarke, W.B., 1860. *Researches in the Southern Goldfields of New South Wales.* Reading and Wellbank, Sydney.

Cloetingh, S. & Wortel, R. 1986. Stress in the Indo-Australian Plate. *Tectonophysics*, 132, 49–67.

Crook, K.A.W., Bein, J., Hughes, R.J. & Scott, P.A. 1973. Ordovician and Silurian history of the southeastern part of the Lachlan Geosyncline. *Journal of the Geological Society of Australia*, 20(2), 113–138.

Denham, D. 1988. Australian seismicity—the puzzle of the not so stable continent. *Seismological Research Letters*, 59(4), 235–240.

Duncan, R.A. & McDougall, I. 1989. Volcanic time–space relationships. *In* Johnson, R.W. (editor), *Intraplate Volcanism in eastern Australia and New Zealand.* Cambridge University Press, Melbourne. 43–53.

Edgecombe, S.M. 1992. The geochemistry and geological setting of a suite of spinel bearing xenoliths from the Monaro Volcanic Province, southeastern New South Wales. Australian National University, Honours thesis (unpublished).

Frey, F.A., Green, D.H. & Roy, S.D. 1977. Integrated models of basalt petrogenesis: a study of quartz tholeiites to olivine melilitites from south eastern Australia utilizing geochemical and experimental petrological data. *Journal of Petrology*, 19(3), 463–513.

Hopwood, T.P. 1976. Stratigraphy and structural summary of the Cooma Metamorphic Complex. *Journal of the Geological Society of Australia*, 23(4), 345–360.

Johnson, R.W. (editor) 1989. *Intraplate Volcanism in eastern Australia and New Zealand.* Cambridge University Press, Melbourne.

Johnson, R.W. & Duggan, M.B. 1989. Rock classification and analytical data bases. *In* Johnson, R.W. (editor),

Intraplate Volcanism in eastern Australia and New Zealand. Cambridge University Press, Melbourne, 12–13.

Kesson, S.E. 1973. The primary geochemistry of the Monaro alkaline volcanics, southeastern Australia—evidence for upper mantle heterogeneity. *Contributions to Mineralogy and Petrology*, 42, 93–108.

Knutson, J. & Brown, M.C. 1989. Monaro, Snowy Mountains and South Coast. *In* Johnson, R.W. (editor), *Intraplate Volcanism in eastern Australia and New Zealand*. Cambridge University Press, Melbourne, 130–131.

Lambert, I.B. & White, A.J.R. 1965. The Berridale Wrench Fault: a major structure in the Snowy Mountains of New South Wales. *Journal of the Geological Society of Australia*, 12, 25–33.

McQueen, K.G., Taylor, G. & Brown, M.C. 1986. The Cambalong Complex: a new metamorphic complex in southeastern N.S.W. *Proceedings of the Linnean Society of New South Wales*, 108(4), 287–291.

Munksgaard, N.C. 1988. Source of the Cooma granodiorite, New South Wales—a possible role of fluid–rock interactions. *Australian Journal of Earth Sciences*, 35, 363–377.

Ollier, C.D., & Taylor, D. 1988. Major geomorphic features of the Kosciusko-Bega region. *BMR Journal of Australian Geology & Geophysics*, 10, 357–362.

O'Reilly, S.Y. & Griffin, W.L. 1988. Mantle metasomatism beneath western Victoria, Australia: I. Metasomatic processes in Cr-diopside lherzolites. *Geochimica et Cosmochimica Acta*, 52, 433–447.

Pilger, R.H. 1982. The origin of hotspot tracks: evidence from eastern Australia. *Journal of Geophysical Research*, 87, 1825–1834.

Powell, C. McA. 1983. Tectonic relationship between the Late Ordovician and Late Silurian palaeogeographies of southeastern Australia. *Journal of the Geological Society of Australia*, 30, 353–373.

Pratt, G.W., Lewis, P.C., Taylor, G., Brown, M.C., Roach, I.C. & McQueen, K.G. 1993. The Monaro Volcanics of the Cooma district. *Geological Survey of New South Wales Quarterly Notes*, 92.

Price, R.C. & Taylor, S.R. 1977. The rare earth element geochemistry of granite, gneiss and migmatite from the Western Metamorphic Belt of south-eastern Australia. *Contributions to Mineralogy and Petrology*, 62, 249–263.

Roach, I.C. 1991. The petrology and geochemistry of the Monaro volcanic plugs. University of Canberra, Honours thesis (unpublished).

Stockton, I. 1988. Electron probe study of fractionated minerals from the Bull Mountain volcanic plug. Canberra College of Advanced Education, Special Studies Unit (unpublished).

Taylor, G., Taylor, G.R., Bink, M., Foudoulis, C., Gordon, I., Hedstrom, J., Minello, J. & Whippy, F. 1985. Pre-basaltic topography in the Northern Monaro and its implications. *Australian Journal of Earth Sciences*, 32, 65–71.

Taylor, G., McQueen, K.G. & Brown, M.C. 1989. Discussion: major geomorphic features of the Kosciusko–Bega region. *BMR Journal of Australian Geology & Geophysics*, 11, 123–125.

Taylor, G., Truswell, E.M., McQueen, K.G. & Brown, M.C. 1990. Early Tertiary palaeogeography, landform evolution, and palaeoclimates of the Southern Monaro, N.S.W., Australia. *Palaeogeography, Palaeoclimatology, Palaeoecology*, 78, 109–134.

Wass, S.Y. 1973. The origin and petrographic significance of hour-glass zoning in titaniferous clinopyroxenes. *Mineralogical Magazine*, 39(302), 133–144.

Wellman, P. 1989. Upper mantle, crust and geophysical volcanology of eastern Australia. *In* Johnson, R.W. (editor), *Intraplate Volcanism in eastern Australia and New Zealand*. Cambridge University Press, Melbourne.

Wellman, P. & McDougall, I. 1974. Potassium–argon ages on the Cainozoic volcanic rocks of New South Wales. *Journal of the Geological Society of Australia*, 21(3), 247–272.

White, A.J.R., Williams, I.S. & Chappell, B.W. 1975. The Jindabyne Thrust and its tectonic, physiographic and petrogenetic significance. *Journal of the Geological Society of Australia*, 23, (1), 105–112.

Williams, I.S., Compston, W., Chappell, B.W. & Shirahase, T. 1975. Rubidium-strontium age determinations on micas from a geologically controlled composite batholith. *Journal of the Geological Society of Australia*, 22, 497–505.

Burst, J.F., 1965. Subaqueously formed shrinkage cracks in clay. *Journal of Sedimentary Petrology*, 35, 348–353.

Davies, G.R., 1970. Algal-laminated sediments, Gladstone Embayment, Shark Bay, Western Australia. *In* Logan, B.W., Davies, G.R., Read, J.F. & Cebulski, D.E. (editors). Carbonate sedimentation and environments, Shark Bay, Western Australia. *American Association of Petroleum Geologists, Memoir* 13, 169–205.

Friedman, G.M. & Sanders, J.E., 1978. *Principles of Sedimentology*. Wiley, New York.

Wellman, P. & McDougall, I., 1974, Cainozoic igneous activity in Eastern Australia. *Tectonophysics*, 23, 49–65.

Illustrations

Line diagrams or maps should be professionally drafted. (AGSO can provide a full professional drafting service to *Journal* standards at competitive rates. See advertisement below.) Figures should be designed for reproduction at either single column (80 mm) or double column (165 mm) width. Final versions of line drawings should be supplied as high-contrast photographic prints, but photocopies of draft figures may be submitted initially (see **Submissions** above).

All illustrations, both line drawings and photographs, are referred to as figures.

Figures should be numbered consecutively, in the order in which they are referred to in the text, with parts of an individual figure identified, if necessary, by upper case letter.

Do not draft figure titles on the figure. Captions are typeset and should be listed on a separate sheet.

Photographs should be good quality glossy prints. Scale in photographs should be indicated by either a recognisable object or a plain bar scale whose length is given in the figure caption.

Figures are reproduced in black and white unless special arrangements for use of colour have been made with the editor.

Tables

Tables should be set out on separate sheets. When preparing tables, if possible, please use the Tables function of your wordprocessor rather than use tabs to align columns.

Providing a disk version

When your manuscript has been accepted, you will be asked to provide a copy on disk.

The disk can be either 3.5 or 5.25 inch MS-DOS or Apple Macintosh format. The *Journal* is edited using WordPerfect 5.2 for Windows, which can convert from most other word-processing programs. If you are using WordPerfect for DOS version 6, please save your file as WordPerfect 5.1/5.2. Please check with the editor if you have any doubts, and send an ASCII file as backup.

Proofs

Authors will receive one proof of their manuscript, in its final formatted version, but without illustrations, to check before it goes for printing. Authors may be charged for the cost of major changes.

Reprints

The author(s) will receive a total of 50 free reprints of their paper.

Authors may buy extra reprints, which should be ordered when proofs are returned. The cost for 50 additional reprints is $100; special rates apply if more are required.

Please address all correspondence to

The Editor,
AGSO Journal of Australian Geology & Geophysics
Australian Geological Survey Organisation
GPO Box 378
ACT 2601

Tel. (06) 249 9114
Fax (06) 249 9987

CSU for Service

Most of the illustrations in this journal have been professionally produced by AGSO's Cartographic Services Unit, using state-of-the-art CAD facilities. This service is extended to all contributing *AGSO Journal* authors. Please call AGSO's Chief Cartographer on (06) 249 9100 (Fax 06 249 9984) to discuss your requirements and our competitive rates.

AGSO
AUSTRALIAN GEOLOGICAL SURVEY ORGANISATION

AGSO Journal of Australian Geology & Geophysics

Volume 15, Number 3, 1994

CONTENTS

David W. Durney & Hanan J. Kisch
A field classification and intensity scale for first-generation cleavages 257

T.P. Mernagh & W.K. Witt
Early, methane-rich fluids and their role in Archaean gold mineralisation at the Sand King and Missouri deposits, Eastern Goldfields Province, Western Australia 297

Alan J. Whitaker
Integrated geological and geophysical mapping of southwestern Western Australia 313

Marion O. Michael-Leiba
Fluctuations in seismicity in the Dalton area, NSW, Australia, and their relevance to earthquake forecasting 329

C.D. Ollier & C.F. Pain
Landscape evolution and tectonics in southeastern Australia 335

Ian H. Lavering
Marine benthic communities in the Early Carboniferous of New South Wales (Visean—*Delepinea aspinosa* Zone) 347

V. Palmieri, C.B. Foster & E.V. Bondareva
First record of shared species of Late Permian small foraminiferids in Australia and Russia: time correlations and plate reconstructions 359

Robert S. Nicoll
Seximembrate apparatus structure of the Late Cambrian coniform conodont *Teridontus nakamurai* from the Chatsworth Limestone, Georgina Basin, Queensland 367

I.C. Roach, K.G. McQueen & M.C. Brown
Physical and petrological characteristics of basaltic eruption sites in the Monaro Volcanic Province, southeastern New South Wales, Australia 381